REMOTE SENSING INVESTIGATIONS OF FUGITIVE SOIL ARSENIC AND ITS EFFECTS ON VEGETATION REFLECTANCE

by

E. Terrence Slonecker
A Dissertation
Submitted to the
Graduate Faculty
of
George Mason University
in Partial Fulfillment of
The Requirements for the Degree
of
Doctor of Philosophy
Environmental Science and Public Policy

Committee:

_____	Dr. Barry N. Haack, Dissertation Director
_____	Dr. Richard J. Diecchio, Committee Member
_____	Dr. Robert L. Fischer, Committee Member
_____	Dr. George E. Taylor, Committee Member
_____	Dr. Albert Torzilli, Graduate Program Director
_____	Dr. Robert Jonas, Acting Department Chairperson
_____	Associate Dean for Graduate Programs, College of Science
_____	Dean, College of Science

Date: May 4, 2007

Spring Semester 2007
George Mason University
Fairfax, VA

Remote Sensing Investigations of Fugitive Soil Arsenic and Its Effects on Vegetation Reflectance

A dissertation submitted in partial fulfillment of the requirements for the degree of Doctor of Philosophy at George Mason University

By

E. Terrence Slonecker
Masters of Science
George Mason University, 1991

Director: Barry N. Haack, Professor
Department of Geography

Spring Semester 2007
George Mason University
Fairfax, VA

Copyright 2007 E. Terrence Slonecker
All Rights Reserved

DEDICATION

This research is dedicated to the people of Spring Valley and to all the people of the world who live with the legacy of hazardous waste.

ACKNOWLEDGEMENTS

I would like to thank my family and especially my wife Michelle who put up with my long mental and physical absences but who maintained the stable environment that allowed me to complete this journey. I would also give special thanks to my committee, Dr. Richard Diecchio, Dr. Robert Fischer and Dr. George Taylor for their thoughtful and patient oversight. Finally I will be forever grateful to my advisor and mentor, Dr. Barry Haack, who never gave up on me.

TABLE OF CONTENTS

Page
Abstract xii
1. Introduction 1
1.1 The Legacy of Chemical Weapons 6
1.2 Remote Sensing of Hazardous Waste 7
1.3 Aerial Photographic Interpretation 9
1.4 Phytoremediation of Arsenic and Spectroscopy 10
1.5 Hyperspectral Remote Sensing 12
1.6 Research Rationale 13
1.7 Dissertation Organization 18
2. Spring Valley, Arsenic and the American University Experiment Station 19
2.1 The Spring Valley Study Site 19
2.2 World War I and the American University Experiment Station 20
2.3 Unexploded Ordnance and Arsenic Contamination 25
2.4 Arsenic Phytoremediation 30
3. Literature Review 36
3.1 Photographic Interpretation and Historical Aerial Photography 36
3.2 Reflectance Spectroscopy and the Analysis of Vegetation 42
3.3 The Evolution of Remote Sensing Technology 56
3.4 The Analysis of Vegetation by Imaging Spectroscopy 60
4. Data Collection and Analysis Methods 65
4.1 Photographic Interpretation and Historical Aerial Photography 66
4.2 Statistical Methods Used in the Aerial Photographic Analysis 70
4.3 Reflectance Spectroscopy of Arsenic Stress and Uptake 71
4.4 Statistical Methods Used in the Analysis of Laboratory Reflectance Data 79
4.5 Hyperspectral Imagery Processing and Analysis Methods 85
4.6 Land Use and Land Cover Mapping 95
4.7 Statistical Methods Used in HSI Processing and LULC Mapping 97
5. Data Analysis and Results 102
5.1 Aerial Photographic Interpretation 102
5.2 Plant Growth and Arsenic Uptake 119
5.3 Greenhouse Spectral Analysis 132
5.4 Mapping Arsenic Induced Vegetation Stress with Hyperspectral Imagery 154
6. Synthesis and Discussion 166
7. Lessons Learned and the Potential for Additional Research 182
List of References 196
Appendices 221

LIST OF TABLES

Table Page
1. Examples of Vegetation Indices 51
2. Examples of Existing and Planned Hyperspectral Sensors.....61
3. Historical Aerial Photographs of the Spring Valley Area 68
4. Hyperspectral Imagery Processing Methods 94
5. 1918 Aerial Photographic Features and Spring Valley Remedial Activity 109
6. Summary Results for *Nephrolepis exaltata* 122
7. Summary Results for *Pteris cretica mayii* 123
8. Summary Results for *Pteris multifida*.....124
9. Model Results for Predicting Arsenic Concentration from Spectral Data.....142
10. Improved Models for Predicting Arsenic Concentration.....148
11. Predicting Arsenic in Field Ferns 150
12. Hyperspectral Processing and Map Accuracy Results.....157
13. Accuracy Assessment Confusion Matrix.....158
14. Null Hypothesis Test: Aerial Photographic Interpretation Features.....168
15. Null Hypothesis Test: Modeling Arsenic Concentration in *Pteris cretica mayi*i ...169
16. Null Hypothesis Test: Modeling Arsenic Concentration in *Pteris multifida*.....170
17. Null Hypothesis Test: Land Cover Mapping Accuracy.....172

LIST OF FIGURES

Figure Page
1. Remote Sensing Inputs to a and Geospatial Decision Making Process.....17
2. The Spring Valley Study Area.....21
3. Ordnance Testing at the AUES.....23
4. Livens Battery Firing at AUES.....24
5. Examples of UXO.....27
6. The Distribution of Arsenic in *Pteris vittata* 34
7. Basic Vegetation Spectra.....43
8. Spectral Similarity in Vegetation.....45
9. The Red Edge.....47
10. Spectral Derivatives.....55
11. The Evolution of Spectral Remote Sensing Systems.....58
12. Differences in Sensor Spectral Resolution 59
13. GIS Features Extracted by Aerial Photographic Analysis.....71
14. The Three Ferns Used in This Study 73
15. Ferns Growing in the Greenhouse 75
16. General Layout of the Greenhouse Experiment.....76
17. *Pteris* Ferns in the Spring Valley Phytoremediation Pilot.....78
18. Example of HyMAP Hyperspectral Imagery of the Study Area 86
19. N-Dimensional Visualization.....91
20. Training/Validation Data for Hyperspectral Image Processing.....98
21. 1918 Aerial Photograph with Photographic Interpretation Features 104
22. 1991 Aerial Photograph with Photographic Interpretation Features 105
23. Enlargement of the NW section of the 1918 Aerial Photograph of AUES 106
24. Enlargement of the SE section of the 1918 Aerial Photograph of AUES 107
25. Evaluation of 1918 Aerial Photographic Features.....110
26. 1918 and 1991 Aerial Photographs of the Glenbrook Road Pit.....112
27. Glass Containers and Mortar Shells.....113
28. Buried Glass Laboratory Waste from AUES.....114
29. Lot 18 / Small Disposal Area in 1927.....115
30. Lot 18 / Small Disposal Area in 1991.....116
31. Arsenic Concentration and Biomass.....120
32. Arsenic Concentration and Dry Weight.....120
33. Arsenic Uptake Summary for *Nephrolepis exaltata*.....126
34. Arsenic Uptake Summary for *Pteris cretica mayii*.....127
35. Arsenic Uptake Summary for *Pteris multifida* 128
36. Root/Frond Arsenic Distribution 129
37. Spectral Data in Spreadsheet Format.....133
38. The Spectra / Arsenic Correlations. 135

39. Spectral Extremes Over Time 137
40. Reflectance Models of Arsenic Concentration 139
41. The 1st Derivative Models of Arsenic Concentration 140
42. The 2nd Derivative Models of Arsenic Concentration 141
43. Noise and Clustering in Spectral Data 144
44. Improved 1st Derivative Models of Arsenic Concentration 146
45. Improved 2nd Derivative Models of Arsenic Concentration 147
46. Vegetation Index Models 153
47. Lab Spectra of Arsenic Stress 155
48. Land Cover Classification Results 159
49. Laboratory and Imagery Spectra 163
50. An Example of Continuum Removal 191
51. Fluorescence Research with Bioreporters 194

LIST OF ABBREVIATIONS AND ACRONYMS

AHS	Airborne Hyperspectral System
AIS	Airborne Imaging Spectrometer
ARI	Anthocyanin Reflectance Index
AOI	Area Of Interest
As	Arsenic
As(III)	Arsenite
As(V)	Arsenate
ASAS	Advanced Solid state Array Spectrometer
ASD	Analytical Spectral Devices
ATREM	ATmospheric REMoval
ATSDR	Agency for Toxic Substances and Disease Registry
AU	American University
AUES	American University Experiment Station
AVHRR	Advanced Very High Resolution Radiometer
AVIRIS	Airborne Visible/Infrared Imaging Spectrometer
BI	Blue Index
bioconc	bioconcentration
CAA	Clean Air Act
CASI	Compact Airborne Spectrographic Imager
CCA	Canonical Correlation Analysis
Cd	Cadmium
CERCLA	Comprehensive Environmental Response, Compensation, and Liability Act
CFR	Code of Federal Regulations
CIS	Chinese Imaging Spectrometer
cm	centimeter
CRI	Carotenoid Reflectance Index
Cu	Copper
CW	Chemical Weapon
CWA	Clean Water Act
D. C.	District of Columbia
DAIS	Digital Airborne Imaging Spectrometer
DCDOH	District of Columbia Department Of Health
DERP	Defense Environmental Restoration Program
DMA	Dimethyl Arsenic Acid
DOD	Department of Defense
DOQQ	Digital Ortho Quarter Quad
dpi	dots per inch
DVI	Difference Vegetation Index

dw	dry weight
EGFN	Edge Green First-derivative Normalized index
EMS	ElectroMagnetic Spectrum
ENVI	ENvironment for Visualizing Images
EOS	Earth Observing System
ER	Emergency Response
EVI	Enhanced Vegetation Index
FUDS	Formerly Used Defense Site
g	grams
GAO	General Accounting Office
GFP	Green Fluorescent Protein
GGRN	Green/Green + Red + Near infrared
GI	Green Index
GIS	Geographic Information Systems
GNR	Green Near infrared Red index
GR	Green Red index
GVI	Green Vegetation Index
ha	hectares
HIRIS	HIgh Resolution Imaging Spectrometer
HRS	Hyperspectral Remote Sensing
HSI	HyperSpectral Imagery
HYDICE	HYperspectral Digital Imagery Collection Experiment
HyMAP	HYperspectral MAPper
ICP/AES	Inductively Coupled Plasma/Atomic Emission Spectrometry
IR	InfraRed
IUPAC	International Union of Pure and Applied Chemistry
km	kilometer
LAI	Leaf Area Index
LOC	Library of Congress
LULC	Land Use and Land Cover
MAS	MODIS Airborne Simulator
mb	megabyte
MCARI	Modified Chlorophyll Absorption Ratio Index
mm	millimeters
MMA	Monomethyl Arsenic Acid
MNF	Minimum Noise Fraction
MODIS	MODerate resolution Imaging Spectrometer
MSI	Moisture Stress Index
MSR	Modified Simple Ratio
MSS	Multi Spectral Scanner
MTVI	Modified Triangular Vegetation Index
NARA	National Archives and Records Administration
NASA	National Aeronautics and Space Administration
NATO	North Atlantic Treaty Organization
NDVI	Normalized Difference Vegetation Index

NEMO	Navy Earth Map Observer
NG	Nir Green index
NIR	Near InfraRED
nm	nanometers
NNGI	Normalized Near infrared Green Index
NPL	National Priorities List
NRC	National Research Council
NRL	Naval Research Laboratory
Pb	lead
PCA	Principal Components Analysis
PLS	Partial Least Squares
PCM	*Pteris cretica mayii*
PMF	*Pteris multifida*
ppb	parts per billion
PPI	Pixel Purity Index
ppm	parts per million
PRI	Photochemical Reflectance Index
PVI	Perpendicular Vegetation Index
RARS	Ratio Analysis Reflectance Spectra index
RCRA	Resource Conservation and Recovery Act
RDVI	Renormalized Difference Vegetation Index
REP	Red Edge Position
RGRN	Red/Green+Red+NIR
RI	Red Index
RNG	Red Near infrared Green
RSR	Reduced Simple Ratio
RVI	Ratio Vegetation Index
RVSI	Red edge Vegetation Stress Index
SARA	Superfund Amendments and Reauthorization Act
SAS	Statistical Analysis Software
SAVI	Soil Adjusted Vegetation Index
SEM	Structural Equation Modeling
SGI	Sum Green Index
SLR	Stepwise Linear Regression
SPSS	Statistical Package for the Social Sciences
SWIR	Short Wave InfraRed
TM	Thematic Mapper
TNT	TriNitroToluene
TRWIS	TRW Imaging Spectrometer
TSCA	Toxic Substances Control Act
TVI	Triangular Vegetation Index
U.S.	United States
UNEP	United Nations Environmental Programme
USACE	United States Army Corps of Engineers
USC	United States Code

USEPA	United States Environmental Protection Agency
USGS	United States Geological Survey
UV	Ultra Violet
UXO	UneXploded Ordnance
VI	Vegetation Indices
VIMS	Visible Infrared Mapping Spectrometer
VIP	Variable Importance in Projection
VOC	Volatile Organic Compounds
WHO	World Health Organization
WR	White Reference
WWI	World War I
WWII	World War II
Zn	Zinc

ABSTRACT

REMOTE SENSING INVESTIGATIONS OF FUGITIVE SOIL ARSENIC
AND ITS EFFECTS ON VEGETATION REFLECTANCE

E. Terrence Slonecker, PhD

George Mason University, 2007

Dissertation Director: Dr. Barry N. Haack

Three different remote sensing technologies were evaluated in support of the remediation of fugitive arsenic and other hazardous waste-related risks to human and ecological health at the Spring Valley Formerly Used Defense Site in northwest Washington D.C., an area of widespread soil arsenic contamination as a result of World War I research and development of chemical weapons. The first evaluation involved the value of information derived from the interpretation of historical aerial photographs. Historical aerial photographs dating back as far as 1918 provided a wealth of information about chemical weapons testing, storage, handling and disposal of these hazardous materials. When analyzed by a trained photo-analyst, the 1918 aerial photographs resulted in 42 features of potential interest. When compared with current remedial activities and known areas of contamination, 33 of 42 or 78.5 % of the features were spatially correlated with current areas of contamination or remedial activity. The second investigation involved the phytoremediation of arsenic through the use of *Pteris* ferns and the evaluation of the spectral

properties of these ferns. Three hundred ferns were grown in controlled laboratory conditions in soils amended with five levels (0, 20, 50, 100 and 200 parts per million) of sodium arsenate. After 20 weeks, the *Pteris* ferns were shown to have an average uptake concentration of over 4,000 parts per million each. Additionally, statistical analysis of the spectral signature from each fern showed that the frond arsenic concentration could be reasonably predicted with a linear model when the concentration was equal or greater than 500 parts per million. Third, hyperspectral imagery of Spring Valley was obtained and analyzed with a suite of spectral analysis software tools. Results showed the grasses growing in areas of known high soil arsenic could be identified and mapped at an approximate 85% level of accuracy when the hyperspectral image was processed with a linear spectral unmixing algorithm and mapped with a maximum likelihood classifier. The information provided by these various remote sensing technologies presents a non-contact and potentially important alternative to the information needs of the hazardous waste remediation process, and is an important area for future environmental research.

1. Introduction

The intentional or accidental release of hazardous substances into the environment is an inevitable consequence of anthropogenic activity. Industrial, commercial, mining, military and even domestic activities can result in the release of substances into the air, land and water that are harmful to environmental quality and human health. The combined industrialization and population growth of the twentieth century has resulted in an unprecedented release of fugitive contamination that today threatens many plant and animal species and may ultimately threaten the survival of the human race (Nriagu 1994). The discovery, detection and remediation of many hazardous waste problems consists of a variety of monitoring and analysis strategies that are time-consuming and expensive, such as laboratory chemical analysis. One of the technologies that has an established and growing potential to provide a non-contact and cost-effective alternative to traditional sampling methods is remote sensing. The purpose of this research is to evaluate the potential for relevant information to be provided to the hazardous waste remediation process by both traditional and emerging remote sensing technologies.

Hazardous waste control, monitoring, remediation and related issues result in a staggering cost to society in terms of human and ecological health effects, negative externalities on real estate values (i.e., the 'stigma' of contamination) and the extraordinary burden of a massive regulatory infrastructure on economic productivity.

The United States Environmental Protection Agency (USEPA) estimates that complying with hazardous waste regulations cost nearly $32 billion in 2000, about 20 % of the cost for all United States (U.S.) pollution control laws (Sigman 1999). In 1998, the U.S. Agency for Toxic Substances and Disease Registry (ATSDR) evaluated the medical and lost productivity costs from health conditions occurring in U.S. communities located near hazardous waste sites that were contaminated with volatile organic compounds (VOCs). For the 258 sites studied, the annual costs were in excess of $300 million (Lybarger et al. 1998).

Substances are considered hazardous wastes if they are ignitable - capable of burning or causing a fire; corrosive - able to corrode steel or harm organisms because of extreme acidic or basic properties; reactive - able to explode or produce toxic cyanide or sulfide gas; or toxic - containing substances that are poisonous to people and other organisms (USEPA 2006b). In the U.S., the regulatory definition of hazardous substances are detailed in the Resource Conservation and Recovery Act (RCRA) and can be found under specific listings, along with accepted testing methods, in Chapter 40, Code of Federal Regulations, Section 261(40 CFR § 261) (USEPA 2006b).

Most hazardous waste is the by-product of industrial or commercial manufacturing processes but significant levels of hazardous substances are associated with agricultural chemicals such as pesticides. However, even household waste contains substances such as bleach, gasoline, batteries and solvents that qualify as hazardous wastes. Hazardous waste can also be naturally occurring substances, such as lead and

mercury, that are brought in much higher than normal exposure concentrations by anthropogenic processes.

The effects of fugitive hazardous waste are multiple and varied. Hazardous wastes may pollute soil, air, surface water or underground water. Pollution of soil may affect people who live on it, plants that put roots into it and animals that move over it. Pollution may concentrate in individual organisms and up the food chain, with serious additive effects in higher trophic organisms in processes called bioaccumulation and biomagnification (IUPAC 1993).

The human health effects from exposure to fugitive hazardous wastes are highly variable but can range from acute toxicity and immediate danger to life to chronic exposures and a wide range of health effects. Many studies have shown that in residential communities near a hazardous waste site, there is an increased risk of birth defects, neuro-toxic disorders, leukemia, cardiovascular diseases, respiratory and skin disorders (Vine et al. 2000; Berry and Bove 1997; Hall et al. 1996; Vianna and Polan 1984). In a comprehensive review of the literature, Vrijheid (2000) noted that there is a general weakness in almost all human health-hazardous waste site studies in that there is a lack of direct exposure measurement and this is a significant research need in order to better understand and quantify the risk of residential exposure to hazardous waste sites.

Hazardous waste sites can have serious economic ramifications on the value of the contaminated property, as well as the value of surrounding properties and neighborhoods. Research suggests that residential dwellings located near hazardous waste sites experience a negative impact on property values and that this impact is

directly related to distance from the site, generally disappearing between 3.2 and 4.8 km from the site (USEPA 2006a). Interestingly some research suggests that the USEPA's listing of a hazardous waste site on the National Priorities List (NPL) actually has a positive effect on surrounding real estate values because it leads to a formal clean-up plan and tends to remove uncertainty that affects market values (USEPA 2006a). Commercial real estate values are often more severely affected by proximity to a hazardous waste site because of the fear of liability issues. In recent years, some companies have actually been able to recover these "stigma damages" through legal action (Honigberg and Nolan 2000).

On a global scale, the issue of hazardous waste is even more serious. During the 1980s, the development of strict environmental controls on hazardous waste in industrialized countries, such as the Superfund Act in the U.S., resulted in a black market for unregulated translocation of hazardous wastes from industrial to third-world countries (de Nava 1996). International outrage at the activities of "toxic traders" led to the drafting and adoption of the Basel Convention of 1989. Both the Basel Convention and the Rotterdam Convention of 1998 seek to stem the trans-boundary movement of hazardous substances and hazardous waste, especially to developing countries. Also the central goal of the Basel Convention is "environmentally sound management" to protect human health and the environment by minimizing hazardous waste production whenever possible and promoting an "integrated life-cycle approach" to hazardous waste management which involves promoting institutional controls from the generation of a

hazardous waste to its storage, transport, treatment, reuse, recycling, recovery and final disposal (UNEP 2006).

In the U.S., hazardous waste and hazardous waste cleanup are regulated by two federal statutes that are administered by the USEPA. The RCRA was enacted by Congress in 1976 in order to (1) protect human health and the environment from the potential hazards of waste disposal, (2) conserve energy and natural resources and to reduce the amount of waste generated, and (3) ensure that waste is managed in an environmentally sound manner. The Comprehensive Environmental Response, Compensation, and Liability Act (CERCLA) of 1980, commonly known as Superfund, and the 1986 Superfund Amendments and Reauthorization Act (SARA) provide strict guidelines regarding the responsibility of past and present property owners, as well as others, for the cost of toxic-waste cleanup. Superfund empowers the USEPA to compel the owner of property contaminated by hazardous substances to clean up the site. Alternatively, the USEPA can conduct the cleanup and obtain reimbursement from the responsible parties at a later date.

A special class of hazardous waste problems relates to current or former military activity at active military facilities and at properties that were formerly owned by, leased to, or otherwise utilized by the U.S. under the jurisdiction of the Secretary of Defense. Such properties are known as Formerly Used Defense Sites (FUDS). The FUDS program is funded under the Defense Environmental Restoration Program (DERP) and administered by the U.S. Army Corps of Engineers (USACE). There are over 4,400 currently identified FUDS with an estimated cost to complete cleanup of between

15 and 20 billion dollars (GAO 2001). One of the costliest and most politically charged cleanups of a FUDS is currently taking place in northwest Washington, D.C., at the American University and the surrounding neighborhood, known as Spring Valley. The objective of the research described in this dissertation is the evaluation of the value of traditional and emerging remote sensing technologies for the cleanup of this hazardous waste site where remediation activity for unexploded ordnance (UXO) and inorganic arsenic is still in progress.

1.1 The Legacy of Chemical Weapons (CW)

Perhaps the most insidious and dangerous forms of hazardous waste are those substances that are precisely engineered and manufactured for the sole purpose of ending human life as quickly as possible.

Chemical weapons, as defined by the United Nations,"… are chemical agents of warfare … whether gaseous, liquid or solid, which might be employed because of their direct toxic effect on man, animals and plants" (United Nations 1969). The North Atlantic Treaty Organization (NATO) definition of a chemical agent is: "A chemical substance which is intended for use in military operations to kill, seriously injure or incapacitate people because of its physiological effects" (U.S. Army 1996).

Poison gas weapons were first developed and extensively deployed during World War I (WWI). Although some accounts differ, the first effective deployment of CW occurred at the battle of Ypres, Belgium, on April 22, 1915. Chlorine gas was released by German forces and killed over 5,000 allied troops. Both sides deployed and continued

to develop CW throughout the conflict with a total of over 92,000 killed and 1.3 million wounded by the end of the war (Heller 1984). Research into new and more deadly types of CW continued throughout the war and saw the development of Mustard Gas, and deadly forms of inorganic arsenic and arsenical compounds such as arsine gas, Lewisite (2-chloroethenyldichloroarsine) and Adamsite (diphenylaminechlorarsine) (Bancroft 1919).

When the U.S. finally entered WWI in 1917, one fact was disturbingly apparent; it was woefully behind in the development and utilization of CW and countermeasures such as protective clothing and gas masks. An intense research and development program was initiated at several locations around the country including the American University, located in what is now northwest Washington, D.C. The U.S. Army leased the entire campus of the college and an additional 243 hectares (ha) for the purpose of research, development and field testing of chemical warfare agents and countermeasures (Bancroft 1919).

The legacy of that CW testing and development still exists in the area today in the form of UXO and soil and groundwater contamination from inorganic arsenic and other chemical compounds. The American University and the surrounding neighborhood, known as Spring Valley, is currently the focus of a major FUDS cleanup.

1.2 Remote Sensing and Hazardous Waste

The process of discovering, characterizing and remediating fugitive contaminants in the environment is typically a long and costly endeavour. The current cleanup of

Spring Valley has been underway for nearly ten years with at least another five to go and has cost in excess of 40 million dollars (Parsons 2003). In the hazardous waste remediation process, one of the key steps is S*ite Characterization*, the determination of the spatial extent and nature of the contamination. Site characterization is often costly and time consuming, requiring extensive field sampling and laboratory analysis. One technology that has been valuable in cleanup efforts and shows promise in providing an alternative to field sampling methods is remote sensing.

Remote sensing is a generic term that encompasses a body of non-contact monitoring techniques that measure energy interactions to determine the characteristics of a target surface or medium. Although remote sensing includes a wide variety of instruments and methods, such as lidar, radar, X-ray technology and acoustic instruments, it is most often associated with overhead imaging techniques, such as aerial photography and satellite imagery that record energy in the solar-reflected part of the electromagnetic spectrum (EMS) between 400 and 2,500 nm wavelengths. Remote sensing has a long history of providing critical information to the process of identifying, characterizing and remediating hazardous waste problems (Titus 1982; Lyon 1987; Barnaba et al. 1991). Further, new and emerging remote sensing techniques show promise for characterizing site conditions and providing critical information to the hazardous waste cleanup process.

The purpose of this study is to evaluate the information derived from three specific remote sensing analysis methods, aerial photographic interpretation, reflectance spectroscopy and imaging spectroscopy in the characterization and remediation of contamination in Spring Valley.

1.3 Aerial Photographic Interpretation

One of the most fundamental forms of remote sensing is that of aerial photographic interpretation. Aerial photographs have been routinely collected over the conterminous U.S. since the 1930s for engineering and agricultural purposes and they represent a rich archive of historical changes on the landscape. The analysis of aerial photographs has been used for decades to assist in hazardous waste investigation and remediation and there is a long history of successful applications of this form of remotely sensed data in environmental monitoring.

The USEPA has produced over 4,000 historical aerial photographic reports on hazardous waste activity that have been instrumental in environmental cleanup programs (Benger 2004). These reports use the interpretation of historical aerial photographs to detail landscape activities, such as burial areas, landfills, vegetation stress and ground disturbance, as indicators of possible surface and sub-surface contamination. While the use of historical aerial photographs has often been employed, there have been few, if any assessments of the accuracy or value of historical aerial photographic interpretation in the hazardous waste site cleanup process. The relevance of historical imagery in hazardous waste cleanup has been documented by Titus (1982), Lyon (1987), Barnaba et al. (1991) and Slonecker et al. (2002). Formal tests for the accuracy and consistency of photographic interpretation were developed by Congalton and Mead (1983) but these largely revolved around inter-analyst variability and were dependent on a relatively recent time frame in which landscape conditions were the same as when the photograph was taken and data could be field-verified. There are inherent difficulties associated with

evaluating subjective interpretation of historical photographs; most notably the inability to perform field checks or obtain reliable ground reference data for accuracy assessment.

The Spring Valley FUDS remediation offers an excellent opportunity to perform a relative accuracy evaluation of photo-derived information by utilizing Geographic Information Systems (GIS) overlay technology. This is the first of the three remote sensing components in this study. By first georegistering historical aerial photographs to a common coordinate system, photo-interpreted features, such as ground scars and pits can be digitized into GIS format and overlaid on a current map of areas of known contamination. This permits direct spatial correlation between features derived from historical aerial photographs and the areas of contamination requiring eventual remediation. The results of this analysis provided a good indication of the value of historical photo-derived information.

1.4 The Phytoremediation of Arsenic and Spectroscopy

The process of remediating hazardous waste has seen the emergence of some interesting alternatives to the standard soil removal techniques, which are expensive, time-consuming and disruptive. When soil is contaminated above certain established chemical concentrations, it must be removed and replaced with clean soil by regulation. Alternative use of innovative technologies for removal of soil contamination is also encouraged and one such innovative alternative for arsenic removal is that of *phytoremediation.*

Phytoremediation is the removal of contamination by plants and in urban areas such as Spring Valley, phytoremediation offers distinct advantages to traditional techniques because it is inexpensive and far less disruptive to the community and the landscape than the standard soil excavation and replacement. Phytoremediation of arsenic is currently being utilized in the Spring Valley cleanup and is the result of the discovery that the *Pteris* genus of ferns hyperaccumulates inorganic arsenic (Ma et al. 2000). The Chinese Brake Fern (*Pteris vittata*), the Spider Brake Fern (*Pteris multifida*) and the Cretan Brake Fern (*Pteris cretica*) have been shown to uptake so much inorganic arsenic that they can actually reduce the soil arsenic concentration of a moderately contaminated site to acceptable levels in just a few growing seasons (Edenspace 2004; Blaylock et al. 2006).

Spectroscopy is the science of measuring the interaction of energy with matter and is a fundamental form of remote sensing investigation. Spectroscopy has been used extensively in chemistry and astronomy for material identification and, with the development of new instrumentation, is being increasingly utilized in traditional remote sensing investigations. The spectral reflectance of vegetation growing in soils containing heavy metals has long been a topic of remote sensing investigation and the spectral analysis of ferns that hyperaccumulate arsenic is an especially interesting application of this form of remote sensing. Early laboratory spectroscopic and remote sensing imaging research successfully identified spectral signatures of heavy metal stress and applied these techniques to applications involving mineral prospecting and environmental contamination (Milton et al. 1983; Milton et al. 1989; Milton et al. 1991).

The second objective of this research is to study the spectral reflectance of *Pteris* ferns, and other common vegetation, subjected to varying levels of soil arsenic, in a controlled greenhouse environment. These results should be a valuable addition to remote sensing science and could potentially lead to the ability to remotely monitor via vegetation reflectance, both the existence of soil arsenic and the level of arsenic extraction.

1.5 Hyperspectral Remote Sensing (HRS)

Spectral reflectance of vegetation and other landscape conditions has received renewed interest by the remote sensing community during the past decade because of the development of a new class of imaging technology called hyperspectral remote sensing, also known as imaging spectroscopy. Many of the early and definitive studies in spectral reflectance utilized spectroscopic measurement instruments in a laboratory setting. These instruments measured reflected energy and produced spectra, which could then be analyzed using standard techniques.

HRS not only collects information about reflected energy, but also collects imagery in very narrow bandwidths across the solar reflected part of the EMS. The result is a digital file of hundreds of bands of imagery, sometimes called a ‘cube”, that can be analyzed with the same methods as laboratory spectra and can identify certain compounds, materials and conditions based on the interaction of photons with the molecular structure of the target material. Spectroscopic analysis techniques can now be employed outside of the laboratory through the use of HRS imaging techniques and

portable field spectroradiometers. The third objective of this research is to evaluate hyperspectral imagery (HSI) and field spectroscopic measurement techniques in the characterization and analysis of arsenic contamination at the Spring Valley site.

1.6 Research Rationale

The primary objectives of this research are the assessment of remote sensing technology's ability to provide information to the decision-making processes in hazardous waste site investigation and remediation. While remote sensing technology, in its various forms, is routinely used in hazardous waste site characterization and remediation, it is typically utilized in very narrow and specific issues. The rationale of this research effort is to link remote sensing information processes from field, laboratory and overhead sensors and to apply the science of remote sensing to the remediation of hazardous waste at an active hazardous waste remediation activity: the Spring Valley site in Washington, D.C. This research will ascertain the value of traditional and emerging remote sensing technologies in these types of clean-up scenarios and will also expand the range of potential applications of remote sensing systems for future hazardous waste remediation.

This research is focused on determining the effectiveness of selected remote sensing technologies to provide critical information along three specific lines of investigation. The first involves the use of historical aerial photography in identifying past landscape activities that relate to current pollution problems. The second involves the use of laboratory spectroscopy and a controlled greenhouse environment to document

the effectiveness of *Pteris* ferns for soil-arsenic phytoremediation and to detect the effects of fugitive arsenic in the soil as expressed by changes in the reflectance patterns of vegetation. The third line is the evaluation of HSI to determine arsenic-induced vegetative stress in areas of known arsenic contamination. This study hypothesizes three specific questions:

1. What is the relative value of information derived from historical imagery to the information needs of the hazardous waste investigation/remediation process? Stated as a set of research hypotheses:

H_0 = Spatially explicit patterns of landscape disturbance, as derived from historical aerial photographs, are NOT spatially related to future hazardous waste remediation requirements.

H_1 = Spatially explicit patterns of landscape disturbance, as derived from historical aerial photographs, ARE spatially related to future hazardous waste remediation requirements.

2. In a controlled laboratory environment, can arsenic phytoextraction be detected and/or quantified, via the spectral reflectance and spectroscopic analysis of hyperaccumulating *Pteris* ferns? Stated as a set of research hypotheses:

H_0 = Arsenic phytoextraction by *Pteris* Ferns can NOT be predicted by spectral reflectance data in the 450 – 2,500 nm region of the EMS.

H_1 = Arsenic phytoextraction by *Pteris* Ferns CAN be predicted by spectral reflectance data in the 450 – 2,500 nm region of the EMS.

3. In a field application, can arsenic stress and/or arsenic phytoextraction be detected and/or quantified via HSI and spectroradiometric data collection and analysis? Stated as a set of research hypotheses:

H_0 = Arsenic stress in common lawn grasses can NOT be identified and mapped by the analysis of HSI in the 450 – 2,500 nm region of the EMS.

H_1 = Arsenic stress in common lawn grasses CAN be identified and mapped by the analysis of HSI in the 450 – 2,500 nm region of the EMS.

The benefits that could be derived from this research are potentially significant. First, although historical imagery has been used for decades, there have been few, if any attempts to quantify its importance or the predictive value of information derived from historical photographic interpretation as related to the actual areas of hazardous waste contamination that require cleanup.

Second, the spectral characterization of the hyperaccumulating *Pteris* ferns would add to the current state of knowledge about this new and potentially very important, phytoremediation option. Although the *Pteris* ferns have been established as legitimate hyperaccumulators of arsenic, little is known about the physiological basis of the arsenic uptake (Bondada and Ma 2003). A study of the reflectance properties of these ferns during the phytoremediation process could lead to an improved understanding of the relationship between the plant physiology and arsenic uptake of the *Pteris* ferns.

Third, the detection of stressor contaminants in the soil by way of changes in vegetation reflectance could be an important new tool in site characterization. The traditional soil sampling process is very time-consuming and expensive. When taking into account quality control factors, the standard laboratory methods and the human labor involved, the cost of the average soil sample today is around $2,000 per sample (Schilling 2004). Further, even with grid sampling procedures, soil samples are still only discrete points taken across a soil continuum, creating the possibility of errors of omission. Reliable spectral signatures from cover vegetation would be more likely to represent the true distribution of contamination across a continuous surface.

Finally, demonstrating the efficacy of information derived from these diverse remote sensing systems across this broad spectrum of remedial data requirements would further not only the science of remote sensing but also its practical application in the area of monitoring and remediating hazardous waste sites and fugitive contamination. Figure 1 shows a conceptual diagram of the information flow in the process of hazardous waste site remediation and how the geospatial products of this type of remote sensing research might fit into a larger context of information management and risk reduction.

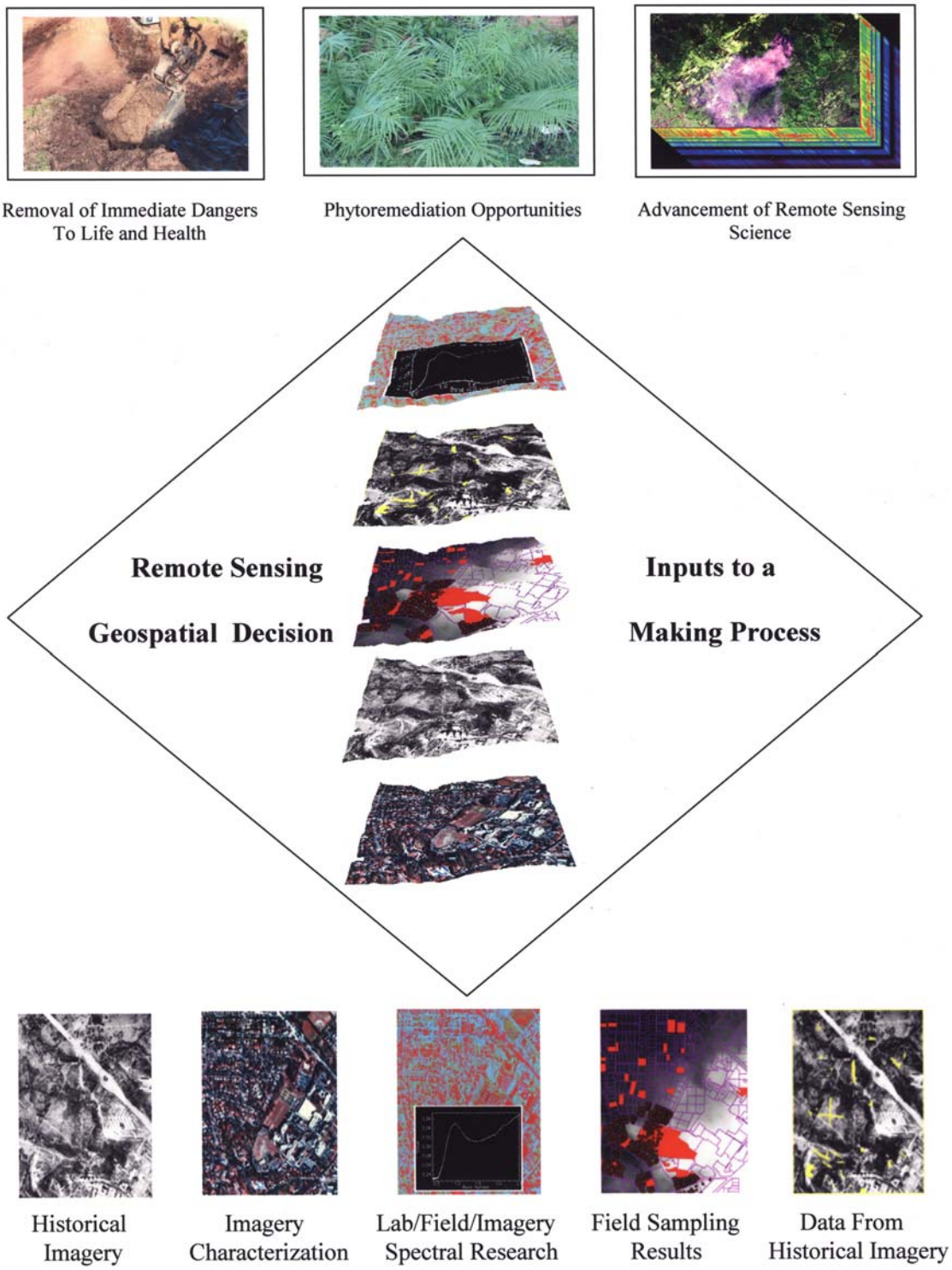

Figure 1. Remote Sensing Inputs to a Geospatial Decision Making Process. The conceptual flow of information from remote sensing systems through the hazardous waste remediation and cleanup process.

1.7 Dissertation Organization

The remainder of this dissertation is organized in the following manner. Chapter 2 presents the details of several key background issues including UXO, arsenic contamination and the phytoremediation of arsenic. Chapter 2 also includes a historical background of WWI and the activities at the American University Experiment Station (AUES), along with a general review of the phytoremediation of arsenic with *Pteris* ferns. Chapter 3 contains a general literature review of remote sensing topics that are relevant to this research. Chapter 4 outlines the data collection and analysis methods. Chapter 5 presents the basic results of analyses. Chapter 6 discusses and synthesizes the results, and Chapter 7 articulates the lessons learned and opportunities for additional research.

2. Spring Valley, Arsenic and the American University Experiment Station

The historical background and context of the hazardous waste contamination and cleanup issues in Spring Valley are an important component to understanding the unique problems and challenges of this type of hazardous waste cleanup. The Spring Valley site is one of the highest profile FUDS remediation efforts in the U.S. New discoveries and remediation activities there attract the attention of the news media and Congressional and District of Columbia officials (Fatz 2001; GAO 2002). See Figure 2.

2.1 The Spring Valley Study Site

The control of hazardous substances and hazardous waste facilities are regulated by a number of key environmental statutes such as the RCRA, CERCLA, SARA, the Toxic Substances Control Act (TSCA), the Clean Water Act (CWA) and the Clean Air Act (CAA). Spring Valley represents a special class of hazardous waste problems resulting from former military activity in areas no longer under the administration of the Department of Defense (DOD). The FUDS program was established as part of the Defense Environmental Restoration Program (DERP) under Section 211 of the SARA of 1986. Section 211 was codified in Title 10 of the United States Code (USC), Section 2701. Under the provisions of CERCLA and SARA, the cleanup and liability for FUDS areas is the responsibility of the DOD.

2.2 World War I (WWI) and the American University Experiment Station

WWI was the first global-scale conflict to employ the technology of the industrial revolution on the battlefield. Although aircraft, submarines, tanks, wireless communication and increasingly sophisticated artillery changed the face of warfare forever, perhaps the most significant of the emerging technologies was the widespread use of CW by both sides in this conflict. WWI was the first widespread use of such weapons in human history.

The first reported use of CW was on the Eastern Front (Germany/Russia) on January 3, 1915, when artillery shells filled with a tearing agent were fired from German positions. The first significant use of gas on the battlefield was the second battle of Ypres on April 22, 1915. German forces released Chlorine Gas, which drifted over allied positions and caused widespread panic and death (Irwin 1915). British and Allied forces started utilizing poison gas by September of 1915 (Heller 1984).

The age of chemical warfare had begun and both sides' use of various types of CW escalated throughout the remainder of the war. When the U.S. formally entered the conflict on April 6, 1917, military leaders were keenly aware that the U.S. did not possess the technology or expertise to deal with the CW that were being deployed on the European battlefields (Fries and West 1921).

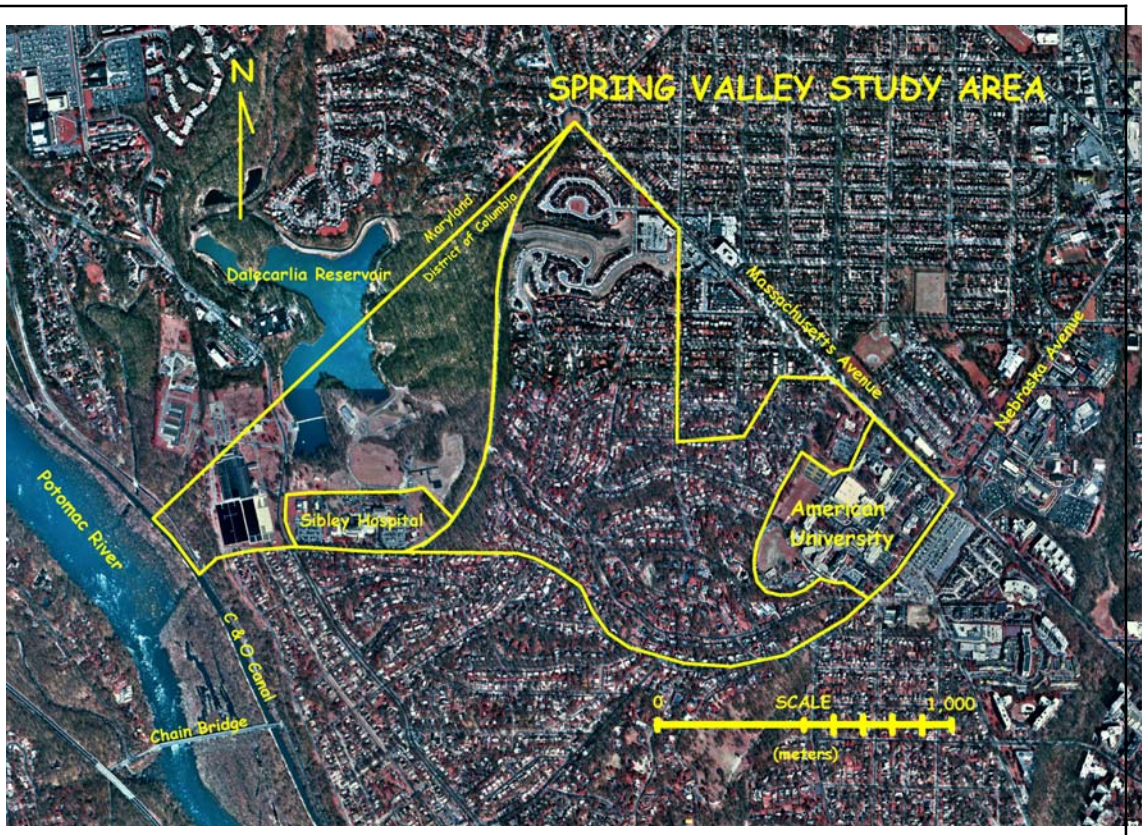

Figure 2. The Spring Valley Study Area. The Boundary of the Spring Valley Study Site in northwest Washington D.C. overlain on the 1994 USGS Digital Orthophoto Quarter Quadrangles (DOQQ), Washington West NW and Washington West SW.

Therefore in order to rapidly develop and test CW and countermeasures, the U.S. Federal Government leased the entire campus of the American University and an adjacent 243 ha from five private landowners. The facility was renamed the American University Experiment Station (AUES) and by October 1917, laboratories, facilities, test ranges and proving grounds had been constructed for the development and testing of CW such as Mustard Gas and Lewisite (Fries and West 1921).

Research and testing included both offensive and defensive measures. This included ordnance and delivery mechanisms such as artillery shells and grenades, human and animal toxicity, chemical persistency in the environment and poison gas countermeasures such as gas masks and protective fabric for clothing, tents and trench curtains. Figures 3 and 4 show ground photos of weapons and smoke candle testing being conducted at the AUES during the 1917–1918 operations.

When the armistice was signed on November 11, 1918, the AUES was in full operation and found itself suddenly without an urgent mission. Over the next several months, the station was shut down. Troops and staff were released, buildings were razed and much of the chemical and munitions inventory was either moved or buried at various locations around the AUES property. As a result, the Spring Valley area was left with a toxic legacy of buried munitions and soil contamination from inorganic arsenic.

The area today mostly consists of single family residential homes. American University occupies most of the original AUES ground in the southeast corner of the study area and Sibley Hospital is located in the southwest corner. See Figure 2.

In spite of anecdotal evidence, the environmental situation went generally unnoticed until March 1986 when officials of American University, because of planned building construction, requested that the USACE conduct an investigation into possible buried chemical munitions on the campus. The USACE completed its investigation in October of that year and concluded that there was no evidence of buried munitions and no further action was necessary.

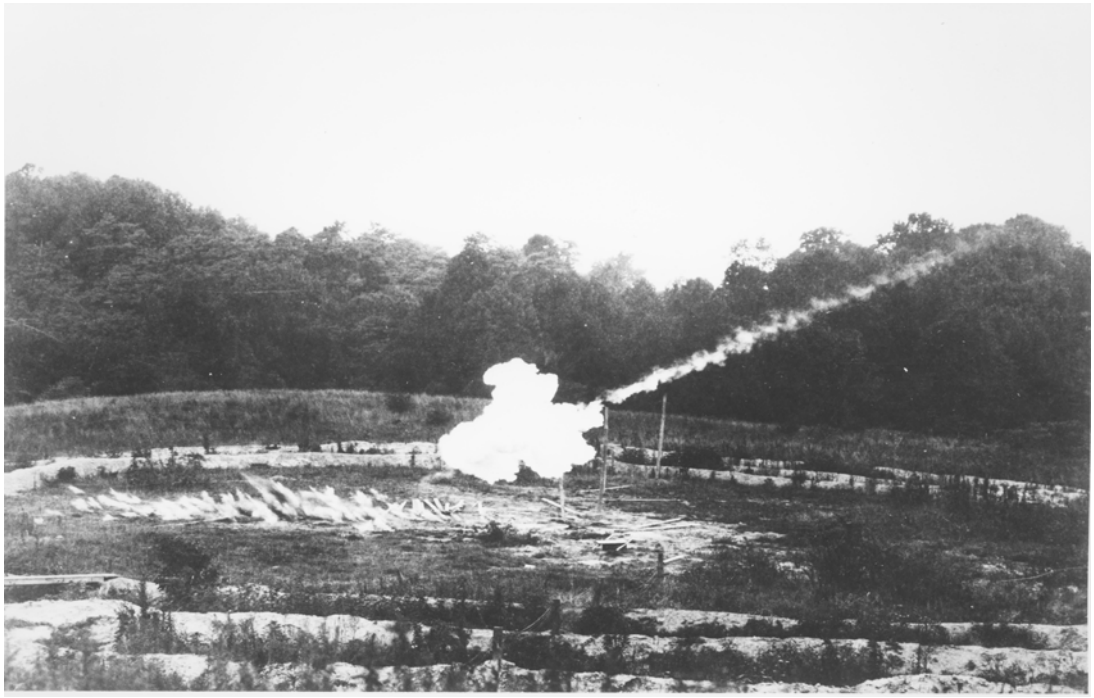

Soldiers entering Smoke Screen produced by candles.

Figure 3. Ordnance Testing at the AUES: Above: A CW-laden mortar shell explodes releasing shrapnel and chemical agent to volatilize in the air. Below: field testing of smoke candles (AUES 1918).

Firing Livin's Drums from Livin's Projector.

Smoke Cloud from Livin's Drum fired from Livin's Projector.

Figure 4. Livens Battery Firing at AUES. Live fire tests utilizing Livens mortars fired from the Western edge of American University to the west towards the Dalecarlia Woods (AUES 1918).

In 1993, a construction crew accidentally unearthed several 75 mm mortar shells near the 52nd Court cul-de-sac in the northwest part of the study area. This resulted in a full Superfund remedial investigation. Although the USACE removed over 200 pieces of ordnance from a burial pit near the 52nd Court cul-de-sac, the final recommendation of the Remedial Investigation, signed by both the USACE and the USEPA was "No further action is necessary" (Parsons 1995).

In 1998, at the request of the Health Department of the District of Columbia (DCDOH), the USACE returned to investigate possible munitions on the property of the Korean Ambassador on Glenbrook Road. Two major burial pits were discovered resulting in the removal of another 200+ pieces of ordnance and other items. This resulted in the initiation of a second Spring Valley investigation (termed Operation Safe Removal) and has resulted in several significant UXO extractions and the discovery of elevated levels of arsenic in the soils around Spring Valley (Parsons 2003). This work is ongoing and this research will contribute to the cleanup and risk assessment decisions in the current remediation effort.

2.3 Unexploded Ordnance (UXO) and Arsenic Contamination

The pollution profile in Spring Valley consists of two primary elements: UXO and inorganic arsenic. An example of unearthed UXO from Spring Valley is shown in Figure 5. Livens and 75 mm mortar shells have been discovered still containing explosives and chemical agents from the AUES operations.

UXO is a legacy of modern warfare and a worldwide threat to human and ecological health and safety. UXO is defined as: Explosive Ordnance that has been (1) primed, fused, armed or otherwise prepared for action; (2) fired, dropped, launched, projected, buried or placed in such a manner as to constitute a hazard to operations installations, personnel or material; and (3) that remains unexploded either by design, malfunction or for any other cause (United Nations 2004). UXO consists of land mines, bombs, grenades, mortars and other types of explosive warfare devices that are left in the upper soil horizons after military activity has ceased. They may have been placed below the soil as a result of direct battlefield tactics, as in land mines, aerial bombing, mortar or artillery warfare or, as in the case of Spring Valley, disposal. UXO devices usually remain explosive and present a serious risk. In addition, some UXO, as in Spring Valley, can carry a secondary and more serious threat, in terms of a chemical warfare agent, which could harm others beyond the immediate impact of the explosion. UXO is a serious problem in countries such as Vietnam, Afghanistan, Angola, Bosnia, Cambodia, Nicaragua and Zimbabwe. Over 800 people are killed each month as a result of accidental UXO explosions (Siegel 1995). In the U.S., it is estimated that there are over 16,000 UXO sites that need remediation (Knickerbocker 2002).

Figure 5. Examples of UXO. Unexploded 75 mm artillery shells excavated from a pit in Spring Valley. Some shells still contained explosives and deadly arsine gas.

Arsenic is the other major contamination problem in Spring Valley and in many of the FUDS locations that were involved with CW development. Because of its toxicity, arsenic and arsenical compounds were used as the basis for many of the chemical warfare compounds that were developed in WWI. Over 200 arsenical compounds were experimented with at the AUES (Fries and West 1921).

Arsenic is an elemental substance that has been known to be highly toxic to human health since Greek times. Arsenic is toxic at very low doses and the current USEPA action level for arsenic removal from soil is only 43 parts per million (ppm)

(CERCLA 1980). Although it has been used throughout history in various medicinal purposes, it is generally associated with its toxicity and killing powers, having gained nicknames like "the inheritance powder" in France and has been one of the most popular substances used in malevolent poisonings through the 19th Century (Gorby 1994). Arsenic is a waste product of many mining processes, has been used extensively in the pesticide industry and until recently, used widely as a wood preservative (Azcue and Nriague 1994).

Although it is often associated with heavy metals, arsenic is classified as a transition element and a metalloid, reflecting the fact that it commonly forms complexes with metals. It also readily reacts to form covalent bonds with carbon, hydrogen and oxygen. Because of these chemical properties, arsenic readily bonds to soil, especially soils that contain iron as are found in Spring Valley.

Arsenic is a major contaminant of soils and waters in the U.S. and other countries. Contamination of surface water, ground water and drinking water by arsenic poses significant health risks to humans and animals. Arsenic is a known carcinogen and mutagen, is detrimental to the immune system and contributes to skin, bladder and other cancers (NRC 1999). According to the U.S. Geological Survey (USGS), in 24 % of the counties in the U.S. where data are available, at least 10 % of water samples have arsenic concentration exceeding 10 parts per billion (ppb), the World Health Organization's (WHO) arsenic limit in drinking water (Focazio et al. 1999). Approximately 6 % of the U.S. small public water supply systems had water arsenic concentrations exceeding 10 ppb and 1 % of such systems had concentrations exceeding 50 ppb, the current U.S.

maximum limit of arsenic in drinking water (Focazio et al. 1999). In some parts of the world, arsenic occurs naturally in groundwater. For example, a recent survey indicates that 80 % of total area, and 40 million people, are at risk of arsenic poisoning in Bangladesh, where more than 7,000 patients are seriously affected by arsenic in drinking water (Karim 2000).

Arsenic is a naturally occurring element in rocks, soils and the waters in contact with them. Before 1968, inorganic forms of arsenic were used extensively in agriculture as insecticides and herbicides. Frequent application at high rates of these chemicals caused significant arsenic accumulation in orchard soils. Inorganic forms of arsenic have since been replaced with organic forms because of their reduced phytotoxicity and overall environmental burden. However, excessive additions of any arsenic compounds can cause pollution of nearby ground and surface waters (Duble et al. 1978). Arsenic concentrations as high as 500 ppm have been reported in soils having a history of arsenic pesticide or herbicide applications. These types of arsenic-contaminated soils can also become a source of contamination in surface water, ground water and drinking water. Fugitive environmental arsenic is still produced today as a result of various mining, industrial and manufacturing operations (Azcue and Nriague 1994).

High levels of soil arsenic have been detected throughout Spring Valley and often require extensive soil sampling and expensive removal for remediation. Arsenic in many places in Spring Valley could be related to ordnance, chemical experiments and production in the AUES laboratories. High soil arsenic could also be the result of outdoor “persistency” testing or the result of air deposition from outdoor tests of weapons

and candles that created arsenic laden clouds that drifted across the landscape and were deposited on the surface by wind and other weather conditions. An innovative, non-contact method for characterizing levels of arsenic contamination through the reflectance characteristics of surface vegetation, such as lawn grasses, would be a tremendously useful and cost-effective alternative to traditional soil sampling here and at many arsenic contaminated areas around the world.

2.4 Arsenic Phytoremediation

Phytoremediation is the process of removing contaminants from the environment using plants. In general, when plants uptake water and nutrients from the soil, they sometimes uptake hazardous chemicals or metals also where they are stored in the plant tissues, reduced to less dangerous forms or changed into gases and released into the air. Plants can also aid cleanup by sorbing hazardous materials to their roots or reducing chemicals to less dangerous forms as a result of microbial or bacterial action from the plant roots (USEPA 2001). Phytoremediation is most often used to remove contaminants from soils, but has also found applications in air and for groundwater (USEPA 2001; Boyajian and Devedjian 1997; Peart 1993). Phytoremediation is an attractive alternative to conventional soil removal and replacement techniques because it is a natural process that does not disturb the landscape, it does not potentially expose workers or citizens to dangerous substances and it is generally much more cost-efficient (USEPA 2001).

In 2001, the Chinese Brake Fern (*Pteris vittata*) was shown to hyperaccumulate inorganic arsenic in soils (Ma et al. 2001). Although there are other plants that are

known to hyperaccumulate metals, the Chinese Brake is the first embryophyte (land plant) to hyperaccumulate arsenic and store it in the leaf cells and with its relatively large biomass, it instantly became a model for phytoremediation of one of the world's major soil contaminants (Bondada and Ma 2003). Since the original discovery of the Chinese Brake Fern, several other ferns from the *Pteris* family, have also been found to be hyperaccumulators of inorganic arsenic. The Cretan Brake Fern (*Pteris cretica*) and the Spider Brake Fern (*Pteris multifida*) appear to be efficient arsenic hyperaccumulators (Wang et al. 2006). Researchers have recently reported several discoveries of new arsenic hyperaccumulating species of *Pteris* taxa. Srivastava et al. (2006) have shown *Pteris biaurita, Pteris quadriaurita* and *Pteris ryukyuensis* to be arsenic hyperaccumulators. Wang et al. (2006) reported *Pteris fauriei, Pteris aspericaulis* and *Pteris oshimensis* from southern China to be similar arsenic hyperaccumulators. However, Wang et al. (2006) also reported that *Pteris ensiformis, Pteris semipinnata* and *Pteris setuloso-costulata* showed no evidence of arsenic hyperaccumulation.

The *Pteris vittata* fern has been shown to accumulate up to 22,630 ppm arsenic in the frond dry weight. Furthermore, the bioconcentration factor, defined as the ratio of shoot arsenic concentration to soil arsenic concentration, was greater than ten although phytotoxic effects were observed once the concentration exceeded approximately 10,000 ppm dry weight (Wang et al. 2002; Tu and Ma 2002). The arsenic hyperaccumulating *Pteris* ferns possesses three key features that are typical of metal/metalloid hyperaccumulating plants; an efficient root uptake, an efficient root to shoot translocation, and a greatly enhanced tolerance to metal/metalloids inside the plant tissues

(Wang et al. 2002; Ma et al. 2001). During the summers of 2004, 2005 and 2006 *Pteri*s ferns were utilized in arsenic phytoremediation pilots in Spring Valley.

2.4.1 The Mechanisms of Arsenic Uptake

Arsenic is a not an essential nutrient for plants, and in its inorganic form is generally highly phytotoxic. In aerobic soils, arsenate is the predominant arsenic form and in anaerobic conditions arsenite dominates (Smith et al. 1998). Arsenate acts as a phosphate analog and can disrupt phosphate metabolism, whereas arsenite reacts with sulfhydryl groups of enzymes and tissue proteins, eventually leading to inhibition of cellular function and death (Meharg and Hartley-Whitaker 2002). Most plant species do not transfer significant levels of arsenic from the soil to the above ground biomass of the plant. This is likely due to generally low bioavailability of arsenic in typical soils and the phytotoxic effects of arsenic in plant tissues (Wang et al. 2002). The speciation of inorganic arsenic in the soil is critical to its availability to plants. Arsenic in soils can exist as the corresponding salts of arsenite [As(III)], arsenate [As(V)], monomethyl arsenic acid (MMA) and dimethyl arsenic acid (DMA). Different arsenic species have different solubilities and mobilities, and thus differing bioavailability to plants.

Several researchers have demonstrated the translocation of arsenic from the soil to the plant and the distribution of arsenic within the plant. Singh and Ma (2006) showed in controlled growth experiments that arsenic distribution was greatest in the fronds, followed by the rhizomes and roots in *Pteris vittata* and *Pteris ensiformis*. Wang et al.

(2006) showed similar results for several *Pteris* species from China. Zhang et al. (2002) showed the same general distribution in both field and in greenhouse conditions.

When growing in soils with moderate or high arsenic concentrations, some plants, such as tomatoes, accumulate arsenic in the root system, probably as part of an exclusion strategy (Carbonell-Barrachina et al. 1997; Dahmani-Muller et al. 2000). When high arsenic concentrations are present in shoots but not in roots an efficient root-to-shoot transport system must be present and is likely an important component of the plant's overall arsenic tolerance. Figure 6 shows the distribution of arsenic with the different parts of *Pteris vittata* fern after growth in arsenic-amended soils in both field (~150 ppm) and greenhouse (~100 ppm) applications. It has been suggested that the translocation of arsenic from the roots to the mature leaves may be part of a detoxification process to remove sequestered arsenic from the plant as the old leaves senesce and fall away (Zhang et al. 2002).

There are several other important factors relating to arsenic uptake in the *Pteris* taxa. The oxidation state of arsenic appears to be very important and even suggest that the *Pteris* ferns converts As(V) arsenate to As(III) arsenite during the translocation from roots to fronds. Singh and Ma (2006) showed that, after one day of exposure, As(V) was the dominant form of arsenic in all tissues of the *Pteris vittata*. However, after five days or more, As(III) was the dominant form in the fronds and the rhizomes even through As(V) was the only form of arsenic supplied in the soil amendments. Since arsenite is generally much more toxic to plants than arsenate, this transformation is not well understood. See Figure 6.

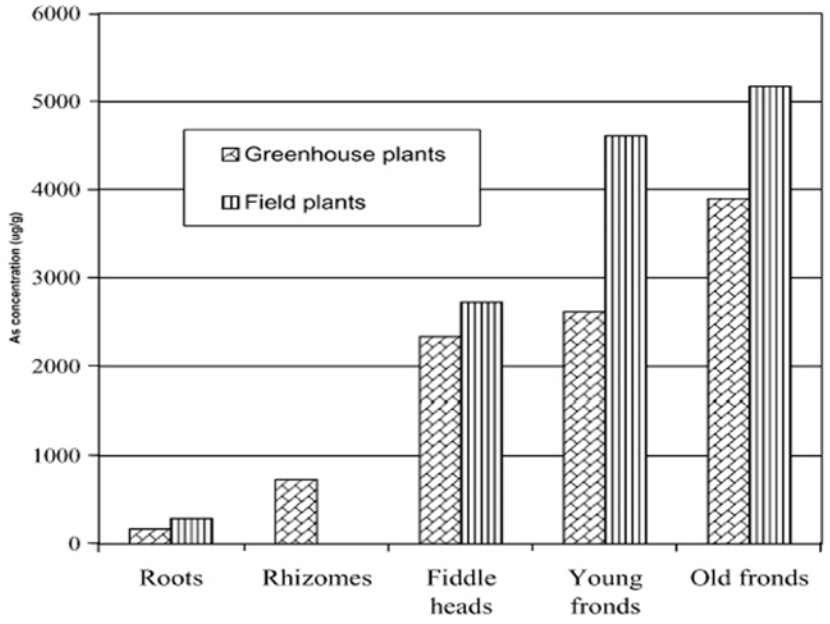

6a

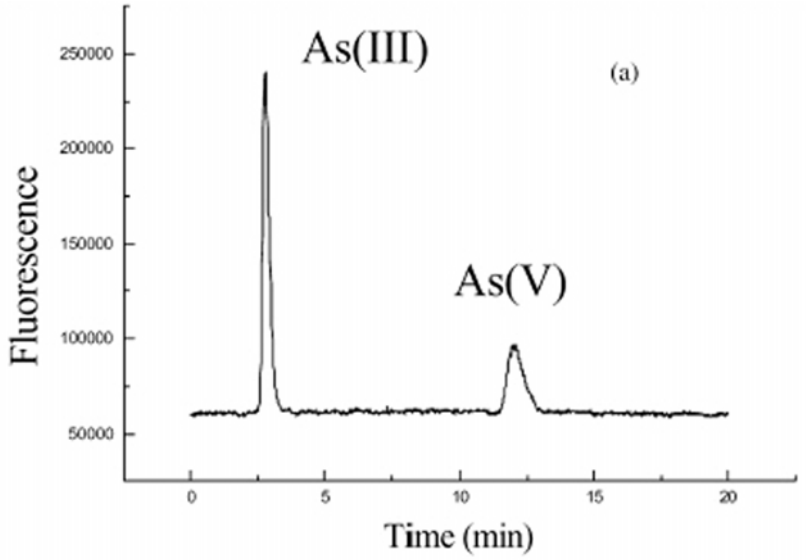

6b

Figure 6a. The Distribution of Arsenic in *Pteris vittata*. The distribution of arsenic with the different parts of *Pteris vittata* fern after growth in arsenic soils in both field and greenhouse environments. Figure 6b. The chromatograms of a *Pteris vittata* frond showing both As(III) and As(V) when only arsenate was available in the soil showing that the *Pteris* ferns, to some extent, reduces arsenate to arsenite internally. From Zhang et al. 2002, pages 171 and 175.

Singh and Ma (2006) showed that the presence of multiple other heavy metals in the soil matrix, can have negative effects on plant growth and arsenic uptake in *Pteris vittata*. They also showed that other heavy metals in the soil tend to decrease arsenic bioavailability and decreases overall arsenic uptake.

The previous chapter has presented some important background information for the current hazardous waste remediation in Spring Valley. The WWI research and development of chemical warfare agents and the role of inorganic arsenic as a base compound for many of these agents along with the innovative use of phytoremediation, establishes the landscape context for the application of remote sensing technologies for providing information to assist in the remediation process. The next chapter will present a review of the relevant scientific literature on the remote sensing technologies applied in this research.

3. Literature Review

This chapter provides a review of the relevant scientific literature on the science of remote sensing and the emerging developments in remote sensing technology as related to the application of the basic remote sensing systems that will collect the primary data for each of the experiments in Spring Valley; aerial photographic interpretation, reflectance spectroscopy and imaging spectroscopy. A core, overall theme in the research is to ascertain the value of remote sensing as an alternative to more traditional methods in collecting the information necessary to remediate hazardous waste problems at locations such as those in Spring Valley.

3.1 Photographic Interpretation and Historical Aerial Photography

The first known aerial photographs were taken in 1858 on board a tethered balloon by a Frenchman named Gaspard Felix Tournachon. Tournachon, who later became known by the nickname "Nadar", successfully photographed the landscape around Paris, France. Shortly thereafter, the aerial perspective proved to be so valuable that General George McClellan used tethered balloons to photograph and study enemy positions in the U.S. Civil War (Babbington-Smith 1957; Simonett et al. 1983). Until the early 1900s, balloons, kites and even pigeons were used as platforms to hoist cameras above the land to photograph the surface below (Colwell 1997). These platforms were,

however, relatively stationary, limited in altitude and range and vulnerable (Slonecker et al. 2002).

After the advent of the airplane in 1903, the value of aircraft-based photography became readily apparent to many, including Wilbur Wright who took the first recorded photographs from an airplane in 1909. The airplane soon became the primary platform for the acquisition of overhead photography. Regular use of cameras from airplanes continued until WWI, when the formal development of reconnaissance systems and photographic interpretation science became so accurate that they completely changed the tactics of battlefield warfare (Colwell 1997). Between WWI and WWII, the continuing development of both aircraft and photographic technology made the use of aerial photographs commonplace for military and intelligence applications, domestic mapping, planning and natural resource management.

During WWII, the role of aerial photography and interpretation was so critical that it prompted German General Oberst von Fritsch to predict in 1938 that the nation with the best photographic interpretation will win the next war (Colwell 1997). It is estimated that between 60 and 90 % of all Allied intelligence was derived from photographic interpretation of enemy-held areas (Colwell 1997).

It was also during this period that the scientific discipline and training in aerial photography and interpretation began to become established. Formal lines of study for basic photographic interpretation, photogrammetry and cartography were developed for military, and, after the war, for civil purposes such as geology, agriculture and forestry.

Universities developed courses on photographic interpretation and photogrammetry and adapted the technology to an ever increasing base of applications.

The art and science of photographic interpretation, along with photogrammetry and cartography, continued to develop throughout the post WW II period and to expand into new areas such as non-photographic imaging sensors like radar and thermal infrared (IR) imaging. In 1961, the first photographs were taken aboard an orbital platform and satellite remote sensing was born. With the application of computer graphics and database management software, the revolution in GIS technology began in the 1980s, and aerial photographs became a regular part of the typical GIS database development process.

As new systems, sensors and technologies became available, it became increasingly clear that the routine use of aerial photographs for a number of purposes had created a tremendous archive of historical information that could not be duplicated by the most sophisticated of current technologies. Applications of historical imagery began to develop and continue to this day based solely on the ability of the aerial photographs to freeze, record and document a moment in time (Slonecker et al. 2002).

In the 1970s, environmental awareness of the hazardous waste problems of the U.S. came to the forefront of public conscientiousness and led to the passage of the CERCLA (Superfund) in 1980. The main goal of the Superfund program was to clean up abandoned hazardous waste sites, and just as in Spring Valley, the archive of historical aerial photographs became an invaluable source of information relating to landscape activities of the past. Historical aerial photographic analysis of abandoned hazardous

waste sites became, and still is, a routine part of the CERCLA remedial investigation process. Titus (1982) documented the critical use of historical photography in the assessment of hazardous waste activity relating to the groundwater contamination from the textile industries in Woburn, Massachusetts. The use of historical aerial photographs and maps in the study of hazardous waste sites was further developed by a number of researchers including Erb et al. (1981), Garofalo and Wobber (1974), Lyon (1982) and Lyon (1987) where a temporal chronology of landscape events was reconstructed from the analysis of aerial photographs and maps. Nelson et al. (1983), Philipson et al. (1988), Barnaba et al. (1989) and Barnaba et al. (1991) used historical and current aerial and satellite photographs to perform area-wide inventories of abandoned waste sites as well as to develop a methodology for prioritizing sites for remedial action.

Interpretation of historical and current aerial photographs has also proved to be extremely valuable to the plant sciences. Even though color and color infrared aerial imagery was impractical to implement on a large scale until the 1950s, early black and white aerial photographs were used in a number of vegetation-related applications. Forestry surveys with aerial photographs date back to 1919 using WWI aircraft and aerial photographs soon became a regular tool in many forestry applications (Parry 1973; Colwell 1997). Interpretation keys based on texture, pattern, branching, height, crown cover, topographic location and other spatial observables were developed for the identification and inventory of forest products. Zsilinsky (1963), Hegg (1967) and Sayn-Wittgenstein (1978) all developed practical methodologies for the identification of tree species.

Similarly, aerial photo applications in agriculture developed rapidly. Thaman (1974) listed 71 specific applications of aerial photography for agriculture including crop analysis, crop maturity, livestock population, disease infestations, soil moisture and fertility and many others. Crop identification with aerial photographs was the subject of intense research and development around 1960 (Goodman 1959, 1964; Colwell 1960; Erb 1968; Wood 1968). Because of the strategic importance of estimating agricultural production globally, crop identification and analysis has continued through the present with complementary research variations with color and color infrared imagery, satellite imagery and combinations of large- and small-scale aerial photographs.

Crop identification remained a primary research topic in agricultural aerial photographic interpretation through the 1980s. Researchers tested airphoto identification capabilities on different types of crops in different parts of the world, comparing the use of panchromatic versus color/color infrared film, and attempting to identify the optimum photo scale for aerial collection that maximized areal extent while preserving the necessary spatial resolution for specific crop identification (Ryerson and Curran 1997).

In terms of Spring Valley research, the most important aspect of the use of analog aerial imagery lies in the techniques that were developed to identify biotic and abiotic stress in vegetation. Pests, diseases, pollution, weather, environmental conditions and other factors that limit yields, and have major economic and human health consequences often affect productivity of forests and agricultural systems. The ability to detect vegetation stress was one of the key aspects in the overall development of the remote sensing profession.

Murtha (1997) traces the earliest known reference for vegetation stress detection to Wood (1910) who described practical infrared photography "…by invisible rays". Taubenhaus et al. (1929) identified cotton root rot from aerial photographs. Bawden (1933) reported that diseased parts of the leaf were clearly evident in infrared photography while negligible to the eye. In 1935, Babel developed the first practical understanding of infrared reflectance in assessing vegetation health (Murtha 1997). Van Atta (1936) and Ives (1939) were successful at utilizing infrared imagery to assess vegetation condition.

However, it was not until after WWII that the potential for the use of infrared imagery in vegetation started to be realized. Three key papers in the late 1940s, Clark (1946) and Spurr (1948, 1949), established the operational parameters for the use of panchromatic and infrared film, filters and procedures (Murtha 1997). Research on photographic interpretation of infrared film and vegetation continued through the 1950s with key works from Keegan and O'Neill (1951), Keegan et al. (1955) and a seminal paper from Colwell (1956) in identifying crop diseases from aerial photography.

As aerial photographic research was progressing, parallel scientific investigations in the laboratory of the more fundamental relationships between vegetation and energy, were starting to yield new, detailed understanding of specific wavelengths of the EMS and how those wavelengths of energy interacted with leaf structure and pigmentation in the process of photosynthesis and this became the basis of future spectral analysis applications of vegetation stress, such as the current application in Spring Valley.

3.2 Reflectance Spectroscopy and the Analysis of Vegetation

During the same period that photographic interpretation and remote sensing research was discovering and developing the value of imagery, and especially near infrared imagery, to monitor and evaluate vegetation condition and stress, other scientists were utilizing laboratory techniques to gain a better understanding of the component wavelengths of the solar reflected part of the EMS and how energy interacts with vegetation, pigments and leaf structure. Laboratory spectroscopic methods generally employ instruments and methods that record reflected energy in very specific wavelengths. These methods do not produce imagery, but instead produce spectra, a graphical plot of the record of energy interactions at specific wavelengths. Figure 7 shows a basic spectra of healthy green vegetation. This type of laboratory spectroscopic analysis of vegetation is directly related to the second remote sensing research issue in Spring Valley; the ability to detect and quantify, with high-resolution spectral reflectance data, the concentration of arsenic within *Pteris* ferns in the phytoremediation process.

The use of laboratory spectral reflectance methods to gain an understanding of photosynthesis and related vegetative processes is a field of scientific study that has been ongoing for decades. Laboratory instruments called spectrometers, spectrophotometers, spectrographs or spectroradiometers are all different names for instruments that essentially use some type of prism to separate light into its component parts and measure the reflectance and absorption of those component parts from a target surface. Early instruments separated light into the basic colors of the spectrum. Modern instruments separate light into individual nanometers of reflectance energy.

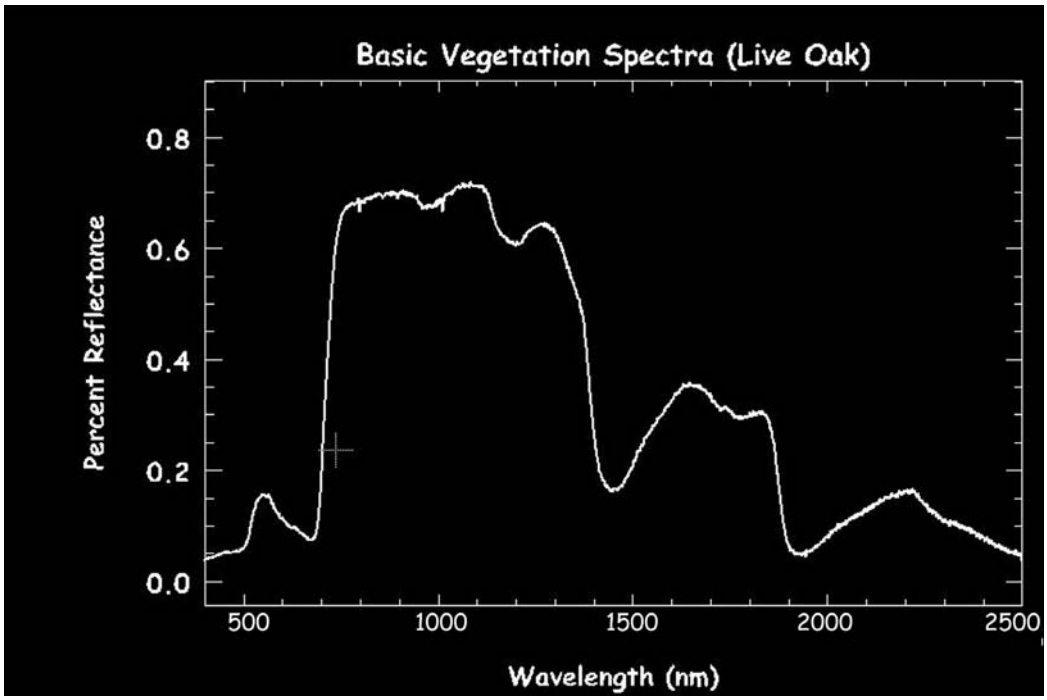

Figure 7. Basic Vegetation Spectra. The basic solar reflected energy spectra of all green vegetation are characterized by reflectance peaks around 550 nm and 780 nm. The absorption well at 680 nm represents the process of photosynthesis. From ENVI (2004).

Using a hand held spectrograph, Rood (1879) analyzed typical vegetation and reported a low reflectance in the blue, a high reflectance in the green, a low reflectance in the red and a rapid rise in reflectance in the infrared. Willstatter and Stoll (1913, 1918) investigated the interaction of light with the typical structure of the leaf using selective spectral absorption (Murtha 1997). Schull (1929) studied and measured the reflectance of various leaves using a prism spectrophotometer to attempt to better explain leaf-energy interactions that occur in photosynthesis. Measuring between 430 and 700 nm, at roughly 20 nm intervals, he was able to determine the basic chlorophyll absorption pattern of most green vegetation and even reported the common chlorophyll absorption

well at 680 nm, increased reflectance in mildew-stressed lilac leaves and a red shift in the reflectance maximum that corresponded to the development of anthocyanins in the leaf. McNicholas (1931), through laboratory methods, defined the spectral characteristics of carotin and xanthophyll, and the absorption changes that occurred during oxidation.

The spectral characteristics of vegetation have enjoyed a wide range of interest through the years for military, agricultural and environmental applications. Key papers by Gates et al. (1965) and Guyot et al. (1992) summarize the diverse applications of laboratory spectral research for vegetation studies.

All green vegetation shows a similar pattern of spectral reflectance in the visible and near infrared regions. Figure 8 shows the library spectra of several different types of vegetation, all showing similar chlorophyll-based reflectance patterns. The highlighted area represents the area of classic bimodal reflectance that is typical of healthy vegetation. The bimodal reflectance pattern is caused by the chlorophyll absorption of blue and red wavelengths, at about 450 and 680 nm respectively, and by the reflectance of chlorophyll in the green wavelengths causing the peak at around 550 nm. The second larger spectral peak around 780 nm is caused by the internal structure of leaf tissue that reflects significant amounts of energy in the near infrared. This internal mesophyll tissue generally consists of irregularly shaped cells separated by interconnected openings. Infrared radiation is strongly scattered by this structure, which combined with a general decrease in pigment absorption at the edge of the visible portion of the spectrum, causes a significant increase in reflected energy at the edge of the infrared part of the spectrum (Campbell 1987).

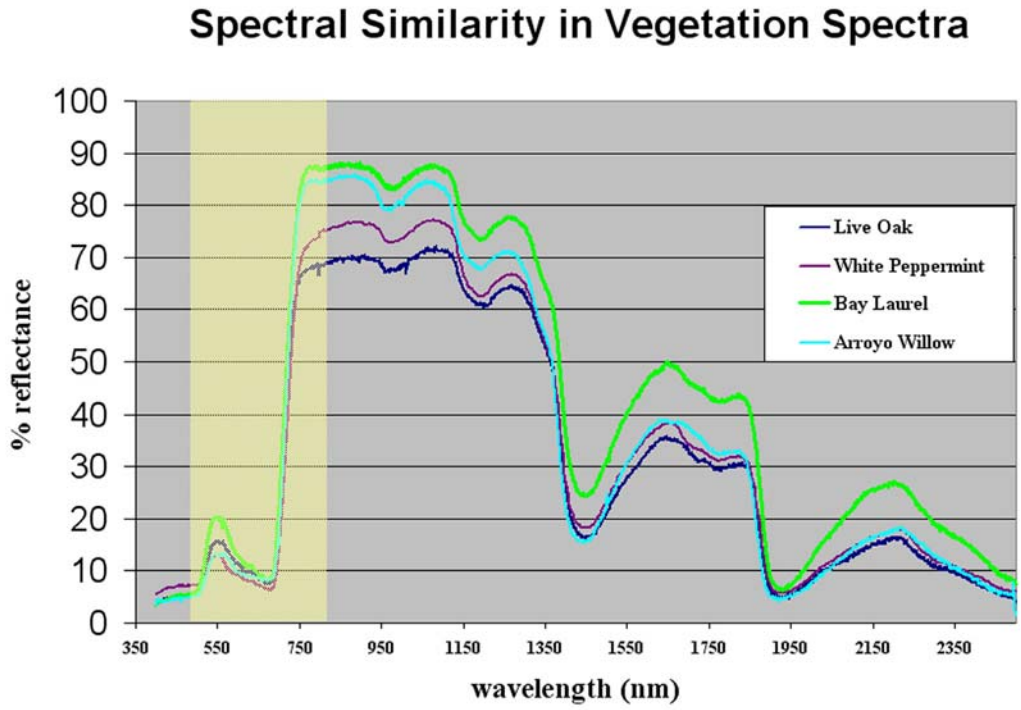

Figure 8. Spectral Similarity in Vegetation. Spectra of several different vegetation species from a standard spectral library (ENVI 2004). Note the same pattern of bimodal reflectance peaks in the green near 550 nm and in the near-infrared around 780 nm.

Gates et al. (1965) performed some of the initial research into the spectral properties of specific vegetation. Using a laboratory spectrophotometer, they measured and reported the reflectance, transmittance and absorption spectra for several different species including magnolias, red rose, cottonwood, oak and several desert succulents. They identified a pattern of temporal change in spectra, especially in the near infrared region, as a result of growing season and chlorophyll content.

3.2.1 The Red Edge

One of the fundamental concepts that has been developed in the spectral analysis of vegetation has been the "Red Edge" of vegetation reflectance. An area usually centered around the 720 nm area and represented by the typical sharp rise in reflectance in the 680–760 nm range of the classic vegetation spectral signature. The location, size, shape and shifts in this Red Edge form one of the central concepts in spectral monitoring of vegetation condition. See Figure 9. Vegetation undergoing stress from exposure to fugitive arsenic in the soil, such as in Spring Valley, is very likely to exhibit symptoms of that stress in the Red Edge region.

Although the general concept of the Red Edge is easily understood as the area of the sharp rise in reflectance, generally between 680 and 760 nm, a variety of definitions and quantitative methods for computing the Red Edge are found in the literature. Ray et al. (1993) define the Red Edge as the sharp transition between absorption by chlorophyll in the visible wavelengths and the strong scattering in the near infrared from the cellular structure of leaves. The Red Edge (λ_{re}) is defined by Horler et al. (1983) as the wavelength of maximum $\Delta R/\Delta\lambda$, where R is reflectance and λ, is the specific wavelength. Guyot et al. (1992) defines the Red Edge as an inflection in the sharp rise in reflectance between 670 and 760 nm.

Horler et al. (1983) studied the feasibility of utilizing a Red Edge measurement as an indication of plant chlorophyll status. Using derivative reflectance spectroscopy in the laboratory, plant chlorophyll status and Red Edge measurements were made of single

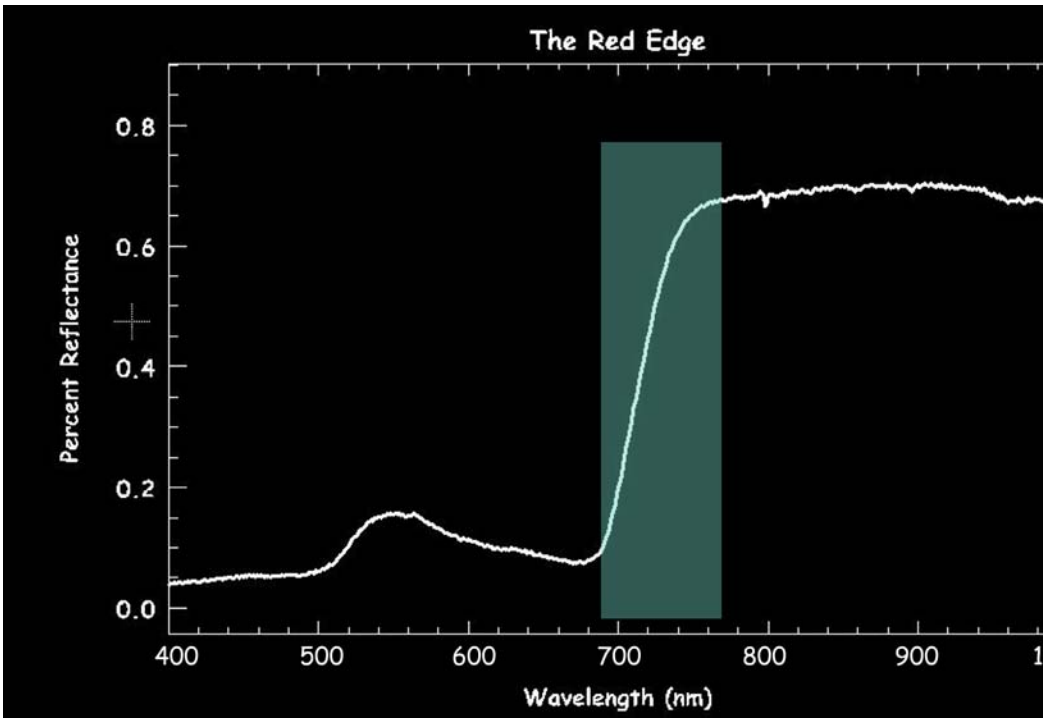

Figure 9. The Red Edge. An important region of vegetation spectra known as the Red Edge. Much research has focused on measuring shifts in this region corresponding to stress or enhancement of chlorophyll. Basic spectra from ENVI (2004).

leaves of several different species. By using spectroscopic and laboratory methods to measure the chlorophyll content of the same leaf samples, direct evidence of the Red Edge - chlorophyll correlation was obtained. Important was the fact that the correlation was strongest when leaf chlorophyll was described on a leaf-area basis and somewhat weaker on a weight or thickness basis. Ray et al. (1993) discovered significant differences in the size and shape of the Red Edge in different types of arid vegetation and found that for a common yellow grass species, there was no chlorophyll “bump” and no detectable Red Edge.

Another critical analytical feature of spectral analysis of vegetation is the shift in absorption and reflectance features that occur as a result of chemical and nutrient exposures. A general relationship between increases in chlorophyll concentration and a "red shift" towards longer wavelengths has been established by several researchers. Gates et al. (1965) showed the basic relationship between the increased chlorophyll and plant health and the shift of the Red Edge towards longer wavelengths. Guyot et al. (1992) similarly showed that the Red Edge inflection point shifts to longer red wavelengths as chlorophyll concentrations increase. This general correlation between chlorophyll content and red shift was confirmed by Horler et al. (1983) and Baret et al. (1987) for different crop species.

More important to the Spring Valley research however, is the "blue shift" of vegetation spectra that occurs when vegetation has undergone stress from some mineral or chemical agent. Collins et al. (1977) showed a basic blue shift in conifers affected by metal sulphide in the 700–780 nm region. Horler et al. (1980) found similar blue shifts in tree species subjected to heavy metal concentration in the soil. Similar blue shift results have been reported by Schwaller and Tkach (1985) and Milton et al. (1989, 1991). Rock et al. (1988) demonstrated a 5 nm blue shift in spruce and fir species in Vermont and Germany as a result of stress caused by airborne acid deposition.

Horler et al. (1980) studied the effects of heavy metals on the reflectance spectra of plants. Utilizing both natural vegetation growing in known areas of metal concentrations, and specific greenhouse experiments, they established relationships of

metal stress to total chlorophyll, chlorophyll a/b ratios, and reduced reflectance at specific wavelengths. Controlled experiments with pea plants and other species showed that the general effect of exposure to cadmium (Cd), copper (Cu), lead (Pb) and zinc (Zn) was growth inhibition. Also the pea plants showed changes in the leaf chlorophyll a/b ratios for exposure to Cd and Cu but showed no changes for Pb and Zn. Metal-treated plants in both controlled and natural environments showed a decrease in reflectance at 850, 1,650 and 2,200 nm and an increase at 660 nm. Metal concentration in the soil has strong negative correlations to reflectance at 1,650 and 2,200 nm and strong positive correlations at 660 nm. In general, the ability to measure stress effects from heavy metals is dependent on species, the phase of the growth cycle, and environment. The pattern of vegetation stress from heavy metals and the band locations at which their effects are observed are likely to be similar to those in the vegetation on Spring Valley.

3.2.2 Vegetation Indices

The use of Vegetation Indices (VIs) has been a fundamental part of the remote sensing analysis of vegetation for decades. VIs are mathematical manipulations of digital number values of two or more bands of data. VIs typically stretch or enhance a particular part of the reflected EMS known to relate to specific vegetation qualities such as chlorophyll content, leaf moisture, pigment ratios and stress level. The search for stressed or unusual growth patterns in cover vegetation, such as the potential arsenic stress patterns that might be seen in Spring Valley, would likely be enhanced by the use of one or more VIs that have been reported in the scientific literature.

The most widely known and used VI is the Normalized Difference Vegetation Index (NDVI), which is calculated by the following general band formula:

$$NDVI = \frac{NIR - Red}{NIR + Red}$$

The NDVI was first proposed by Pearson and Miller (1972) and has been widely utilized as a general measure of vegetation condition and although the NDVI has been the most widely used vegetation index, it has clear limitations. NDVI saturates in areas of multi-layered canopy and shows non-linear relationships with critical vegetation parameters such as Leaf Area Index (LAI). As a result, there has been substantial effort to develop new indices that improve on the shortcomings of NDVI.

For example, the Enhanced Vegetation Index (EVI) (Running et al. 1994) was developed as an improvement to the NDVI for the Moderate Resolution Imaging Spectrometer (MODIS) instrument. While the EVI is calculated similarly to NDVI, it corrects for some distortions in the reflected energy caused by the particles in the air as well as the ground reflectance underneath the vegetation.

Examples of other VIs that have been used with spectroscopic data are listed in Table 1. These, along with several others, will be utilized in the examination of HSI of Spring Valley. Vegetation indices have often been developed for specific purposes and optimized to assess a specific condition or process. Also, the emergence and increasing

Table 1.
Examples of different Vegetation Indices (VI) derived from the literature.

Index Name	Acronym	General Formula	Source
Ratio Vegetation Index	RVI	NIR/RED	Jordon 1969
Transformed Vegetation Index	TVI	SQRT((B/B+G+R) + 0.5)	Rouse et al. 1973
Red Index	RI	RED/(BLUE+GREEN+RED)	Kleman & Fagerlund 1981
Green Index	GI	GREEN/(BLUE+GREEN+RED)	Kleman & Fagerlund 1981
Blue Index	BI	BLUE/(BLUE+GREEN+RED)	Kleman & Fagerlund 1981
Perpendicular Vegetation Index	PVI	-.8736(RED) + .4866(NIR)	Richardson et al. 1983
NIR-Green	NG	NIR/GREEN	Demetrides-Shah & Court 1987
Green-Red	GR	GREEN/RED	Demetrides-Shah & Court 1987
Soil Adjusted Vegetation Index	SAVI	$\frac{(1+L)(R_{800} - R_{670})}{(R_{800} + R_{670} + L)}$	Huete 1988
Green(NIR/Red)	GNR	GREEN(NIR/RED)	Vygodskaya et al. 1989
Red(NIR/Green)	RNG	RED(NIR/GREEN)	Vygodskaya et al. 1989
Normalized NIR Green Index	NNGI	NIR-GREEN/NIR+GREEN	Vygodskaya et al. 1989
RED/(Green+Red+NIR)	RGRN	RED/(GREEN+RED+NIR)	Bracher 1991
Enhanced Vegetation Index	EVI	G * NIR –RED/ NIR+ACred – ACBlue + L	Running et al. 1994
Renormalized Difference Vegetation Index	RDVI	$(R_{800} - R_{670}) / (R_{800} + R_{670})^{1/2}$	Rougean & Breon 1995
Modified Simple Ratio	MSR	$(R_{800} / R_{670} - 1) / (R_{800} / R_{670} + 1)^{1/2}$	Chen 1996
Yellowness Index	YI	$\Delta^2 R / \Delta^2 \lambda$	Adams et al. 1999
Reduced Simple Ratio	RSR	$SR\ (1 - \frac{(SWIR - SWIR_{min})}{(SWIR_{max} - SWIR_{min})}$	Brown et al. 2000

availability of hyperspectral data and imagery has resulted in a new class of VIs, known as “narrow-band” indices that capitalize on the increased spectral resolution of hyperspectral data.

For example, Chappelle et al. (1992) developed the Ratio Analysis of Reflectance Spectra (RARS) index to estimate the concentrations of chlorophyll a, chlorophyll b and carotenoids in soybean leaves. Gamon et al. (1992) developed the Photochemical Reflectance Index (PRI) to estimate physiological parameters of sunflowers undergoing nitrogen stress. A Reduced Simple Ratio (RSR) index was developed specifically to estimate LAI for Jack Pine and Blue Spruce canopies (Brown et al. 2000).
The Modified Chlorophyll Absorption Ratio Index (MCARI) (Daughtry et al. 2000) and the Triangular Vegetation Index (TVI) (Broge and Leblanc 2000) were developed as very precise measures of chlorophyll concentration and absorption and depend on very specific narrow wavelengths. Haboudane et al. (2004) successfully modified the MCARI and TVI indices to be less sensitive to chlorophyll effects and more sensitive to LAI. Penuelas et al. (1994) developed several narrow-band VIs, such as the Edge Green First derivative Normalized difference (EGFN) index which correlates with nitrogen content and was used successfully by Reusen et al. (2003) to identify stress from zinc deposition in pine trees using Compact Airborne Spectrographic Imager (CASI) data.

3.2.3 Spectral Derivatives

One of the key concepts in the analysis of spectral phenomena is the ability to extract hidden absorption and reflectance features based on the use of derivative functions of the polynomial spectral curve. In situations like Spring Valley where the expression of vegetation stress or arsenic uptake may be only a very subtle spectral feature, derivatives can play a critical role in isolating and identifying those types of subtle, but critical features.

The derivative is a basic concept from calculus that is defined as the limiting value of the rate of change of a process. At any point on a curve, the y value is changing with respect to x and the derivative is often defined, in its simplest terms as the change in y over the change in x, or $\Delta y/\Delta x$. In spectroscopy, the derivative is often defined as $\Delta R/\Delta\lambda$, where R is the reflectance and λ is a specific wavelength. The $\Delta R/\Delta\lambda$ function is often called the first derivative and subsequent or higher derivatives are created from simply repeating the process. Figure 10 shows a graphic example of the first four derivative curves that are derived from a Gaussian band shape.

Many researchers have utilized derivatives to bring out critical, subtle features in spectral analyses. Martin et al. (1998) used the first difference spectra of forest canopies to identify species based on the specific patterns of nitrogen and lignin concentrations in the leaf. Chen et al. (1992) used derivative reflectance spectroscopy to estimate suspended sediment concentrations and found that the derivative relationship was much less affected by environmental/atmospheric variables than the direct spectra record. Demetriades-Shah et al. (1990) showed that derivative spectral indices were superior to

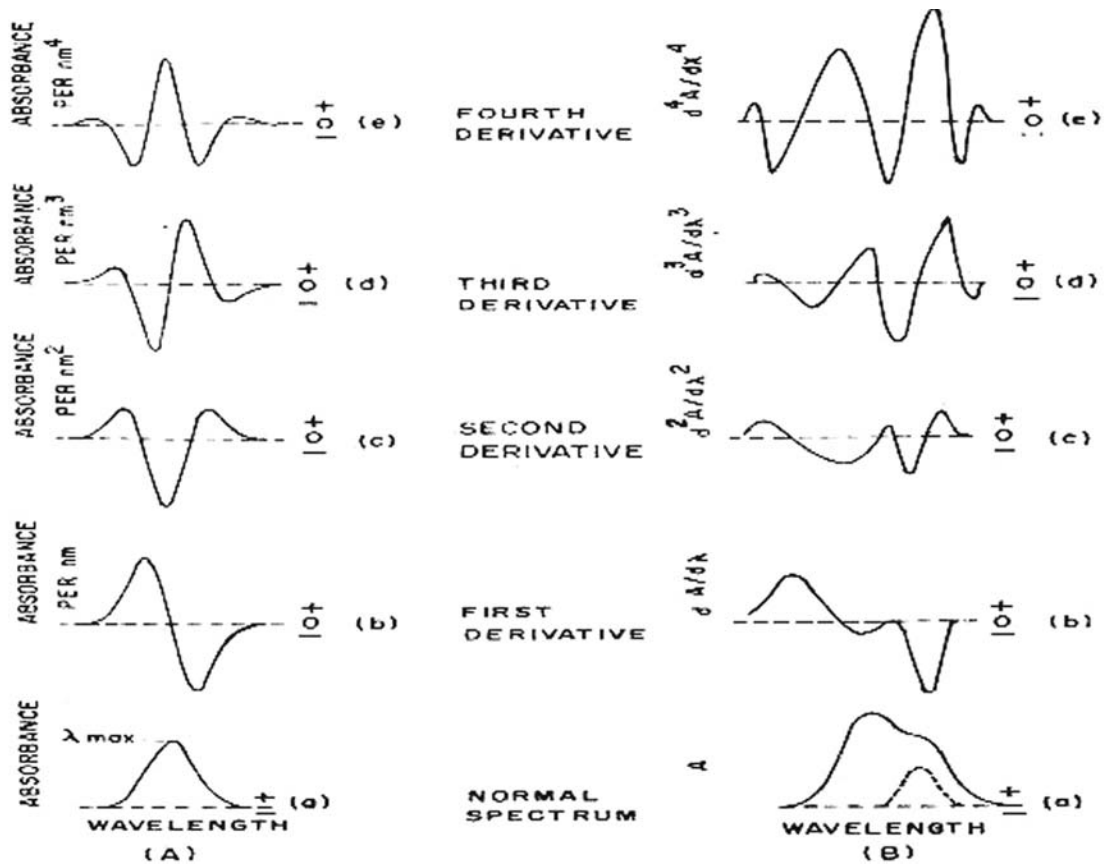

Figure 10. Spectral Derivatives. A normal Gaussian curve and a band pair with the first four derivatives of each. Different levels of derivatives bring out different and subtle characteristics of the spectral curve that may not be readily apparent in the original spectra. From , and Ram (1985, page 318).

broad-band measures, such as NDVI, for monitoring chlorosis in vegetation. Tsai and Philpot (1991) showed that derivatives could be used to minimize the effects of atmospheric conditions.

Derivatives have been used extensively in analytical chemistry to reduce the effects of background noise and resolve overlapping spectra. The first derivative has

often been used to isolate the specific Red Edge inflection point in vegetation spectra (Dockray 1981; Horler, et al. 1983). Wessman et al. (1988) and Yoder and Pettigrew-Crosby (1995) used the first derivative of hyperspectral reflectance data to investigate canopy chemistry such as nitrogen and lignin.

Derivatives of a second order or higher can be valuable for analysis of hyperspectral remote sensing data because they are relatively insensitive to variations in illumination, sun angle, cloud cover and topographic shadow (Tsai and Philpot 1998). Kosmas et al. (1984) used the second derivative of reflectance spectra for the analysis of iron oxide minerals. Adams et al. (1999) developed a yellowness index as a measure of chlorosis, which approximated the second derivative and correlated well with NDVI measurements from Advanced Visible InfraRed Imaging System (AVIRIS) data. Chen et al. (1993) developed a derivative-based green vegetation index (GVI) that showed a greatly enhanced ability to estimate green cover levels and minimize the effect of background noise.

All spectra are essentially sets of x, y pairs that represent energy interactions against some scale of magnitude. For imaging spectroscopy applications, the x variable is wavelength and the y variable is radiance or percent reflectance. From Dixit and Ram (1985), the first order derivative is defined as the change in y over the change in x, or simply, $\Delta y/\Delta x$, and can be computed for spectral data with the formula:

$$\Delta y/\Delta x = (y_{i+1} - y_i) / (x_{i+1} - x_i)$$

that determines the complete first derivative when applied to the all pairs in the spectra. The same formula, when applied to the results of the first derivative, results in the second derivative and so on.

Analysis of derivative data can be approached in much the same way as direct spectral measurements. Values for specific band locations, such as R_{680} can be calculated for the first-, second- and nth-order derivatives. Also, spectral features of the derivative graph, such as the wavelength maximum and minimum reflectance can be evaluated.

In the Spring Valley application, the spectral effects of arsenic on cover vegetation and in the phytoremediation applications are generally unknown and the use of derivatives, along with statistical tools, may help to isolate, or even quantify, the level of arsenic exposure and/or uptake.

3.3. The Evolution of Remote Sensing Technology

The science of remote sensing has undergone tremendous change in the last twenty years. In addition to significant changes in the commercial, legal and policy arenas in which remote sensing scientists operate, there has been a virtual revolution in the mechanics and technical capabilities of sensors, platforms and processing. One of the most significant developments has been in the evolution of HSI (Green et al. 1998).

Traditional multispectral imaging sensors, such as the Landsat Multi-Spectral Scanner (MSS) which was developed in the early 1970s, utilized a complex system of optical/mechanical filters and discrete detectors to capture four individual bands at broad spectral resolutions on the order of 100 - 200 nm, and a spatial resolution of

approximately 80 m. These detectors transmit reflected photons for each individual pixel through specific filters that pass broad portions of the visible and near-infrared spectrum and turn these signals into electronic, digital measurements. The Landsat Thematic Mapper (TM) has seven bands with similar spectral resolutions and a spatial resolution of 30 m. These detectors transmit reflected and emitted energy for each individual pixel through specific filters that pass broad portions of the visible, near-infrared, and for the TM, also the mid- and thermal-infrared parts of the spectrum and turn these signals into electronic, digital measurements. The bands were selectively placed in the spectrum to correspond to atmospheric transmission windows and maximize information content.

HRS became possible in the late 1970s with the development of dispersing elements, grating spectrometers and line detector arrays that were capable of capturing the reflected electromagnetic energy over hundreds of narrow, discrete, contiguous, spectral bands (Green et al. 1998). Figure 11 graphically shows the evolution of spectral bandwidth capabilities. Early HRS instruments, such as the NASA Advanced Solid state Array Spectrometer (ASAS) and the Advanced Imaging System, developed by NASA in the late 1970s and early 1980s served as test bed systems that provided not only valuable advances in detector technology, but also provided critical proof-of-concept research for the continuing development of hyperspectral technology. Commercial development of systems also provided critical research during the 1980s.

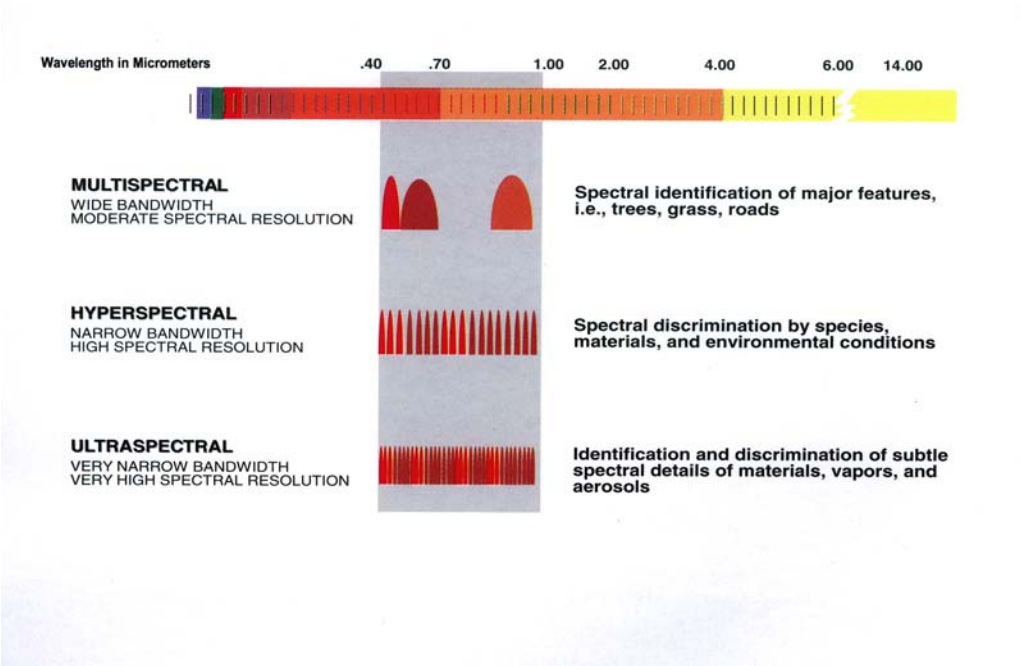

Figure 11. The Evolution of Spectral Remote Sensing Systems.This graphic demonstrates spectral resolution from basic multispectral systems into hyper- and ultra- spectral sensors capable of discriminating materials based on molecular structure. Adapted from the Multispectral Users Guide (1995, Pages 1-7).

The power of hyperspectral technology can be seen in Figure 12 which compares the spectral resolution capabilities of multispectral and hyperspectral systems. With the advent of HRS imaging systems were capable of providing spectroscopic analysis information that was previously conducted only in the laboratory.

A major development in hyperspectral technology came with the NASA AVIRIS instrument which first flew in 1987. Still operational today, this instrument images 224 bands across the 400–2,500 nm range of the EMS and has provided data for numerous successful research applications in imaging spectroscopy (Green et al. 1998). Significant

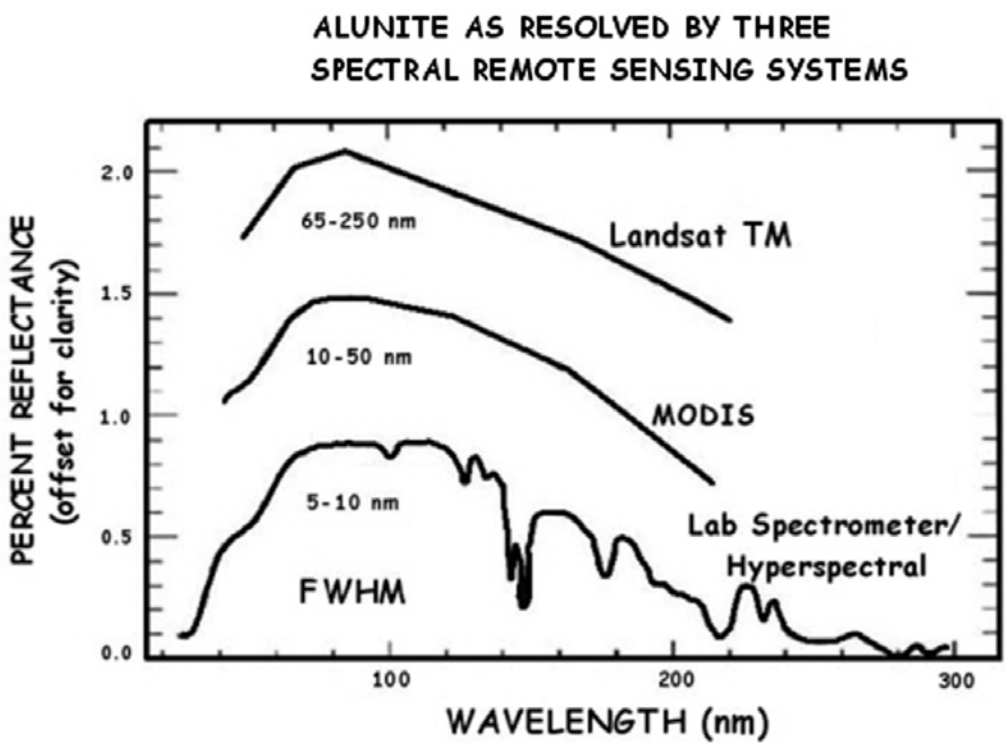

Figure 12. Differences in Sensor Spectral Resolution The reflectance spectra for the mineral, Alunite, as derived from the Landsat TM, MODIS and a hyperspectral laboratory spectrometer. The advantages of the narrow bandwidth, as indicated in the figure above, and the continuous nature of the hyperspectral data for analytical purposes are readily apparent in the detailed reflectance and absorption patterns in the hyperspectral data. From Clark (1997, page 5).

commercial hyperspectral instrument developments have also followed and HSI can now be purchased commercially.

Two unfortunate events in the development of HRS should be noted here. First, the HIgh Resolution Imaging Spectrometer (HIRIS) instrument that was planned to be part of the NASA Earth Observing System (EOS) suite of sensors, was canceled due to funding considerations. Second, the loss of the LEWIS instrument due to launch failure in 1996 denied the research community its first orbital hyperspectral instrument. However, NASA has since successfully deployed both the MODIS and Hyperion

satellites that are now operational. Table 2 lists some early hyperspectral instruments, manufacturers and spectral ranges.

Because of area wide sampling in the study area, there are significant data on soil arsenic levels and distribution. The vegetation and soil arsenic patterns in Spring Valley will be analyzed with a HSI data set acquired by the HyMAP sensor in October 2000.

3.4 The Analysis of Vegetation by Imaging Spectroscopy

As a final stage in technological evolution of sensors and systems, it is now possible to link the analysis of vegetation from laboratory spectroscopy (Section 3.2) with the development of hyperspectral imaging technology (Section 3.3) and emerge with the synoptic imaging capabilities of remote sensing, coupled with the spectral analysis capabilities of spectroscopy, to achieve one of the major research goals in Spring Valley; determining the ability to identify arsenic-stressed vegetation from overhead, HSI. Imaging spectroscopy is a relatively new scientific capability within the field of remote sensing that has emerged as a result of technical improvements in sensor array and electronic systems. Airborne and satellite hyperspectral imaging systems can now measure the response of reflected and emitted electromagnetic energy in hundreds of individual bands across the EMS. In many cases, the measurement of this energy gives unique information related to the structural or chemical composition of the material or substance being sensed.

Table 2
Examples of Existing and Planned Hyperspectral Instruments

Sensor	Name	Manufacturer	Bands	Spectral Range
ASAS	Advanced Solid-State Array Spectrometer	NASA (Goddard)	62	400 - 1,200
AHS	Airborne Hyperspectral Scanner	Daedalus	48	433 - 12,700
AIS-1	Airborne Imaging System 1	NASA (JPL)	128	800 - 1,600 1,200 - 2,400
CIS	Chinese Imaging Spectrometer	Shanghai Institute of Technical Physics	91	400 - 12,500
Dais 7915	Digital Airborne Imaging Spectrometer	GER Corp	79	400 - 12,000
VIMS-V	Visible Infrared Mapping Spectrometer	ASI	512	300 - 1,050
AVIRIS	Advanced Visible and Infrared Imaging Spectrometer	NASA (JPL)	224	400 - 2,500
HYDICE	Hyperspectral Digital Imagery Collection Experiment	NRL	210	400 - 2,500
HYMAP	Airborne Hyperspectral Scanner	Integrated Spectronics	128	400 - 12,000
MAS	Modis Airborne Simulator	Daedalus	50	530 - 14,500
TRWIS III	TRW Imaging Spectrometer	TRW	384	300 - 2,500
MODIS	Moderate Resolution Infrared Spectrometer	NASA	36	400 - 14,400
Hyperion	Hyperion	TRW	384	300 - 2,500
NEMO	Navy Earth Map Observer	U.S. Navy	210	400 - 2,500
Warfighter 1	Warfighter	U.S. Air Force	280	400 - 5,000

A vector of the reflected energy of a reflectance-calibrated hyperspectral image is a profile of an individual pixel location through all of the hyperspectral bands. When viewed in graphical form, it represents the same energy and matter interactions that are recorded in the spectra that are derived in standard laboratory methods of reflectance spectroscopy. These two data sources can be analyzed with the same techniques.

Although early applications of HSI were focused on the identification of minerals, vegetation applications soon followed. The chlorophyll absorption features centered at 480 and 680 nm are the result of photosynthesis and are clearly evident in hyperspectral image data. It was soon discovered that subtle changes in the reflectance of these regions were the result of biochemical changes, often in response to external factors. The earliest applications of HSI for vegetation revolved around mineral exploration and the identification of geochemical stress in vegetation from mineral deposits (Collins et al. 1983; Milton et al. 1983; Chang and Collins 1983). Airborne hyperspectral data have been used to investigate canopy chemistry by Peterson et al. (1988), Curran (1989) and Martin and Aber (1993, 1997). Ecological patterns of vegetation productivity have been identified from HSI by Gamon and Qiu (1999), Ustin et al. (1993) and Wessman (1994). Vegetation type and in some cases, actual species identification has been accomplished with AVIRIS data by Martin et al. (1998) and Roberts et al. (1998).

Agricultural applications of HSI analysis have been conducted by Strachan et al. (2002) and Thenkabail et al. (2000) where very-narrow, crop-specific VIs were developed from HSI and applied to the assessment of agricultural productivity. In general, the use of VIs has seen a significant increase with the development and

availability of HSI. Elvidge and Chen (1995), Blackburn (1998) and Thenkabail et al. (2000) have demonstrated the effectiveness of narrow-band VIs which continues as one of the most important analytical approaches in the area of spectroscopic analysis of vegetation.

This literature review has presented the historical background and relevant literature relating to several aspects of remote sensing technology that will be utilized in Spring Valley research. First, the process of utilizing historical imagery to identify patterns of landscape disturbance and their relationship to possible hazardous waste disposal or exposure is not cutting-edge science but it is an unusual and often-overlooked source of information. Also, the extraction of information by the qualitative photographic interpretation process is sometimes viewed as less-than fully scientific and may account, to some extent, for the lack of full exploitation of this information resource. This study will evaluate the potential of this historic information source in the operational context of Spring Valley remediation.

Second, the review of laboratory reflectance spectroscopy and vegetation-specific research is directly related to the second Spring Valley research issue of arsenic stress and arsenic uptake in the phytoremediation process. The ferns and grasses grown in the laboratory in soils amended with arsenic afford the opportunity to study the spectral phenomenon of arsenic stress and uptake in a controlled environment and potentially provide a “stand-off “ method for the identification of fugitive arsenic. This review described the background science and techniques that have evolved in the laboratory for

vegetation analysis and that will be relevant to the laboratory spectral study of the effects of arsenic on ferns and grasses.

Third, while the spectral study of arsenic and vegetation in the laboratory is important in its own right, it is also an important connection to the third aspect of this Spring Valley research, the analysis of HSI. The background on the evolution of remote sensing systems to the point where they can now record the same energy-matter interactions as spectroscopy in the laboratory, as well as provide the advantages of synoptic spatial coverage, shows the emerging potential of this technology and its direct potential application for identifying fugitive arsenic in Spring Valley.

4. Data Collection and Analysis Methods

Each of the three phases of this research are related to the direct information needs of the hazardous waste remedial process and to different aspects of remote sensing in providing that information. The first phase involves an evaluation of the landscape-level information derived from the interpretation of historical aerial photographs. The second phase is centered on the investigation of the spectral properties of arsenic stress and uptake in vegetation in a laboratory environment. The third phase focuses on the analysis of HSI in the identification and mapping of the spectral indicators of arsenic stress in Spring Valley vegetation.

This chapter is organized in the following manner. Section 4.1 discusses the basic process of historical aerial photographic research, acquisition, analysis and reporting. Section 4.2 presents the spatial overlay and analysis methodology that was used to evaluate photo-interpreted data against known remediation requirements. Section 4.3 explains the information about the greenhouse growth chamber, chemistry procedures and the laboratory spectral data collections. Section 4.4 outlines the statistical analysis methods used to evaluate the relationship between reflectance spectra and arsenic concentration. Section 4.5 examines the methods typically used for processing and analyzing HSI and Section 4.6 reviews the concept of land cover mapping as related to

Spring Valley. Section 4.7 describes the techniques used in the statistical evaluation of remote sensing classification accuracy as will be employed for the Spring Valley HSI.

4.1 Photographic Interpretation and Historical Aerial Photography

The goal of the historical aerial photographic analysis in this study is the determination of the accuracy and relative value of information derived from interpretation of historical aerial photographs for the hazardous waste investigation process. Historical aerial photographic interpretation has often been used to investigate past landscape activities that might be related to the disposal of hazardous waste (Lyon 1987). However, because of the inherent problems with verifying historical data, there has been little or no evaluation of the accuracy or practical value of this information. Since active clean-up operations have been taking place in Spring Valley for several years, there is extensive data available on soil sampling, geophysical investigations, UXO and contaminated soil removal and other potential environmental effects. This information represented an excellent reference data set and was used to assess the spatial correlation between of data derived from the interpretation of historical aerial photographs and actual remediation requirements.

This section describes the basic methodology used to develop the original photographic interpretation report on Spring Valley by Stout (1986). This report, performed by an independent imagery analyst, Kristen K. Stout, is the only photographic analysis being evaluated in this study. Although several detailed investigations of historical imagery of Spring Valley have been accomplished (Stout 1986; Kartman and

Slonecker 2001; Mata 2002; Williams 2002), this analysis focused only on the 1986 report since it was performed before any discovery of hazardous waste or remedial activity had started and was conducted with little or no collateral information about the facility available to the analyst.

4.1.1. Basic Historical Aerial Photographic Methods

A search of government and commercial imagery archives was conducted in order to identify historical imagery in a time frame that may be of value for the identification of landscape activities that were the direct result of historical AUES-related activity. Imagery research was conducted at the U.S. National Archives and Records Administration (NARA), the U.S. Library of Congress (LOC), American University (AU) and other places for aerial photographs, reports, monographs, newspaper articles and any other records that potentially contained information about the WWI activities at the AUES. Although several historical aerial photographs were discovered and acquired, three proved to be critical to the eventual hazardous waste investigation and are listed in Table 3.

Duplicate negatives of all relevant images and copies of all reports and maps identified in the historical research were obtained. Aerial photographic interpretation was accomplished according to standard USEPA methods (USEPA 2005). Photo analysis was conducted by viewing film positives on a backlit light table with double ocular microscopes/stereoscopes. When available, overlapping aerial photographs were analyzed in three-dimensional stereo, which gives the analyst a depth and topographic

perspective of the landscape. Specific photo-identified features were extracted first as graphics markings and annotations on a mylar overlay to photographic print of the same

Table 3
Historical Aerial Photographs of the Spring Valley Area

Photo Source	Date of Acquisition	Original Scale	Film Type	Comments
AU	8/17/1918	1:7,500	B&W Positive	uncontrolled mosaic
USACOE	1922	unknown	B&W Print	uncontrolled mosaic
NARA	1927	1:10,000	B&W Positive	frames 53, 96-98, 557-558

image, along with the analysts written description of the features and the surrounding landscape context. In the context of hazardous waste, photographic interpretation involves the identification of a distinct set of photographic observables, activities or conditions such as ground scars, active digging or waste disposal, that are identified and extracted to meet the specific information needs of the investigation. The formal definitions of the specific photographic observables and standard operating procedures can be found in the report "Photo Interpretation: Hazardous Waste Sites. Standard Operating Procedure" (USEPA 2005).

For GIS analysis, all historical photographs were scanned at a minimum resolution of 1,300 dpi and registered to the Maryland State Plane Coordinate System for entry into a GIS database. The overall registration accuracy for the 1918 image 8.34 m. All photo-interpreted features were then digitized as points, lines and polygons in a GIS format and attributed with appropriate descriptions.

4.1.2. Reference Data from Remedial Activities

As reference points for the evaluation of historical photographic information, a verification dataset was developed from a variety of actual hazardous waste cleanup activities that have taken place over the past eight years in Spring Valley. These include the following activities/events:

1. UXO burial areas.
2. Chemical waste burial areas.
3. Properties with high soil arsenic concentrations, from site-wide soil arsenic screening.
4. Properties with detected levels of chemical warfare agents or their breakdown products.
5. Areas of relevant and confirmed contextual activities, such as the mustard field testing area, derived from historical document research.
6. Areas of unusual human health problems or other activities that were reported, and verified by the Area of Interest Task Force, a multi-agency team established to investigate all potential problems in Spring Valley.

These features, derived from ongoing remedial activities, provide documentation and defensible information about landscape level effects of AUES activities and establish

an excellent source of reference information for the evaluation of historical photographic interpretation features. Features derived from aerial photographic interpretation were overlain with the reference data in a GIS environment to determine the spatial correlation between photo-interpreted features and the future requirements for hazardous waste remediation. An example of photo-derived information displayed on a georegistered image of part of the American University area is shown in Figure 13.

4.2 Statistical Methods Used in the Aerial Photographic Analysis

The first phase of this research, the evaluation of the relative relationship between the landscape features derived from 1918 aerial photographs and current remediation activities, is basically a spatial overlay/correlation process. It is a deterministic evaluation of a single set of geospatial data points through time and their relationship to current spatial features related to hazardous waste remediation. A test for significance can be accomplished by comparing the relationship between historical aerial photographic points of interest with a set of random points and their relationship to remediation (i.e., the number of aerial photographic points that fall within known remediation areas and the number of random points that fall within remediation areas). These two sets of binary data points can be tested with a chi-square statistic in a logistic regression model (SAS 2004).

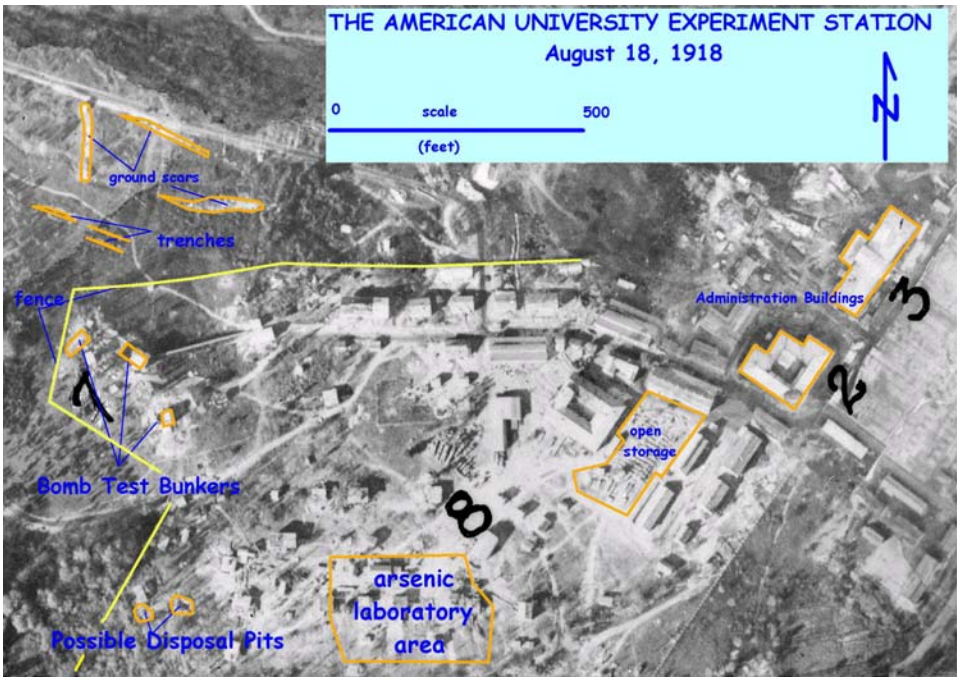

Figure 13. GIS Features Extracted by Aerial Photographic Analysis. An example of features derived from historical aerial photographic interpretation displayed as vectors on a georegistered image in a GIS environment. Adapted from Kartman and Slonecker (2001).

4.3 Reflectance Spectroscopy of Arsenic Stress and Uptake

A laboratory environment was used to investigate the spectral reflectance properties of arsenic stress and uptake in vegetation. The primary goal of this phase of the research was the identification of any potential spectral signature, index, shift or other spectral observable that was linked to, and was predictive of, arsenic stress and/or arsenic uptake during phytoremediation. To do this, *Pteris* ferns and common lawn grasses were grown in a controlled laboratory environment under contract to Edenspace Incorporated,

the holder of the patent on phytoremediation of arsenic with ferns. Plants were harvested every 4 weeks, dried and sent to a commercial chemistry laboratory for analysis of total metals. Spectral reflectance data were collected for each plant just prior to harvest.

4.3.1 Growth Chamber Methods

From April to October 2004, 300 individual ferns and 20 individual pots of common lawn grasses were grown in soils amended with varying levels of sodium arsenate to achieve five distinct concentrations of arsenic from 0 to 200 ppm (Blaylock 2005).

The ferns consisted of 100 each of two arsenic-hyperaccumulating varieties, *Pteris cretica mayii* and *Pteris multifida* and one non-arsenic accumulating variety, *Nephrolepis exaltata*, used as a control. See Figure 14. Twenty individual sporelings from each variety were transplanted in 10 cm pots of each of the five soil-arsenic concentrations.

Seeds from two types of lawn grasses common to the Spring Valley area, rye (*Secale cereale*) and fescue (*Festuca arundinacea*) were planted in 20 pots, two in each soil concentration. All ferns and grasses were maintained and grown for specified periods up to a total period of 20 weeks. Weekly fertilizer supplements were provided using a .025-.025-.025 (Nitrogen-Phosphorous-Potassium plus micronutrients) solution applied as part of the regular watering schedule.

The soil consisted of clean, homogeneous sandsodium arsenate to achieve approximate concentrations of 0, 20, 50, 100 and 200 ppm. The sand was limed to

Figure 14. The Three Ferns Used in This Study. The three ferns grown in the greenhouse study of the spectral qualities of arsenic uptake. From left to right, *Pteris cretica mayii*, *Pteris multifida* and the control fern, *Nephrolepis exaltata*.

achieve a neutral pH of 7 and fertilized to 100 ppm nitrogen, 50 ppm phosphorous and 100 ppm potassium plus other micronutrients. The soil medium was equilibrated for two wetting and drying cycles to homogenize the arsenic and fertilizer mixtures. Samples from each of the five concentration batches were collected for laboratory analysis by USEPA 3050 method for total metals (USEPA 2004). The analysis showed final, pre-concentrations of < 2.5, 18, 34, 64 and 183 ppm respectively (Blaylock 2005).

The open air greenhouse environment was controlled by ambient temperature and solar lighting conditions for the April–October time frame. Pots containing fern plants were placed in trays grouped by soil arsenic concentration to avoid cross contamination of arsenic between different levels. The open air greenhouse (cold frame) was covered with 60 % shade cloth to reduce light transmittance and provide improved growing conditions for the fern plants. Figure 15 shows the actual plants in the greenhouse at the

Figure 15. Ferns Growing in the Greenhouse The 300 ferns in the greenhouse, arsenic-uptake experiment at the beginning of the experiment. Three types of ferns were grown in five different arsenic soil treatments.

beginning of the experiment and Figure 16 is a diagram of the general layout of the plants in the greenhouse experiment.

The main purpose of this phase of the research was to grow accumulating and non-accumulating ferns in different levels of bioavailable soil arsenic and measure the spectral vegetation reflectance response, as a function of the arsenic concentration in the above ground biomass of the plant. This design did not address the assumptions of parametric statistics such as a Latin Square randomization. The primary analytical endpoints of this phase of the research were the arsenic concentrations in each individual

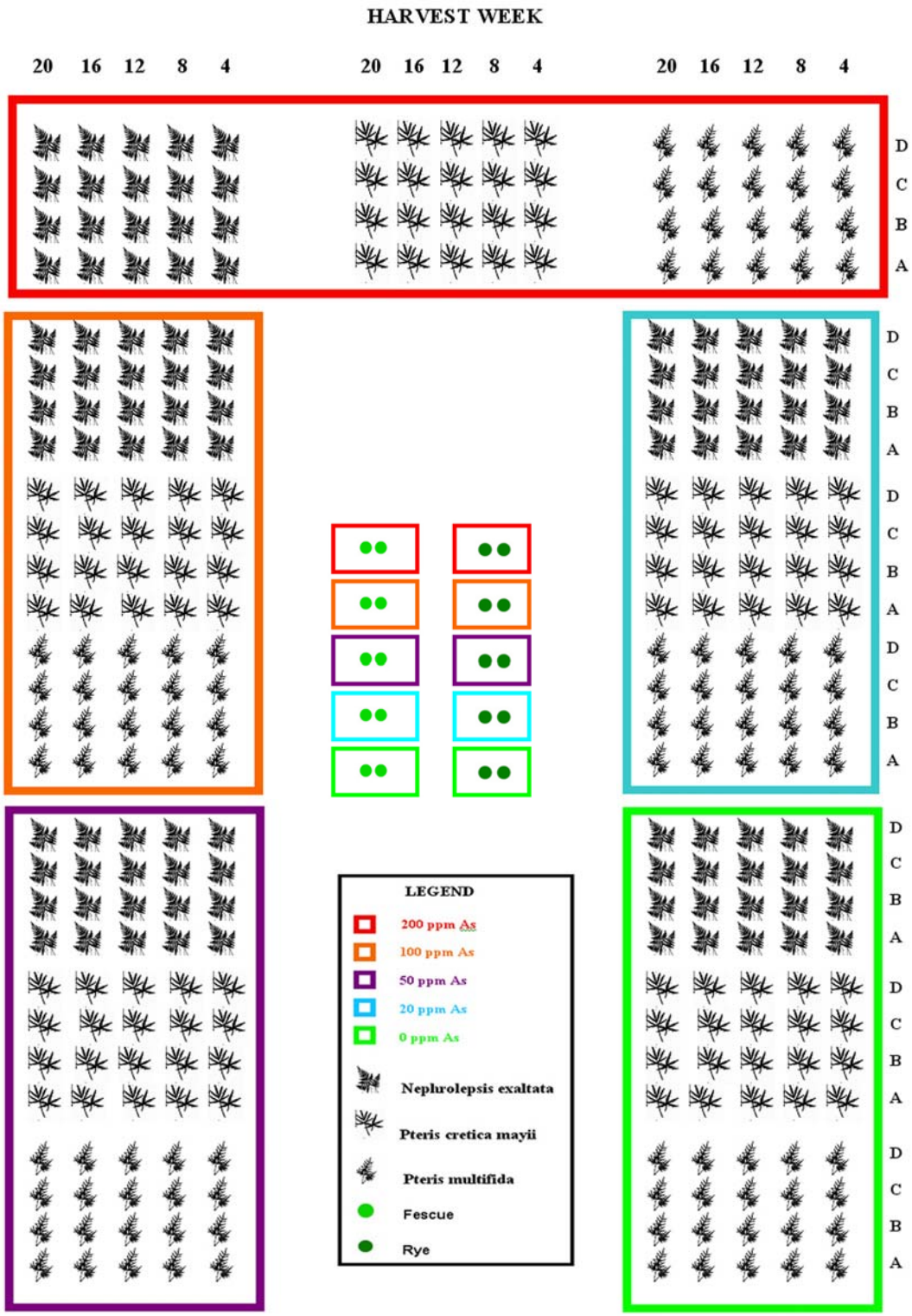

Figure 16. General Layout of the Greenhouse Experiment. The layout of the ferns and grasses in the greenhouse as part of the experiment on controlled growth and exposure to soil arsenic.

plant which were to be determined by standard chemistry methods and the corresponding spectral reflectance response as measured by an Analytical Spectral Devices (ASD) Full Range spectrometer. Therefore, biases in local greenhouse conditions were not a primary concern. After data analysis was completed, there was no detectable pattern in plant growth or arsenic uptake that would indicate any type of critical bias based on greenhouse conditions.

4.3.2 Chemical and Spectral Data Collection

Four replications of each fern variety and two replications of each grass variety were harvested at 4 week intervals after transplanting for a total of 20 weeks (4, 8, 12, 16 and 20 weeks). The plants were harvested by cutting the above ground material 2.5 cm above the soil surface. The vegetation samples were oven dried at 85°C for 24 hours and the dried samples were weighed and shipped to a commercial laboratory and analyzed for total metals via USEPA Method 6010b, Inductively Coupled Plasma/Atomic Emission Spectrometry (ICP/AES) (USEPA 2004). Soil samples were collected at the end of the study from the pots of each plant species at each soil concentration for evaluation. Soils were analyzed for arsenic and total metals by USEPA Method 3050 (USEPA 2004).

Reflectance spectra of ferns and grass were collected just prior to each 4 week harvest using an ASD spectrometer. This instrument utilizes grating prisms, three separate detector arrays and fiber optics to collect reflected energy in the 400 - 2,500 nm range, known as the “solar reflected” part of the EMS. The spectral resolution of this instrument is 1 nm (ASD 1997). A Dell Latitude C640 laptop computer was connected to

the spectrometer and used to execute the spectral collection instrument software. The fiber optic cable of the spectrometer is housed in a pistol grip assembly and mounted on a standard camera tripod to be perpendicular to the target. Spectra were calibrated against a white Spectralon surface and processed according to the standard techniques outlined in ASD (1997). A Lowell lamp was used as a light source for all spectral collections and was mounted on a 60 degree angle to the spectral target. Each spectral collection event utilized nine observations and was conducted according the following standard procedure:

1. Optimization of the spectrometer (internal calibration).
2. Collection of two white references (WR) from the Spectralon standard.
3. Collection of five spectral readings from the target, altering the plant orientation or slightly moving the fern after each reading.
4. Collection of two white references from the Spectralon standard.

Spectra were processed by standard techniques based on the following general formula for relative reflectance (ASD 1997):

$$\textbf{Reflectance}_{(Band_x)} = ((\textbf{Radiance}_{(Band_x)} / \textbf{White Ref.}_{(Band_x)} * 100) * \textbf{Ref. Std.}_{(Band_x)})$$

4.3.3 Field Phytoremediation Spectral Data

As a result of widespread soil testing conducted in Spring Valley as part of the remedial investigation process, several areas of high soil arsenic have been identified and scheduled for remediation according to standard procedures. See Figure 17. Because of

Figure 17. *Pteris* Ferns in the Spring Valley Phytoremediation Pilot. *Pteris* ferns being used in a phytoremediation pilot study next to the Van Ness Reservoir in Spring Valley.

the dynamic nature of the urban setting and the complexities of large-scale excavations in urban areas, phytoremediation techniques, using *Pteris* ferns, are also being tested in several areas of moderate arsenic concentration as an alternative to the traditional soil-removal and replacement techniques. The collection of spectral data of some of these ferns growing in an actual phytoremediation application presented an excellent opportunity to test any predictive model of arsenic concentration that may have been developed as part of the laboratory spectra data collection and analysis.

One of these phytoremediation tests was conducted in a high soil arsenic area adjacent to the Van Ness reservoir. During the summer of 2004, *Pteris* ferns were planted in April and were harvested and tested for arsenic in September. Just prior to harvest, field spectra were collected with the ASD field spectrometer for 24 individual

ferns (12 *Pteris cretica mayii* and 12 *Pteris multifida)* distributed throughout the remediation area. These individual ferns were separately bagged, marked and sent to the USACE laboratory in Vicksburg, Mississippi for chemical analysis of arsenic concentration.

4.4 Statistical Methods Used in the Analysis of Laboratory Reflectance Data

The statistical analysis of the relationship between the spectral reflectance of the ferns and grasses and their corresponding biomass arsenic concentration were conducted with standard summary statistical methods and with two multivariate techniques; partial least squares (PLS) and stepwise liner regression (SLR). These methods were used to develop linear and predictive models of the relationship between plant reflectance and plant arsenic concentration.

The analysis of spectra reflectance data presents unique problems for standard multivariate techniques because of the large numbers of independent variables (> 2,000 spectral bands) and the highly correlated nature of those variables, which stems from the fact that each individual spectral band is only 1 nm away from the spectral bands above and below it. The result is that each spectral band records an energy pattern that is a very similar to its neighboring bands and is thus highly correlated. Highly correlated independent variables create a condition known as collinearity, which violates the assumptions of linear regression. To develop a predictive and effective linear model, variables must be independent. The overall result of a collinearity condition is that correlated independent variables have unstable coefficients, and although the model

developed may have a high R^2 value and low residuals, it will perform poorly outside of the immediate data set that was used to develop it.

Partial least squares was first introduced by Swedish mathematician Herman Wold (1966) as an exploratory analysis technique in the field of econometrics and was specifically designed to help researchers in situations of small, non-normally distributed data sets with numerous but highly correlated explanatory variables. General PLS and all of its variants consist of a set of regression and classification tasks as well as dimension reduction techniques and modeling tools. Sometimes called a "soft" modeling technique, the strength of PLS resides in its relaxation, or "softening" of the distribution, normality and collinearity restrictions that are inherent in standard multiple linear regression techniques (Tobias 1997; Abdi 2003).

The underlying assumption of all PLS methods is that the observed data are generated by a system or process which is driven by a small number of latent (not directly observed or intuitive) variables. Projections of the observed data to its latent structure by means of PLS is a variation of principal component analysis (PCA). PLS generalizes and combines features from PCA and multiple regression and is similar to Canonical Correlation Analysis (CCA) in that it can also relate the set of independent variables to a set of multiple dependent response variables and extract latent vectors with maximum correlation (Höskuldsson 1988; Rosipal and Kramer 2006).

PLS is one of a number of covariance-based statistical methods which are often referred to as structural equation modeling or SEM. Also known as a "latent variable" approach to modeling the covariance structures, the PLS model attempts to find the

multidimensional direction in the X space that explains the maximum multidimensional variance direction in the Y space. According to its developer, Herman Wold, the term "PLS" is also and more correctly termed "Projection to Latent Structures" (Wold 1975; Wold 1985). Wold's son, Svante, has been largely responsible for the development and widespread use of PLS methods in the field of chemometrics and chemical engineering (Wold et al. 2001). Statistician John F. MacGregor (2004) had great success applying PLS techniques to industrial process control (Kresta et al. 1991). It has also been used successfully in the study of spatial pattern analysis of imagery of human brain functions (Nyberg et al. 1996; Macintosh et al. 1996; Habeck et al. 2005). More recently, in the field of landscape ecology, PLS has been used to describe how structural variation in landscape metrics are related to biological and chemical properties of surface water (Nash et al. 2005).

Instead of finding hyperplanes or vectors of maximum variance, as in PCA, PLS attempts to find a linear model between a matrix of predicted values and a matrix of observed values. PLS regression is especially useful in cases where the number of descriptors (independent variables) is comparable to or greater than the number of dependent variables and/or there exist other factors leading to correlations between variables (Abdi 2003). In this case the solution of the classical least squares problem does not exist or is unstable and unreliable. Such is the case with spectral reflectance data where the 1 nm difference between band centers leads to highly correlated data that could not be analyzed in a traditional multiple regression model because the data would

violate the collinearity assumption (Höskuldsson 1988; Martens 1989; Eriksson et al. 2001).

PLS is also used as an exploratory/data mining and analysis tool in remote sensing. As a relatively new technique, the full utilization of PLS is still evolving but it is clear that it has a major application in several types of spectral, remote sensing analyses, due to the large numbers of potential predictive variables and the highly correlated nature of hyperspectral reflectance and hyperspectral imaging data.

Kooistra et al. (2004) used two spectral VIs, the Difference Vegetation Index (DVI) and the Red Edge Position (REP), along with PLS regression to predict the level of metal contamination in the soil based on the spectral reflectance of grasses. Bogrekci and Lee (2005a, 2005b, 2006) utilized PLS in evaluating visible and infrared reflectance data to predict soil phosphorus concentrations. Rossel et al. (2006) used PLS techniques to predict a number of complex soil properties from mid-infrared data. ElMasry et al. (2006) demonstrated the very practical application of PLS and hyperspectral analysis as a nondestructive method of determining the moisture content, total soluble solids and acidity in strawberries.

Xu et al. (2007) suggests extending the variable selection capabilities of PLS by weighting variables through the use of a particle swarm optimization algorithm. The variable weighting method is demonstrated by optimizing calibrations of near-infrared (NIR) spectral data of meat and pharmaceutical quality control. However, Kruse et al. (2006) showed that standard VIs like NDVI, Stress1 (R706/R760) and Stress2

(R706/R813) ratios did a better job than PLS at predicting chlorophyll content and nitrogen status in creeping bent grass.

Although there are several variations on the basic PLS process, the general method applied to spectral studies is shown in Appendix A on one of the applications of fern data in this study. The overall goal of PLS processing of spectral data in this study is the reduction of 2,151 variables (bands 350–2,500) down to a manageable number of 20 to 25 variables that have a high probability of significance in a predictive model. The PLS regression produces a number of significant factors using a "leave-one-out" cross-validation method (Nash et al. 2005). At several stages in the PLS process, diagnostic checks are performed, sometimes graphically, to help isolate variables for deletion in the model that do not have any significant predictive value or are outliers. The end result of a PLS run is a Variable Importance for Projection (VIP) table. The VIP represents the value of each variable in fitting the PLS model for both predictors and response. The VIP for each factor is defined as the square root of the weighted average times the number of predictors. If a predictor has a relatively small coefficient (in absolute value) and a small value of VIP, then it is a prime candidate for deletion (Nash et al. 2005). Wold (1995) considers a value less than 0.8 to be "small" for the VIP.

Variables with VIP values less than 0.8 and outliers are dropped from the model. The VIP table results are then typically divided into 4 to 9 groups. The PLS analysis process is then repeated on the individual groups of variables. Typically the process is iterated 2 to 5 times until a manageable subset of variables can be identified based on the top VIP scores in each group and some a priori knowledge of the process being modeled.

PLS can itself be used to construct a predictive model but has some drawbacks. One of the strengths of PLS is its relaxation of collinearity and distribution assumptions but this also can result in a set of collinear or redundant independent variables. Also, the best combinations of variables are not necessarily reflected in the VIP table values. In spectral applications, a common practice is to take the final subset of variables and then place them into a SLR model. The stepwise method is a modification of the forward variable selection technique and differs in that variables already in the model do not necessarily stay there. A SLR model computes the F-statistic for each variable and contains parameters for significance levels for variables to ENTER and to STAY in the model. The SLR process computes all possible combinations of linear variables and ends when none of the variables outside the model has a significance (p-value) at or below the ENTRY level and every variable in the model is significant at the STAY level. Using this sigma-restricted parameterization and general linear model methods, the SLR process simply regresses all possible combinations of input variables and returns the model with the best regression coefficient and the lowest residuals (Nash et al. 2005).

This combination of PLS and SLR techniques was the primary analytical method used to develop predictive models of arsenic concentration from spectral reflectance data. Analysis was conducted for all three fern species and the PLS procedure was used to reduce the number of potential predictive variables. These variables were input into a SLR model which then developed and optimized a linear regression model.

4.5 Hyperspectral Imagery Processing and Analysis Methods

Hyperspectral remote sensing represents a merger of laboratory spectroscopic analysis methods with the spatial and synoptic advantages of overhead imagery. Hyperspectral imaging systems record, at lower spatial and spectral resolution, the same energy-matter interactions that are recorded by spectroradiometer instruments in controlled laboratory environments. The third experiment in this research attempts to extend the concept of spectral analysis of vegetation health that was developed from the laboratory spectral analysis of arsenic stress in grasses during the greenhouse experiment, to the spectral patterns of vegetation recorded by a hyperspectral imaging system. Patterns of known soil-arsenic contamination in Spring Valley were used to test the ability of HSI to detect the same patterns of vegetation stress that were observed in the laboratory spectral data.

Hyperspectral Imagery of the Spring Valley area were acquired on October 20, 2000, by the HyMAP System (Mission HY20001020f06r06, HyVISTA Corporation, Sydney, Australia). HYMAP is a commercially available hyperspectral sensor with 126 bands in the 450–2,500 nm region of the EMS and an approximate 4 m spatial resolution. An example of the HyMAP imagery of Spring Valley is shown in Figure 18.

Image preprocessing consisted of a radiance calibration, an atmospheric removal correction, a spectral noise reduction filtering and calibration to apparent surface reflectance, all of which are described in the following section. Geometric corrections are typically not performed on hyperspectral data until after the analysis phase so as to preserve the spectral integrity of the data which might be reduced by resampling.

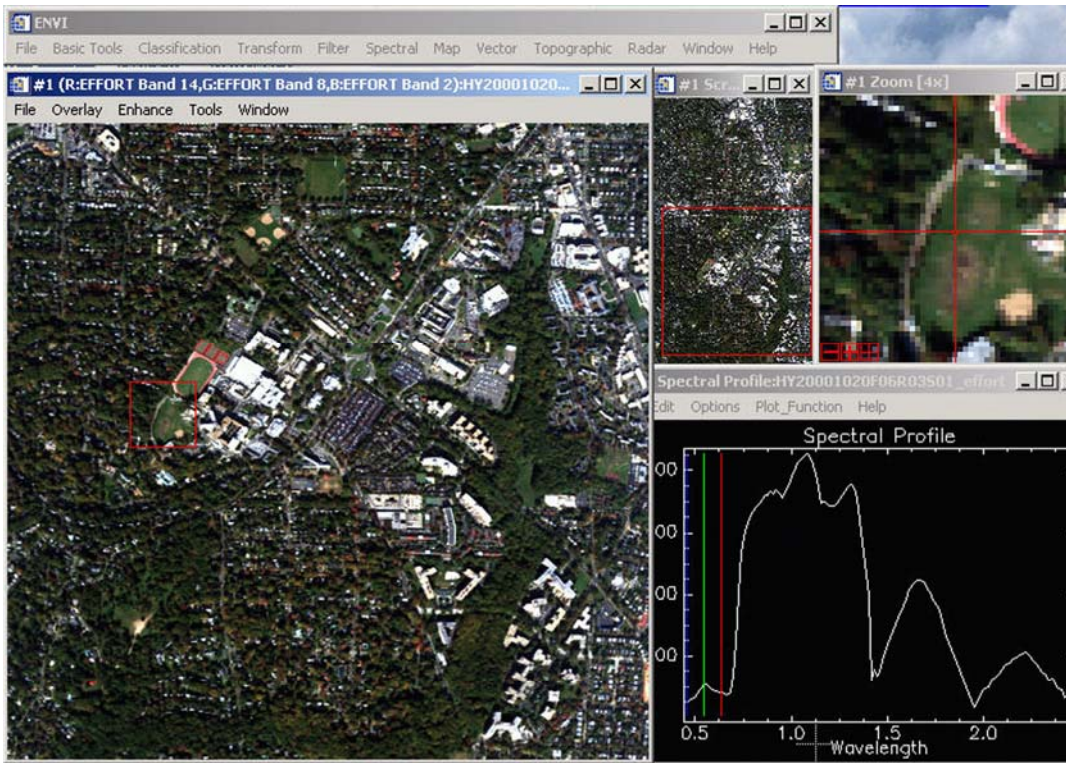

Figure 18. Example of HyMAP Hyperspectral Imagery of the Study Area. A portion of the HyMAP hyperspectral image that was collected over Spring Valley in October 2000. Spectra of arsenic stress in grasses, developed during the greenhouse experiment, were used to map potential area of arsenic contamination.

However, the analysis of HSI and the information that can be extracted from it are still in a developmental stage largely because of the interference that is caused by atmospheric conditions. As energy travels through the atmosphere from the sun and is reflected back to the sensor, it is absorbed, scattered and attenuated by atmospheric gases and conditions. Water vapor, oxygen, ozone, carbon dioxide, nitrogen dioxide, carbon monoxide and methane, along with some chlorofluorocarbons all have undesirable effects on the spectral integrity of reflected solar energy. Although new and better algorithms

for correcting atmospheric interference are constantly being developed, the process is not yet 100 % accurate and enough artifacts of atmospheric noise remain in the data to prevent the use of standard laboratory methods such as spectral library matching.

Hyperspectral imagery is also affected by the "mixed pixel" problem that has often been a difficulty with multispectral image systems. The mixed pixel occurs when the reflectance value of a single spatial unit (pixel) is influenced by a heterogeneous combination of surfaces. This can occur when the spatial footprint of the pixel encompasses different surfaces, with different reflectance values, or when the reflectance of a single pixel is influenced by stronger material reflectances in the surrounding location.

Hyperspectral imagery does offer a unique advantage of spectral over-sampling. The word "hyper" is derived from the Greek *huper* meaning "over" or "too many" and oversampling occurs when there are more spectral samples than there are spectral dimensions in the imagery (Boardman 1995). Goetz and Calvin (1987) demonstrated in the laboratory that most earth materials could be spectrally identified with a spectral resolution of 20 nm and a spectral resampling interval of at least 10 nm across the EMS. Laboratory spectrometers and HSI instruments exceed these spectral requirements by factors ranging from 2 to 20 times. Research in HRS has developed a number of unique image processing methods to take advantage of this oversampling and extract an increased information content from HSI.

The minimum noise fraction (MNF) transform is commonly used in HSI processing to determine and reduce the inherent dimensionality of image data. The MNF

transform also segregates noise in the data and reduces the size of the data set and computational requirements for subsequent processing (Boardman and Kruse 1994). A variation on PCA, the MNF transform is based on the spectral oversampling and inherent redundancy of HSI data. Hunt and Sierra (2003) demonstrated that spectral oversampling could be traded for spectral precision and improved classification accuracy using both supervised and unsupervised algorithms. Vélez-Reyes et al. (2004) utilized the spectral oversampling of HSI data to enhance spectral resolution across the image, resulting in improved classification and material identification accuracy.

4.5.1 Basic Processing of HSI

Although there are different approaches to processing HSI, the following general approach and processing steps were adapted from the spectral processing tools contained within the Environment for Visualizing Images (ENVI) image processing software (ENVI 2004).

4.5.1.1 Atmospheric Correction

HSI data are typically delivered in the form of raw radiance values of reflected energy. However, these values are not absolute and are significantly affected by specific temporal conditions such as relative humidity, sun angle and several atmospheric gases. To compensate for this, data are typically processed to correct for atmospheric interferences. Atmospheric corrections were performed on the Spring Valley HyMAP data set with the ATmospheric REMoval (ATREM) software program (Gao et al. 1993).

ATREM is an operational code for retrieving "scaled surface reflectance" from spectral imaging data to model water vapor and atmospheric gas absorption as well as molecular and aerosol scattering effects and converts the calibrated sensor radiance measurements to apparent surface reflectance (Gao et al. 1993).

4.5.1.2 Minimum Noise Fraction (MNF) Transformation

Because HSI systems record energy in hundreds of very narrow bands, there is significant redundancy and noise in the data set. Reducing the data to the most significant bands of spectral information is a key processing step that minimizes computational requirements of the subsequent processing steps (Green et al. 1998; ENVI 2004). This is accomplished using a variation on PCA called the Minimum Noise Fraction (MNF). The minimum noise fraction utilizes two principal component transformations. The first transformation decorrelates and rescales the noise in the data and results in transformed data in which the noise has unit variance and no band-to-band correlation (ENVI 2004). The second step is a standard principal components transformation of the noise-whitened data (Boardman and Kruse 1994). Typically the result of MNF processing, just like the principal components transformation used in traditional multispectral image processing, is a dataset reduced to only the bands that have any significant variance and that can provide information to the subsequent image processing steps. With HyMAP data over a heterogeneous urban environment, the MNF transform typically results in a 60–68 band data set, reduced from the original 128 bands.

4.5.1.3 Pixel Purity Index

HSI processing theory assumes that in every scene, the recorded spectral reflectance in most pixels is a mixture of a limited number of spectrally pure pixels, known as endmembers. Establishing these image endmembers is fundamental to understanding the basic dimensionality of a data set and in successfully identifying spectral targets of interest. A unique, automated method of identifying the spectrally purest pixels within a scene has been developed for spectral image processing called the Pixel Purity Index (PPI) (Boardman 1993; Boardman et al. 1995). The PPI is computed by repeatedly projecting the MNF transformed data cloud (scatterplots of pixels in hyperspectral space) onto a series of random vectors. When a pixel "hits" a vector, it is counted in the distribution for that vector. After each projection, the distribution of pixels and vectors is computed and a running total is kept for all vectors. This process is repeated, usually a minimum of 10,000 times. The vectors that have the most hits are considered to be extreme and are likely candidates to be the endmembers in the image.

4.5.1.4 N-Dimensional Visualizer

Multidimensional data distributions are difficult conceptualize. To help the image analyst understand the identity of the spectral complexities in an image, ENVI has developed a visualization tools called the N-Dimensional Visualizer. The N-Dimensional Visualizer is an interactive tool that shows the results of the PPI in N-space and allows the users to investigate image and spectral properties of the HSI data by moving through

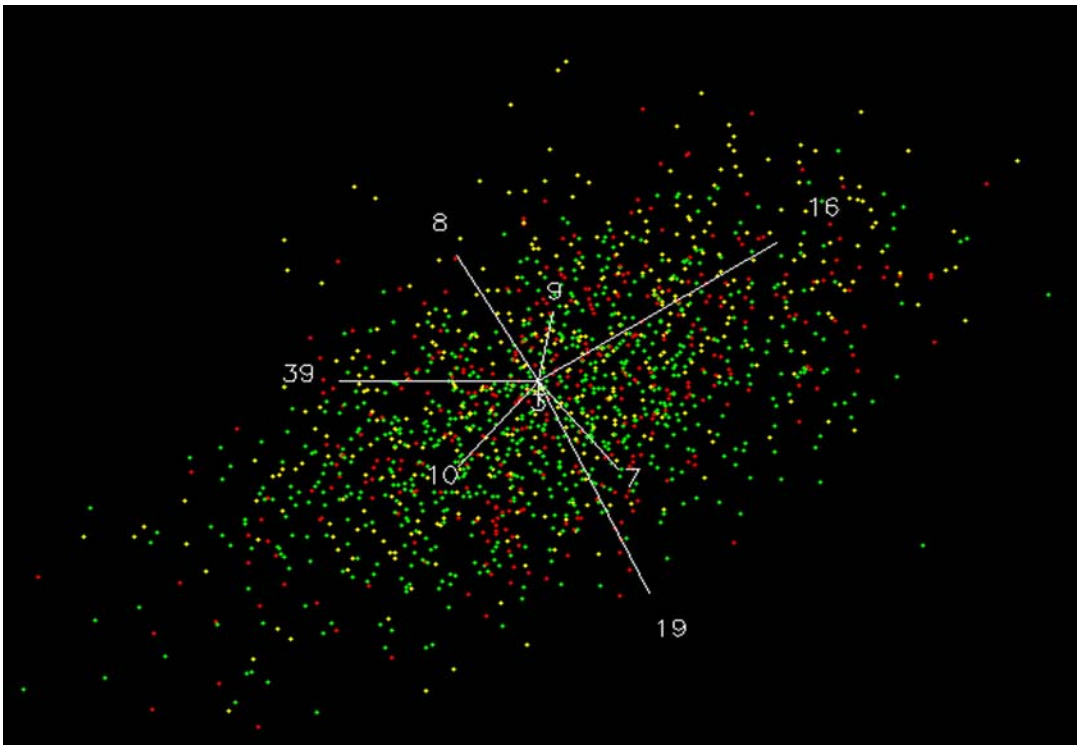

Figure 19. N-Dimensional Visualization. The N-Dimensional visualization of part of the Spring Valley HSI dataset. In hyperspectral space, the red pixels represent arsenic-affected grass and the green pixels represent unaffected grass. The inherent problems with the separability of these two classes are evident.

and manipulating the N-Dimensional clouds of data and endmembers and by visually correlating these with the image pixels. Figure 19 shows an example of the N-Dimensional Visualizer displaying the results of the PPI data of the Spring Valley HyMAP dataset used for this research. The vectors are the result of the PPI processing showing the number of hits for each vector.

The N-Dimensional display is interactive and can be rotated on the axes of the PPI vectors to better display a grouping or distribution of pixels. A subset of pixels can also be selected by manually drawing a polygon around them and those particular pixels

will then be highlighted in the image. This tool allows the analyst to graphically picture the spectral dimensions of the image and relate the statistical distributions back to the original image.

4.5.2 Intermediate and Final HSI Processing

Hyperspectral data processing involves a number of novel processing applications that are generally different from standard multispectral methods because they are specifically designed to explore the range of spectral information content of hyperspectral image data sets and maximize the advantage of the spectral "over-sampling" with special statistical tools (Hunt and Sierra 2003). However, standard multispectral image classification approaches are also used with hyperspectral image processing depending on the specific application. A basic hyperspectral image may be processed into one of several intermediate forms before a classification process is attempted. These include a linear spectral unmixing, which is a linear transformation of each pixel into its component percentages based on training signatures or spectra; spectral feature fitting which is a least squares match between image and reference spectra; and a pixel purity index which is an automated method of determining the purest, or endmember pixels in the image (ENVI 2004). Table 4 lists the combinations of basic and intermediate processing and classification algorithms used in this Spring Valley study (ENVI 2004).

Spectral profiles, or raw spectral signatures, are the necessary information components that drive all of the hyperspectral mapping methods. Spectral profiles can

usually only be generated in one of three ways: (1) statistically from the dimensionality of the image, such as the pixel purity index; (2) from supervised interaction in the image processing to identify known areas of the image as target spectra, analogous to supervised classification; and (3) from external or library spectral of materials or specific conditions. All three methods of developing spectral profiles were utilized in this experiment.

Table 4
Hyperspectral Imagery Processing Methods
(from ENVI 2004)

Base Processing	**Method**
Minimum Noise Fraction	Layered Principal Components reduces noise and data dimensionality.
Continuum Removal	Removes atmospheric constants and standardize spectral band depths.
Intermediate Processing	
Pixel Purity Index	Random selection of pixels identifies endmembers in spectral space.
Linear Spectral Unmixing	Linear transformation to determine the subpixel composition of each raster element based on endmember statistics.
Matched Filter	A method of spectral identification based on linear spectral unmixing results and detailed and refined spectral endmembers.
Mixture Tuned Matched Filter	A specialized form of spectral matched filtering that creates and utilizes an infeasibility image, a pixel by pixel map of the probability of a false positive, to identify unique spectral signatures, relatively noise-free.
Spectral Feature Fitting	A least squares fit between reference and image absorption spectra. Requires Continuum Removal.
Specialized Intermediate Processing	
Vegetation Indices	A set of spectral index values, as take from the remote sensing literature, for specific vegetation parameters.
Classification Decision Rules	
Parallelepiped	Classification based on a range of specific band values in n-dimensions.
Mahalanobis Distance	A direction-sensitive distance classifier that classifies each pixel into the statistically closest class of training or endmember data.
Maximum Likelihood	Classifies each pixel into the class of highest probability based on a normal distribution of the training classes.
Minimum Distance	Calculates the Euclidean distance from each pixel to the mean vector for each class. The pixel is assigned the classification of the shortest vector.
Binary Encoding	Classification technique that encodes the data and endmember spectra into zeros and ones, and utilizes Boolean functions to match image to reference spectra.
Spectral Angle Mapper	Spectral classification that matches image to reference spectra based on the similarity between the two spectra and by calculating and treating the angle between them as a vector in a space with dimensionality equal to the number of bands.

The primary goal of this image processing research was the classification and mapping of accurate land cover and especially the identification and discrimination of grasses growing in and stressed by fugitive arsenic from other normal grass cover. A subset of polygons of confirmed land cover classes was used as a "training" data set from which various image classification algorithms could establish statistical and/or spectral parameters for classification of the whole image. A second, independent set of known land cover classes was used as a reference file for accuracy assessment and statistical analysis of the quality of each of several classification processes. After the classification has been accomplished, the result is a raster GIS map of pixels as they have been assigned into land cover classes by a particular classification method.

4.6 Land Use and Land Cover Mapping

The final phase of this research involves the identification and mapping of arsenic stress in common lawn grasses in the study area using HSI. The identification of the areal extent of specific vegetation, cover condition or any surface phenomena is a process called land use and land cover (LULC) mapping and is one of the most fundamental uses of remotely sensed data. LULC maps provide critical information in a variety of applications and are typically developed from spectral imagery based on the differences in reflectance of major categories of land cover (i.e., forests, urban, open water, etc.). Thematic LULC mapping involves generalizing certain spectral and spatial landscape characteristics into regions or polygons of LULC categories.

While the primary goal of this image processing research was the identification and discrimination of grasses growing in and stressed by fugitive soil arsenic from other normal grass cover, a more robust land cover classification system was developed in order to put the results of grass classification in a full LULC context, and to help identify the LULC classes that might contribute to the misclassification of grass and arsenic-grass land cover classes. An eight-class LULC classification was developed and used to guide the rest of the LULC mapping process. The classification scheme follows.

Land Cover Classification Scheme

1. Arsenic-affected grass areas.
2. Non-Arsenic affected grass areas.
3. Tree and forest cover.
4. Buildings 1 (commercial).
5. Buildings 2 (residential).
6. Asphalt surfaces.
7. Bare and exposed soil.
8. Concrete surfaces.

After a working knowledge of the spectral properties of the data set had been established through field work, image analysis or the development of spectral data in the laboratory, two subsets of LULC data were developed from the HSI data for the Spring Valley area. The first subset of LULC classes was used to calibrate various classification

algorithms on the statistical and/or spectral parameters of each LULC class. The second subset was used as a validation data set for the accuracy assessment of each classification method. Figure 20 shows both the calibration and validation data sets overlain on a single band of the Spring Valley HSI data.

4.7 Statistical Methods Used in HSI Processing and LULC Mapping

After the classification has been accomplished, the result is a raster GIS map of pixels as they have been assigned into one of the eight land cover classes by a particular classification method. Remote sensing and mapping accuracy assessment is typically accomplished by comparison of the independent file of reference classes to the classification results and the computation of the standard remote sensing "Confusion Matrix" (Story and Congalton 1986; Congalton 1991). The confusion matrix classifies errors of omission (false negatives) and commission (false positives) per land cover class and also calculates two general measures of agreement; the overall accuracy percentage and the Kappa coefficient which is a measure of the number of pixels classified correctly versus the number of pixels that might be classified correctly by random chance.

The statistical evaluation and quality control of land cover mapping is complicated by the uneven distribution of land cover categories of general interest, and by the fact that some categories often do not display unique reflectance signatures in spectral space. Further, because of the large areal extents of many land cover mapping applications and the high cost of field verification, it is impractical to collect independent

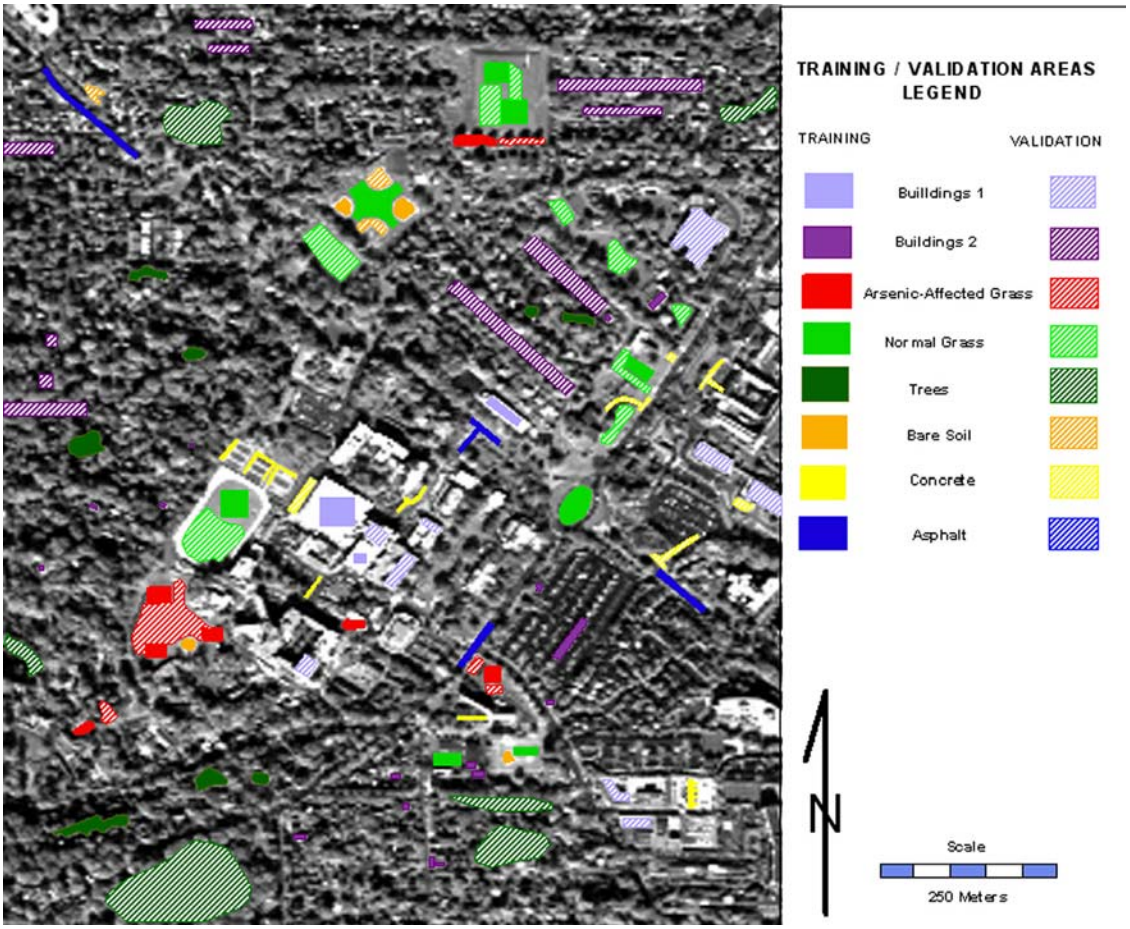

Figure 20. Training/Validation Data for Hyperspectral Image Processing. A single band of HyMAP imagery of American University and the surrounding area showing calibration and verification polygons digitized for a basic LULC classification including grass growing in areas of arsenic-contaminated soil.

data for accuracy assessment without the use of a statistical sampling design and that creates a number of issues with respect to edge effects, sampling units, sample size and rare classes (Fiztpatrick-Lins 1981).

A distinct paradigm in remote sensing and thematic mapping accuracy assessment has evolved since the mid-1980s (Story and Congalton 1986) centered around some type

of random or stratified random sample and the use of the error (sometimes called "confusion matrix"). The confusion matrix provides a quantification of pixel by pixel errors of omission and commission as measured against field derived samples or some source information of a higher spatial and/or spectral resolution and reliability.

In addition to the matrix classification of errors of omission and commission, the key metric in map accuracy evaluation is a statistical measure of agreement known as the Kappa Coefficient (Congalton et al. 1983). In typical map accuracy evaluations and reporting, two overall metrics are calculated and reported; the overall accuracy percentage and the Kappa, or K-hat, statistic. K-hat is calculated by the formula:

$$k = (d-q)/(N-q)$$

where d is the number of cases classified correctly and located in the diagonal cells of the confusion matrix and q is the number of cases expected to be classified correctly and located in the diagonal cells by chance. N is the total number of cases (Congalton 1991). K-hat is one for perfectly accurate data (all N cases on the diagonal), zero for accuracy no better than chance.

The K-hat metric was adapted from the Cohen's Kappa coefficient used in education and psychology research. Cohen's Kappa is a measure of statistical concordance designed to measure agreement in dichotomous or classification data (Cohen 1960). It was originally developed as a measure of inter-rater reliability and is

generally thought to be a more robust measure of agreement that the simple percentage because Kappa is influenced by a measure of chance agreement.

A variation of Cohen's Kappa is Fleiss' Kappa which was developed to assess agreement between more than two groups (Fleiss 1981). Where Cohen's Kappa only measured two raters, Fleiss' Kappa can utilize multiple raters

There exists a significant level of criticism of the use of the Kappa statistic in both education and psychology (Mclure and Willett 1987) and in mapping and remote sensing (Stehman 1997, 2000). Especially used as a reliable metric of accuracy and quantification in areas outside of subjective scoring of categorical attributes, the use of the Kappa metric may be especially inappropriate. As Stehman (1997) points, adjusting for the level of random agreement may be completely inappropriate in assessing map accuracy.

Because most remote sensing and mapping software packages do not report a significance value with Kappa, to test the null hypothesis in this study, it was necessary to compute Kappa separately in another software application. Cohen's Kappa can be computed in SAS as an option in "Process Frequency" and Fleiss' Kappa can be computed in SAS with the 'magree_macro' (SAS 2002). An alternative significance testing method of calculating the 95 % confidence intervals from the confusion matrix was also used.

For the purposes of this research, a separate raster data layer was created that represents a sample of the areas of known arsenic contamination in the soil. Also, to understand the context of the arsenic contamination with an urban community and to

enable the evaluation of the classifier in a full land cover context, a basic land cover classification was adopted. Reference data were developed from USACE and USEPA soil sampling results and DOQQ data and used to assess the accuracy of each HSI processing method and to create an error matrix for evaluation.

This chapter has presented the details of the analytical methods and statistical tests that were used to evaluate three separate remote sensing systems; historical aerial photographs, laboratory reflectance spectroscopy and HSI/imaging spectroscopy for their ability to provide information in the Spring Valley hazardous waste remediation context. Chapter 5 presents the results of these analyses.

5. Data Analysis and Results

The results of the three main experiments conducted in the course of this research are presented in this chapter along with a discussion of significant findings. This chapter is organized in the following manner. Section 5.1 presents the analysis of the aerial photographic results. Section 5.2 reviews the results of the uptake and stress from the greenhouse experiment. Section 5.3 explains the results of the analysis of laboratory reflectance of the arsenic uptake and stress from the greenhouse data. Section 5.4 examines the results of the processing and classification of HSI of the Spring Valley area.

5.1 Aerial Photographic Interpretation

The purpose of the investigation of aerial photographs was not to provide a rigorous statistical analysis of photographic interpretation results but rather to provide a practical measure, by simple percentage, of the relative value of the information derived from the acquisition and analysis of historical aerial photographs. While the analysis of historical photographs is somewhat subjective and very basic in terms of modern scientific analysis, information derived by this means has a long history of practical value, and sometimes critical significance, to the investigation and remediation of hazardous waste. In 1986, the EPA produced a photographic interpretation report, "Historical Aerial Photographic Analysis, American University, Washington, D.C."

(Stout 1986). The photo-analysis in that report was performed prior to any public knowledge of the nature or extent of the contamination issues in Spring Valley. It was also performed without benefit of the extensive collateral information that has resulted from 15 years of historical research in libraries, archives and historical holdings of American University, the U.S. Federal Government and the government of Washington, D.C.

The photo-analyst, using standard hazardous waste imagery analysis techniques identified 50 features on the 1918 aerial photograph that were of potential relevance to hazardous waste disposal and the current environmental cleanup activities. Figure 21 shows the photographic interpretation features overlaid on the 1918 aerial photograph and Figure 22 shows the same features overlaid on a 1991 image of the Spring Valley area. Figures 23 and 24 depict enlargements of the 1918 aerial image with the photographic interpretation features. These are presented here for improved clarity of the landscape detail.

Eight of the photographic interpretation features identified in the 1986 report were omitted from this analysis because they were provided in the original report for locational context only. These features include: tents, barracks, support buildings, general buildings (B1 - B10), the Weaver Farm House, Massachusetts Avenue and Nebraska Avenue.

Of the remaining 42 features, each was investigated for spatial correlation to any potential environmental contamination or cleanup issue. This was accomplished by digitizing and georeferencing the photographic interpretation features into a vector GIS data layer. Another GIS data layer was created consisting of all known areas of past,

Figure 21. 1918 Aerial Photograph with Photographic Interpretation Features. Potential areas of environmental significance derived from the interpretation of 1918 aerial photographs. Adapted from Stout (1986).

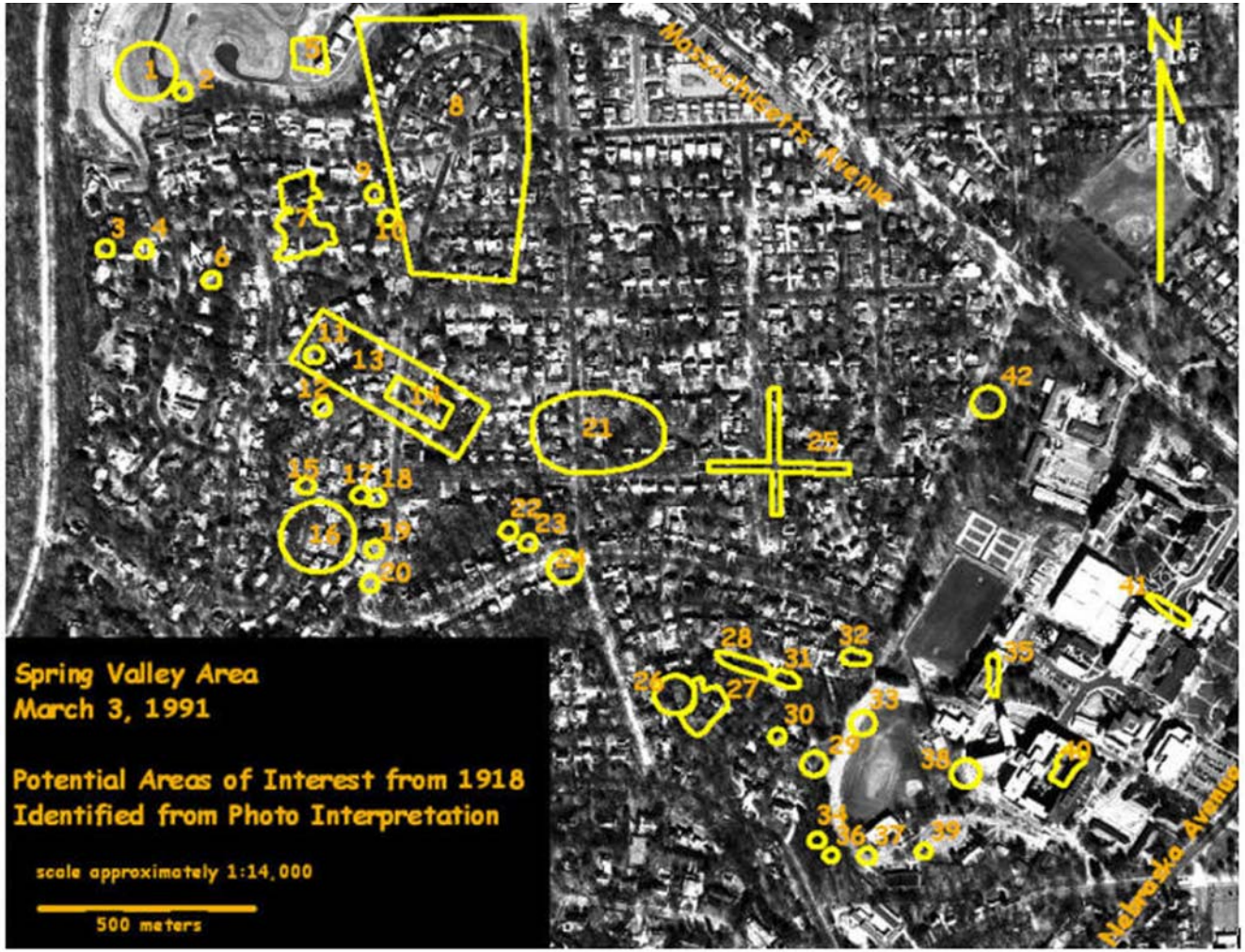

Figure 22. 1991 Aerial Photograph with Photographic Interpretation Features. Potential Areas of Interest derived from the photographic interpretation of 1918 aerial imagery overlaid on a 1991 image of the same area with Geographic Information Systems (GIS) technology. Photo source: USACE 1991.

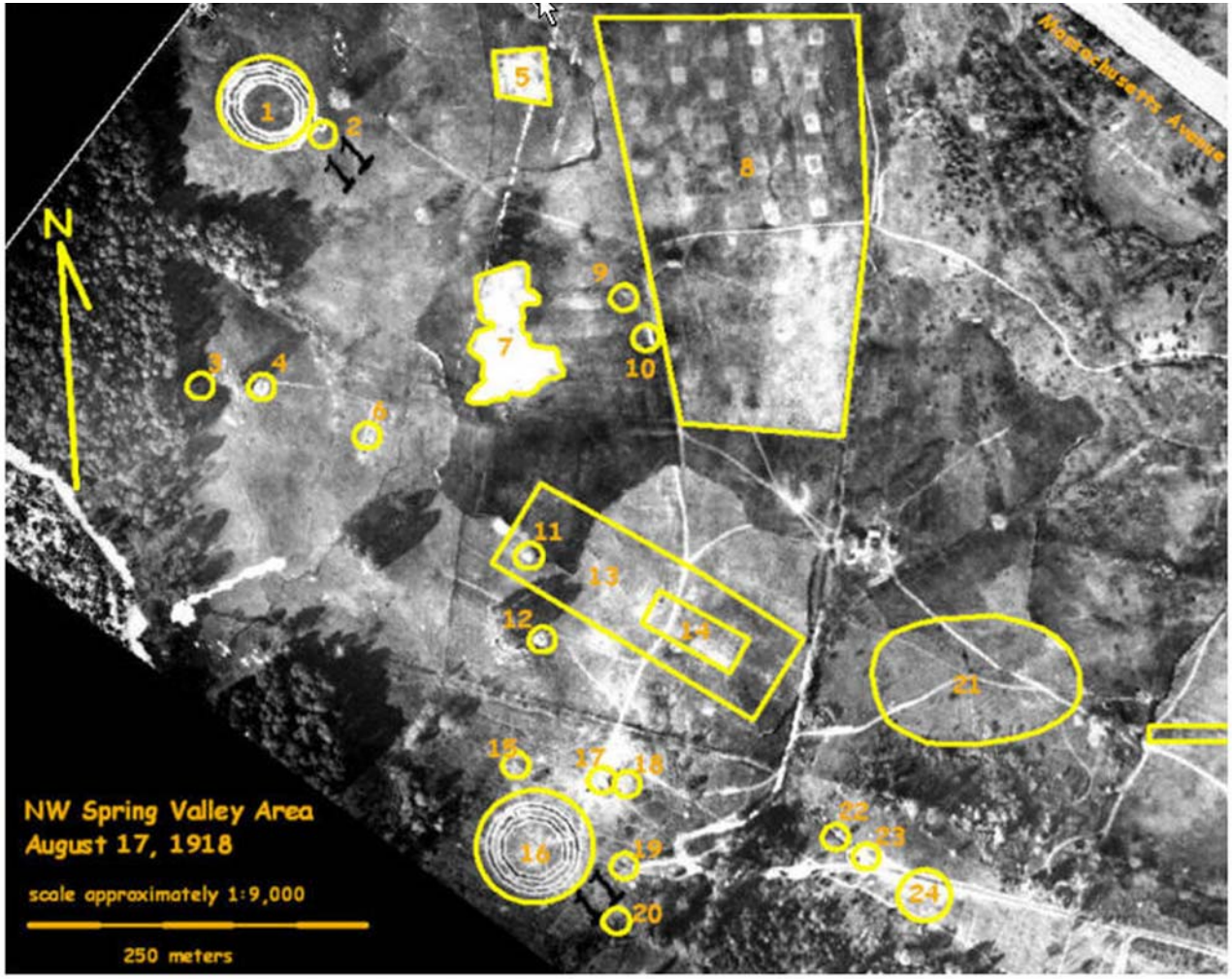

Figure 23. Enlargement of the NW section of the 1918 Aerial Photograph of AUES. Enlargement of the northwest section of the 1918 aerial image along with the key photographic interpretation features. From Stout (1986).

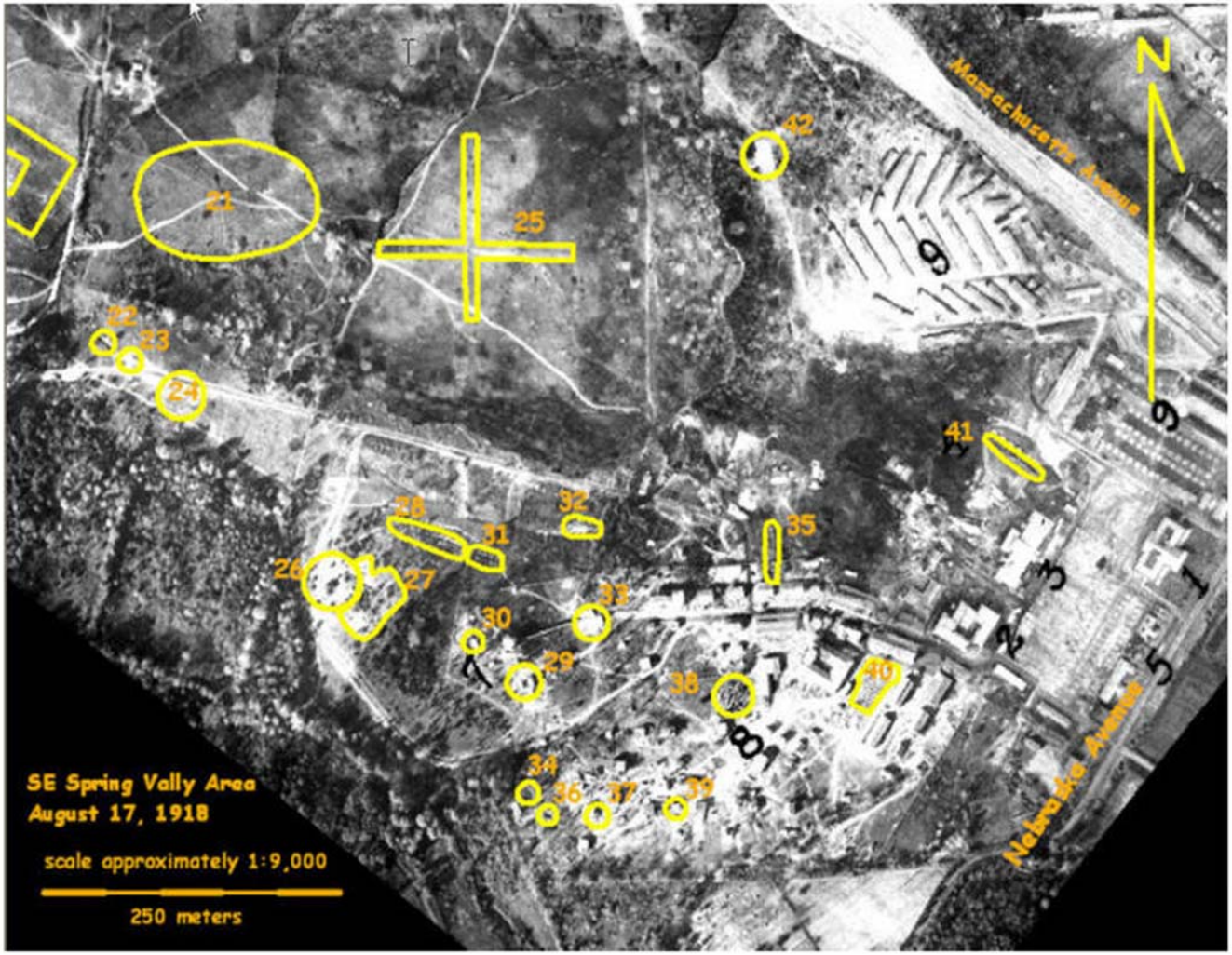

Figure 24. Enlargement of the SE section of the 1918 Aerial Photograph of AUES. Enlargement of the southeast portion of the 1918 aerial image with the key photographic interpretation features. From Stout (1986).

current and future remediation activity. These consisted of (1) all known areas of CW or UXO removal; (2) all known parcels with arsenic levels exceeding the residential standard; (3) any parcels that specialty sampling results showing detectable levels of other (non-arsenic) contaminants of concern; (4) areas of known contextual activities (areas of documented AUES activities, such as animal toxicity testing) that have not been cleared by subsequent investigations; and (5) verified citizen reports of unusual activities, events or documented health problems.

Of the 42 features analyzed, 33, or over 78.5 %, were spatially related to a past or present FUDS cleanup issue. Table 5 lists the site by site analysis and the contamination issue related to each location and Figure 25 shows this graphically.

Fourteen of the photo-identified areas of interest were related to properties of confirmed soil arsenic contamination. The arsenic contamination thresholds currently being utilized in Spring Valley are 20 ppm for residential properties and 43 ppm for all other properties (Parsons 2003).

Ten of the photo-identified features were related to actual ordnance or specific areas of known ordnance testing. Three areas were related to reported human health problems and six areas correlated with known activities of contextual importance, such as animal toxicity testing and chemical persistency testing. One area was related to known mercury and antimony contamination.

Table 5
1918 Aerial Photographic Features and Spring Valley Remedial Activity

Photo-interpreted Features	Feature ID #	Past/Current FUDS Investigation?	Relevant Finding or Remedial Activity
Double Ring of Trenches	1	YES	52nd Court Trench - ER Removal
Pit	2	YES	Soil As & Ordnance / 4700 Block Woodway
Scattered Ground Scars	3	NO	
Possible Test or Target Site	4	NO	
Ground Scar	5	NO	
Possible Firing or Observation Stalls	6	YES	High Soil As / 4000 Block 52nd Street
Smoke	7	YES	Confirmed Smoke Candle & Gas Testing Area
Possible Munition Storage Pads	8	YES	Chemical Persistency Test area / High Soil As
Possible Graded Area	9	YES	AOI 8 / Reported Health Issues
Light-Toned Feature	10	YES	AOI 8 / Reported Health Issues
Possible Target or Test Site	11	YES	Partial Livens Shell Casing
Possible Target or Test Site	12	NO	
Possible Test Area	13	YES	Area of Animal Toxicity Testing / High Soil As
Possible Fence	14	YES	Area of Animal Toxicity Testing / High Soil As
Small Crater Scars	15	YES	AOI Investigation Sedgewick Ground Scars
Double Ring of Trenches	16	YES	Sedgewick Trenches / Several Actions
Probable Structure	17	YES	High Soil As / 5000 Block Sedgewick Street
Possible Pit	18	YES	High Soil As / 5000 Block Sedgewick Street
Possible Pit	19	YES	High Soil As / 4700 Block Fordham Street
Probable Tent Platform	20	YES	High Soil As / 4700 Block Fordham Street
Old Mustard Field	21	YES	High Soil As / 4800 Block Sedgewick Street
Deep Erosion Gully	22	YES	High Soil As / 4900 Block Rodman Street
Turnout	23	NO	
Small Crater Scars	24	YES	High Soil As / 4900 Block Quebec Street
Possible Old Airstrip	25	YES	AOI 1 / Reports of Health Problems
Structures (3)	26	YES	AOI 4 - Magazine Gunpowder Area
Ground Scars	27	YES	AOI 4 - Magazine Gunpowder Area
Trenches	28	YES	Mercury and Antimony Contamination Areas
Shell Pit	29	YES	High Soil As & Ordnance / 4700 Block Woodway
Possible Pit	30	YES	High Soil As & Ordnance / 4700 Block Woodway
Possible Trench	31	YES	High Soil As & Ordnance / 4700 Block Woodway
Small Crater Scars	32	YES	High Soil As / 4900 Block Quebec Street
Concrete Shell Pit	33	YES	Known Ordnance Testing
Probable Vertical Tank	34	YES	High Soil As & Ordnance / 4800 Block Glenbrook
Probable Trench or Ditch	35	NO	
Probable Pit	36	YES	High Soil As & Ordnance / 4800 Block Glenbrook
Stacked Materials	37	YES	High Soil As / American University
Crates	38	YES	High Soil As / American University
Probable Vertical Tank	39	YES	High Soil As / American University
Open Storage Area	40	NO	
Probable Trench or Ditch	41	NO	
Ground Scar	42	NO	

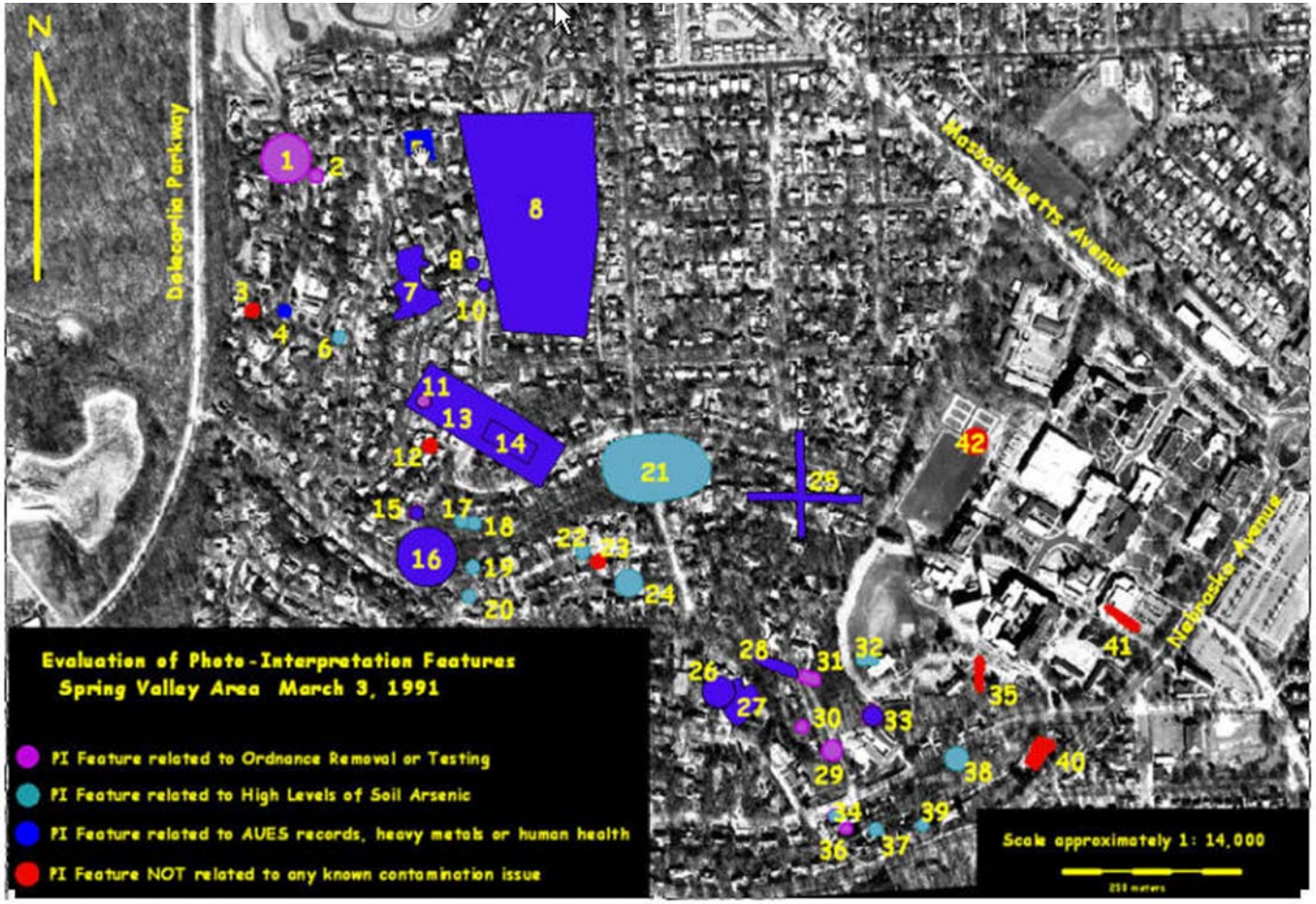

Figure 25. Evaluation of 1918 Aerial Photographic Features and Current Remedial Requirements. The features identified in the 1986 EPA Photo Interpretation Report reconciled against past and present emergency and remedial cleanup activities. Thirty-three out of a total of forty-two features (78.5%) identified by the photo-analyst were later correlated with some type of FUDS environmental cleanup activity, such as high soil arsenic or unexploded ordnance removal. Photo source: USACE 1991

Ongoing photo research and interpretation has also led to the discovery of two additional major contamination areas in Spring Valley that might have been otherwise missed in the normal remedial process. First, the location of an undiscovered ordnance burial pit, located on Glenbrook Road, was identified and mapped from historical aerial and ground photographs. The pit appears on the 1918 photograph and in the 1986 report and a pit was excavated in the same vicinity in 1998. The issue revolved around the question of whether the previously excavated pit and the photo-identified pit were actually the same. After numerous photogrammetric and GIS analyses, the photo-analyst concluded that the previously excavated pit and the photo-identified pit were not one and the same, meaning that another pit likely existed in the general area. After several months of debate among the partnering regulatory agencies (USACE, USEPA and the DCDOH) concerning the location and significance of the aerial photographic evidence, an intrusive ground investigation was undertaken in the summer of 2002 to determine if a third pit did actually exist and presents any risk to human or ecological health in the area.

In the first test pit excavated, WWI-era mortar shells were discovered and over 200 mortar shells have since been located and removed. Subsequent analysis revealed that many of these shells were filled with highly toxic arsine gas. Also, several glass containers filled with chemical warfare agents were also recovered. These items represented a serious environmental hazard and their discovery and remediation removed a potentially major environmental risk from a residential area. Figure 26 shows the pit location on the 1918 and 1991 aerial images and Figure 27 shows examples of the mortar shells and glass containers recovered from the pit.

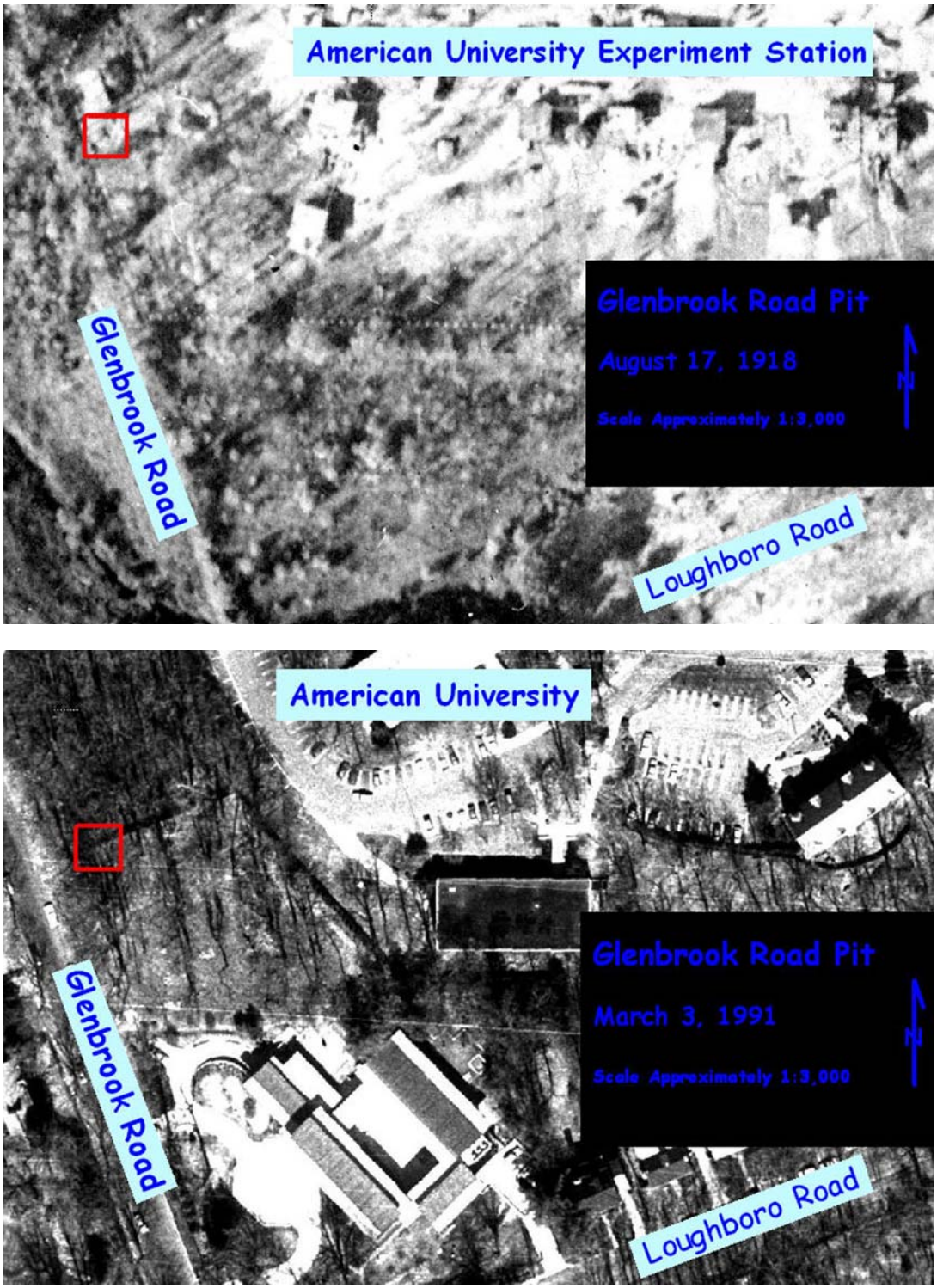

Figure 26. 1918 and 1991 Aerial Photographs of the Glenbrook Road Pit . The discovery of the Glenbrook Road Pit from interpretation and mapping of historical aerial photographs.

Figure 27. Glass Containers and Mortar Shells. WWI glass containers of chemical warfare agents and unexploded 75 mm mortar shells that were discovered in the disposal pit along Glenbrook Avenue. Photographic interpretation played a critical role in the discovery and remediation of this major environmental threat.

Second, in 2004, interpretation of a newly-discovered 1927 aerial photo revealed a series of trails leading to a ravine in the back portion of the American University property. Initial investigations revealed the presence of very high arsenic as well as laboratory glassware and equipment of the WWI era. Subsequent investigations have identified a large landfill area containing chemical laboratory equipment and containers that has yielded confirmed CW materials and other dangerous contaminants. Figure 28 shows an example of the laboratory glassware in the soil and Figures 29 and 30 show the trails and disposal area on both 1927 and 1991 aerial photographs. These trails were present on the imagery in the 1986 report but were not identified as significant, because the general area of the AUES had been razed and small trails were common in the image.

Figure 28. Buried Glass Laboratory Waste from AUES. A piece of glass tubing from one of the AUES chemistry laboratories that was discovered as part of an investigation triggered by the identification of a series of trails on a 1927 aerial photo.

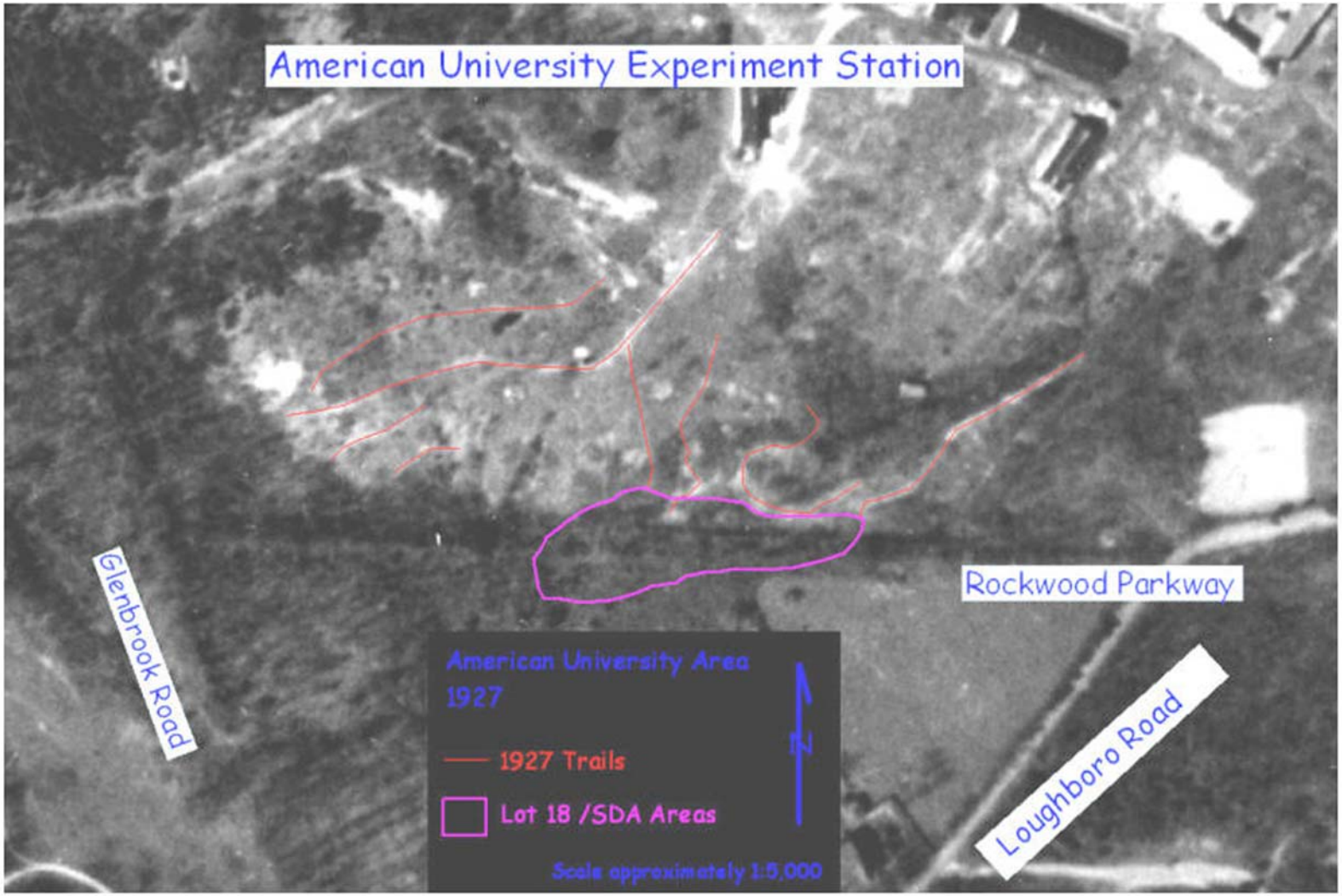

Figure 29. Lot 18 / Small Disposal Area in 1927. Photo interpretation of this 1927 aerial photograph identified several linear foot trails leading to a low-lying area bounded by the AUES, Rockwood Parkway and Glenbrook Road. From Kartman and Slonecker 2001.

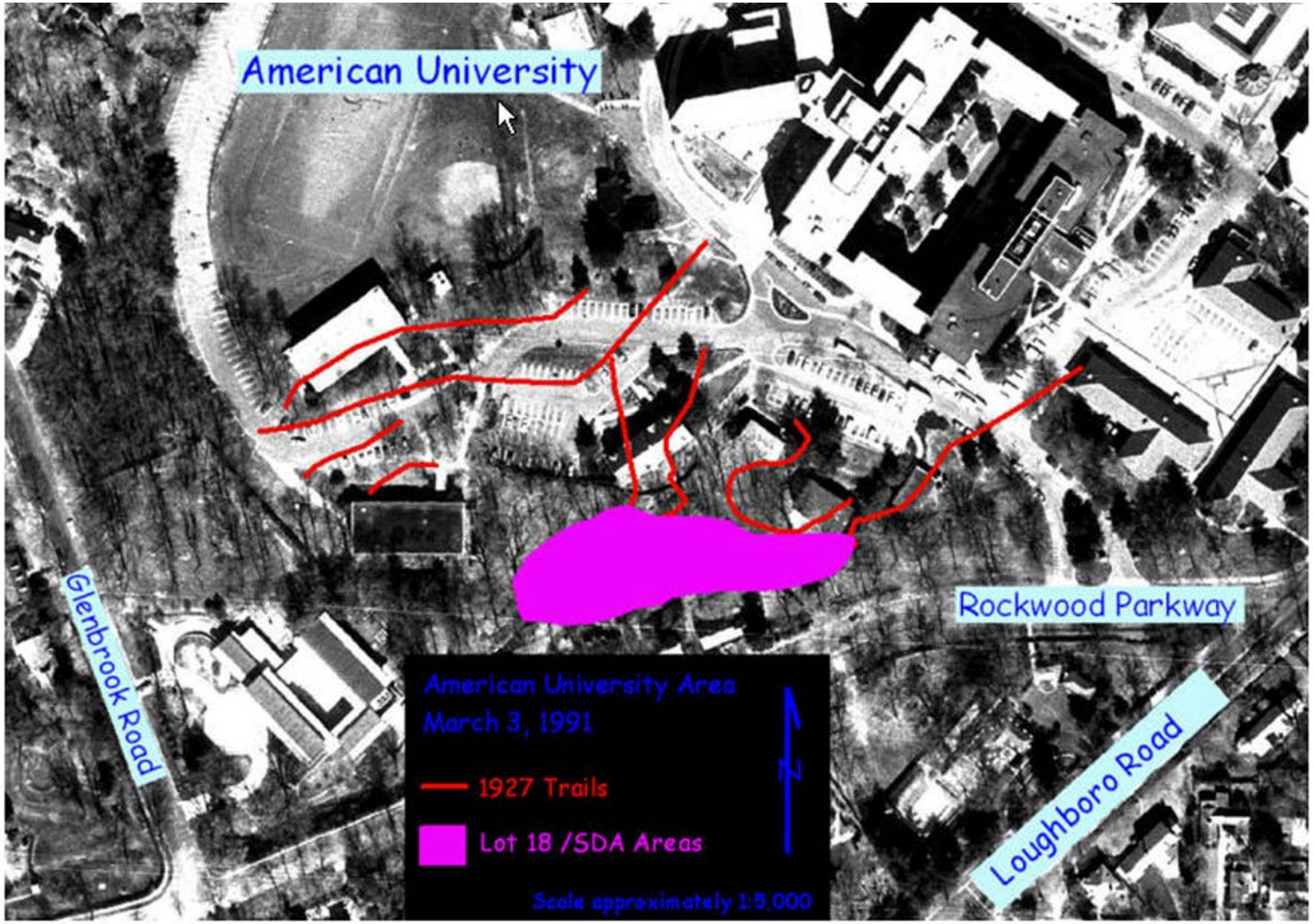

Figure 30. Lot 18 / Small Disposal Area in 1991. The trails from the 1927 aerial photo overlaid on a 1991 aerial photo showing the relationship between the 1927 trails and the large laboratory waste disposal area known as Lot 18. Photo Source: USACE 1991

5.1.1 Summary and Discussion of Aerial Photographic interpretation Results

Although sometimes overlooked in a world of dynamic scientific instrumentation and emerging information processes from sophisticated satellite sensors, historical aerial photographs represent a rich and sometimes invaluable source of landscape level information related to hazardous waste disposal and remediation, or any issue where past activity on the landscape is relevant.

As pointed out by Philipson (1997), the importance of photographic interpretation can not and should not be downplayed or minimized because it is a fundamental information process in itself but, perhaps more importantly, it is the foundation of many sophisticated, digital, remote sensing analysis techniques. A cursory review of current literature reveals numerous applications of photographic/imagery interpretation in providing critical land use and land cover information that includes time frames that predate satellite image availability (Imbernon 1999); verification of computer models predictions of earthquake damage (Marzorati et al. 2003); and as a more reliable method of developing specific landscape metrics in describing holistic aspects of complex landscapes (Antrop and Eetvelde 2000).

In this application in Spring Valley, information derived from the interpretation of historical aerial photographs was directly responsible for the discovery and removal of several serious risks to human and ecological health and these sites might still be undiscovered if it had not been for the utilization and interpretation of this basic form of information.

Also, used as a screening tool in the early stages of a remedial investigation, a 78.5 % correlation with specific areas and conditions that will eventually require remedial action, could make this type of information a very cost-effective screening tool in a time when resources for environmental cleanups are dwindling. A more detailed scientific investigation of the relationship between information derived from historical imagery interpretation and confirmed hazardous waste conditions across a statistically significant sample of hazardous waste sites, could reveal a quantifiable level of information confidence related to human and ecological risk. Additionally, it could facilitate a cost-benefit type of economic analysis that could document efficiencies and cost savings over other investigative techniques. Finally, a study of the effectiveness of information provided by aerial photographic interpretation could underscore the need to invest in archival sciences and preserve invaluable sources of historical photographic information.

5.2 Plant Growth and Arsenic Uptake

To study the spectral response of arsenic uptake and stress, 100 plants of each of three ferns, *Pteris multifida, Pteris cretica mayii* and *Nephrolepis exaltata* were grown in greenhouse conditions in soils amended with sodium arsenate in concentrations of 0, 20, 50, 100 and 200 ppm. Two common lawn grass species, fescue and rye, were also grown in identical soil, arsenic and greenhouse conditions. Plants were harvested at 4-week intervals, dried and tested for arsenic concentration by standard acid digestion and ICP/AES methods.

5.2.1 Fern Uptake Results

Plant growth in soils contaminated with arsenic is generally inhibited and the effects range from depressed biomass production to extreme toxicity (Eisler 1994). The *Nephrolepis exaltata* control fern showed moderate to severe symptoms of phytotoxicity, including chlorosis, diminished growth, leaf necrosis and plant death and these symptoms increased with the soil arsenic concentration. The *Pteris* ferns showed a pattern of decreased biomass as arsenic concentrations increased. In all ferns and grasses, including the *Pteris* ferns, there was a general inverse relationship between the soil arsenic concentration and the plant biomass at harvest. See Figures 31 and 32. Tables 6, 7 and 8 show the results of the chemical analysis for arsenic for each of the three fern species over the entire study period. Summary statistical results for Tables 6, 7 and 8 are located in Appendix B.

Figure 31. Arsenic Concentration and Biomass. *Nephrolepis Exaltata* ferns at 8 weeks in soil/arsenic concentrations of (from left to right) 0, 20, 50, 100 and 200 ppm, showing the general effect of soil arsenic on plant growth.

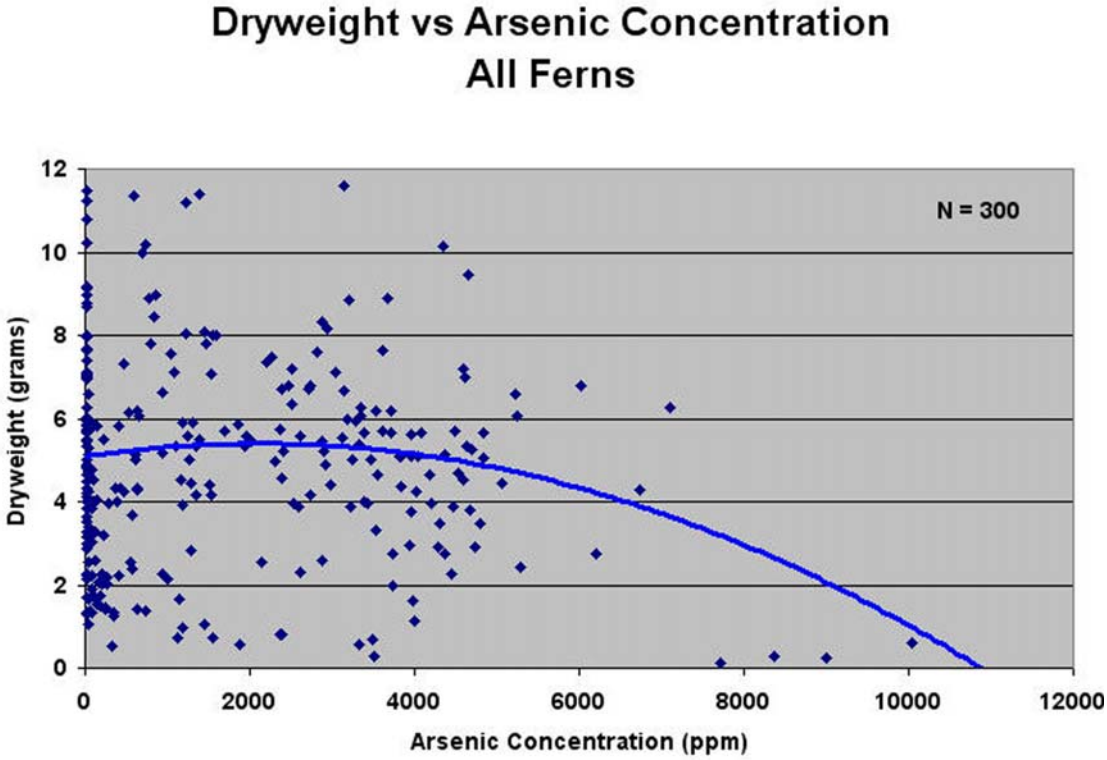

Figure 32a. Arsenic concentration and dryweight. The general inverse relationship between arsenic and plant biomass for all ferns in this study.

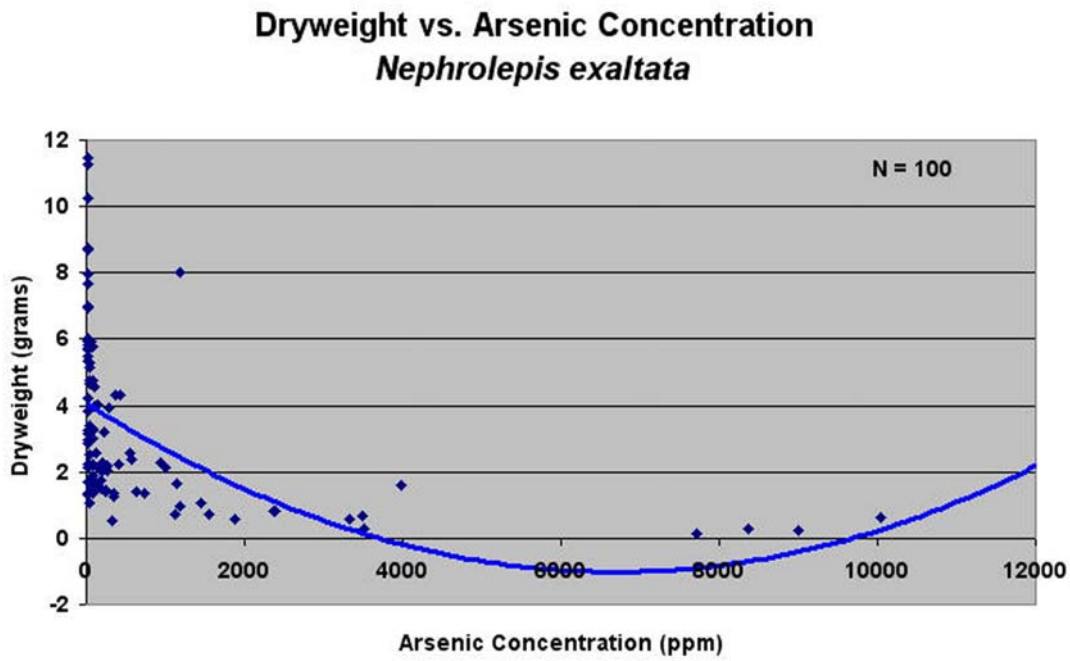

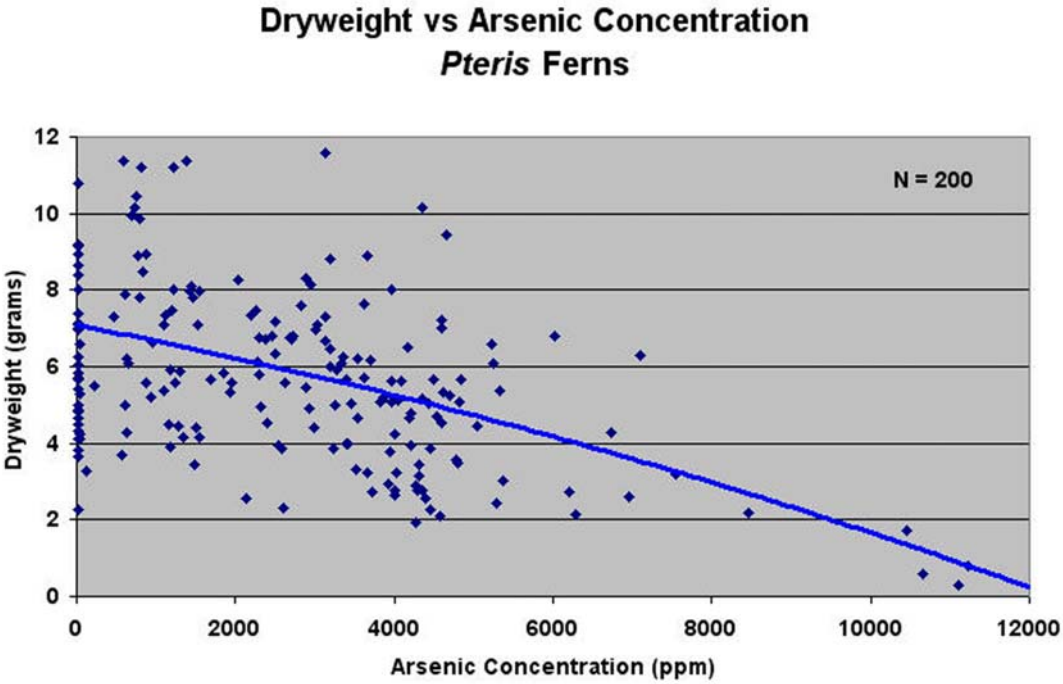

Figure 32b. Arsenic concentration and dryweight. The general relationships between arsenic and plant biomass for the non-accumulating control fern, *Nephrolepis exaltata* and for the two hyperaccumulating *Pteris* species.

Table 6
Summary Results for *Nephrolepis exaltata*

Plant Species	Soil As (ppm)	Harvest Week	Frond As	SE	Biomass (g DW)	SE	Bioconc Factor
Nephrolepis exaltata	0	4	ND	NA	2.29	0.91	NA
		8	ND	NA	4.32	1.70	NA
		12	ND	NA	6.46	0.61	NA
		16	ND	NA	9.22	1.54	NA
		20	ND	NA	9.21	1.83	NA
	20	4	33	14	1.56	0.50	1.83
		8	33	12	3.01	0.38	1.83
		12	28	4	5.38	0.49	1.56
		16	67	25	4.66	1.23	3.72
		20	19	9	5.08	0.76	1.06
	50	4	64	27	1.90	0.77	1.88
		8	143	74	2.72	0.66	4.21
		12	78	27	4.82	0.73	2.29
		16	181	132	3.29	1.04	5.32
		20	241	151	3.20	1.50	7.09
	100	4	508	694	1.34	0.44	7.94
		8	649	457	1.45	0.64	10.14
		12	509	152	2.57	1.05	7.95
		16	467	364	2.59	1.18	7.30
		20	1422	700	1.22	0.37	22.22
	200	4	248	70	1.54	0.36	1.36
		8	5695	3532	0.36	0.15	31.12
		12	4920	4938	1.01	0.42	26.89
		16	5179	6872	0.57	0.06	28.30
		20	4036	2605	2.35	3.78	22.05

Table 7
Summary Results for *Pteris cretica mayii*

Plant Species	Soil As (ppm)	Harvest Week	Frond As	SE	Biomass (g DW)	SE	Bioconc Factor
Pteris cretica mayii	0	4	ND	NA	4.99	1.59	NA
		8	ND	NA	5.14	2.30	NA
		12	ND	NA	7.37	2.17	NA
		16	ND	NA	6.86	1.17	NA
		20	ND	NA	6.37	2.01	NA
	20	4	887	400	4.57	0.60	49.28
		8	1326	577	5.04	2.18	73.67
		12	743	405	5.70	0.92	41.28
		16	1025	370	6.07	2.01	56.94
		20	670	76	6.06	2.01	37.22
	50	4	1157	959	5.40	1.64	34.03
		8	1625	749	4.91	0.87	47.79
		12	2359	589	4.37	0.45	69.38
		16	2806	1193	5.72	2.63	82.53
		20	1868	620	6.06	1.57	54.94
	100	4	2725	1071	3.54	2.17	42.58
		8	3463	574	5.71	1.58	54.11
		12	4138	401	4.56	1.27	64.66
		16	5584	1322	5.54	1.86	87.25
		20	3792	350	3.99	1.05	59.25
	200	4	3428	398	3.55	1.64	18.73
		8	3727	490	3.76	0.22	20.37
		12	4894	329	5.14	1.22	26.74
		16	4436	605	5.46	2.58	24.24
		20	4009	264	3.77	1.14	21.91

Table 8
Summary Results for *Pteris multifida*

Plant Species	Soil As (ppm)	Harvest Week	Frond As	SE	Biomass (g DW)	SE	Bioconc Factor
Pteris multifida	0	4	ND	NA	4.19	0.86	NA
		8	ND	NA	5.00	0.49	NA
		12	ND	NA	7.07	1.86	NA
		16	ND	NA	6.62	2.45	NA
		20	26	13	6.11	3.17	NA
	20	4	1097	376	5.59	2.15	60.94
		8	1322	189	6.30	1.63	73.44
		12	837	289	7.66	1.35	46.50
		16	1053	363	8.46	3.38	58.50
		20	843	155	12.67	3.01	46.83
	50	4	2415	292	5.29	0.90	71.03
		8	3189	677	6.77	1.23	93.79
		12	3095	787	6.21	0.88	91.03
		16	2702	623	6.04	0.56	79.47
		20	1830	549	8.09	2.09	53.82
	100	4	3684	592	4.38	1.50	57.56
		8	3659	1098	5.53	1.00	57.17
		12	4079	780	6.13	1.83	63.73
		16	4058	1898	6.24	1.42	63.41
		20	3498	753	6.28	0.78	54.66
	200	4	3790	1138	4.52	1.40	20.71
		8	5510	1675	6.29	1.45	30.11
		12	4723	1074	7.81	3.42	25.81
		16	3707	1025	7.87	2.96	20.26
		20	4441	736	4.29	1.67	24.27

Both *Pteris* ferns displayed significant uptake of arsenic at the first 4-week harvest and consistently throughout the study. At the 200-ppm soil concentration, the control fern *Nephrolepis exaltata* showed significant concentrations of frond arsenic beginning at the 8-week harvest and through the rest of the study. However, as the *Nephrolepis exaltata* fern was generally displaying symptoms of phytotoxicity at the 200 ppm soil concentration, the plant arsenic concentrations are probably due to processes and effects other than uptake alone. Figures 33–35 show the arsenic concentration and total arsenic removed for each fern species.

The *Pteris* ferns are known to concentrate arsenic in the fronds and the harvested frond arsenic concentrations generally correlated with the soil arsenic concentration for both *Pteris multifida* ($r^2 = .55$) and *Pteris cretica mayii* ($r^2 = .57$). There were some notable exceptions. *Pteris cretica mayii,* at the 8- and 16-week harvests, and the *Pteris multifida* at the 16- and 20-week harvests, both show that either arsenic concentration or total arsenic was higher at the 100 ppm soil level than the 200 ppm soils, suggesting that there may be an upper boundary for soil arsenic concentrations and conditions between 100 and 200 ppm and that there are species-specific differences in uptake rate and tolerance between *Pteris* species.

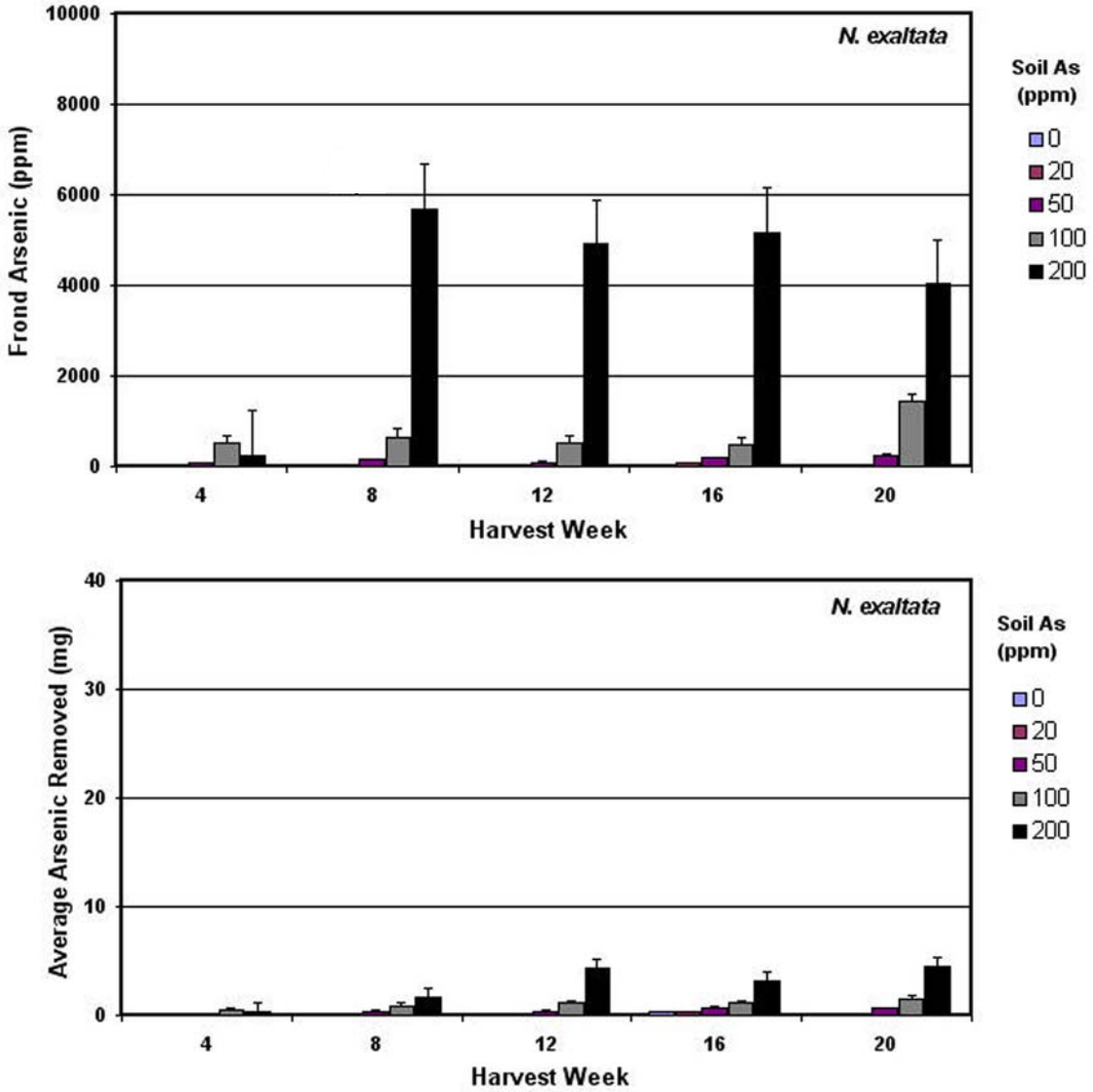

Figure 33. Arsenic Uptake Summary for *Nephrolepis exaltata.* Arsenic concentration and content in the control fern *Nephrolepis exaltata* in this study. One of the surprising results was the consistently high frond arsenic concentrations of *Nephrolepis exaltata* ferns grown in the 200 ppm arsenic/soil concentration. Whiskers show the standard error.

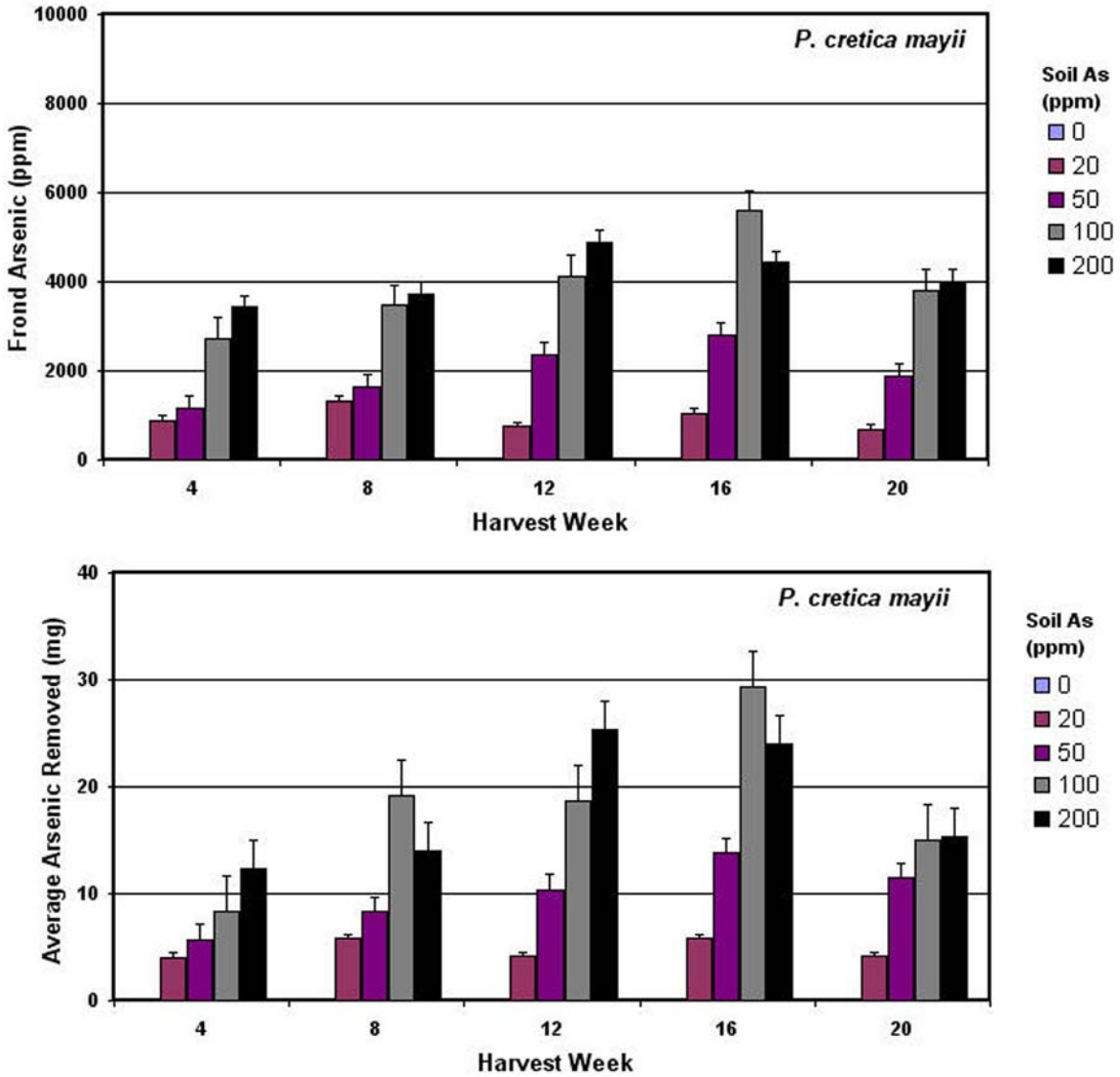

Figure 34. Arsenic Uptake Summary for *Pteris cretica mayii.* Arsenic concentration and content in the arsenic-hyperaccumulating fern *Pteris cretica mayii*. Peak concentration and content were observed after 16 weeks and, in several cases, *Pteris cretica mayii* seemed to accumulate more arsenic from the 100 ppm concentration than the 200 ppm concentration.

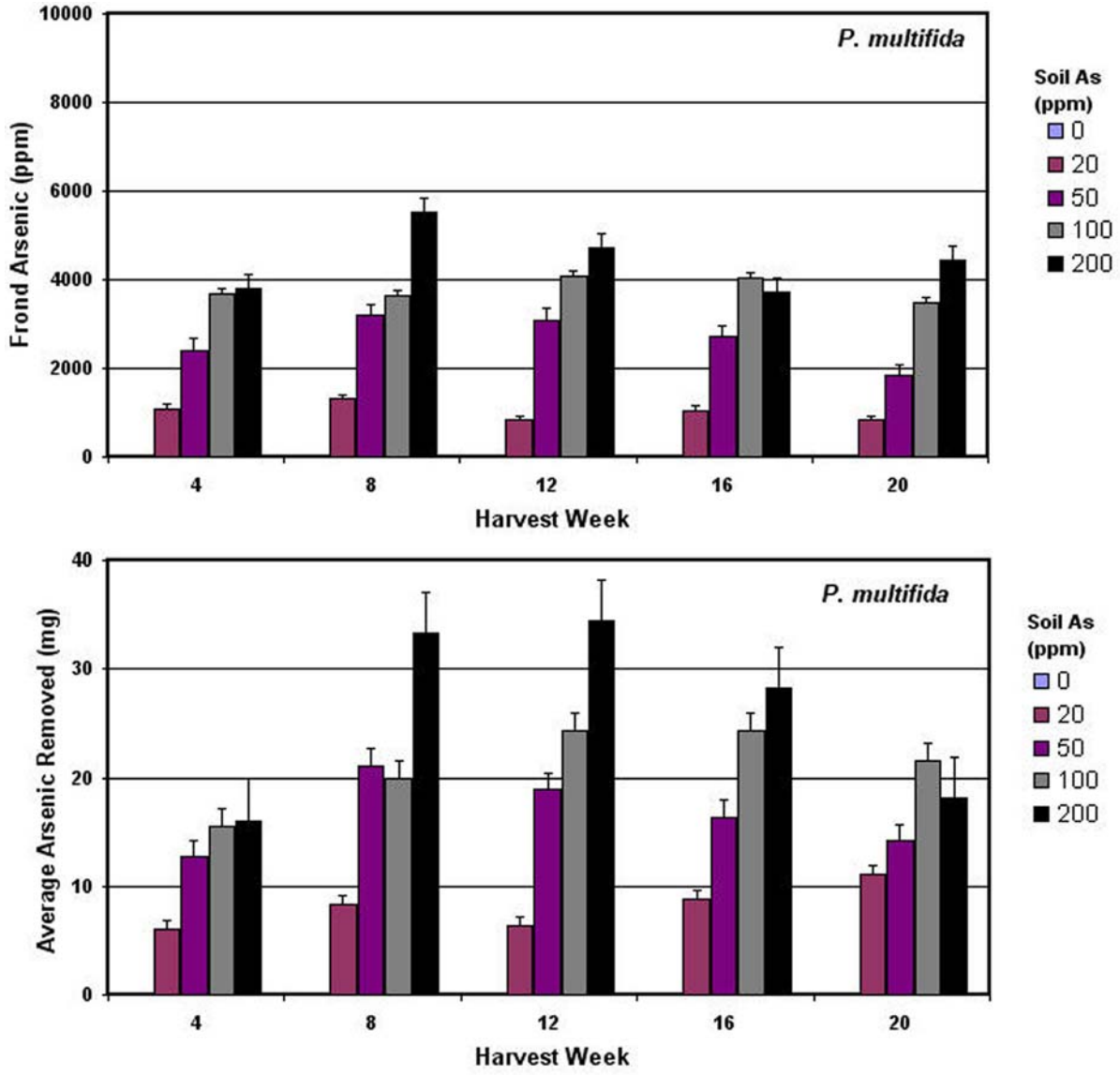

Figure 35. **Arsenic Uptake Summary for *Pteris multifida*. Arsenic concentration and content in the arsenic-hyperaccumulating fern *Pteris multifida*. Peak concentration and content were observed between eight and 12 weeks and, like, *Pteris cretica mayii* accumulated more arsenic from the 100 ppm concentration than from the 200 ppm concentration in some cases.**

On the final fern harvest at 20 weeks, the roots of the ferns were also collected and tested for arsenic concentration using the same methods as the fronds. Results showed that *Nephrolepis exaltata, Pteris cretica mayii* and *Pteris multifida* had root arsenic levels of 154, 701 and 776 ppm respectively. Figure 36 shows the distribution of root/frond arsenic levels for all three ferns for the 200 ppm soil level at 20 weeks.

The root/frond distribution of arsenic in the *Pteris* species is consistent with previously published results by Bondata and Ma (2003), Srivastava et al. (2006) and Wei and Chen (2006). One of the working definitions of a hyperaccumulating plant is the ability to rapidly translocate a metal or metalloid from the roots to the above ground biomass.

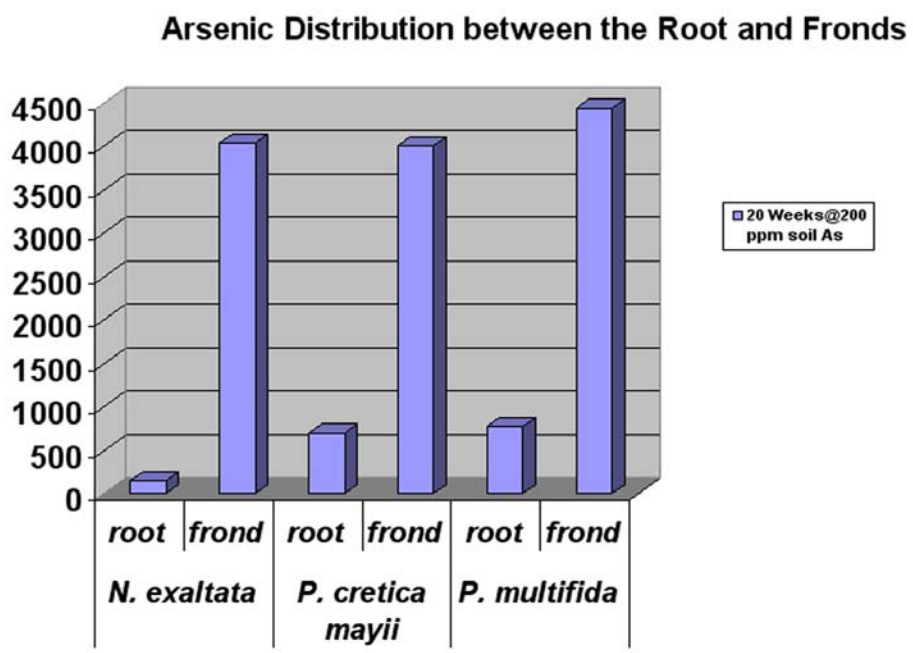

Figure 36. Root/Frond Arsenic Distribution. Arsenic concentration in the roots and fronds of the three fern species. *Nephrolepsis exaltata* was near death for all replicates.

5.2.2 Grass Uptake and Stress Results

The two grass species, fescue and rye, sprouted from seed, generally showed moderate to severe symptoms of phytotoxicity, including chlorosis, diminished growth, leaf necrosis and plant death. In the 200 ppm arsenic soil concentration, neither of the grass species sprouted or grew to any appreciable degree. In the 100 ppm arsenic soil concentration only one replicate of each grass species grew and survived for 20 weeks.

Significant concentrations of arsenic were observed in the grass samples that were harvested at 16 and 20 weeks. However, at the 100 ppm soil arsenic level, all plants of both species were showing signs of extreme stress and, like the *Nephrolepis exaltata* ferns at the 200 ppm arsenic soil concentration, the resultant levels of arsenic detected by analysis are probably related to processes other than normal plant uptake.

5.2.3 Summary and Discussion of Greenhouse Results

Although previously reported by Wei and Chen (2006), Wang et al. (2006) and others, this study reconfirms that *Pteris cretica mayii* and *Pteris multifida* are arsenic hyperaccumulators. Both *Pteris* ferns achieved frond arsenic concentrations in excess of 5,000 ppm with no visual phytotoxic effects, although decreased biomass was observed at the 200 ppm soil arsenic level. The *Pteris multifida* ferns removed more arsenic than the *Pteris cretica mayii* ferns. The maximum level of frond arsenic concentration was achieved at 8 weeks for *Pteris multifida* and at 16 weeks for *Pteris cretica mayii* suggesting individual species differences in arsenic uptake. Also, at several harvests, both species showed that the maximum concentration of frond arsenic and/or the

maximum total arsenic was higher in the 100 ppm soil arsenic category than in the 200 ppm soil arsenic category, suggesting that there may be a upper limit for optimal arsenic hyperaccumulation for both species in the 100 to 200 ppm soil arsenic concentration range.

The control fern *Nephrolepis exaltata* and the rye and fescue turf grasses showed extreme phytotoxic effects in soil arsenic levels of 100 ppm or greater. Significant concentrations of arsenic were detected in the fronds of *Nephrolepis exaltata* growing in the 200 ppm soil arsenic concentration but with decreased biomass and with extreme phytotoxic effects.

Even though there was significant uptake of arsenic by both *Pteris* ferns, they still were negatively affected by arsenic uptake and there was a general negative relationship between fern biomass (dry weight) and frond arsenic concentration.

5.3 Greenhouse Spectral Analysis

Reflectance spectra of all ferns and grasses were collected at 4-week intervals prior to harvesting for chemical analysis. Spectra were collected with an ASD full range spectroradiometer under controlled light conditions. Reflectance spectra of all ferns and grasses grown in the laboratory study were analyzed to establish predictive relationships between soil and plant arsenic and plant spectral reflectance parameters as expressed in either enhanced growth or stress effects. Spectra for each individual fern in each of the three species was summarized in spreadsheets showing the laboratory control values, plant dry weight, arsenic concentration, arsenic content and the 2,151 spectral values representing 1 nm wavelength increments of the solar visible wavelength range of 350 - 2,500 nm. Figure 37 shows an example spreadsheet and graph of the basic management of spectral data.

Spectral analysis was conducted with three statistical methods including simple correlation analysis, PLS regression and SLR. All statistical analyses were conducted with SAS, version 9.0 (The SAS Institute, Apex, North Carolina) software, and SYSTAT 10 (SPSS Inc., Cambridge, Massachusetts).

Three tracks were investigated for establishing predictive relationships between spectral response and arsenic concentration: (1) reflectance spectra, (2) derivative spectra, and (3) spectral indices. Because of the highly correlative nature of hyperspectral data, analysis presents special statistical problems with autocorrelation and two statistical techniques, PLS and SLR have emerged in the literature as successful approaches for the

	A	B	C	D	E	F	G	H	I	J	K	L	M
1													
2			Harvest	Plant	Soil					Arsenic	Arsenic	Bioconc	Reflectance
3	Lab #	edenlog	Week	Species	As	Replicate	DW	Dig.W	Dilution	Uptake	Removed	Factor	Spectra File
20	9917599	ME04-0439	8	*N. exaltata*	100	D	1.48	0.25	1	184	0.27	183.50	NE_100_HW8_T58D
21	9917600	ME04-0440	8	*N. exaltata*	200	A	0.28	0.25	1	8,377	2.35	8376.70	NE_200_HW8_T58A
22	9917601	ME04-0441	8	*N. exaltata*	200	B	0.3	0.25	1	3,519	1.06	3519.20	NE_200_HW8_T58B
23	9917602	ME04-0442	8	*N. exaltata*	200	C	0.26	0.25	1	9,005	2.34	9004.80	NE_200_HW8_T58C
24	9917603	ME04-0443	8	*N. exaltata*	200	D	0.58	0.25	1	1,880	1.09	1880.30	NE_200_HW8_T58D
25	9917604	ME04-0444	8	*P. mayii*	0	A	4.322	0.25	1	25	0.11	25.00	PCM_0_HW8_T58A
26	9917605	ME04-0445	8	*P. mayii*	0	B	2.25	0.25	1	25	0.06	25.00	PCM_0_HW8_T58B
27	9917606	ME04-0446	8	*P. mayii*	0	C	7.02	0.25	1	25	0.18	25.00	PCM_0_HW8_T58C
28	9917607	ME04-0447	8	*P. mayii*	0	D	6.96	0.25	1	25	0.17	25.00	PCM_0_HW8_T58D
29	9917608	ME04-0448	8	*P. mayii*	20	A	2.55	0.25	1	2,136	5.45	2135.70	PCM_20_HW8_T58A
30	9917609	ME04-0449	8	*P. mayii*	20	B	4.46	0.25	1	1,286	5.74	1286.30	PCM_20_HW8_T58B
31	9917610	ME04-0450	8	*P. mayii*	20	C	5.35	0.25	1	1,094	5.85	1094.10	PCM_20_HW8_T58C
32	9917611	ME04-0451	8	*P. mayii*	20	D	7.79	0.25	1	789	6.15	789.10	PCM_20_HW8_T58D
33	9917612	ME04-0452	8	*P. mayii*	50	a	5.32	0.25	1	1,934	10.29	1934.00	PCM_50_HW8_T58A
34	9917613	ME04-0453	8	*P. mayii*	50	B	4.97	0.25	1	2,309	11.47	2308.50	PCM_50_HW8_T5CB
35	9917614	ME04-0454	8	*P. mayii*	50	C	3.68	0.25	1	569	2.09	568.80	PCM_50_HW8_T58C
36	9917615	ME04-0455	8	*P. mayii*	50	D	5.68	0.25	1	1,690	9.60	1690.20	PCM_50_HW8_T58D
37	9917616	ME04-0456	8	*P. mayii*	100	A	3.94	0.25	1	4,213	16.60	4212.90	PCM_100_HW8_T58A
38	9917617	ME04-0457	8	*P. mayii*	100	B	7.6	0.25	1	2,820	21.43	2820.20	PCM_100_HW8_T5CB
39	9917618	ME04-0458	8	*P. mayii*	100	C	6.27	0.25	1	3,352	21.02	3352.10	PCM_100_HW8_T58C
40	9917619	ME04-0459	8	*P. mayii*	100	D	5.02	0.25	1	3,465	17.39	3465.00	PCM_100_HW8_T58D
41	9917620	ME04-0460	8	*P. mayii*	200	A	3.46	0.25	1	4,304	14.89	4303.50	PCM_200_HW8_T58A
42	9917621	ME04-0461	8	*P. mayii*	200	B	3.76	0.25	1	3,950	14.85	3949.60	PCM_200_HW8_T58A
43	9917622	ME04-0462	8	*P. mayii*	200	C	3.86	0.25	1	3,234	12.48	3234.20	PCM_200_HW8_T58A
44	9917623	ME04-0463	8	*P. mayii*	200	D	3.97	0.25	1	3,420	13.58	3419.90	PCM_200_HW8_T58A
45	9917624	ME04-0464	8	*P. multifida*	0	A	4.87	0.25	1	25	0.12	25.00	PMF_0_HW8_T58A
46	9917625	ME04-0465	8	*P. multifida*	0	B	4.47	0.25	1	25	0.11	25.00	PMF_0_HW8_T58B

	A	B	C	D	E	F	G	H	I
1	Spectra File	PCM_0_HW4_T31D	PCM_20_HW4_T31D	PCM_50_HW4_T31D	PCM_100_HW4_T31D	PCM_200_HW4_T31D	PCM_0_HW8_T58A	PCM_0_HW8_T58B	PCM_0_HW8_T58C
2	Lab #	9917465	9917477	9917489	9917501	9917513	9917604	9917605	9917606
3	edenlog	ME04-0314	ME04-0326	ME04-0338	ME04-0350	ME04-0362	ME04-0444	ME04-0445	ME04-0446
4	DW (g)	3.26	3.91	3.94	2.31	4.00	4.322	2.25	7.02
5	Frond As	125	1189	2539	2602	3396	25	25	25
6	As Removed	0.41	4.65	10.00	6.01	13.58	0.11	0.06	0.18
7	350	4.67	-4.65	0.05	7.26	0.78	6.69	5.47	-3.31
8	351	5.91	2.84	-21.18	-17.73	1.59	-0.19	-0.81	0.43
9	352	5.93	3.29	-24.20	-22.05	2.89	-5.89	-5.36	-2.06
10	353	4.79	0.60	-11.72	-8.99	4.59	-10.91	-8.72	-7.48
11	354	5.20	4.39	-3.73	11.48	6.26	-16.38	-7.24	-4.64
12	355	10.43	13.22	-1.47	11.64	6.33	-12.95	-3.52	-2.29
13	356	15.06	18.21	-0.51	7.50	8.49	-7.18	1.45	-0.48
14	357	16.88	13.82	1.99	9.62	17.23	-2.21	6.45	1.00
15	358	9.16	6.71	3.86	7.95	11.95	2.44	3.71	-0.62
16	359	2.92	2.01	4.63	6.84	6.01	2.41	0.95	-2.65
17	360	2.73	2.68	4.15	7.35	4.63	-5.11	0.65	-4.26
18	361	2.80	3.64	3.87	5.67	5.02	-3.42	2.15	-0.94
19	362	2.38	3.95	2.39	4.97	5.39	-1.64	2.14	0.04
20	363	1.87	3.86	-0.35	5.34	5.51	-0.05	1.17	-0.42
21	364	4.29	5.16	1.34	7.41	3.47	1.98	1.49	2.13
22	365	4.02	4.62	1.63	8.07	3.54	1.73	1.54	3.00
23	366	2.75	3.13	1.89	8.10	4.51	0.26	1.26	2.54
24	367	2.64	1.57	3.63	8.36	5.08	-1.88	0.34	0.32
25	368	3.07	2.46	3.48	9.58	6.90	-1.68	0.24	-0.77
26	369	2.92	3.12	2.70	10.97	7.70	-0.60	0.86	-0.95
27	370	1.50	2.23	1.64	12.12	6.31	0.97	2.34	-0.11
28	371	5.00	2.89	2.55	10.70	5.45	2.31	3.23	1.09
29	372	5.90	3.33	2.86	8.69	5.26	2.77	3.12	1.30

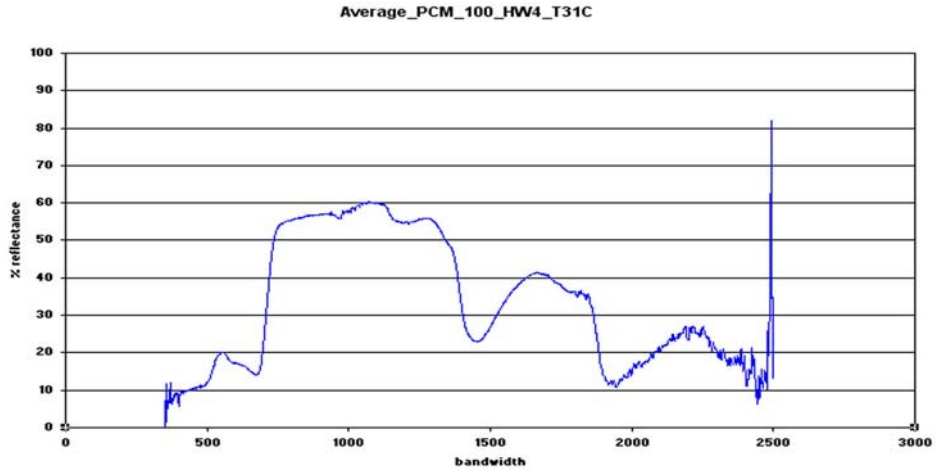

Figure 37. Spectral Data in Spreadsheet Format. The basic management of laboratory and spectral data through spreadsheet software.

analysis of hyperspectral data, especially as it relates to vegetation (Hansen et al. 2002; Kooistra et al. 2004; Schmidtlein 2005).

Each of the three fern species-specific data sets, collected at 4-week intervals, resulted in 85 individual plant observations and 2,151 spectral values for each observation. As an initial data mining step, the spectral values for each band were correlated against the known arsenic concentration and content for each plant. Figure 38 shows the results of this analysis for all three fern species. Although none of the correlation coefficients show a strong relationship, it is still evident that there is a pattern between plant arsenic and wavelength that is likely related to basic photosynthetic processes. Several key peaks and valleys in this spectral range are located in areas of known plant phenomena.

The fern that was most efficient at arsenic uptake, *Pteris multifida*, shows the least amount of spectral variation and *Nephrolepis exaltata*, the non-accumulating fern, shows the greatest amount of spectral variation. Each of the ferns shows a negative correlation in the area of 530 nm (green reflectance peak) and a positive correlation at 680 nm (red light absorption). Other spectral areas of potential interest include a trough at 750 nm, commonly referred to as the "Red Edge" and related to plant stress. Shoulders near 980 nm and 1,180 nm are likely related to leaf or atmospheric water. Peaks near 1,460 nm and 1,950 nm probably also relate to atmospheric water vapor absorption and

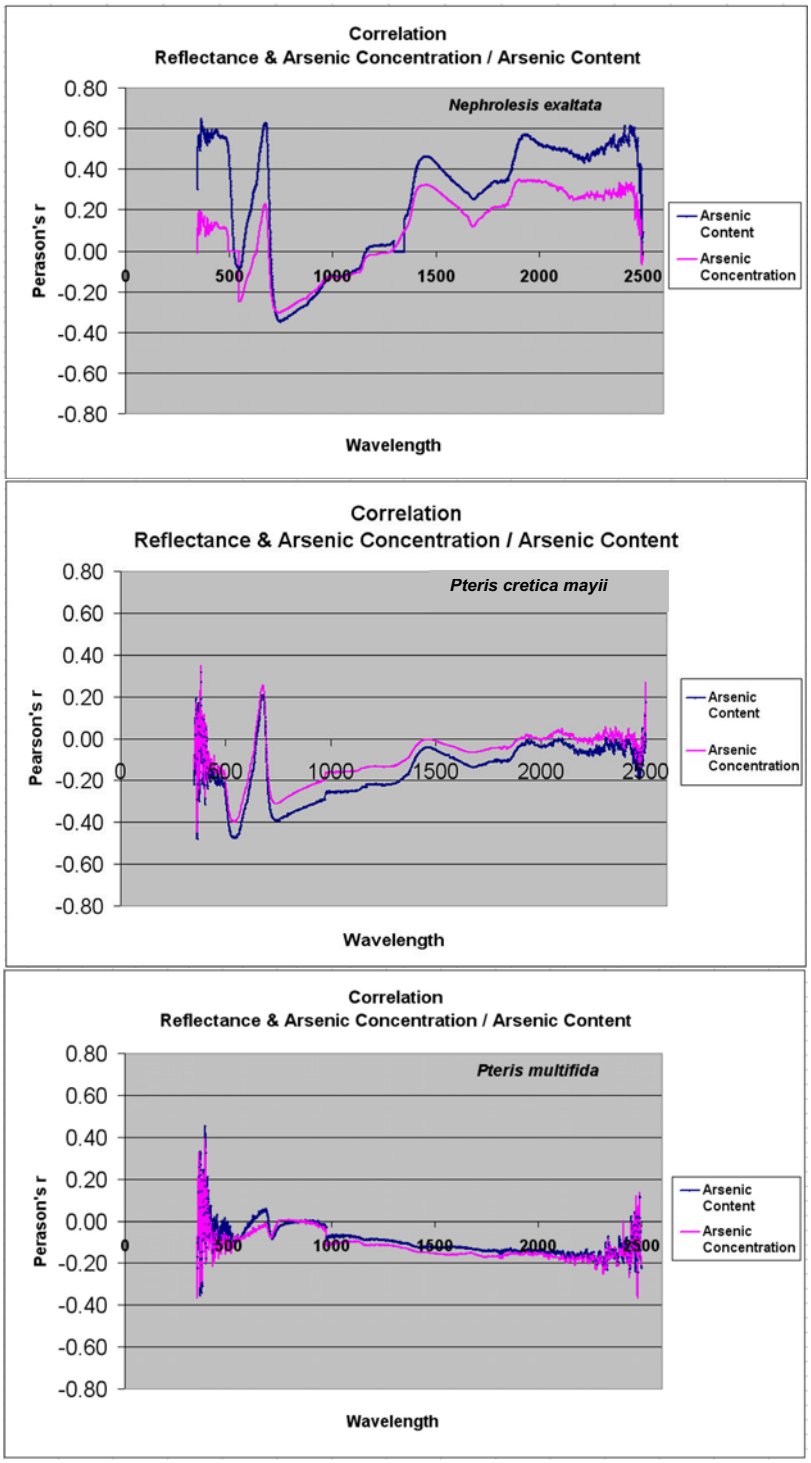

Figure 38. The Spectra - Arsenic Correlations. The first data visualization investigates the correlation between spectral bands and arsenic concentration and content, that shows the areas of the spectrum that might be sensitive to yield information about the levels of arsenic in the plant.

the trough at 1,685 could potentially be related to nitrogen or proteins containing nitrogen.

A second basic data visualization technique is shown in Figure 39 that displays the extreme arsenic exposure over time and the resulting spectra. The average spectra of four replicates for each species is displayed at 4 weeks in the 0 ppm soil arsenic, at 12 weeks in 50 ppm soil arsenic and at 20 weeks in 200 ppm soil arsenic. These three collections of spectra generally show the entire range of change effects that have occurred with arsenic exposure. Distinct patterns are evident in all three fern species. These include changes in the green peak around 560 nm, changes in the red absorption trough at 680 nm and loss of the infrared shoulder around 750 nm. Other potential diagnostic features include peaks at 1,120, 1,310, 1,685, 1,860, 2,020 and 2,230 nm and absorption features at 1,150, 1,200, 1,460, 1,685, 1,940 and 2,170 nm.

5.3.1 Analysis of Spectral Reflectance Data

One of the three main objectives of this research is the development of a predictive model for arsenic uptake based on reflectance data collected in the laboratory. Reflectance data were acquired for each fern just prior to harvest under controlled conditions. See Section 4.3.2 for details.

The PLS and SLR techniques were used to identify the best-fit linear and non-linear equations for each fern for basic reflectance, and the first and second derivative data sets. Cross correlation was used to test for the collinearity condition. Figures 40, 41

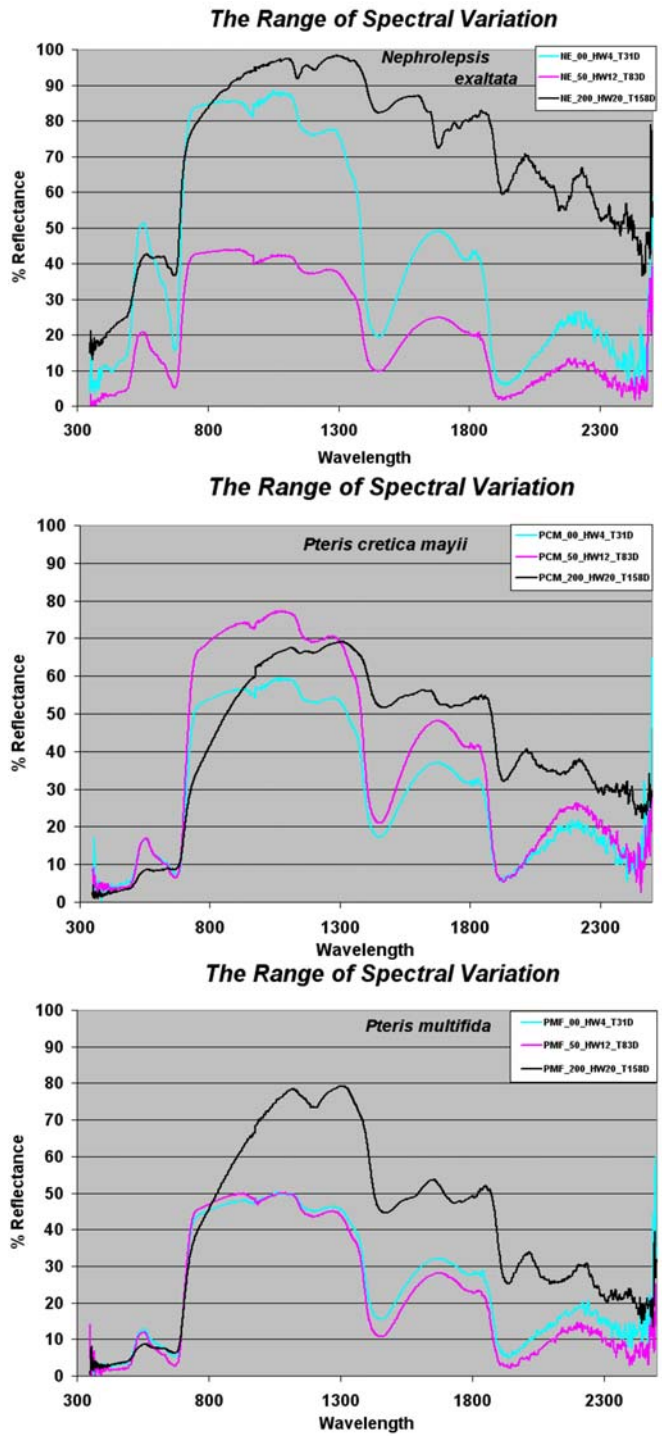

Figure 39. Spectral Extremes Over Time. A second data visualization technique plots the extremes of spectral variations of all three fern species; 0 ppm arsenic at 4 weeks, 50 ppm arsenic at 12 weeks and 200 ppm arsenic at 20 weeks. Distinct changes are evident.

and 42 graphically shows the best arsenic prediction models, based on spectral reflectance for each fern. Table 9 shows the models and the R^2 values for each.

As is evident from the R^2 value for each model, as well as graphically from the plots on Figures 40, 41 and 42, none of the models does a very good job at predicting the known arsenic concentration value in the plants. Reasonable linear and second order polynomial models were achieved for the *Nephrolepis exaltata* for the reflectance and first derivative data sets. However, since *Nephrolepis exaltata* is the non-accumulating control fern, it is unlikely that the spectra, and the derived models, are actually measuring arsenic since the concentrations are very low. Given the bands involved in the models, 463, 558 and 654 nm roughly correspond to the blue trough, the green peak and red trough, and 736, 818 and 946 nm are all associated with the shoulder at the top of the red/infrared edge and the loss of definition that corresponds to arsenic exposure in the *Nephrolepis exaltata* fern. This is graphically evident in all three species in Figure 39 and is likely the result of photosynthetic stress because the change in all of these areas indicates a decrease in chlorophyll production.

At this point, a review of the data and approaches in the literature revealed two possible methods for improving the spectral models of arsenic prediction from the reflectance data of the ferns. First, the primary reflectance data showed that there was a significant noise signal in many of the individual spectra at both ends of the solar reflected spectrum. At the mid-infrared edge (2,400 - 2,500 nm) the noise is likely due to atmospheric moisture in the form of high ambient humidity. At the blue edge (350 - 450 nm) the noise is probably due to ambient light in the laboratory. Even though the

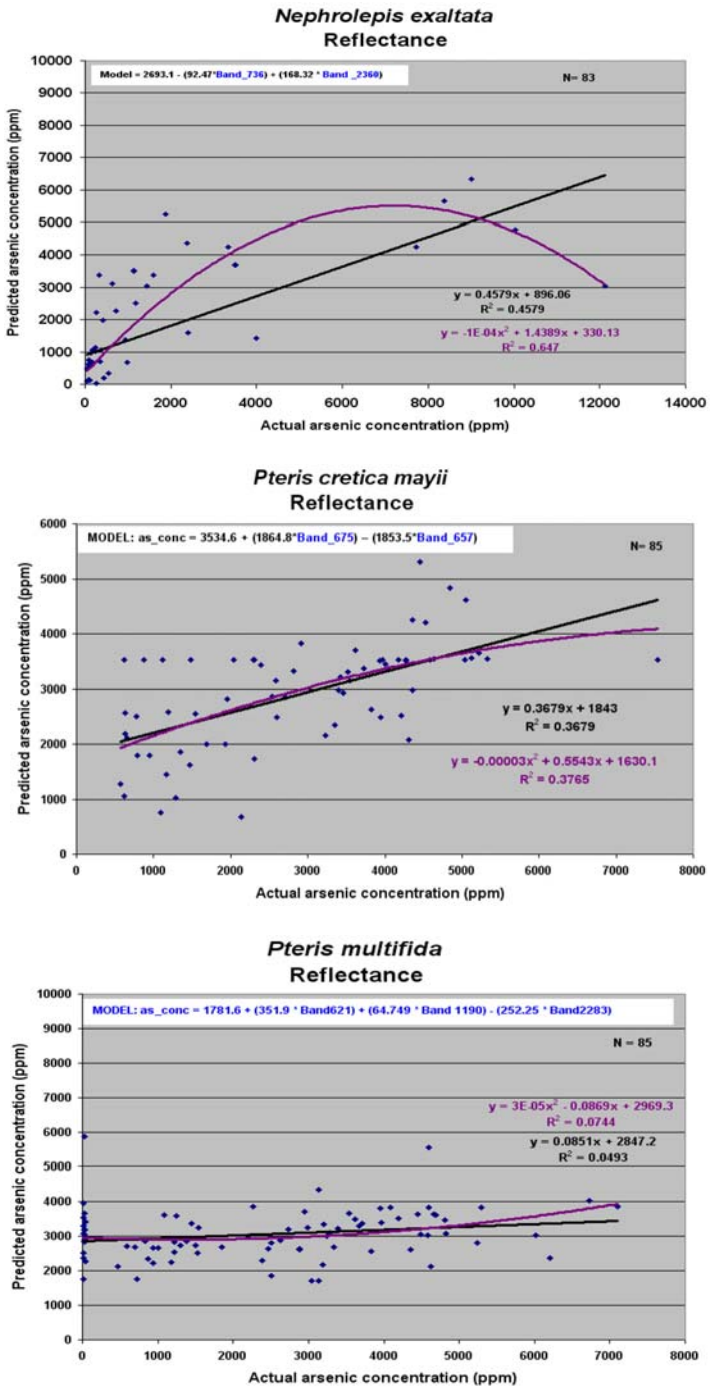

Figure 40. Reflectance Models of Arsenic Concentration. Linear and Polynomial Models between Arsenic Concentration and basic spectral reflectance. Models were developed with PLS and SLR techniques.

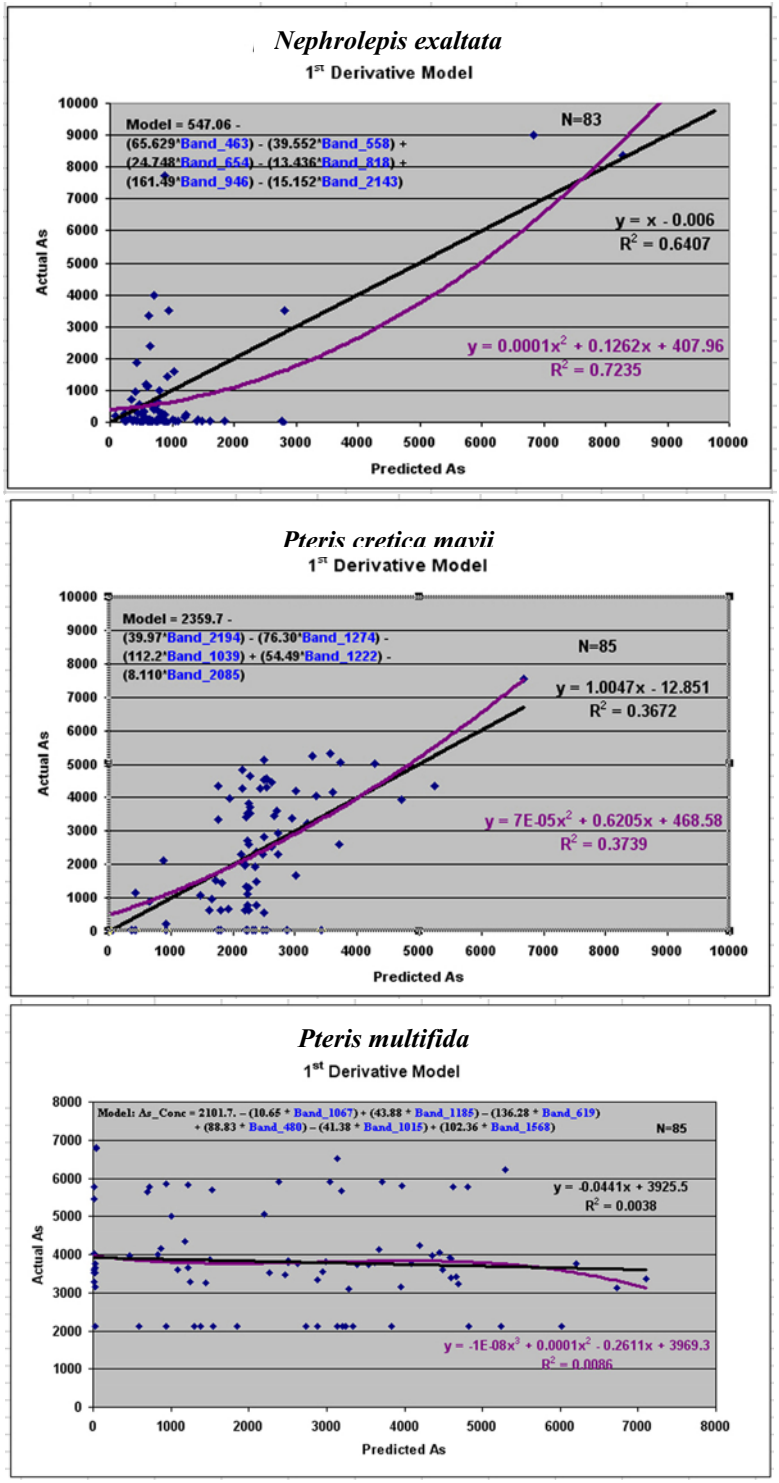

Figure 41. The 1st Derivative Models of Arsenic Concentration. The linear and non-linear models of arsenic concentration from the 1st Derivative of spectral reflectance for all three fern species.

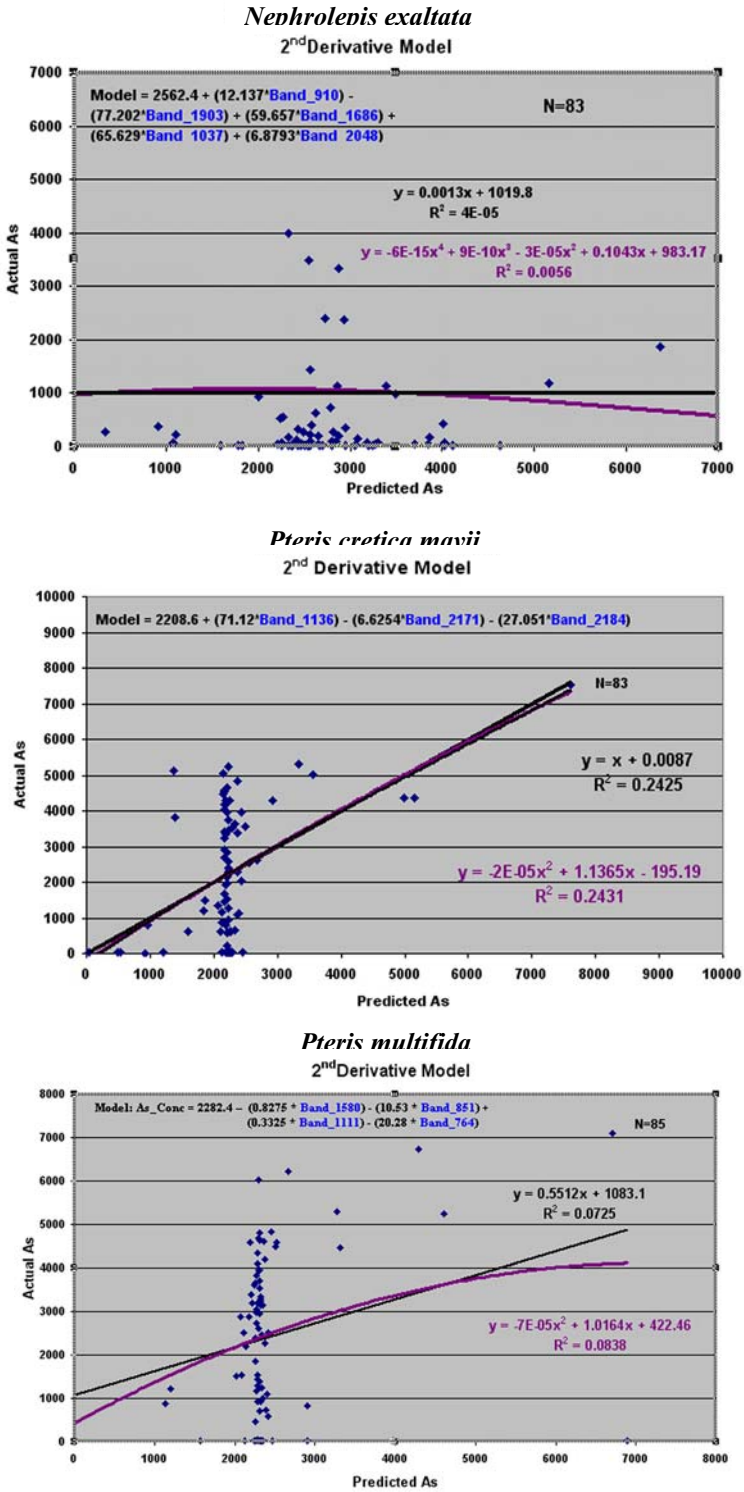

Figure 42. The 2nd Derivative Models of Arsenic Concentration. The linear and non-linear models of arsenic concentration from the 2nd Derivative of spectral reflectance for all three fern species.

Table 9
Model Results for Predicting Arsenic Concentration from Spectral Data

Nephrolepis exaltata			**Reflectance**
Model: as_conc =	**2693.1 + (92.47 * Band_736) + (168.32 * Band_2360)**		
linear equation / R^2	y = 0.0915x	/	**.47**
non-linear equation / R^2	y = $0.0002x^2$ + 0.2111x +162.53	/	**.52**
Pteris cretica mayii			**Reflectance**
Model: as_conc =	2260.3 - (411.59 * Band_548) + (384.17 * Band_679) – (99.2 * Band_1894) + (115.92 * Band_1689)		
linear equation / R^2	y = -0.273x + 3507.4	/	**.021**
non-linear equation / R^2	y = $5E\text{-}05x^2$ – 0.5184x + 3661.4	/	**.023**
Pteris multifida			**Reflectance**
Model: as_conc =	1781.6 - (351.9 * Band_621) + (64.75 * Band_1190) – (252.25 * Band_2283)		
linear equation / R^2	y = 0.0851x + 2847.2	/	**.05**
non-linear equation / R^2	y = 3E-05x2 - 0.0869x + 2969.3	/	**.07**
Nephrolepis exaltata			**1st Derivative of Reflectance**
Model: as_conc =	547.06 - (65.629*Band_463) - (39.552*Band_558) + (24.748 * Band_654) - (13.436*Band_818) + (161.49*Band_946) – (15.152*Band_2143)		
linear equation / R^2	y = x - 0.006	/	**.64**
non-linear equation / R^2	y = 0.0001x2 + 0.1262x + 407.96	/	**.72**
Pteris cretica mayii			**1st Derivative of Reflectance**
Model: as_conc =	2359.7 - (39.97*Band_2194) - (76.30*Band_1274) -(112.2*Band_1039) + (54.49*Band_1222) - (8.110*Band_2085)		
linear equation / R^2	y = 1.0047x - 12.851	/	**.37**
non-linear equation / R^2	y = 7E-05x2 + 0.6205x + 468.58	/	**.37**
Pteris multifida			**1st Derivative of Reflectance**
Model: as_conc =	2101.7. – (10.65 * Band_1067) + (43.88 * Band_1185) – (136.28 Band_619) + (88.83 * Band_480) – (41.38 * Band_1015) + (102.36 * Band_1568)		
linear equation / R^2	y = -0.0441x + 3925.5	/	**.004**
non-linear equation / R^2	y = -1E-08x3 + 0.0001x2 - 0.2611x + 3969.3	/	**.009**
Nephrolepis exaltata			**2nd Derivative of Reflectance**
Model: as_conc =	2562.4 + (12.137*Band_910) - (77.202*Band_1903) + (59.657 * Band_1686) + (65.629*Band_1037) + (6.8793*Band_2048)		
linear equation / R^2	y = 0.0013x + 1019.8	/	0
non-linear equation / R^2	y = -6E-15x4 + 9E-10x3 - 3E-05x2 + 0.1043x + 983.17	/	**.006**
Pteris cretica mayii			**2n Derivative of Reflectance**
Model: as_conc =	2208.6 + (71.12*Band_1136) - (6.6254*Band_2171) + (27.051*Band_2184)		
linear equation / R^{22}	y = x + 0.0087	/	**.24**
non-linear equation / R^2	y = -2E-05x2 + 1.1365x - 195.19	/	**.24**
Pteris multifida			**2n Derivative of Reflectance**
Model: as_conc =	2282.4 – (0.8275 * Band_1580) - (10.53 * Band_851) + (0.3325 * Band_1111) - (20.28 * Band_764)		
linear equation / R^2	y = 0.5512x + 1083.1	/	**.073**
non-linear equation / R^2	y = -7E-05x2 + 1.0164x + 422.46	/	**.084**

protocol called for a high-intensity solar lamp, it is nearly impossible, without being in an isolated room, to completely eliminate other light sources and this resulted in significant noise in that part of the spectrum.

Second, it was clear from several of the plots of the data in the PLS routine and in the spreadsheet figures that there was a dual distribution or clustering in the data set. Approximately 18 to 20 data points were consistently isolated from the rest of the spectral files for each fern. Figure 43 shows graphic examples of both the noise in the data and the distribution of data points

These spectral noise conditions were rectified by trimming the basic spectrum for each plant by 100 nm on each end, from the original 350–2,500 nm to 450–2,400 nm. This removed a major portion of the noise in the data set and creating a very different statistical data set for analysis. See Figure 43.

In addition, by working back though the graphs, the isolated data clusters turned out to be the ferns growing in the soils with the zero arsenic concentrations and subsequently with little or no arsenic in the fronds, this meant that there were no spectral characteristics relating to the arsenic concentration. Reviewing the data further, it appears that the threshold for the spectral expression of arsenic stress is in the 400–500 ppm range. To correct for this problem, all ferns with a confirmed laboratory analysis of less than 500 ppm were eliminated from the two *Pteris* ferns data sets.

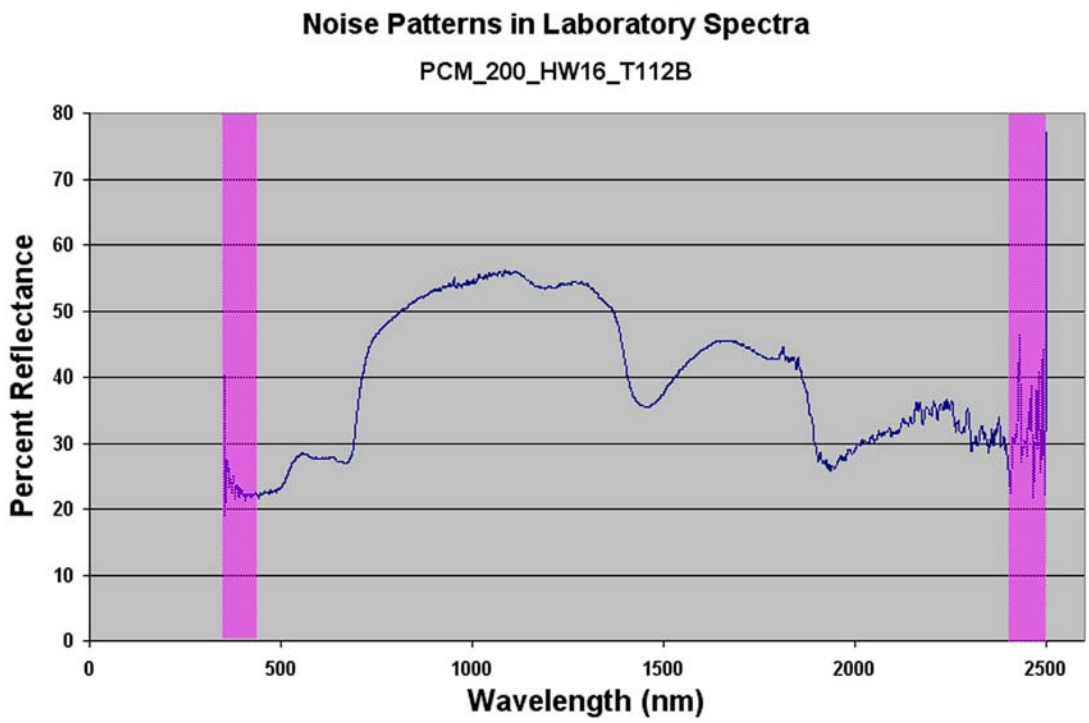

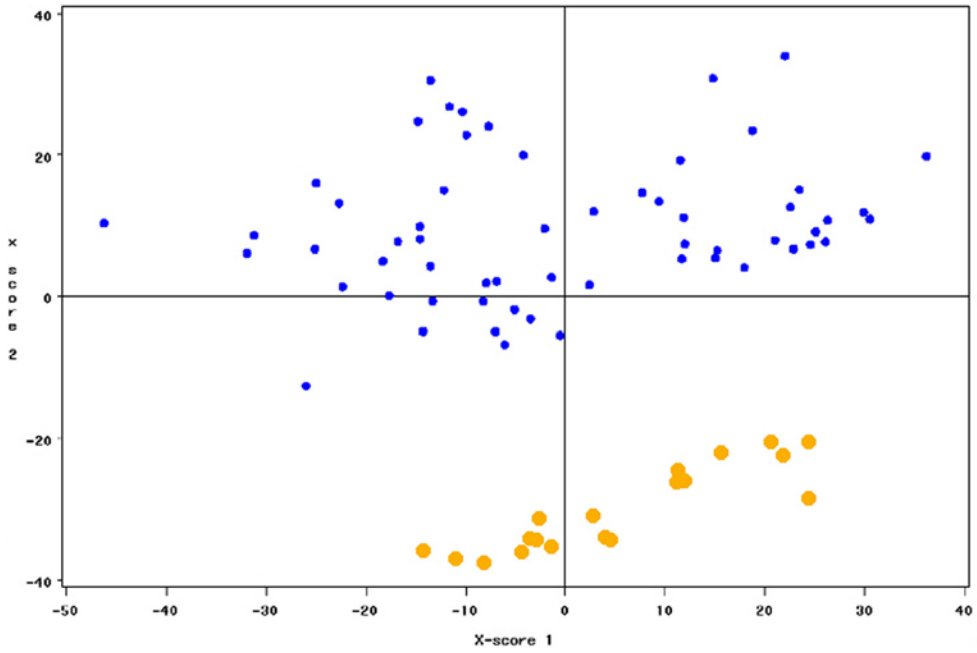

Figure 43. Noise and Clustering in Spectral Data. Two spectral conditions discovered after reevaluation of all spectral data. The top figure shows noise at both ends of the spectrum which was eliminated by trimming the spectral trace by 100 nm on each end. Below an obvious cluster of data points did not add to the predictive models. This cluster, show n in gold, was eventually determined to be the zero soil treatments and the lowest detectable arsenic concentrations in the ferns and were withheld from the fern observations for each species.

5.3.2 Second Analysis of Spectral Reflectance Data

After the data edits for trimming away the noisy edges of the spectra and subsetting the observations to include only those with arsenic concentrations greater than 500 ppm, the basic PLS methodology was reapplied to the reflectance, and the first and second derivative data for the two arsenic accumulating ferns. The reanalysis of reflectance revealed no improvement in the predictive models for arsenic concentration. The raw reflectance data are so highly correlated that finding several components that will pass the collinearity condition for a predictive model is nearly impossible. The first and second derivatives of the reflectance spectra, on the other hand, are very uncorrelated, and make the discovery and use of multiple components and factors much more feasible.

The reanalysis of the first and second derivatives for the *Pteris cretica mayii* and the *Pteris multifida* data yielded four very improved models for relating arsenic concentration to spectral reflectance. All four models had R^2 values of .70 or greater. Figures 44 and 45 show the improved models and graphs for the first and second derivatives for both *Pteris* ferns. Table 10 summarizes the models and improved R^2 values.

Model components appear to vary significantly between species especially with respect to the most important wavelengths selected in the PLS regression process. However, some similarities are present. All four models had at least one component in, or very close to, the water absorption areas of 1,400 and 1,900 nm, possibly indicating

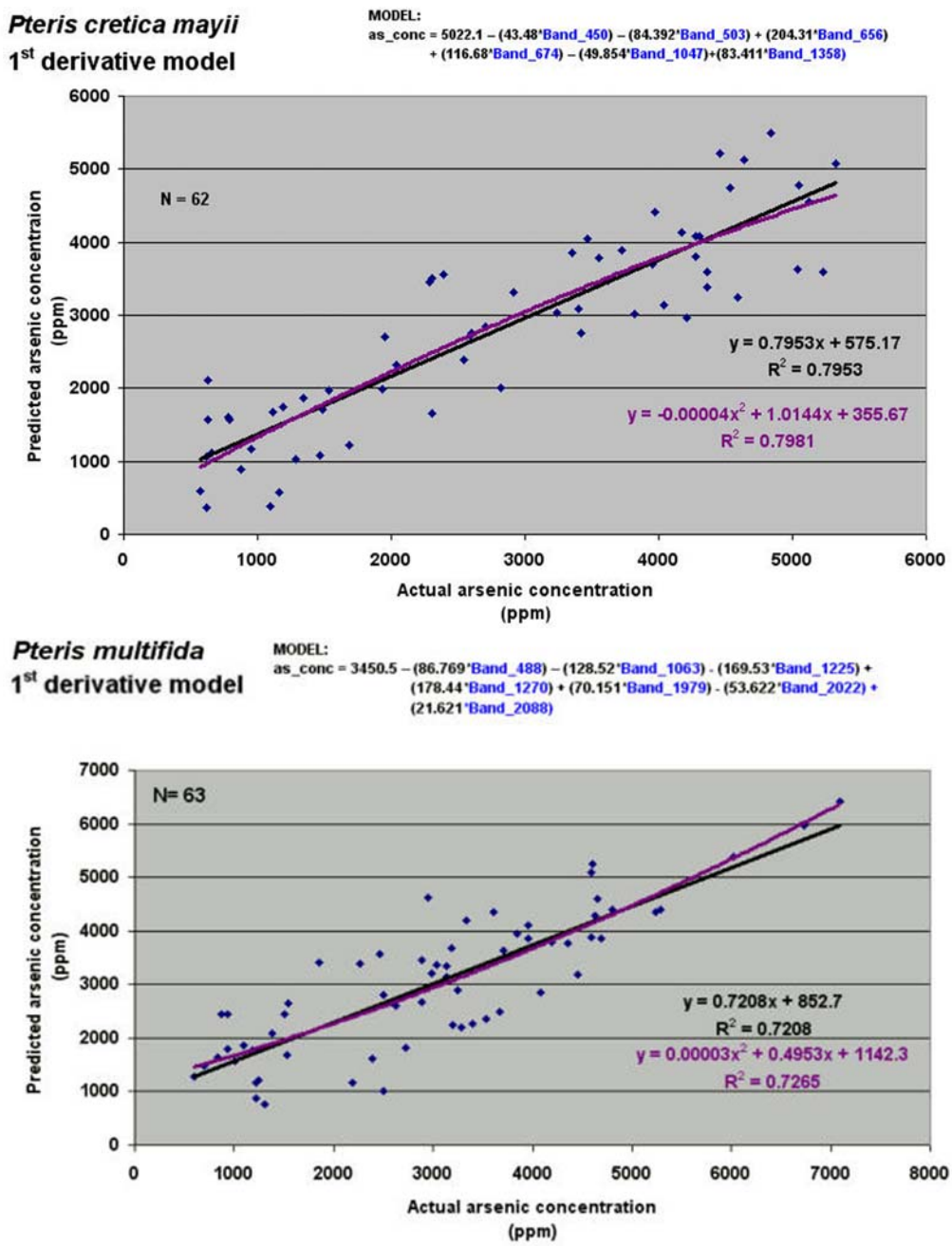

Figure 44. Improved 1st Derivative Models of Arsenic Concentration. Models of arsenic concentration in the fronds of two *Pteris* ferns derived from the 1st derivative of reflectance after data were trimmed and subsetted to include only arsenic concentration greater than 500 ppm.

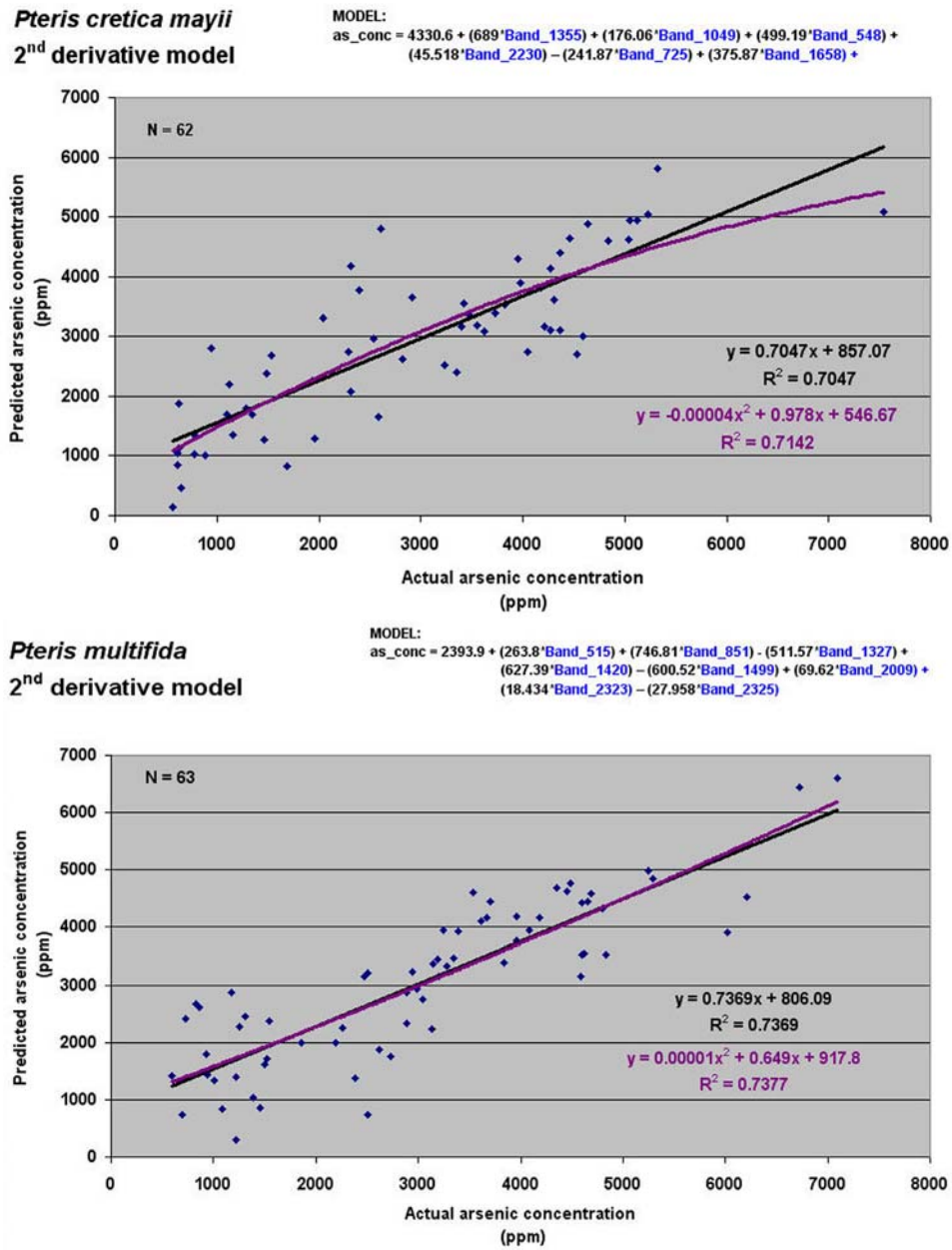

Figure 45. Improved 2nd Derivative Models of Arsenic Concentration. Improved models of arsenic concentration in the fronds of two Pteris ferns derived from the second derivative of reflectance after data were trimmed and subsetted to include only arsenic concentration greater than 500 ppm.

Table 10.
Improved Linear and Non-linear Models for Predicting Arsenic Concentration from Spectral Data.

Pteris cretica mayii **1st Derivative of Reflectance**

Model: as_conc = 5022.1 – (43.48*Band_450) – (84.392*Band_503) + (204.31*Band_656) + (116.68*Band_674) – (49.854*Band_1047)+(83.411*Band_1358)

linear equation	/ R^2 / prev R^2	y = 0.7953x + 575.17	**.79 / .37**
non-linear equation	/ R^2 / prev R^2	y = -0.00004x2 + 1.0144x + 355.67	**.79 / .37**

Pteris multifida **1st Derivative of Reflectance**

Model: as_conc = 3450.5 – (86.769*Band_488) – (128.52*Band_1063) – (169.53*Band_1225) + (178.44*Band_1270) + (70.151*Band_1979) - (53.622*Band_2022) + (21.621*Band_2088)

linear equation	/ R^2 / prev R^2	y = 0.7208x + 852.7	**.72 / .073**
non-linear equation	/ R^2 / prev R^2	y = 0.00003x2 + 0.4953x + 1142.3	**.73 / .084**

Pteris cretica mayii **2n Derivative of Reflectance**

Model: as_conc = 4330.6 + (689*Band_1355) + (176.06*Band_1049) + (499.19*Band_548) + (45.518*Band_2230) – (241.87*Band_725) + (375.87*Band_1658) + (198.09*Band_1251)

linear equation	/ R^2 / prev R^2	y = 0.7047x + 857.07	**.70 / .24**
non-linear equation	/ R^2 / prev R^2	y = -0.00004x2 + 0.978x + 546.67	**.70 / .24**

Pteris multifida **2nd Derivative of Reflectance**

Model: as_conc = 2393.9 + (263.8*Band_515) + (746.81*Band_851) – (511.57*Band_1327) + (627.39*Band_1420) + (600.52*Band_1499) + (69.62*Band_2009) + (18.434*Band_2323) – (27.958*Band_2325)

linear equation	/ R^2 / prev R^2	y = 0.7369x + 806.09	**.74 / .073**
non-linear equation	/ R^2 / prev R^2	y = 0.00001x2 + 0.649x + 917.8	**.74 / .084**

---

some interactions between sequestered arsenic and leaf moisture. All of the derived models had a component which was a bandwidth in the blue-green transition zone, between 450 and 550 nm and except for the *Pteris cretica mayii* first derivative model, none of the other models utilized components or information from the traditional red or Red Edge regions that are known to relate to plant health and photosynthetic activity. Several bands in the short wave infrared region (SWIR), from 1,400 nm to 2,400 nm, proved to be valuable for predicting plant arsenic concentration. Three out of four new models used at least two component bands from the SWIR region.

5.3.3 Testing Spectral-Arsenic Prediction Models

In September 2004, field reflectance spectra were collected for 24 ferns (12 *Pteris cretica mayii* and 12 *Pteris multifida*) that had been grown in Spring Valley as part of a phytoremediation pilot. These ferns were then harvested and independently analyzed for arsenic by the USACE Laboratory in Vicksburg, Mississippi. The spectra from these ferns were input into spreadsheets and processed into reflectance and the first and second derivatives. The original intent of this data collection was to provide a field test of the arsenic prediction models developed from the laboratory spectra data analysis.

Unfortunately, field conditions are generally very different and, although the ferns were successfully utilized for remediation of soil arsenic, the arsenic concentrations in these particular ferns were generally very low and below the 500 ppm threshold that was used in the model development. However, six ferns contained arsenic concentrations levels at or near 500 ppm level and the spectral data from these ferns were used to

compute the first and second derivatives and specific band values were inserted into the corresponding models. Table 11 shows the results.

Table 11
Arsenic Concentrations (ppm) and Spectral Model Prediction

Spring Valley Phytoremediation Ferns

		1st Derivative Model		2nd Derivative Model	
Sample	**Fern**	**Predicted**	**Actual**	**Predicted**	**Actual**
ts1	*P. cretica*	1313	593	3278	593
ts13	*P. multifida*	1024	1060	1042	1060
ts14	*P. multifida*	1111	483	1857	483
ts17	*P. multifida*	980	907	2144	907
ts18	*P. multifida*	340	383	3669	383
ts21	*P. multifida*	830	694	3111	694

Although this is a very limited test because of the number of subjects, it still demonstrates the potential for predicting arsenic concentration from spectral data. In general, it appears that the first derivative model works better than the second derivative model and the better predictions were the ferns with the higher actual arsenic concentrations, which is consistent with the model statistics. Much more data are needed to fully evaluate the model effectiveness.

5.3.4 Vegetation Indices

VIs are numerical formulas of spectral reflectance data that are designed to maximize specific properties or relationships among parts of the EMS. VIs can be a general indicator of overall condition, such as the NDVI, or can be quite specific, such as the anthocyanin reflectance index (ARI). Anthocyanins are the red pigments in most leaves and have one main absorption around 529 nm in the green region of the EMS. Anthocyanins levels tend to have an inverse relationship with photosynthetic activity and therefore they can be an effective measure of stress.

Sixty six VIs were extracted from the literature and programmed into spreadsheets for each spectral measurement. Appendix C lists the VIs, the formulas and the reference for each. Broadband indices, such as those that might have been developed for Landsat or AVHRR were computed by taking an average of hyperspectral bands in the target region. For example, a value for broadband blue was computed by the summation of bands 445 to 515, divided by 71.

The values for all 66 VIs were appended to the spectral reflectance values for each file prior to the PLS analysis, resulting in 2,217 total bands. After all PLS processing, none of the VIs for any of the ferns were selected for inclusion in the final model.

The 66 VI values were then input into SLR models for each fern to determine if any significant statistical relationships were present. For the *Nephrolepis exaltata* fern, a good linear relationship was found with the Moisture Stress Index (MSI), the Photochemical Reflectance Index (PRI), the Red Edge Vegetation Stress Index (RVSI),

the Red Near Infrared Green (RNG) Index and the Modified Triangular Vegetation Index 2 (MTVI2). The model R^2 is .7026 and has a p value of .0001.

The SLR process was repeated for *Pteris multifida* and *Pteris cretica mayii*. The SLR process for *Pteris cretica mayii* returned an acceptable model using the Green Index (GI), the Sum Green Index, (SGI) and Carotenoid Reflectance Index 1 (CRI1). The model R^2 is .6939 and has a p value of .0001. No model could be developed for the *Pteris multifida* data. Figure 46 displays the graphs and equations for both the *Nephrolepis exaltata* and *Pteris cretica mayii* models.

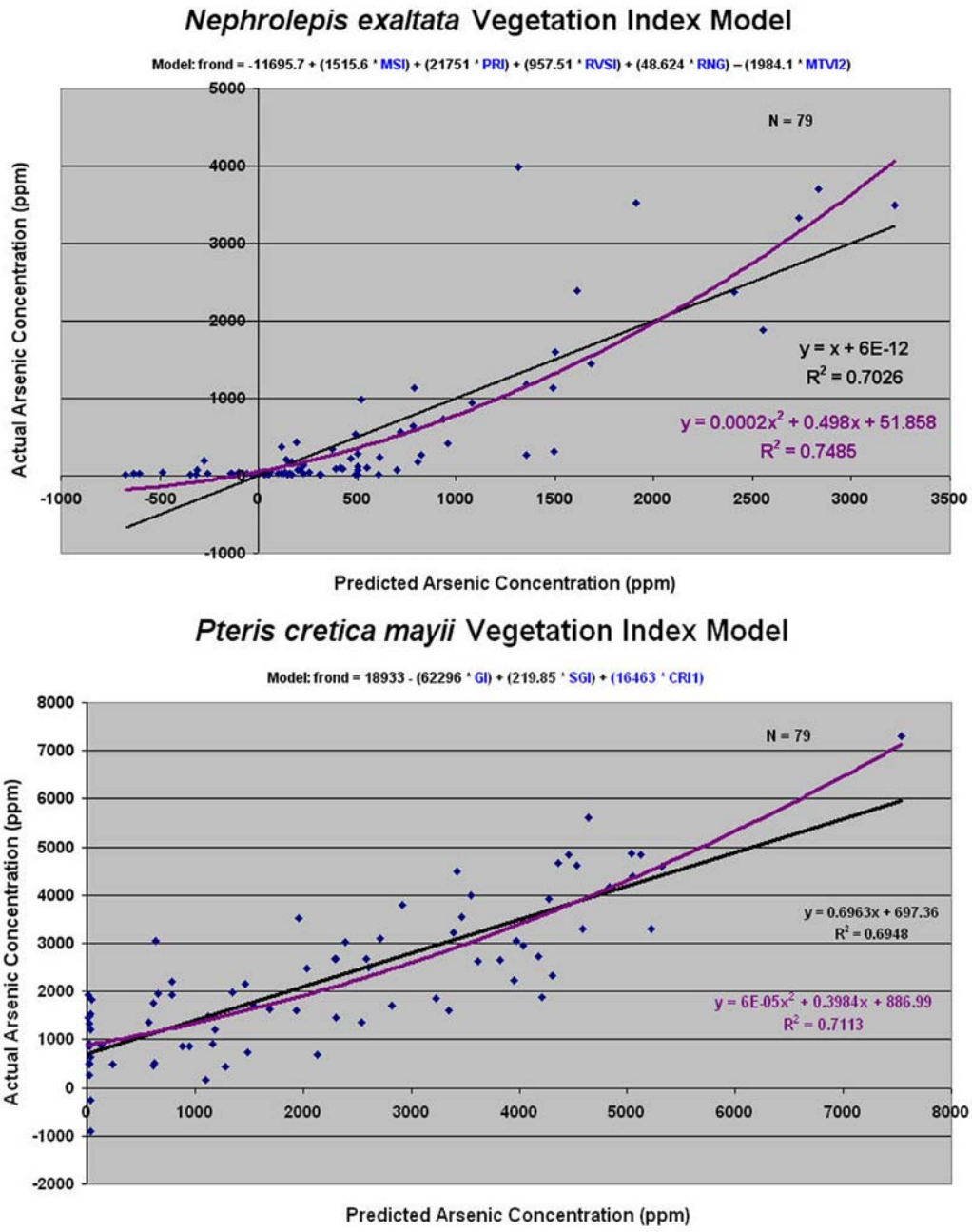

Figure 46. Vegetation Index Models. The two linear models that were developed from VIs for *Nephrolepis exaltata* and *Pteris cretica mayii*. No model was significant for *Pteris multifida*.

5.4 Mapping Arsenic Induced Vegetation Stress with Hyperspectral Imagery

Hyperspectral imagery data were processed and analyzed to identify and map the spectral signature of known areas of arsenic-induced stress in vegetation. HSI systems record, at a lower spatial and spectral resolution, the same energy interactions as a laboratory spectrometer and there has been much research over the past ten years in applying HSI analysis to the identification of unique substances or conditions on the landscape.

As a result of the spectral data collected for the two grass species grown in the laboratory in the five soil-arsenic concentrations, a spectral profile of arsenic stress has been acquired and serves as a starting point in the attempt to identify high soil arsenic based on the spectral signature of the grass growing in it. As is typical in a vegetation stress scenario, spectral expressions of stress are indicated by the changes in the Green and Red Edges (around 400 and 700 nm, respectively), the Red Trough around 680 nm and the infrared shoulder near 750 nm. These areas, and possibly others, have the best potential to discriminate arsenic affected vegetation in HSI. Figure 47 shows two spectra from unstressed and arsenic-stressed ferns with the graphic outline of the key areas of stress identification.

HyMAP HSI were collected in October 2000 over the Spring Valley area and prior to any remediation of high soil arsenic. HyMap is an aircraft-mounted commercial hyperspectral sensor operated by the HyVista Corporation (Sydney, Australia). The system is a whiskbroom scanner utilizing diffraction gratings and four 32 element detector arrays to provide 126 spectral channels covering the 450–2,500 nm spectral

range over a 512 pixel swath. The bandwidths vary between 10 and 20 nm with a greater than 1000:1 signal-to-noise ratio. The HyMap sensor acquires imagery at spatial resolutions of between 3 and 10 m, depending on the flight height. The pixel size of the HyMap imagery of Spring Valley is 4 m (Cocks et al. 1998).

The imagery cube, 133 mb in size, was preprocessed according to ENVI standard methods, including an ATREM atmospheric correction, (Gao et al. 1993; Clark et al. 1984), dark current noise removal and internal and external calibration to apparent relative reflectance (Bachman et al. 2002; Kruse et al. 2003).

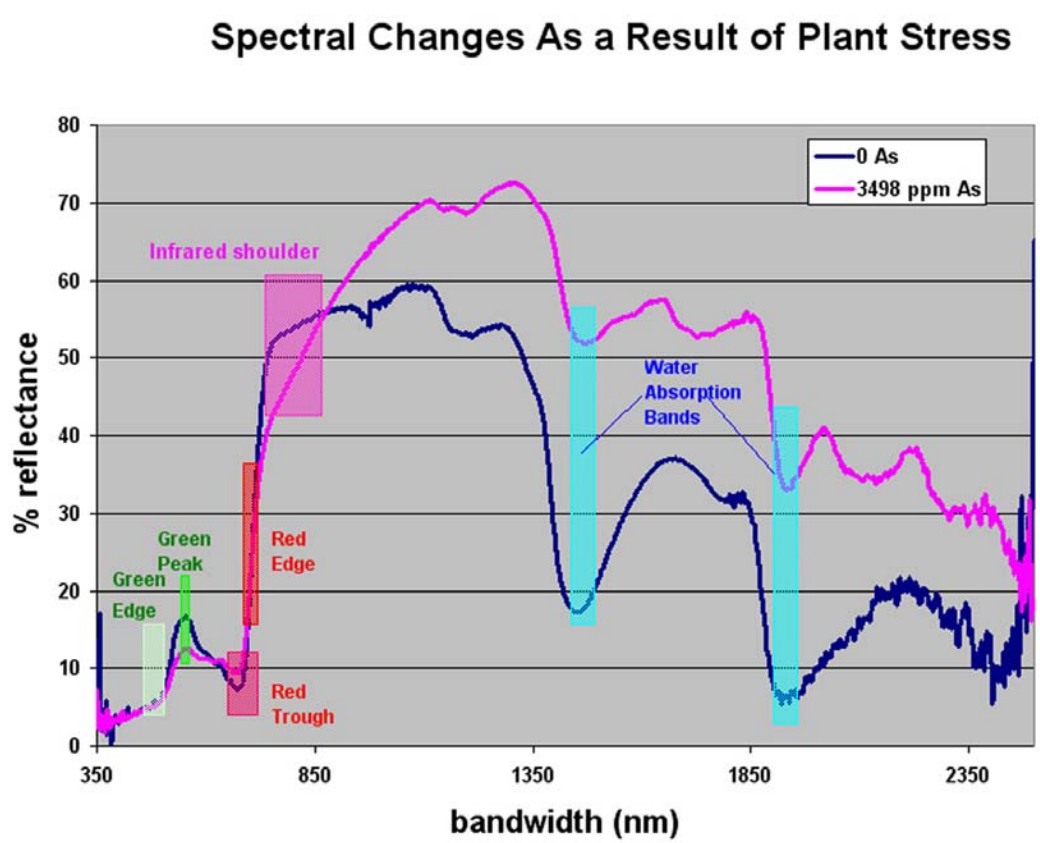

Figure 47. Lab Spectra of Arsenic Stress. Spectra from two *Pteris cretica mayii* ferns with and without arsenic stress. The primary regions of spectral separation for identifying and measuring stress are highlighted.

The first image processing trial utilized the automated spectral hourglass wizard in ENVI and produced transformed files for the Minimum Noise Fraction, Pixel Purity Index, Linear Unmixing, Endmembers and a Matched Filter. Unfortunately, none of the endmembers uniquely identified the known arsenic-affected grass areas and all of the classification attempts resulted in poor accuracies.

A series of mapping methods were attempted covering the range of spectral processing capabilities utilizing different intermediate processing files and using the six classification decision rule algorithms. Table 12 outlines the different base imagery files and classification approaches that were attempted along with the overall accuracy statistics.

The highest overall mapping accuracy was achieved with linear spectral unmixing as the base processing and Maximum Likelihood as the decision rule. The overall accuracy of this classification was 83 % with a Kappa Coefficient of 0.77. Further, the mapping accuracy of the arsenic grass category was 55.8 % for producers accuracy and 82.7 % for users accuracy.

Several other image processing/classification methods had accuracies around 70 % or higher and invariably the classification method was either Maximum Likelihood or Mahalanobis Distance. In terms of overall classification accuracy, the Mahalanobis Distance routine performed the best with an average accuracy of 64.2 % and the Maximum Likelihood was second at 61.5 %. The confusion matrix for the best classification is shown in Table 13, and Figure 48 shows a classified image of the Spring

TABLE 12.
Hyperspectral Processing and Map Accuracy Results

Base Image	Classifier	Overall Accuracy %	Kappa Coefficient
Minimum Noise Fraction	Binary Encoding	17.1	.10
Minimum Noise Fraction	Mahalanobis Distance	38.1	.26
Minimum Noise Fraction	Maximum Likelihood	42.4	.29
Minimum Noise Fraction	Minimum Distance	58.8	.47
Minimum Noise Fraction	Parallelepiped	24.3	.15
Minimum Noise Fraction	Spectral Angle Mapper	22.2	.12
Matched Filter	Binary Encoding	11.1	.02
Matched Filter	Mahalanobis Distance	71.0	.61
Matched Filter	Maximum Likelihood	70.1	.61
Matched Filter	Minimum Distance	66.1	.56
Matched Filter	Parallelepiped	17.5	.08
Matched Filter	Spectral Angle Mapper	18.9	.12
Mix-Tuned Matched Filter	Binary Encoding	5.5	.00
Mix-Tuned Matched Filter	Mahalanobis Distance	77.2	.70
Mix-Tuned Matched Filter	Maximum Likelihood	70.4	.60
Mix-Tuned Matched Filter	Minimum Distance	51.6	.38
Mix-Tuned Matched Filter	Parallelepiped	15.5	.10
Mix-Tuned Matched Filter	Spectral Angle Mapper	56.2	.45
Continuum Removal	Binary Encoding	32.4	.20
Continuum Removal	Mahalanobis Distance	73.1	.64
Continuum Removal	Maximum Likelihood	49.0	.39
Continuum Removal	Minimum Distance	54.9	.42
Continuum Removal	Parallelepiped	53.9	.41
Continuum Removal	Spectral Angle Mapper	58.5	.49
Linear Spectral Unmixing	Binary Encoding	34.9	.21
Linear Spectral Unmixing	Mahalanobis Distance	79.6	.73
Linear Spectral Unmixing	Maximum Likelihood	83.0	.77
Linear Spectral Unmixing	Minimum Distance	39.2	.21
Linear Spectral Unmixing	Parallelepiped	16.5	.06
Linear Spectral Unmixing	Spectral Angle Mapper	58.5	.49
Spectral Feature Fitting	Binary Encoding	5.5	.00
Spectral Feature Fitting	Mahalanobis Distance	46.2	.39
Spectral Feature Fitting	Maximum Likelihood	54.1	.47
Spectral Feature Fitting	Minimum Distance	46.7	.38
Spectral Feature Fitting	Parallelepiped	35.2	.27
Spectral Feature Fitting	Spectral Angle Mapper	45.0	.37

Table 13
Accuracy Assessment Confusion Matrix
Linear Spectral Unmixing / Maximum Likelihood Classification

Overall Accuracy = (9636/11610) 82.9 % Kappa Coefficient = 0.77

	As Grass	Grass	Trees	Bldg1	Bldg2	Soil	Asphalt	Concrete	Total
				(pixels)					
As_Grass	263	55	0	0	0	0	0	0	318
Grass	41	448	0	0	0	0	0	0	489
Trees	68	0	5082	0	44	0	2	4	5200
Bldg1	0	0	0	889	3	0	19	30	941
Bldg2	94	323	293	295	1509	18	262	272	3066
Soil	1	0	0	0	5	945	2	0	953
Asphalt	0	0	0	0	1	0	239	0	240
Concrete	4	73	0	35	4	25	1	261	403
Total	471	899	5375	1219	1566	988	525	567	11610
				(percent)					
As_Grass	55.84	6.12	0	0	0	0	0	0	2.74
Grass	8.7	49.83	0	0	0	0	0	0	4.21
Trees	14.44	0	94.55	0	2.81	0	0.38	0.71	44.79
Bldg1	0	0	0	72.93	0.19	0	3.62	5.29	8.11
Bldg2	19.96	35.93	5.45	24.2	96.36	1.82	49.9	47.97	26.41
Soil	0.21	0	0	0	0.32	95.65	0.38	0	8.21
Asphalt	0	0	0	0	0.06	0	45.52	0	2.07
Concrete	0.85	8.12	0	2.87	0.26	2.53	0.19	46.03	3.47
Total	100	100	100	100	100	100	100	100	100

Class	Commission%	Omission%	Commission%	Omission%
As_Grass	17.30	44.16	55/318	208/471
Grass	8.38	50.17	41/489	451/899
Trees	2.27	5.45	118/5200	293/5375
Bldg1	5.53	27.07	52/941	330/1219
Bldg2	50.78	3.64	1557/3066	57/1566
Soil	0.84	4.35	8/953	43/988
Asphalt	0.42	54.48	1/240	286/525
Concrete	35.24	53.97	142/403	306/567

Class	Prod. Acc. %	User Acc.%	Prod. Acc.%	User Acc.%
As_Grass	55.84	82.70	263/471	263/318
Grass	49.83	91.62	448/899	448/489
Trees	94.55	97.73	5082/5375	5082/5200
Bldg1	72.93	94.47	889/1219	889/941
Bldg2	96.36	49.22	1509/1566	1509/3066
Soil	95.65	99.16	945/988	945/953
Asphalt	45.52	99.58	239/525	239/240
Concrete	46.03	64.76	261/567	261/403

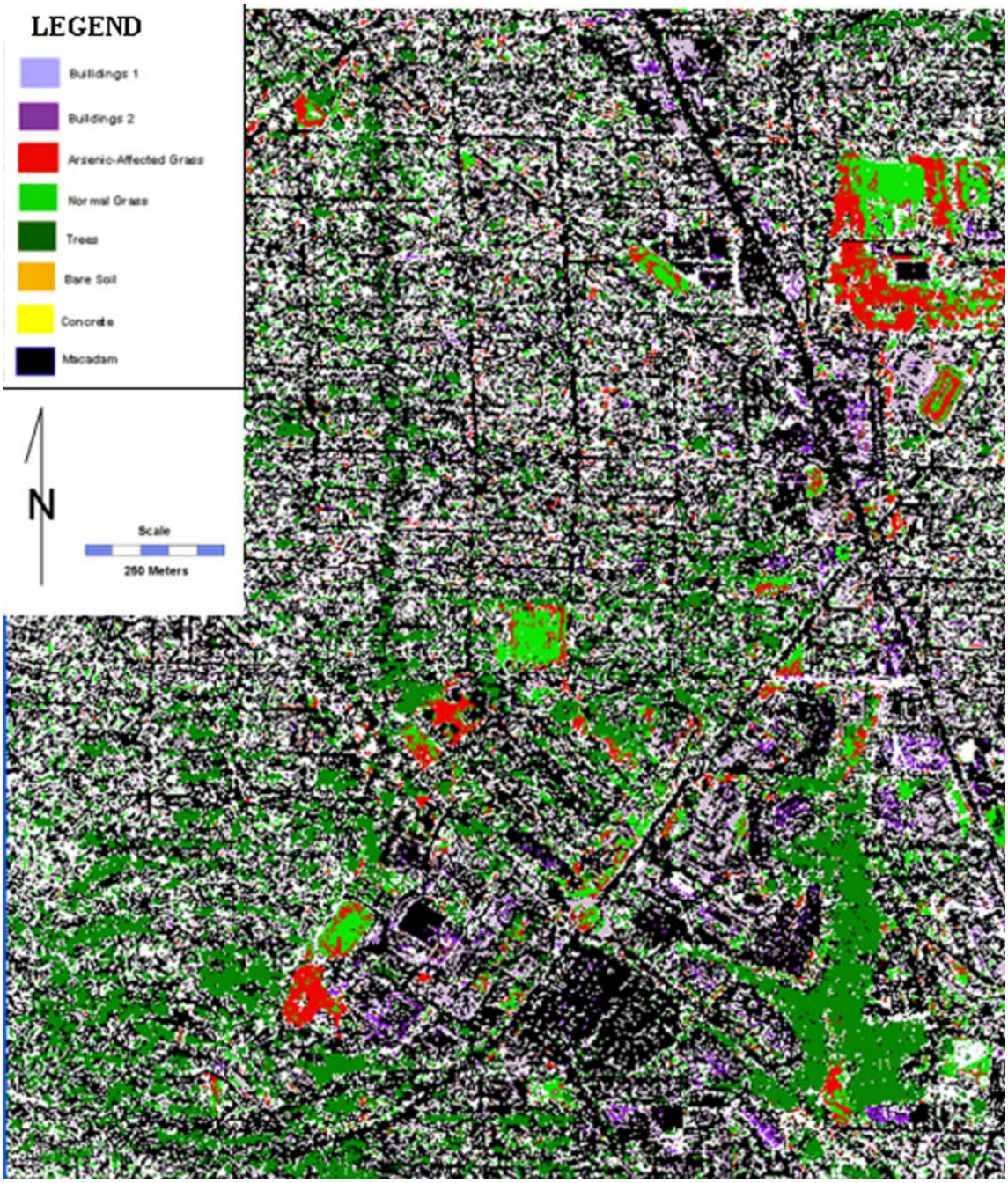

Figure 48. Land Cover Classification Results. Linear Spectral Mixing / Maximum Likelihood classification results of the Spring Valley / American University Area. Red is arsenic-affected grass.

Valley area from the highest accuracy combination of intermediate processing and classification decision rule algorithm (Linear Spectral Unmixing / Maximum Likelihood).

The range of overall accuracy measures from the 36 image/classifier combinations yielded some interesting and potentially useful information for future applications. The Binary Encoding classification decision rule performed poorly in all tests. This classifier divides the endmember and image data into ones and zeros based on the spectral mean and uses an exclusive Boolean OR function to compare each encoded reference spectrum with the encoded data spectra and produces a classification image. Image pixels are classified to the endmember with the greatest number of matches (ENVI 2004). The classic Parallelepiped classifier also performed poorly with an average accuracy of 27.2 %.

The best overall classification decision rule algorithm was the Mahalanobis Distance classifier with an average of 64.2 % follow by the Maximum Likelihood classifier at 61.5 %. Both of these classifiers calculate statistics for each class, assume that the covariances of all classes are equal and utilize probabilities to assign a pixel to a specific class (ENVI 2004). The significance of these results lies in the fact that the classifiers developed specifically for hyperspectral applications, the Binary Encoding and the Spectral Angle Mapper, did not produce any meaningful results and the best classification decision rules were those developed for multispectral applications.

In terms of the image processing format, the best overall accuracy was achieved by the Continuum Removal method with an average accuracy of 53.6 % followed closely by Linear Spectral Unmixing at 52.0 %. The image format that performed at the poorest

level is the Minimum Noise Fraction at 33.8 %. The Minimum Noise Fraction is really an initial basic format for HSI, and therefore, the low accuracy is not surprising. The Continuum Removal is a method that has been gaining acceptance in the scientific literature. The Continuum Removal fits a convex hull over the spectra and subtracts the spectral maxima, leaving only the normalized absorption features. Linear Spectral Unmixing is a form of subpixel processing that has gained a wide acceptance and application in recent years. It is appealing in that it can produce continuous surface results instead of a limited number of thematic classes.

Also worth noting are the results of the image processing using the Vegetation Index (VI) functions in the ENVI software. The complete suite of VIs were calculated for each pixel and stored as layers in a multiband image. The VI images were processed with the same algorithms listed in Table 12 but produced no significant classification results. Just as in the laboratory spectral applications, where limited results were observed, the performance of these VI metrics is confusing given their relative popularity in the scientific literature.

5.4.1 Discussion of Hyperspectral Image Processing Results

The hyperspectral image processing of arsenic stress in grass was severely constrained because of the extreme crown closure of the Oak trees that line the streets in the area. Many of the arsenic-contaminated grass areas were not accessible to the sensor and thus severely limited the scope of this analysis. Further, because Oak trees in the

Washington, D.C., area were starting to senesce in mid-October, they were displaying natural stress characteristics and therefore were unacceptable for spectral analysis.

Even under these conditions the statistical and image processing results can be viewed as promising. The level of users classification accuracy between arsenic-affected (82.7 %) and non-affecting grasses (91.6 %) was surprisingly high although there obviously appear to be some significant false positives. These could be due to error or confusion in the training signature or the classification process or could be due to other forms of stress, such as moisture deficiency or pesticides, that create a similar reflectance pattern. Also, it is unlikely but possible that there are additional arsenic-affected areas that have been overlooked.

It is clear that the HSI and analysis process is identifying and mapping a significant level of arsenic stress. Although HSI is far less sensitive in spatial and spectral resolution than the laboratory spectrometer (1 cm vs. 4 m, 126 bands vs. 2,151 bands), there are known and consistent spectral relationships that enable HSI to identify important conditions in vegetation status. For example, the same key spectral regions of stress that are displayed in Figure 47 can be seen in the HSI spectra in Figure 49 which shows spectra of healthy and arsenic-stressed grass from both the laboratory spectrometer and the HSI.

The same classic areas and patterns of spectral changes due to stress can be seen in both sets of data and are well founded in the scientific literature. Horler et al. (1980, 1983) showed that stressed vegetation often shows a general increase in reflectance magnitude as a general non-specific response usually due to a loss of chlorophyll

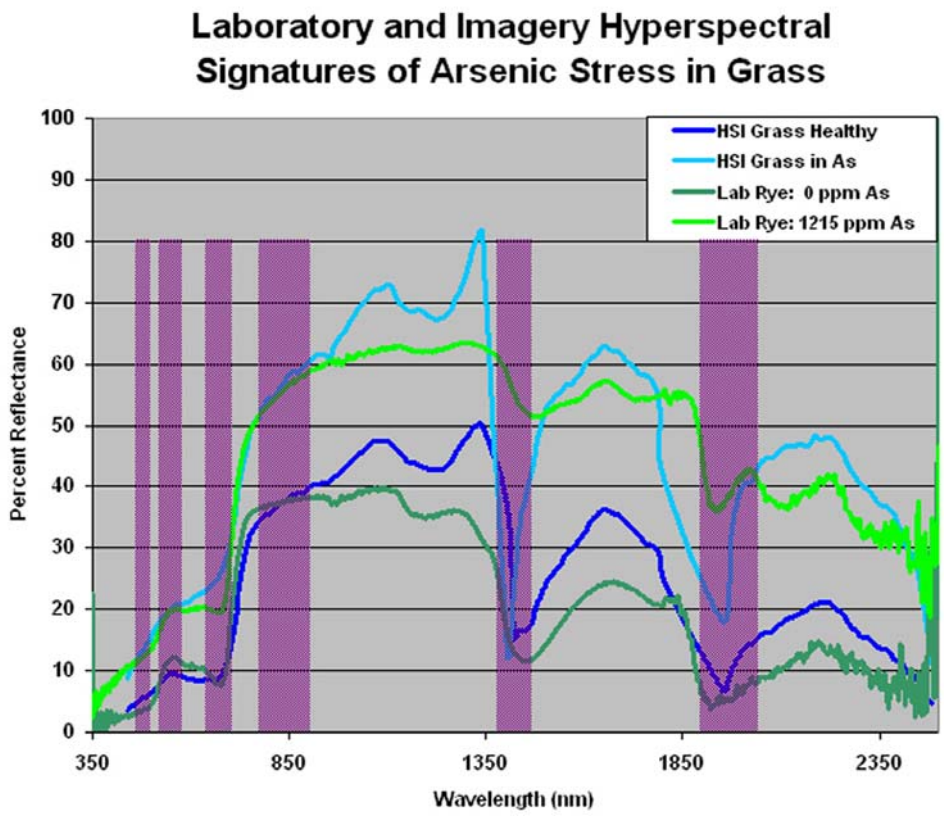

Figure 49. Laboratory and Imagery Spectra. Healthy and stressed grass signatures from both the laboratory and hyperspectral imagery. The same critical areas in the green, red, near-infrared and SWIR show the patterns of spectral separation between the healthy and stressed grass that enable the image processing algorithm to separate, identify and map these areas.

synthesis. Horler et al. (1983), Bammel and Birnie (1994) and Reusen et al. (2003) documented the general flattening of the green peak at 450 nm and the red trough at 680 nm in stress scenarios as a result of decreasing chlorophyll and photosynthetic activity.

The stressed-induced blue shift of the Red Edge inflection point, around 700 nm has been documented by numerous researchers including Collins et al. (1977), Rock et al. (1988), Milton et al. (1989), Ray (1993) and Kooistra et al. (2003). Changes in the

infrared shoulder around 800 nm due to water stress have been documented by Hunt and Rock (1989), Ceccato et al. (2001) and Zhang et al (2003) and changes in the band depths and band depth centers around the water absorption bands and in the SWIR region in general have been documented by Ceccato et al. (2001), Fensholt and Sandholt (2003) and Noomen et al. (2006).

All of these spectral signatures of vegetation stress are visible in both the laboratory and imagery spectra and these spectral differences enabled the identification and mapping of healthy and arsenic-stressed grass cover in the Spring Valley test areas.

Identification of specific arsenic stress in these areas in Spring Valley required prior knowledge of their spatial location and extent and this information provided a critical content for this research. It cannot be confirmed that this process was able to identify or classify arsenic-specific vegetation stress as opposed to nutrient, pesticide, moisture or any other types of typical vegetation stresses.

The research literature in this area is promising. Horler et al. (1980) found both general and metal-specific stresses in the reflectance data from peas dosed with cadmium, copper, lead and zinc. Milton et al. (1989) identified arsenic- and selenium-specific stress changes in the spectra of soybeans. Bammel and Birnie (1994) found specific patterns of hyperspectral changes in the green edge and red trough in relation to surface plant stress from underground hydrocarbon seepage.

Sims and Gamon (2002) developed a hyperspectral photochemical reflectance index (PRI) to measure specific leaf pigments and the distributions within the leaf structure which is an indicator of plant health and specific types of stress. Schuerger et

al. (2003) utilized hyperspectral reflectance and laser-induced fluorescence to identify specific signatures of zinc stress chlorophyll concentration in Bahia grass. Rosso et al. (2005) used field spectroscopy to identify crude oil and heavy metal stresses in California wetlands vegetation and found very specific differences based on the specific pollutant and the level of contamination.

The logical next step in the evolution of this research is building the knowledge base about pollutant-specific vegetation stress responses and how they affect a wide variety of potentially susceptible species. Even if these pollutant-specific signatures can be developed through laboratory or imaging spectroscopy, these are likely to be very small shifts in spectral band centers or very sensitive VIs and will require a new level of attention to atmospheric correction, cross-sensor calibration, spectral processing standards and quality control procedures.

6. Synthesis and Discussion

6.1 Hypothesis Testing: Historical Aerial Photography

In the historical aerial photographic phase of this research, features derived from the photographic interpretation of 1918 aerial photography were georeferenced and digitized into a GIS format and overlaid on a GIS coverage of areas requiring remediation in the current Spring Valley clean up efforts. Out of 42 polygons from the 1918 photos, 33, or 78.5 %, intersected areas on the remediation coverage. For this study component, the research hypotheses were stated as:

H_0 = Spatially explicit patterns of landscape disturbance, as derived from historical aerial photographs, are NOT spatially related to future hazardous waste remediation requirements.

H_1 = Spatially explicit patterns of landscape disturbance, as derived from historical aerial photographs, ARE spatially related to future hazardous waste remediation requirements.

To test the null hypothesis, a data set of 42 random point values was generated and buffered to a 23.5 m distance, giving each circular polygon the same area as the average of the 1918 polygons. Ten random point/polygon coverages were overlaid on a GIS data layer of the combined areas of required remediation and an average of 13

intersections occurred between the random polygons and the remediation areas. Thus a random sample of the study area resulted in 13 areas requiring remediation. There are now two binary data sets, "photo", and "random", each with 42 points and each with the variable "remedial" set to 0 = no or 1 = yes.

The null hypothesis, involving non-normal binary data can be modeled with a log transformation and tested with a logistic regression model. The test statistic is the Chi-Square Goodness of Fit (SAS 2002). The summarized results are in Table 14. The Chi-Square statistic is 20.0868 and well above the random effects value of 2.1016 and the p value is < .0001. Therefore, the Null Hypothesis is rejected.

6.2 Hypothesis Testing: Modeling Arsenic Uptake with Laboratory Reflectance Data

In the modeling of arsenic uptake with laboratory reflectance spectra, PLS and SLR techniques were utilized to develop and model the relationship between spectral reflectance and arsenic concentration in *Pteris* ferns. The research hypotheses for this component were stated as:

H_0 = Arsenic phytoextraction by *Pteris* ferns can NOT be predicted by spectral reflectance data in the 450 – 2,500 nm region of the electromagnetic spectrum.

H_1 = Arsenic phytoextraction by *Pteris* ferns CAN be predicted by spectral reflectance data in the 450 – 2,500 nm region of the electromagnetic spectrum.

As the final step in the arsenic concentration - spectral reflectance model development process, a limited number of variables (spectral bands) that were identified

Table 14
Null Hypothesis Test
Aerial Photographic Interpretation Features

The SAS Logistic Procedure

Model Information

Data Set	WORK.SVPOINTS
Response Variable	remedial
Number of Response Levels	2
Number of Observations	84
Model	binary logit
Optimization Technique	Fisher's scoring

Testing Global Null Hypothesis: BETA=0

Test	Chi-Square	F	Pr > ChiSq
Likelihood Ratio	20.0686	1	<.0001
Score	19.2220	1	<.0001
Wald	17.4702	1	<.0001

Analysis of Maximum Likelihood Estimates

Parameter	DF	Estimate	Standard Error	Wald Chi-Square	Pr > ChiSq
Intercept	1	-1.2993	0.3760	11.9374	0.0006
Random	1	2.1016	0.5028	17.4702	<.0001

Table 14. Results of the logistic regression for the null hypothesis of remedial = random. The null hypothesis is rejected and the alternate hypothesis is accepted.

by an iterative PLS analysis, were input into a SLR process. The summary results for both ferns are shown in Tables 15 and 16.

Table 15
Null Hypothesis Test
Modeling of Arsenic Concentration in *Pteris cretica mayii*

The SAS Stepwise Linear Regression Procedure

Model: PCM_1D > 500

Dependent Variable: Frond

Stepwise Selection: Step 8
Analysis of Variance

Source	DF	Sum of Squares	Mean Square	F Value	Pr > F
Model	**6**	**109180440**	**18196740**	**35.62**	**< .0001**
Error	55	28097091	510856		
Corrected Total	61	37277532			

Variable	Parameter Estimate	Standard Error	Type II SS	F Value	Pr > F
Intercept	5022.12158	468.87371	58608602	114.73	< .0001
_450	-43.48019	14.84948	4379845	8.57	0.0050
_503	-84.39237	26.66967	5115285	10.01	0.0025
_656	204.30538	48.87576	8926295	17.47	0.0001
_674	116.67897	41.19318	4098578	8.02	0.0064
_1047	-49.85354	15.36349	5379118	10.53	0.0020
_1358	83.41086	36.53512	2662704	5.21	0.0263

Summary of Stepwise Selection

Step	Variable Entered	Variable Removed	Num Vars	Part R^2	Model R^2	C(p)	F Value	Pr > F
1	_656		1	0.545	0.545	59.723	71.76	< .0001
2	_674		2	0.099	0.643	36.239	16.30	0.0002
3	_1047		3	0.049	0.693	25.493	9.30	0.0035
4	_503		4	0.049	0.742	14.758	10.87	0.0017
5	_450		5	0.034	0.776	7.925	8.54	0.0050
6	_1358		6	0.019	0.795	4.911	5.21	0.0263
7	_956		7	0.012	0.807	3.907	3.25	0.0770

Table 15. The Analysis of Variance and summary of the stepwise model selection for the *Pteris cretica mayii* first derivative model, showing the F Statistic and p value at levels to reject the Null Hypothesis at the 99 % confidence interval.

Table 16
Null Hypothesis Test
Linear Modeling of Arsenic Concentration from *Pteris multifida*

The SAS Stepwise Linear Regression Procedure

Model: PMF_1D > 500

Dependent Variable: Frond

Stepwise Selection: Step 9
Analysis of Variance

Source	DF	Sum of Squares	Mean Square	F Value	Pr > F
Model	10	125480622	12548062	16.25	< .0001
Error	56	43240283	772148		
Corrected Total	66	168720905			

Root MSE	878.71948	R-Square	0.7437
Dependent Mean	3063.86119	Adj R-Sq	0.6980
Coeff Var	28.68013		

Variable	Parameter Estimate	Standard Error	Type II SS	F Value	Pr > F
Intercept	2596.32676	154.45431	229438857	282.57	<.0001
_474	121.06626	30.31060	12954049	15.95	0.0002
_488	-120.88362	26.07079	17457214	21.50	<.0001
_1016	64.68674	20.54666	8048155	9.91	0.0026
_1063	-135.62926	26.67813	20986703	25.85	<.0001
_1118	-170.70110	39.01920	15540473	19.14	<.0001
_1979	51.10332	12.68716	13173996	16.22	0.0002
_2022	-43.29900	10.23812	14523252	17.89	<.0001
_2088	36.07435	11.11538	8552575	10.53	0.0020
_2360	12.96350	3.68947	10024530	12.35	0.0009

Summary of Stepwise Selection

Step	Variable Entered	Variable Removed	Vars	Num R2	Part R2	Model C(p)	F Value	Pr > F
1	_1063		1	0.1208	0.1208	119.679	8.93	0.0039
2	_1118		2	0.1211	0.2419	96.5234	10.22	0.0022
3	_2022		3	0.1304	0.3723	71.4281	13.09	0.0006
4	_1979		4	0.0788	0.4511	57.0511	8.90	0.0041
5	_2088		5	0.0680	0.5191	44.9184	8.63	0.0047
6	_2360		6	0.0672	0.5864	32.9454	9.75	0.0028
7	_488		7	0.0325	0.6189	28.1850	5.04	0. 0286
8	_474		8	0.0591	0.6780	17.9117	10.64	0.0019
9	_1016		9	0.0477	0.7257	10.0000	9.91	0.0026

Table 16. The Analysis of Variance and summary of the stepwise model selection for the *Pteris multifida* first derivative model, showing the F statistic and p value at levels to reject the Null Hypothesis at the 99 % confidence interval.

6.3 Hypothesis Testing: Arsenic Stress and Hyperspectral Imagery

In the third segment of this research, HSI data were analyzed with a variety of methods to identify and map grasses stressed by arsenic and especially to distinguish them from non-affected grass areas, as well as map overall land cover in the Spring Valley area. For this study component, the research hypotheses were stated as:

H_0 = Arsenic stress in common lawn grasses can NOT be identified and mapped by the analysis of hyperspectral imagery in the 450 – 2,500 nm region of the electromagnetic spectrum.

H_1 = Arsenic stress in common lawn grasses CAN be identified and mapped by the analysis of hyperspectral imagery in the 450 – 2,500 nm region of the electromagnetic spectrum.

Three different versions of the Kappa statistic were computed with SAS, (SAS 2002) statistical software to test for significance at the 95 % confidence interval. The Cohen's Kappa, Fisher's Exact and Fleiss' Kappa were all applied to the confusion matrix for Linear Spectral Unmixing / Maximum Likelihood classification that resulted in the best overall mapping accuracy (83 %) of all the methods tested. Testing the number of pixels classified correctly for each class against the total number of pixels for each class, all p-values confirm the rejection of the Null Hypothesis. See Table 17.

As an alternative, significance was tested by the calculation of the confidence intervals and in each case, the weighted Kappa value fell within the 95 % confidence interval, supporting the alternative hypothesis that the land cover mapping accuracy was not due to chance.

Table 17
Null Hypothesis Test
Land Cover Mapping Accuracy

HYPOTHESIS TEST for three KAPPA Coefficients **Sample Size = 8**

Weighted Kappa Coefficient	**Cohen's KAPPA**	**Fisher's Exact**	**Fleiss' Kappa**
Weighted Kappa	0.937	0.9866	0.9866
ASE	0.0490	0.0110	0.0110
95% Lower Conf Limit	0.8410	0.9649	0.9649
95% Upper Conf Limit	1.0000	1.0000	1.0000
Test of H_0: Weighted Kappa = 0			
ASE under H_0	0.2693	0.1336	0.2665
Z	3.4795	5.3452	3.7025
One-sided p > Z	0.0003	<.0001	0.0001
Two-sided p > |Z|	0.0005	<.0001	0.0002

Table 17. Three different calculations of the Kappa statistic as a measure of agreement between the correctly classified and total number of pixels in each of eight land cover classes. p values and the upper and lower 95 % confidence interval levels all indicate that the null hypothesis is rejected at the alpha .05 level.

6.4 Significant Results and Discussion

6.4.1 Historical Aerial Photography

The most important result of the historical aerial photographic phase of this research is the relatively high spatial correlation of 78.5 % between the 1918 photo-interpreted features and contemporary hazardous waste remediation requirements. If this percentage, or something similar to it, were to hold true over a significant sample of sites, it could be a potentially important information source for all types of hazardous waste remediation in the future.

The availability of historical imagery in the 1918 time frame is surprising to some extent but it also underscores the fact that the range of historical photo coverage often approaches 90 years or more, especially in urban areas. Only diligent research through a variety of governmental, commercial and educational institutions will reveal the historical profile of imagery available for any given area.

A process-oriented but still important result is that the historical photos in this ongoing project have become a “living” resource that are consulted on a routine basis as new problems or issues arise. Such was the case with the discovery of the second pit on Glenbrook road and the waste disposal areas in the rear portion of the AUES area. This emphasizes the fact that any particular remotely sensed image contains a nearly infinite level of information that may be relevant to a specific issue.

In this case study, the discovery and removal of potentially disastrous threats to the life and health of thousands of residents of the Spring Valley, in the form of CW and

munitions, is but an extreme example of the value of the flow of information from remote sensor to land manager, and the impact it can potentially have on the present day. While the significance of a 78.5 % correlation between 1918 landscape disturbance and contemporary remediation requirements in Spring Valley are notable, it still only represents one site.

It is also significant to this study that, in spite of a variety of available technological capabilities, such as geophysical instrumentation, magnetometers and ground piercing radar, the information derived from historical aerial photographs is, in several instances, the best and most reliable source of information. In all likelihood it was probably also the easiest to obtain and the most cost efficient.

Additional significant results in the historical aerial photographic research are related to the importance of landscape patterns and how they are recorded by imagery and extracted for informational purposes. The relationship between identifiable features of disturbance and future landscape conditions, including risks to human and ecological health might seem straightforward, but it is an often overlooked source of basic, and sometimes critical, information. The current model of remote sensing and information flow is often biased towards space-based systems and the cutting edge sensor technology. While emerging technology improves scientific understanding every day, in some cases, the most important source of information is to be found in the archives of historical data.

An important result of this research is the potential value of the temporal record of landscape-level information recorded on analog historical imagery. Beyond the immediate importance of hazards waste remediation, what is potentially intriguing is that

these historical images record patterns of disturbance that are representative of a larger set of landscape interactions. The features identified by photographic interpretation and related to hazardous waste remediation were really nothing more than signatures of landscape disturbance in a hazardous waste setting. Perturbations and patterns of landscape disturbance are key concepts in ecology that influence both the development and the loss of biodiversity at multiple spatial and temporal scales. Applying this same type of spatial correlation analysis between historical aerial photographic features and landscape conditions could become a rich area of remote sensing research.

Society is often aware of the role that major natural disasters, such as the eruption of Mount Saint Helens in 1980 or the great Mississippi floods in 1988, have had in reshaping the landscape and our ecosystems on a regional or continental scale. In fact, much of ecological theory is based on disturbance as a driving factor in many natural processes. Often though, the role of disturbance on the landscape or local level is not afforded the same level of importance. This type of information is available and potentially critical, as it proved to be in Spring Valley.

6.4.2 Modeling Arsenic Uptake with Laboratory Reflectance Spectra

In this segment, the significant outcomes relate to the results of both the greenhouse growth chamber phase and the results of the spectral modeling. The results of the greenhouse data confirm the fact that ferns *Pteris multifida* and *Pteris cretica mayii* are, in fact, arsenic hyperaccumulators. Average concentrations of frond arsenic were nearly all above 4,000 ppm for both ferns after 12 weeks in the 100 ppm and 200 ppm

levels of soil arsenic. *Pteris multifida* was slightly more efficient at arsenic extraction than *Pteris cretica mayii* with average frond arsenic concentrations of 2,976 and 2,773 ppm respectively. *Pteris multifida* was more tolerant of high arsenic concentrations than was *Pteris cretica mayii* with average biomass yields of 6.5 and 5.2 g respectively.

The control fern *Nephrolepis exaltata* displayed symptoms of stress and phytotoxicity early and throughout the 20-week study with the level of severity directly related to the level of soil arsenic. See Figure 30. There was a significant inverse relationship between frond arsenic and biomass yield in the highest two soil arsenic concentrations ($R^2 = .48$, $p = .004$). One important result for *Nephrolepis exaltata* was the frond arsenic concentrations at the 200 ppm soil arsenic level. At 8 weeks and to the end of the study *Nephrolepis exaltata* had arsenic concentrations at this level, in excess of 4,000 ppm. It is important to note that the biomass yields of these ferns at this level were very low as they were near biological death. It is likely that the high arsenic concentrations were not related to an uptake process as in the *Pteris* ferns but rather other processes such as the fronds coming in direct contact with the soil due to osmotic stress and loss of turgor pressure (Jones et al. 1989).

One of the unique aspects of this experiment was that the soil arsenic was prepared so as to be highly bioavailable to the ferns and both of the *Pteris* ferns had significant uptake of arsenic at the first harvest at 4 weeks. *Pteris cretica mayii* continued to show increases in arsenic uptake through harvest week 16 and then a slight decrease at harvest week 20. This is probably due, at least in part, to environmental conditions as this part of the study extended into October and both day and night ambient

temperatures were falling. An interesting point is that *Pteris cretica mayii* displayed its highest level of frond arsenic concentration and its highest level of phytoextraction at harvest week 16 and from the 100 ppm arsenic soils, not the 200 ppm arsenic soils. *Pteris multifida* had its highest concentration of frond arsenic at harvest week 8 and its highest level of phytoextraction at harvest week 12. This all suggests that there are species-specific differences in the uptake profile of *Pteris* ferns and that specific phytoremediation applications might be developed for different ferns of the *Pteris* genus.

An obvious next step would be another greenhouse uptake experiment, perhaps with *Pteris* ferns that are native to a more temperate climate, in a variety of soil characteristics and with a completely randomized statistical design. A full climate-controlled greenhouse facility would also be desirable.

There are several significant results from the analysis of reflectance spectra. Of the three forms of spectral data evaluated, reflectance, the first derivative and the second derivative, the first derivative was the best for developing a statistical model. The reflectance data are so highly correlated that it becomes very difficult, if not impossible, to find enough components to build a robust and significant model that does not violate the collinearity condition of regression. The second derivative was very noisy and in spite of several different professional spectral processing software applications, is harder to calculate in reality than originally assumed. The key is in the smoothing algorithms that are used in spectral graph processing. Most of the literature in reflectance spectroscopy and imaging spectroscopy suggests employing a Savitsky-Golay smoothing algorithm that performs a local polynomial regression to determine the smoothed value

for each point and offers the advantage of preserving spectral features of the distribution such as subtle absorption features, key edges, relative maxima and minima which are often destroyed by other smoothing techniques (Savitsky and Golay 1964).

The investigation of the relationship between the computed VIs and the actual arsenic concentrations had mixed results. The fact that none of the VIs stayed in the PLS model is a disappointment, as is the failure to achieve any type of model relationship with the *Pteris multifida* data. The models for *Pteris cretica mayii* and *Nephrolepis exaltata* are good and show promise for areas of future research.

The *Nephrolepis exaltata* model selected the Moisture Stress Index (MSI), PRI, RVSI, RNG and MTVI2, which are all measures of some aspect of vegetation stress. Since *Nephrolepis exaltata* is not a hyperaccumulating fern variety, it makes sense that VIs based on stress would stand out as predictors. Further, the RNG, MTVI2, and PRI all have strong components in the green bandwidth of the EMS. The MTVI2 was developed specifically to be an indicator of green LAI (Haboudane et al. 2004). Further, the *Pteris cretica mayii* model utilized the GI, the SGI and the CRI1, which is calculated based on the spectral reflectance values at 510 and 550 nm (the green part of the EMS). It appears that arsenic stress in ferns and the green bandwidths are a potentially important area for further research.

The development of the linear models of arsenic concentration was one of the primary goals of the study, and the results of the model development between the reflectance characteristics and the level of frond arsenic concentration are significant because of the potential to develop a non-contact monitoring tool for phytoremediation

and in the larger context of "bio-reporting", the use of plants to report back important information about landscape conditions. The ability to predict soil and geologic conditions based on vegetation spectra was first developed and explored as a form of biogeophysical mineral exploration by Milton et al. (1983) and with continuing development and deployment of hyperspectral systems, this concept could be advanced to new capabilities.

One of the interesting results in the development of the spectral models of arsenic concentration was the completely different set of wavelengths for each *Pteris* species that proved to be optimal for prediction. The *Pteris cretica* models tended to use bands in the 450–700 nm range, where photosynthetic absorption and reflectance are very pronounced and known to relate to plant physiology. The *Pteris multifida* models mostly used bands in the infrared areas well beyond the range of photosynthetic absorption. One possibility is that the bands in the near and SWIR regions are related to leaf chemistry and specific chemical absorptions. For example, Kokaly and Clark (1999) demonstrated that there were narrow infrared band centers that were related to absorptions of specific chemical compounds. *Pteris* models bands at 1,658, 2,088 and 2,324 nm have been shown to relate to cellulose, nitrogen and lignin respectively.

6.4.3 Mapping Arsenic Induced Vegetation Stress with Hyperspectral Imagery

The third component of this research attempted to map vegetation stress from soil arsenic with HSI acquired by the HyMAP sensor in October 2000. As part of the laboratory spectral work, two species of grasses common to the Spring Valley area were grown in the same concentration of soil arsenic that were used for the ferns. Spectroradiometer readings for the grasses were acquired at the same time as the ferns and were used as a basis to create a basic land cover map of the Spring Valley area including two classes of grass, arsenic-stressed and unaffected.

Significant results from this imaging processing and classification include the overall classification accuracies of 82.9 % with a Kappa coefficient of 0.77. Especially important were the producers and users accuracy of 55.8 % and 82.7 % respectively for the arsenic-affected grass category. Further, a strong signature relationship was demonstrated for this critical land cover class by comparison of the spectra of arsenic-affected grass collected in the laboratory and spectra of arsenic-affected grass derived from the HSI. Both spectra showed very similar patterns of stress-related change in the green, red, NIR and SWIR regions. This ability to extend spectral analysis from the laboratory to the overhead sensor to the identification of a critical landscape condition represents a potentially important capability for remote sensing science.

Other significant results of the HSI processing and analysis include the comparison of 36 combinations of HSI formats and classification decision rule algorithms. With respect to classification decision rule algorithms, the best overall mapping accuracies were obtained with a Mahalanobis Distance classifier at 64.2 %

followed closely by the Maximum Likelihood classifier at 61.5 %. A surprising aspect of these results is that the HSI-specific algorithms, Binary Encoding and the Spectral Angle Mapper, performed poorly in terms of overall accuracy and the older, probability-based statistical classifiers that have been used in multispectral processing for decades, such a Maximum Likelihood, performed very well. In terms of the intermediate image processing formats of HSI, the Continuum Removal and Linear Spectral Unmixing showed the highest overall accuracies with 53.6 % and 52.0 % respectively. Also worth noting is that the VIs calculated and used to map land cover performed poorly in this application.

7. Lessons Learned and the Potential for Additional Research

All major research endeavors involve missteps and errors and science requires researchers to constantly evaluate activities, protocols and paradigms and to correct flaws or improve in basic research activities. In the course of this research effort, several valuable lessons were identified as a result of unforeseen circumstances. Also, several unique and exciting opportunities for subsequent remote sensing research can be articulated.

7.1 Lessons Learned

7.1.1 Greenhouse Procedures and Experimental Design

A limitation in this entire effort was the failure to employ a "Latin Square" design in the greenhouse study. Latin square designs randomize the treatment units and trial order, and allow for "nuisance" factors, such as variability in heat and light or other environmental gradients, to be controlled and accounted for between experimental treatments (NIST/SEMATECH 2003). Although the major objective of this phase of the research was the collection and analysis of spectral reflectance data from ferns growing in a range of known soil-arsenic concentration values, and there was some concern over cross-contamination of soil treatments, a better experimental design would have provided more statistically defensible data about the specific ferns and the factors affecting arsenic

concentration, uptake, exposure, growth rates and a variety of other parameters relating to plant physiology and life strategies of these unique arsenic hyperaccumulating ferns.

An additional minor lesson from this process relates to the procedures for the growing conditions and exposure of the grass samples. The sprouting of grass from seeds was hindered and sometimes completely failed at the high soil-arsenic levels. The grass that sprouted from seeds at the 100 ppm level were severely reduced in biomass and health and the grass seeds in the 200 ppm level did not sprout or grow to any effective degree. It would have likely been much more effective to have transplanted fully formed sod into the arsenic soils than to sprout them from seed. This would have provided a uniform and consistent base condition for spectral and physiological changes due to arsenic exposure.

7.1.2 Sampling and Analysis Procedures for Soil Arsenic

Soil sampling procedures and laboratory analysis methods for inorganic arsenic have been an ongoing concern in both this specific project and in the overall Spring Valley phytoremediation work as well. EPA methods 3050 and 6010B were used for the acid digestion and ICP/AES analysis of inorganic arsenic and total metals (USEPA 1986a, 1986b). Although these are widely accepted methods, the variability in the analytical results has been surprising. Post harvest soil sampling performed for this research showed standard errors as high as 88 % of the sample value, even in a controlled laboratory environment (Blaylock 2005) and similar post harvest sampling results from the Spring Valley phytoremediation have shown that in certain lots, soil arsenic

concentrations have actually *increased* even after six months of verified phytoextraction (Blaylock et al. 2005; Blaylock et al. 2006). Excluding cross- or re-contamination from an unknown source during the active phytoremediation period, results such as these can only be attributed to non representative sampling and/or analysis procedures. In other words, the pre- and post-phytoremediation soil sample results are not reliable, or have far more variability than is acceptable.

Whether the source of variability is in the soil sampling procedures or in the laboratory analysis methods is unknown. Field soil sampling procedures generally consist of compositing five surface samples (one in the center and one at each corner) for each 20 x 20 m grid location (Blaylock et al. 2005; Blaylock et al. 2006). Composite samples are then mixed, ground and prepared for acid digestion. Sample procedures such as this might be very unreliable in this type of environment. The contamination profile of a site such as Spring Valley is related to a variety of anthropogenic activities, and not natural conditions. The distribution of arsenic is not due to the weathering of parent geologic materials or other natural processes that might result in a distribution profile of a continuous or near-continuous surface. In Spring Valley, soil arsenic contamination might have been the result of a mortar or hand grenade explosion, direct application on the soil surface for persistency testing or leakage from a defective artillery shell resulting in a random distribution of arsenic "hot spots" that make composite sample procedures problematic.

While the spatial sampling procedures are undoubtedly a contributing factor, the laboratory methods and results are also suspect. In this study, soils were prepared from a

clean sand, wetted with a solution of sodium arsenate, mixed and dried in bulk for several cycles until a target concentration was achieved. After the final wetting and drying cycle, the soils were mixed and bulk samples from each of the five soil arsenic classes were sent to the lab for analysis. After the last fern harvest at 20 weeks, soils from each arsenic concentration class were composited and samples sent to the lab for a post harvest analysis. Results showed that for at least one class, the arsenic concentration increased and several other classes displayed inconsistent and suspect results for arsenic concentration.

When ICP/AES laboratory analysis of plant biomass shows that a particular fern extracted 25 mg of arsenic from the soil in a 10 cm pot, it is difficult to explain why the soil concentration in that pot increased. Results such as these create inconsistent and sometimes suspect science and casts unfair doubt on a phytoremediation capability that could become a viable alternative clean up method. Different laboratory methods, more rigorous spatial sampling, better quality control and alternative characterization methods, such as x-ray fluorescence, should be fully investigated as possible methods to reduce this level of uncertainty.

7.1.3 Laboratory Collection of Spectral Data

The collection of spectral data under controlled conditions was a key element of this project. Established protocols and methods, such as the use of a calibrated Spectralon standard as a white reference and the use of a Lowell lamp as a primary illumination source, were employed to insure precise and consistent spectral data

collection. Problems were still encountered in the spectral data collections with the introduction of spectral noise at both ends of the solar-visible spectrum (400–2,500 nm). In the ultraviolet/blue region (350–450 nm), spectral noise is typically caused by "dark current", electrical radiation from the instrument itself or nearby electronic devices, or by "stray light" from ambient internal, non-coherent light sources (Lam 2004; Robinson and Dewitt 1983). On the infrared side of the spectrum, noise is usually caused by atmospheric humidity (Myers and Andreas 2004). Even in laboratory conditions, the humid mid-Atlantic summers affected this spectral data collection. Neither of these parts of the spectrum are associated in the literature with vegetation stress or vegetation analysis. In any future spectral data collections of this type, ambient light and atmospheric moisture should be controlled to the highest degree possible.

7.2 Research Opportunities

7.2.1 Historical Aerial Photo/Landscape Pattern Analysis

The results of the spatial correlation between the aerial photographic interpretation results and future remediation needs immediately raises the question of a larger landscape pattern analysis. Is there a quantifiable and significant relationship between landscape disturbance patterns and future soil contamination at hazard waste sites, or in the general industrial land use zone? Further, could this basic disturbance pattern be correlated to other landscape issues beyond soil pollution, such as vegetation communities, urban development patterns or human health issues?

With an archive of over 4,000 reports such as the one performed in Spring Valley, the USEPA holds a rich and unusual source of landscape level information that could reveal new relationships concerning landscape level attributes. A more detailed scientific investigation of the patterns from historical imagery across a sample of hazardous waste sites, might reveal a quantifiable level of information related to aerial photographic signatures and eventual risks to human and ecological health. Further, a study of this type that identified and correlated the landscape pattern of disturbance with future conditions, such as remediation, might also yield a new level of quantification of historical air photo-derived variables and the importance that they might play in landscape ecology.

Many of the archives of historical aerial photographs, dating back to the 1920s, are reaching their effective shelf life and will soon be lost if not recovered digitally or reproduced. Without some resource and policy attention from a national level, many of the priceless archives of these historical aerial photographs, and the landscape information that they contain, will be lost forever. A study that quantifies the value of this information, beyond simple feature identification, could provide the scientific basis and enough justification to obtain the resource commitment necessary to advance archival sciences and preserve invaluable sources of historical photographic information.

7.2.2 Pteris Ferns and Heavy Metal Stress in a Laboratory Environment

There are a number of logical research extensions related to the *Pteris* ferns and the identification of stress in a controlled, laboratory environment. Tests with different

species of *Pteris* ferns, especially temperate climate varieties, would result in additional quantification of arsenic uptake and phytoextraction potential, but might also help to determine if some varieties of *Pteris* ferns could over-winter and if there would be any advantage to that beyond eliminating the need to replant in Spring. What would be the uptake rate over an annual period? Would there be any significant uptake in the spring and fall periods and what is the relationship between ambient temperatures and uptake potential per *Pteris* species?

An interesting result of this research was the fact that both *Pteris* ferns showed significant levels of uptake at 4 weeks and reached uptake maximums at 8 and 12 weeks. If the arsenic uptake rate could be better quantified over time, more optimum phytoextraction strategies might be developed. For example, if the arsenic uptake profile is characterized by a large initial pulse and then a linear relationship related to biomass, as the data in this research suggest, would more arsenic be removed by two successive *Pteris* plantings of 8 weeks each rather than one plant over 16 weeks? Could this be quantified and monitored by hyperspectral analysis?

The development of linear models between arsenic uptake spectral reflectance is also a promising area for research. The initial model development here could be followed by model refinement and model development applications related to specific chemical stressors and/or individual phytoremediation or sentinel vegetation. This might also include a more robust field test of the predictive ability of the current models for *Pteris* ferns.

The identification of arsenic stress in the lawn grasses also leads to a larger issue of sources of stress and the spectral profile development that might be possible. Collecting regular spectral readings, while growing common lawn grasses in a controlled environment and simultaneously subjecting different individual plants or pots to different levels of stress from arsenic, lead, zinc, volatile organic compounds and other stress-inducing agents, could help identify subtle but unique spectral signatures that identify the stressor.

7.2.3 Hyperspectral Imagery Research

The potential applications for HSI as a result of this research are numerous. First, continued development of spectral signatures and mapping strategies for the identification of vegetation stress from fugitive contaminants is an area that should be a research priority. The potential benefits from spectral overhead monitoring of vegetation condition has implications for environmental issues at the local to global scales. An especially important component is the connection between controlled laboratory spectral analysis and the transfer of that information to overhead systems. This was successfully demonstrated in this project and has potential in a wide variety of environmental applications.

Second, additional development of specific HSI processing and classification decision rule strategies is clearly needed. The comparative results of the different image processing and classification decision rules in this project was not what might have been expected from current HSI literature or theory. Needed is basic research on HSI

processing strategies for specific imagery analysis tasks such as LULC mapping, material identification, ecological condition assessment and many other possible tasks.

Third, new methods development in HSI processing should be a part of an evolving paradigm. One of the processing strategies that is receiving increased interest in the remote sensing community is Continuum Removal and band-depth analysis of HSI data. Continuum Removal is a spectral data reduction technique that is used to normalize reflectance spectra and allow comparison of individual absorption features from a common baseline. The continuum is a convex hull fit over the top of a spectrum using straight line segments that connect local spectra maxima. The continuum is removed by dividing it into the actual spectrum for each pixel in the image. The resulting image spectra are equal to 1.0 where the continuum and the spectra match and less than 1.0 where absorption features occur (ENVI 2004). Figure 50 shows a typical vegetation spectra of coast sage as derived from a standard spectroradiometer or hyperspectral imaging sensor and the same spectra after Continuum Removal.

Continuum Removal is very effective at reducing the variability in spectral measurements that is inherent in remote sensing due to a variety of solar, environmental and atmospheric factors. This standardization of the spectral signal allows for a more precise analysis of absorption features in a related analysis technique known as band depth analysis. Subtle differences in the band depth at specific wavelengths relate to species differences, foliar biochemistry and leaf water content.

First proposed as a hyperspectral processing technique by Clark and Rousch (1984) the effectiveness of the Continuum Removal approach was fully demonstrated by

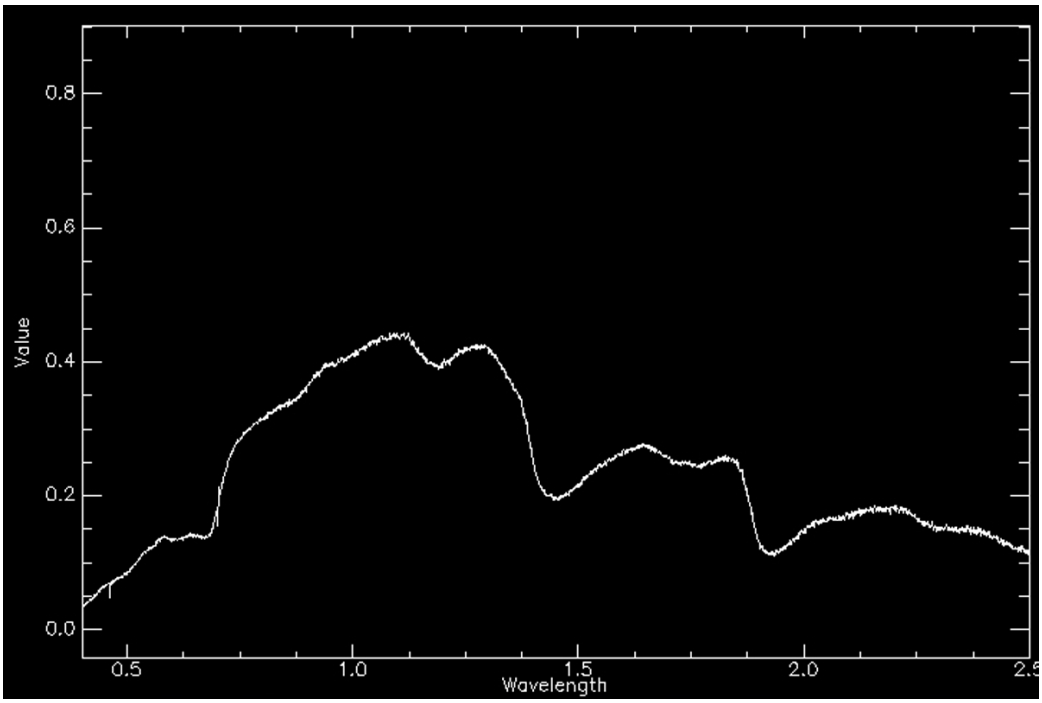

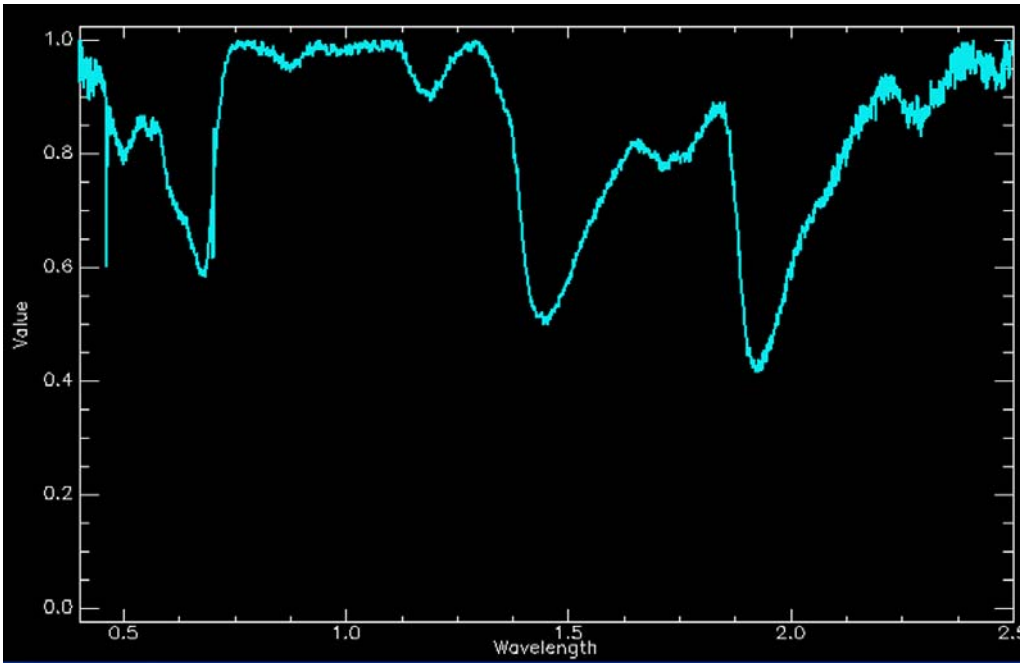

Figure 50. An example of Continuum Removal. Above is the original vegetation spectra of Coast Sage and below is the same spectra after the Continuum Removal processing leaving only the absorption features represented as "band depths". This process provides a high degree of standardization in hyperspectral remote sensing analysis. From ENVI (2004).

Kokaly and Clark (1999) who used laboratory reflectance data of dried and ground leaves to determine leaf biochemistry, theorizing that leaf water content was the most important factor inhibiting and masking the spectral signal from nitrogen, lignin and cellulose.

The Continuum Removal/band depth analytical approach appears to be gaining in popularity with hyperspectral imaging researchers. Mutanga and Skidmore (2004) used band-depth analysis of continuum-removed hyperspectral data to map grass biomass under heavy canopy conditions and were able to correlate VIs with grass biomass at a coefficient of determination of greater than 0.8 and beyond the saturation point of the NDVI. Noomen et al. (2006) showed the Continuum Removal and band depth analysis could detect stress in vegetation from fugitive releases of natural gas from underground pipes. Subtle reflectance changes in the water absorption bands of 1,400 and 1,900 nm and blue shifts in the 560–590 nm region were indicative of ethane-induced stress. Mutanga and Skidmore (2003) were able to apply Continuum Removal to identify and map foliar nitrogen concentrations in African grasslands. Two absorption features located in the visible and the SWIR were detected from an atmospherically corrected HyMAP image and, along with Neural Network Analysis, explained 60 % of the variation in nitrogen concentration in savanna grasses.

As in this study, the ability of HSI data to identify the leaf pigments, metal uptake or cellulose/lignin parameters within an individual plant or at the canopy layer, is where HSI technology starts to represent the merger of geospatial technologies with the analytical methods of chemistry. Continuum Removal techniques normalize spectral absorptions depths and band feature positions, eliminate noise and generally permit very

fine spectral resolutions and feature distinctions in spectral data that are not possible with current methods.

7.2.4 Fluorescence Remote Sensing of Arsenic Phytoextraction

The detection and analysis of arsenic uptake through fluorescence remote sensing is one of the most promising future applications of this study. The analysis of vegetation by fluorescence remote sensing is an area of growing interest in the research community. The fluorescence of chlorophyll is a natural emission in the red part of the spectrum that shows a strong inverse relationship with the level of photosynthetic activity and is one of the natural mechanisms by which plants release excess energy (Schrieber 1983; Lichtenthaller 1988; Lichtenthaller and Rinderle 1988).

A fluorescence emission also occurs in the blue region of the EMS and this has been the subject of intense plant physiological research over the past decade. This is especially with the advent of "active" ultraviolet (UV) and laser induced fluorescence instruments, which create greater quantum yields than passive systems, with spectral resolution sufficient to detect trace metals (Dibennetto 2003) and protein/nitrogen interactions at the leaf level (Corp et al. 1997).

A developmental application of plant fluorescence can be found in the emerging field of monitoring genetically modified vegetation. Transgenic plants can be implanted with a green fluorescence protein (GFP) that fluoresces under UV light enabling long term monitoring and identification of these plants for tracking and safety reasons (Stewart 1996; Stewart et al. 2005). See Figure 51.

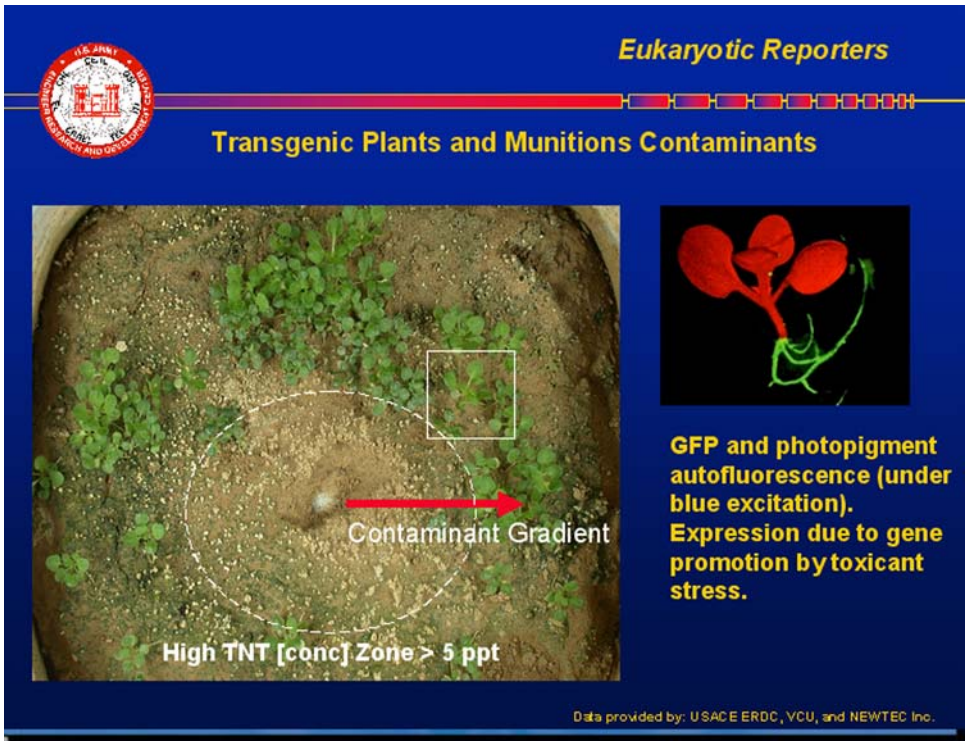

Figure 51. Fluorescence Research with Bioreporters. Transgenic *Arabidopsis* fluoresces in the presence of explosives from a fugitive land mine. From Anderson et al. (2004).

A very specialized but important application of this technology has been developed by the USACE for the bio-reporting of fugitive land mines (Anderson et al. 2004). *Arabidopsis* is genetically modified to fluoresce in the presence of trinitrotoluene (TNT) and can identify fugitive land mines, one of the major threats human health and safety in the world (Siegel 1995).

Research is currently being conducted to genetically modify *Pteris* ferns to fluoresce in the presence of high levels of arsenic in the same way as *Arabidopsis* fluoresces in the presence of TNT. The implications could be important for many areas affected by arsenic contamination.

The results of this study have shown not only the ability of remote sensing technology to deliver critical information to hazardous waste remediation investigations, but also the rich potential for research in emerging remote sensing capabilities. The ability of historical imagery to document past landscape conditions is a unique source of potentially critical information that may never be equaled by any level of technological sophistication. The spectroscopic analysis of plant physiology and condition has the potential to create new, stand-off methods of monitoring and HSI systems are currently delivering new analytical capabilities on a regular basis.

Especially important is the merger of laboratory and imaging spectroscopic methods. The ability of overhead imaging systems to provide analytical capabilities that parallel bench procedures in chemistry represents the evolution of remote sensing from mapping to material identification, and from landscape to molecular analysis, while retaining the geospatial and analytical advantages of each. The research and development and potential new applications for these emerging remote sensing systems are only just beginning.

List of References

List of References

Abdi, H. 2003. Partial Least Squares Regression (PLS-regression). In *Encyclopedia for Research Methods for the Social Science,* edited by M. Lewis-Beck and B.T. Futing: 792-795. Thousand Oaks, California, Sage.

Adams, M.L., W.D. Philpot and W.A. Norvell. 1999. Yellowness index: an application of spectral second derivatives to estimate chlorosis of leaves in stressed vegetation. *International Journal of Remote Sensing,* 18: 3663-3675.

Anderson, J.E., R.L. Fischer and J.D. Nelson. 2004. Trace chemical detection through vegetation sentinels and fluorescence spectroscopy. In *Proceedings: Monitoring Science and Technology Symposium*, September 20-24, 2004, Denver, Colorado.

Antrop, M. and V.V. Eetvelde. 2000. Holistic aspects of suburban landscapes: visual image interpretation and landscape metrics. *Landscape and Urban Planning*, 50: 43-58.

ASD. 1997. *FieldSpec Users Guide*. Analytical Spectral Devices. Boulder, Colorado.

AUES (American University Experiment Station). 1918. Records Collection of the American University Experiment Station, United States Army, Chemical Warfare School, Fort Leonard Wood, Missouri.

Azcue, J.M. and J.O. Nriague. 1994. Arsenic: Historical Perspectives. In *Arsenic in the Environment, Part I: Cycling and Characterization*, edited by J.O. Nriagu, 1-16. John Wiley and Sons, New York.

Babington-Smith, C. 1957. *Air Spy: The Story of Photo Intelligence in World War II*. New York, Harpers.

Bachman, C.M., T.F. Donato, G.M. Lamela, W.J. Rhea, M.H. Bettenhouse, R.A. Fusina, K.R. Du Bois, J.H. Porter and B.R. Truitt. 2002. Automatic classification of land cover on Smith Island, VA. Using HyMAP imagery. *IEEE Transactions on Geoscience and Remote Sensing*, 40 (10): 2313-2330.

Bammel, B.H. and R.W. Birnie. 1994. Spectral reflectance response of big sagebrush to hydrocarbon-induced stress in Bighorn Basin, Wyoming. *Photogrammetric Engineering and Remote Sensing*, 60 (1): 87-96.

Bancroft, W.D. 1919. Bancroft's History of the Chemical Warfare Service in the United States. Research Division, Chemical Warfare Service, American University Experiment Station. Technical Library, Edgewood Arsenal, U.S. Army.

Baret, F.I., G. Champion, G. Guyot and A. Podaire. 1987. Monitoring wheat canopies with a high spectral resolution radiometer. *Remote Sensing of Environment*, 22: 367-378.

Barnaba, E.M., W.R. Phillipson, A.W. Ingram and J. Pim. 1989. Countywide inventory of waste disposal sites: a case study of historic airphoto analysis. In *Proceedings 55th Annual Meeting of the American Society for Photogrammetry and Remote Sensing (ASPRS*), Baltimore, Maryland. ASPRS, Bethesda, Maryland. 1: 167-174.

Barnaba, E.M., W.R. Phillipson, A.W. Ingram and J. Pim. 1991. The use of aerial photographs in county inventories of waste disposal sites. *Photogrammetric Engineering and Remote Sensing* 57: 1289-1296.

Bawden, F.C. 1933. Infra-red photography and plant virus diseases. *Nature* 132: 168.

Benger, M.J. 2004. Fact Sheet: The EPA Remote Sensing Archive. The U.S.E.P.A. Environmental Photographic Interpretation Center (EPIC), Reston, Virginia.

Berry, M. and F. Bove. 1997. Birth weight reduction associated with residence near a hazardous waste landfill. *Environmental Health Perspectives*, 105: 856-861.

Blackburn, G.A. 1998. Spectral indices for estimating photosynthetic pigment concentrations: a test using senescent tree leaves. *International Journal of Remote Sensing*, 19 (4): 657-675.

Blaylock, M.J. 2005. Final Report: The controlled growth of arsenic hyperaccumulating ferns to support EPA spectral imaging studies. Dulles, Virginia, Edenspace Systems Corporation.

Blaylock, M.J., M.P. Elless, C.A. Bray and C.L. Teeter. 2005. Phytoremediation of arsenic contaminated soil, Spring Valley FUDS, Washington, DC., Phase 1 Field Verification Study. Dulles, Virginia, Edenspace Systems Corporation.

Blaylock, M.J., M.P. Elless, C.A. Bray and C.L. Teeter. 2006. Phytoremediation of arsenic contaminated soil, Spring Valley FUDS, Washington, DC., Phase 2 Field Verification Study. Dulles, Virginia, Edenspace Systems Corporation.

Boardman, J.W. 1993. Automated spectral unmixing of AVIRIS data using convex geometry concepts. In *Summaries, Fourth JPL Airborne Geoscience Workshop*, JPL Publication 93-26, 1: 11-14.

Boardman, J.W. and F.A. Kruse. 1994. Automated spectral analysis: a geological example using AVIRIS data, North Grapevine Mountains, Nevada, In *Proceedings of the Tenth Thematic Conference on Geological Remote Sensing*, 407-18. Ann Arbor, Michigan, Environmental Research Institute of Michigan.

Boardman, J.W. 1995. Analysis, understanding and visualization of hyperspectral data as convex sets in n-space. *Optical Engineering*, 2480: 14-22.

Boardman, J.W., F.A. Kruse and R.O. Green. 1995. Mapping target signatures via partial unmixing of AVIRIS data. In *Summaries of the 5nd Annual JPL Airborne Geoscience Workshop*, JPL Publication 95-1, 1: 23-26.

Bogrekci, I. and W.S. Lee. 2005a. Spectral phosphorus mapping using diffuse reflectance of soils and grass. *Biosystems Engineering*, 91 (3): 305–312.

Bogrekci, I. and W.S. Lee. 2005b. Spectral phosphorus mapping using diffuse reflectance of soils and grass. *Biosystems Engineering*, 92 (4): 527–533.

Bogrekci, I. and W.S. Lee. 2006. Comparison of ultraviolet, visible, and near infrared sensing for soil phosphorus. *Biosystems Engineering*, In Press.

Bondada, B.R. and L.Q. Ma. 2003. Chapter 28, Tolerance of Heavy Metals in Vascular Plants: Arsenic Hyperaccumulation by Chinese Brake Fern (Pteris vittata L). In *Pteridology in the New Millennium*, edited by S. Chandra and M. Srivastava, 397-420. The Netherlands, Kluwer Academic Publishers.

Boyajian, G.E. and D.L. Devedjian, 1997. Phytoremediation: it grows on you. *Soil and Groundwater Cleanup*, February/March, 22-26.

Bracher, G.A. 1991. Detection Of Nutrient Stress In Douglas-Fir Seedlings Using Spectroradiometer Data. PhD Thesis. University of British Columbia, Vancouver. 236 pages.

Broge, N.H. and E. LeBlanc. 2001. Comparing prediction power and stability of broadband and hyperspectral vegetation indices for estimation of green leaf area index and canopy chlorophyll density. *Remote Sensing of Environment,* 76: 156–172.

Brown, L., M.C. Jin, S.G. Lablanc and J. Cihlar. 2000. A shortwave infrared modification to the simple ratio for LAI retrieval in boreal forests: an image and model analysis. *Remote Sensing of Environment*, 71: 16-25.

CAA. 1963. Clean Air Act. Public Law 88-206, [As Amended Through P.L. 101–549, November 15, 1990]. 42 U.S.C. § 7401 *et seq*.

Campbell, J.B. 1987. *Introduction to Remote Sensing.* Guilford. Press, New York. 551 Pages.

Carbonell-Barrachina A.A., F. Burlo, A. Burgos-Hernandez, E. Lopez and J.T. Mataix. 1997. The influence of arsenic concentration on arsenic accumulation in tomato and bean plants. *Scientia Horticulturae,* 71: 167–176.

Ceccato, P., S. Flasse, S. Tarantola, S. Jacquemoud, and J.M. Gregoire, 2001. Detecting vegetation leaf water content using reflectance in the optical domain. *Remote Sensing of Environment* 77: 22-33.

CERCLA 1980. Comprehensive Environmental Response, Compensation, and Liability Act (commonly known as Superfund). Public Law 96-510, 42 U.S.C. §§ 9601 *et seq*.

Chang, S.H. and W. Collins. 1983. Confirmation of airborne biogeophysical mineral exploration technique using laboratory methods. *Economic Geology*, 78 (4): 723-736.

Chappelle, E.W., M.S. Kim, and J.E. McMurtrey. 1992. Ratio Analysis of Reflectance Spectra (RARS): an algorithm for the remote estimation of the concentrations of chlorophyll a, chlorophyll b, and the carotenoids in soybean leaves. *Remote Sensing of Environment*, 39: 239-247.

Chen, Z., P.J. Curran and J.D. Hansom. 1992. Derivative reflectance spectroscopy to estimate suspended sediment concentration. *Remote Sensing of Environment*, 40: 67-77.

Chen, Z., C.D. Elvidge, and W.T. Jansen. 1993. Description of a derivative-based high spectral-resolution (AVIRIS) green vegetation index. In *Proceedings of Imaging Spectrometry of the Terrestrial Environment*, Orlando, FL, SPIE 1937: 43–54.

Chen, J. 1996. Evaluation of vegetation indices and modified simple ratio for boreal applications. *Canadian Journal of Remote Sensing*, 22: 229-242.

Clark, W. 1946. *Photography by Infrared*. New York: John Wiley and Sons, 472 p.

Clark, R.N. and T.L. Roush. 1984. Reflectance spectroscopy: quantitative analysis techniques for remote sensing applications: *Journal of Geophysical Research*, 89 (7): 6329-6340.

Clark, R.N., 1997. Chapter 1: Spectroscopy of Rocks and Minerals, and Principles of Spectroscopy. In *Manual of Remote Sensing, Volume 3, Remote Sensing for the Earth Sciences*, edited by A.N. Rencz. 3-58. New York, John Wiley and Sons.

Cocks, T., R. Jenssen, A. Stewart, I. Wilson and T. Shields. 1998. The HYMAP airborne hyperspectral sensor: the system, calibration and performance. Presented at 1st EARSEL Workshop on Imaging Spectroscopy, Zurich, Switzerland, October 1998.

Cohen, J. 1960. A coefficient of agreement for nominal scales. *Educational and Psychological Measurement*, 20: 37-46.

Collins, W., G.L. Raines and F.C. Canney. 1977. Geological Society of America. 1977 Annual Meeting, Seattle, Washington, 7-9 November. Abstracts with programmes, 932-933.

Collins, W., G.L. Raines and F.C. Canney, and R. Ashley. 1983. Airborne biogeophysical mapping of hidden mineral deposits. *Economic Geology*, 78 (4): 737-749.

Colwell, R.N., 1956. Determining the prevalence of certain cereal crop diseases by means of aerial photography. *Hilgardia* 26: 223-286.

Colwell, R.N., Editor. 1960. *Manual of Photographic Interpretation.* Washington, D.C. American Society of Photogrammetry.

Colwell, R.N. 1997. Chapter 1: History and Place of Photographic Interpretation. In *The Manual of Photographic Interpretation, Second Edition*. Edited by Warren R Phillipson. American Society for Photogrammtery and Remote Sensing, Bethesda, Maryland, 3-47.

Congalton, R.G. and R A. Mead. 1983. A quantitative method to test for consistency and correctness in photointerpretation. *Photogrammetric Engineering and Remote Sensing*. 49 (1): 69-74.

Congalton, R.G., R. Oderwald and R.A. Mead. 1983. Assessing Landsat classification accuracy using discrete multivariate analysis statistical techniques. *Photogrammetric Engineering and Remote Sensing*, 49 (12): 1671-1678.

Congalton, R.G. 1991. A review of assessing the accuracy of classification of remotely sensed data. *Remote Sensing of Environment*, 37: 35-46.

Corp, L.A., J.E. McMurtrey, E.W. Chappelle, C.S.T. Daughtry and M.S. Kim. 1997. UV band fluorescence (in vivo) and its implications for the remote assessment of nitrogen supply in vegetation. *Remote Sensing of Environment*, 61 (1): 110-117.

Curran, P.J. 1989. Remote sensing of foliar chemistry. *Remote Sensing of Environment*, 29: 271-278.

CWA. 1948. Federal Water Pollution Control Act. Public Law 80-845, [As Amended Through Public Law 107–303, November 27, 2002]. 33 U.S.C. §§ 1251 *et seq*.

Dahmani-Muller, H., F. van Oort, B. Gelie, and M. Balabane. 2000. Strategies of heavy metal uptake by three plant species growing near a metal smelter. *Environmental Pollution*, 109: 231–238.

Daughtry, C.S., C.L. Walthall, M.S. Kim, E. Brown de Colstoun and J.E. McMurtrey III. 2000. Estimating corn leaf chlorophyll concentration from leaf and canopy reflectance. *Remote Sensing of Environment*, 74: 229-239.

de Nava, C.C. 1996. World wide overview of hazardous wastes. *Toxicology and Industrial Health*, 12 (2): 127-38.

Demetriades-Shah, T.H., M.D. Steven and J.A. Clark. 1990. High resolution derivative spectra in remote sensing. *Remote Sensing of Environment*, 33: 55-64.

DERP (Defense Environmental Restoration Program), Title 10, Subtitle A, Part IV, Chapter 160, United States Code § 2701 *et seq*.

DiBenedetto J. 2003. Laser-induced fluorescence remote sensing. Abstracts of the Spectral Remote Sensing of Vegetation, March 12-14, 2003, U.S. Environmental Protection Agency, Las Vegas, Nevada.

Dixit L. and S. Ram. 1985. Quantitative analysis by derivative electronic spectroscopy. *Applied Spectroscopy Reviews*, 21 (4): 311-418.

Dockray, M. 1981. Verification of a new method for determining chlorophyll concentration in plants by remote sensing. Masters of Science Thesis, Imperial College, University of London.

Duble, R.L., J.C. Thomas and K.W. Brown. 1978. Arsenic pollution from underdrainage and runoff from golf greens. *Journal of Agronomy*, 70: 71-74.

Edenspace. 2004. Case Study: Arsenic.
http://www.edenspace.com/casestudy-arsenic.html
Last accessed January 25, 2007.

Eisler, R. 1994. A review of Arsenic Hazards to Plants and Animals with Emphasis on Fishery and Wildlife Resources. In *Arsenic in The Environment. Part II: Human Health and Ecosystem Effects, e*dited by J.O. Nriagu, 185-261. New York, John Wiley & Sons.

ElMasry, G.N., A.E. Wang, L. Sayed and M. Ngadi. 2006. Hyperspectral imaging for nondestructive determination of some quality attributes for strawberry. *Journal of Food Engineering*. *In Press.*

Elvidge, C.D. and Z. Chen. 1995. Comparison of broad-band and narrow band red and near-infrared vegetation indices. *Remote Sensing of Environment*, 54: 38-48.

ENVI (Environment for Visualizing Images). 2004. Image Processing Software. Research Systems Incorporated, Boulder Colorado. Version 4.0
http://www.rsinc.com/envi/
Last accessed January 25, 2007

Erb, D.K. 1968. The identification of fruit trees by aerial photograph analysis and interpretation for census purposes. In *Proceedings, Second Seminar of Air Photo Interpretation in the Development of Canada*, (Ottawa), 97-99.

Erb, T.L., W.R. Philipson, W.L. Teng and T. Liang. 1981. Analysis of landfills with historical airphotos. *Photogrammetric Engineering and Remote Sensing,* 47 (9): 1361-1369.

Eriksson, L., E. Johansson, N. Kettaneh-Wold and S. Wold. 2001. Multi- and megavariate data analysis: principles and applications. Kinnelon, N.J., Umetrics Incorporated.

Fatz, R.J. 2001. Testimony: Subcommittee On The District Of Columbia Committee On Government Reform U.S. House Of Representatives July 27, 2001, Raymond J. Fatz, Deputy Assistant Secretary of the Army (Environment, Safety and Occupational Health).
http://www.nab.usace.army.mil/projects/WashingtonDC/springvalley/Minutes/~Testimony/FatzTestimony2001.pdf. Last Accessed January 22, 2007.

Fensholt, R. and I. Sandholt. 2003. Derivation of a shortwave infrared water stress index from MODIS near and shortwave infrared data in a semiarid environment. *Remote Sensing of Environment*, 87: 111–121.

Fitzpatrick-Lins, K. 1981. Comparison of sampling procedures and data analysis for a land use and land cover maps. *Photogrammetric Engineering and Remote Sensing,* 47 (3): 343-351.

Fleiss, J.L. 1981. *Statistical methods for rates and proportions, 2ed*. Chapter 13: The Measurement of Interrater Agreement, 212-236. New York, John Wiley & Sons.

Focazio, M.J., A.H. Welch, S.A. Watkins, D.R. Helsel and M.A. Horn. 1999. A retrospective analysis on the occurrence of arsenic in ground-water resources of the United States and limitations in drinking-water-supply characterizations: *U.S. Geological Survey Water-Resources Investigations Report 99-4279.*

Fries, A.A. and C.J. West. 1921. *Chemical Warfare*. New York: McGraw-Hill.

Gamon, J.A., J. Penuelas and C.B. Field. 1992. A narrow-waveband spectral index that tracks diurnal changes in photosynthetic efficiency. *Remote Sensing of Environment*, 41: 35-44.

Gamon, J.A. and H. Qiu. 1999. Ecological Applications of Remote Sensing at Multiple Scales. In *Handbook of Functional Plant Ecology*, edited by F.I. Pugnaire and F. Valladares, New York: Marcel Dekker.

Gao, B.-C., K.B. Heidebrecht and A.F.H. Goetz. 1993. Derivation of scaled surface reflectances from AVIRIS data. *Remote Sensing of Environment*, 44: 145-163.

GAO (U.S. General Accounting Office). 2001. Environmental Contamination: Cleanup Actions at Formerly Used Defense Sites. Report to Congressional Requesters. GAO-01-557, U.S. General Accounting Office, Washington, D.C.

GAO (U.S. General Accounting Office). 2002. Environmental Contamination: Many Uncertainties Affect the Progress of the Spring Valley Cleanup. Report to the Subcommittee on the District of Columbia, Committee on Government Reform, House of Representatives.GAO-02-556. U.S. General Accounting Office, Washington, D.C.

Garofalo, D. and F. Wobber. 1974. Solid waste and remote sensing. *Photogrammetric Engineering,* 40 (1): 45-59.

Gates, D.M., H.J. Keegan, J.C. Schleter, and V.R. Weidner. 1965. Spectral properties of plants. *Applied Optics*, 4 (1): 11-20.

Goetz, A.F.H. and W.M. Calvin. 1987. Imaging spectrometry: spectral resolution and analytical identification of spectral features. SPIE, *Imaging Spectroscopy II*, 834: 158-165.

Goodman, M.S. 1959. A Technique for the identification of farm crops on aerial photographs. *Photogrammetric Engineering,* 25: 131-138.

Goodman, M.S. 1964. Criteria for the identification of types of farming on aerial photographs. *Photogrammetric Engineering,* 30: 984-991

Gorby, M.S. 1994. Arsenic in Human Medicine. In *Arsenic in the Environment, Part II: Human Health and Ecosystem*, edited by J.O. Nriagu, 1-16. John Wiley and Sons, New York.

Green, A.A., M. Berman, P. Switzer and M.D. Craig. 1988. A transformation for ordering multispectral data in terms of image quality with implications for noise removal. *IEEE Transactions on Geoscience and Remote Sensing*, 26 (1): 65-74.

Green, R.O., M.L. Eastwood and O. Williams. 1998. Imaging Spectroscopy and the Airborne Visible/Infrared Imaging Spectrometer (AVIRIS). *Remote Sensing of Environment*, 65: 227-240.

Guyot G., F. Baret and S. Jacquemoud. 1992. Imaging Spectroscopy for Vegetation Studies. In *Imaging Spectroscopy: Fundamentals and Prospective Applications*, Edited by F. Toselli and J. Bodechtel, 145-165. ECSC, EEC, EAEC, Brussels and Luxembourg.

Habeck, C., J. W. Krakauer, C. Ghez, H.A. Sackeim, D. Eidelberg, Y. Stern and J.R. Moeller. 2005. A New Approach to Spatial Covariance Modeling of Functional Brain Imaging Data: Ordinal Trend Analysis. *Neural Computation*, 17 (7): 1602-1645.

Haboudane, D., J.R. Miller, E. Pattey, P.J. Zarco-Tejada and I.B. Strachan. 2004. Hyperspectral vegetation indices and novel algorithms for predicting green LAI of crop canopies: Modeling and validation in the context of precision agriculture. *Remote Sensing of Environment*, 90 (3): 337-352.

Hall, H.I., W.E. Kaye, L.S. Gensburg and E.G. Marshall. 1996. Residential proximity to hazardous waste sites and risk of end-stage renal disease. *Journal of Environmental Health,* 59: 17-21.

Hansen, P.M., J.R. Jorgenson and A. Thomsen. 2002. Predicting grain yield and protein content in winter wheat and spring barley using repeated canopy reflectance measurements and partial least squares regression. *The Journal of Agricultural Science,* 139: 307-318.

Hegg, K.M. 1967. A Photo identification guide for the land and forest types of Alaska. Juneau, Alaska: Northern Forest Experiment Station. USDA Forest Research Paper NOR-3, 55p.

Heller, C.E. 1984. *The Leavenworth Papers, Number 10. Chemical Warfare in World War I: The American Experience, 1917-1918.* Combat Studies Institute, U.S. Army Command and General Staff College, Fort Leavenworth, Kansas 66027-6900.

Honigberg, C. and M. Nolan. 2000. Who pays for the stigma of environmental contamination? Commercial Investment Real Estate. http://www.ciremagazine.com/article.php?article_id=406 Last Accessed April 22, 2006

Horler, D.N.H., J. Barber and A.R. Barringer. 1980. Effects of heavy metals on the absorbance and reflectance spectra of plants. *International Journal of Remote Sensing*, 1 (2): 121-136.

Horler, D.N.H., M. Dockray, J. Barber and A.R. Barringer. 1983. Red edge measurements for remote sensing plant chlorophyll content. *Advances in Space Research,* 3 (2): 273-277.

Höskuldsson, A. 1988. PLS regression methods. *Journal of Chemometrics,* 2 (3) 211-228.

Huete, A.R. 1988. A Soil Adjusted Vegetation Index (SAVI). *Remote Sensing of Environment,* 17: 5-53.

Hunt, S.D.and H. Sierra. 2003. Spectral oversampling in hyperspectral imagery. In *Proceedings of the SPIE. Algorithms and Technologies for Multispectral, Hyperspectral, and Ultraspectral Imagery IX*. Edited by S.S. Shen, and P.E. Lewis, 5093: 643-650.

Hunt, E.R. Jr., and Rock, B. N. 1989. Detection of changes in leaf water content using near- and middle-infrared reflectances. *Remote Sensing of Environment,* 30: 43–54.

Imbernon, J. 1999. Pattern and development of land-use changes in the Kenyan highlands since the 1950. *Agriculture, Ecosystems and Environment,* 76: 67–73.

Irwin, W. 1915. The German Army dispersed chlorine gas over Allied lines at Ypres on 22 April 1915. New York Tribune, April 25, 1915.

IUPAC (International Union of Pure And Applied Chemistry). 1993. Glossary For Chemists Of Terms Used In Toxicology: Pure and Applied Chemistry, 65(9): 2003-2122 (on-line version posted by the U.S. National Library of Medicine). http://sis.nlm.nih.gov/enviro/glossarymain.html
Last Accessed December 7, 2006

Ives, R.L. 1939. Infrared Photography As an Aid in Ecological Surveys. *Ecology,* 20: 433-439.

Jones, H.G., T.L. Flowers and M.B. Jones. 1989. *Plants Under Stress*. Cambridge New York, University Press.

Jordan, C.F. 1969. Derivation of leaf area index from quality of light on the forest floor, *Ecology*, 50: 663-666.

Karim, M.M. 2000. Arsenic exposure modeling and risk assessment in Bangladesh using geographic information system, In *The Second International Health Geographics Conference,* 35-42. Washington D.C. March 17 - 19, 2000.

Kartman A.S. and E.T. Slonecker. 2001. Historical Aerial Photographic Analysis, Spring Valley Site, Washington, D.C. Report TS-PIC-20103439S, Volumes 1 and 2, U.S. Environmental Protection Agency, Environmental Sciences Division, Las Vegas, Nevada.

Keegan, H.J. and H.T. O'Neill. 1951. Spectrophotometric study of autumn leaves. *Journal of the Optical Society of America*, 41: 284.

Keegan, H.J, J.C. Schleter and W.A. Hall. 1955. Spectrophotometric and Colorimetric Change in the Leaf of a White Oak Tree Under Conditions of Natural Drying and Excessive Moisture. National Bureau of Standards Report Number 4322. Government Printing Office, Washington, D.C.

Kleman, J. and E. Fagerlund. 1981. Spectral signature measurements of barley crops the influence of irrigation and fertilization. In *Proceedings of International Colloquium on Spectral Signatures of Objects in Remote Sensing.* (Avignon, France). *International Society of Photogrammetry and Remote Sensing*, 417-424.

Knickerbocker, B. 2002. Former military sites littered with bombs. Christian Science Monitor November 22, 2002
http://www.csmonitor.com/2002/1127/p02s02-usgn.html
Last accessed January 25, 2007.

Kokaly, R.F. and R.N. Clark. 1999. Spectroscopic determination of leaf biochemistry using band-depth analysis of absorption features and stepwise multiple linear regression. *Remote Sensing of Environment,* 67: 267-287.

Kooistra, L., J. Wanders, G.F. Epema, R.S.E.W. Leuven, R. Wehrens and L.M.C. Buydens. 2003. The potential of field spectroscopy for the assessment of sediment properties in river floodplains. *Analytica Chemica Acta,* 484: 189–200.

Kooistra, L , E.A.L. Salas, J. Clevers, R.R. Wehrens, R.S.E.W. Leuvena, P.H. Nienhuisa, and L.M.C. Buydens. 2004. Exploring field vegetation reflectance as an indicator of soil contamination in river floodplains. *Environmental Pollution,* 127: 281–290.

Kosmas, C.S., N. Curi, R.B. Bryant and D.P. Franzmeier. 1984. Characterization of iron oxide minerals by second derivative visible spectroscopy. *Journal of the Soil Science Society of America*, 48: 401-405.

Kresta J.V., J.F. Macgregor and T.E. Marlin. 1991. Multivariate statistical monitoring of process operating performance. *Canadian Journal of Chemical Engineering,* 69 (1): 35-47.

Kruse, F.A., J.W. Boardman and J.F. Huntington. 2003. Comparison of airborne hyperspectral data and EO-1 Hyperion for mineral mapping. *IEEE Transactions on Geoscience and Remote Sensing*, 41 (6): 1388-1400.

Kruse, J.K., N.E. Christians and M.H. Chaplin. 2006. Remote sensing of nitrogen stress in creeping bentgrass. *Journal of Agronomy*, 98: 1640-1645.

Lam, H. 2004. Performance of UV-Vis spectrophotometers. Calibration & Validation Group (CVG), Glaxo-Wellcome Inc.
http://www.cvg.ca/images/Performance_UV_Vis.pdf
Last Accessed January 22, 2007.

Lichtenthaler, H.K. 1988. Remote sensing of chlorophyll fluorescence in oceanography and in terrestrial vegetation: an introduction. In *Applications of Chlorophyll Fluorescence*, edited by H.K. Lichtenthaler, 287-297. Kluwer, Dordrecht.

Lichtenthaler, H.K., and U. Rinderle. 1988. The Role of chlorophyll fluorescence in the detection of stress conditions in plants. *Critical Reviews in Analytical Chemistry*, 19 (Suppl. 1): s29-s85.

Lybarger, J.A., R. Lee, D.P. Vogt, R.M. Perhac, Jr, R.F. Spengler and D.R. Brown. 1998. Medical costs and lost productivity from health conditions at volatile organic compound-contaminated superfund sites. *Environmental Research* 79: 9–19.

Lyon, J.G. 1982. The use of aerial photographs and remote sensing data in the management of hazardous waste sites. In *Hazardous Waste Management for the 80's*, edited by T. Sweeny, H. Bhatt, R. Sykes, and O. Sproul, 163-171. Ann Arbor, Michigan, Ann Arbor Science Publications.

Lyon, J.G. 1987. The use of maps, aerial photographs and other remote sensing data for practical evaluation of hazardous waste Sites. *Photogrammetric Engineering and Remote Sensing,* 53: 515-519.

Ma, L.Q., K.M. Komar, C. Tu, W. Zhang, and Y. Cai. 2001. A fern that hyperaccumulates arsenic. *Nature*, 409: 579.

Maclure, M. and W.C. Willett. 1987. Misinterpretation and misuse of the kappa statistic. *American Journal of Epidemiology*, 126: 161-169.

MacGregor, J.F., C. Jaeckle, C. Kiparissides and M. Koutoudi. 2004. Process Systems. Engineering: Process monitoring and diagnosis by multiblock PLS methods. *AIChE Journal,* 40 (5): 826–838.

Martens, H. and T. Naes. 1989. *Multivariate Calibration*. Chichester, Wiley.

Martin, M.E. and J.D. Aber. 1993. Measurements of canopy chemistry with 1992 AVIRIS data at Blackhawk Island and Harvard forest. In *Summaries of the Fourth Annual JPL Airborne Geoscience Workshop: AVIRIS,* Edited by R.O. Green, 1:113-116. Jet Propulsion Laboratory, Pasadena, California.

Martin, M.E. and J.D. Aber. 1997. Estimation of forest canopy lignin and nitrogen concentrations and ecosystems processes by high resolution remote sensing. *Ecological Applications,* 7: 431-443.

Martin, M.E., S.D. Newman, J.D. Aber, and R.G. Congalton. 1998. Determining forest species composition using high spectral resolution remote sensing data. *Remote Sensing of Environment,* 65: 249-254.

Marzorati, S., L. Luzia, V. Petrini, F. Meronia and F. Pergalani. 2003. Detection of local site effects through the estimation of building damages. *Soil Dynamics and Earthquake Engineering,* 23: 497–511.

Mata, L. 2002. Historical Drainage Channel Analysis of Spring Valley Site, Washington, D.C. TS-PIC-20203486S, U.S. Environmental Protection Agency, Environmental Sciences Division, Las Vegas, Nevada.

Maclure, M. and W.C. Willett. 1987. Misinterpretation and misuse of the kappa statistic. *American Journal of Epidemiology,* 126: 161-169.

McNicholas, H.J. 1931. The visible and ultraviolet absorption spectra of carotin and xanthophyll and the changes accompanying oxidation. *Bureau of Standards Journal of Research,* 7 (1): 171-193.

Meharg A.A. and J. Hartley-Whitaker. 2002. Arsenic uptake and metabolism in arsenic resistant and nonresistant plant species. *New Phytologist,* 154 (1): 29-43.

Milton, N.M., W. Collins and S.H. Chang. 1983. Confirmation of airborne biogeophysical mineral exploration technique using laboratory methods. *Economic Geology*, 78 (4): 723-736.

Milton, N.M., C.M. Ager, B.A. Eisworth and M.S. Powers. 1989. Arsenic and selenium induced changes in spectral reflectance and morphology of soybean plants. *Remote Sensing of Environment,* 30: 263-269.

Milton, N.M., B.A. Eisworth and C.M. Ager. 1991. Effect of phosphorous deficiency on spectral reflectance and morphology of soybean plants. *Remote Sensing of Environment,* 36: 121-127.

Multispectral Users Guide. 1995. Spectral Imagery Technology Applications Center (SITAC), Logicon/Geodynamics Incorporated, Fairfax, Virginia, 1-7.

Murtha, P.A. 1997. Chapter 5: Vegetation. In *The Manual of Photographic Interpretation, Second Edition*, edited by Warren R. Phillipson. American Society for Photogrammetry and Remote Sensing, Bethesda, Maryland.

Mutanga O. and A.K. Skidmore. 2003. Integrating imaging spectroscopy and neural networks to map grass quality in the Kruger National Park, South Africa. *Remote Sensing of Environment,* 90 (1): 104-115.

Mutanga O. and A.K. Skidmore. 2004. Hyperspectral band depth analysis for a better estimation of grass biomass (Cenchrus ciliaris) measured under controlled laboratory conditions. *International Journal of Applied Earth Observation and Geoinformation,* 5 (2): 87-89.

Myers, D.R. and A.A. Andreas. 2004. Sensitivity of spectroradiometric calibrations in the near infrared to variations in atmospheric water vapor. National Renewable Energy Laboratory, NREL/CP-560-36037, NREL, Golden, Colorado. http://www.nrel.gov/docs/fy04osti/36037.pdf
Last accessed January 22, 2007.

Nash, M.S., D.J. Chaloud and R.D. Lopez. 2005. Applications of Canonical Correlation And Partial Least Squares in Landscape Ecology. Environmental Sciences Division, U.S. Environmental protection Agency, Las Vegas, Nevada. EPA/600/X-05/004. 82 p.

NATO (North Atlantic Treaty Organization). 1954. Protocol No. III: On the Control of Armaments

Nelson, A.B., L.A. Hartshorn and R.A. Young. 1983. A methodology to inventory, classify and prioritize uncontrolled waste disposal sites. Report EPA-600/4-83-050. U.S. Environmental Protection Agency, Las Vegas, Nevada.

NIST/SEMATECH. 2003. e-Handbook of Statistical Methods, 5.3.3.2.1. Latin square and related designs.
http://www.itl.nist.gov/div898/handbook/
Last accessed January 22, 2007.

Noomen, M.F., A.K. Skidmore, F.D. van der Meer and H.H.T. Prins. 2006. Continuum removed band depth analysis for detecting the effects of natural gas, methane and ethane on maize reflectance. *Remote Sensing of Environment,* 105 (3): 262-270.

Nriagu, J.O., Editor. 1994. *Arsenic in the Environment, Part I: Cycling and Characterization*. New York, John Wiley and Sons.

NRC (National Research Council). 1999. Arsenic in Drinking Water. National Academy Press, National Academy of Sciences, Washington, D.C.

Nyberg, L., C. Forkstam, K.M. Petersson, R. Cabeza, M. Cabeza and M. Ingvar. 2002. Brain imaging of human memory systems: between-systems similarities and within-system differences. *Cognitive Brain Research,* 13: 281–292.

Parry, J.D. 1973. The development of air photo interpretation in Canada. *The Canadian Observer,* 27 (4): 320-351.

Parsons Engineering Science, Incorporated. 1995. Final Remedial Investigation Report For The Operation Safe Removal Formerly Used Defense Site, Washington, D.C. U.S. Army Corps of Engineers, Huntsville Division, Baltimore District.

Parsons Engineering Science, Incorporated. 2003. Engineering Evaluation / Cost Analysis For Arsenic In Soil Spring Valley Operable Units 4 And 5 Washington, D.C. Contract Daha90-94-D-0010, Task Order DA01 DERP-FUDS HTRW Project No. C03DC091802. 3 Volumes.

Pearson, R.I. and L.D. Miller. 1972. Remote Mapping of Standing Crop Biomass for Estimation of the Productivity of the Shortgrass Prairie, Pawnee National Grasslands, Colorado. In *Proceedings of Eight International Symposium of Remote Sensing for the Environment*, 1355-1379. Ann Arbor, Michigan, Environmental Research Institute of Michigan (ERIM).

Peart, V. 1993. Indoor Air Quality in Florida: Houseplants to Fight Pollution. Publication FCS 3208, Department of Family, Youth and Community Services, Florida Cooperative Extension Service, Institute of Food and Agricultural Sciences, University of Florida;
http://edis.ifas.ufl.edu/HE356
Last Accessed January 25, 2007.

Penuelas, J., F. Baret, and I. Filella. 1994. Semi-empirical indices to assess carotenoids/chlorophyll-a ratio from leaf spectral reflectance. *Photosynthetica,* 31: 221-230.

Peterson, D.L., J.D. Aber, P.A. Matson, D.H. Card, N.A. Swanberg, C.A. Wessman and M.A. Spanner. 1988. Remote sensing of forest canopy leaf biochemical contents. *Remote Sensing of Environment*, 24: 85-108.

Philpot, W.D. 1991. The derivative ratio algorithm: avoiding atmospheric effects in remote sensing. *IEEE Transactions on Geoscience and Remote Sensing,* 29: 350-357.

Philipson, W.R., E.M. Barnaba, A. Ingram, and V.L. Williams. 1988. Land cover monitoring with spot for landfill investigations. *Photogrammetric Engineering and Remote Sensing,* 54 (2): 223-228.

Philipson, W.R., Editor. 1997. Manual of Photographic Interpretation. Bethesda, Maryland: American Society for Photogrammetry and Remote Sensing.

Ray, T.W., B.C. Muray, A. Chehbouni and E. Njoku. 1993. The Red Edge in Arid Region Vegetation: 340-1060 nm Spectra. In *Summaries of the Fourth Annual JPL Airborne Geoscience Workshop*, 149-152. JPL Publication 93-26, Jet Propulsion Laboratory, Pasadena, California.

RCRA. 1976. Resource Conservation and Recovery Act. Public Law 94-580. 42 U.S.C. §§6901-6992.

Richardson, A.J., J.H. Everitt and H.W. Gausman. 1983. Radiometric estimation of biomass and nitrogen contents of Alicia grass. *Remote Sensing of Environment,* 13: 179-184.

Reusen, I., L. Bertels, W. Debruyn, B. Deronde, D. Fransaer, S. Sterckx. 2003. Species identification and stress detection of heavy-metal contaminated trees. In: *Proceedings of the Spectral Remote Sensing of Vegetation Conference*, Las Vegas, Nevada, March 12-14, 2003. http://www.epa.gov/nerlesd1/land-sci/srsv/images/bertels.pdf Last Accessed January 22, 2007.

Roberts, D.A., M. Gardner, R. Church, S. Ustin, G. Scheer and R.O. Green. 1998. Mapping chaparral in the Santa Monica mountains using multiple endmember spectral mixture models. *Remote Sensing of Environment,* 65: 267-279.

Robinson, B. F., and D.P. Dewitt. 1983. Electro-optical non-imaging sensors. In: *Manual of Remote Sensing,* edited by R. N .Colwell, American Society of Photogrammetry, Falls Church, VA, pp. 293-333.

Rock, B.N., T. Hoshizake, and J.R. Miller. 1988. Comparison of *in situ* and airborne spectral measurements of the blue shift with forest decline. *Remote Sensing of Environment*, 24 (1): 109-127.

Rood, J.W, Jr. 1879. *Modern Chromatics With Applications to Art and Industry*. New York, D. Appleton & Company.

Rosipal, R. and N. Krämer. 2006. Overview and recent advances in partial least squares. In *Subspace, Latent Structure and Feature Selection Techniques*, edited by C. Saunders, M. Grobelnik, S. Gunn, and J. Shawe-Taylor, 34-51. New York, Springer.

Rossel, R.A., D.J.J. Walvoort, A.B. McBratney, L.J. Janik and J.O. Skjemstad 2006. Visible, near infrared, mid infrared or combined diffuse reflectance spectroscopy for simultaneous assessment of various soil properties. *Geoderma,* 131: 59–75.

Rosso, P.H., J.C. Pushnik, M. Lay and S.L. Ustin. 2005. Reflectance properties and physiological responses of Salicornia virginica to heavy metal and petroleum contamination. *Environmental Pollution*, 137 (2): 241-252.

Rougean, G. and F.M. Breon. 1995. Estimating PAR absorbed by vegetation from bi-directional reflectance measurements, *Remote Sensing of Environment*, 51: 375-384.

Rouse, J.W., R.H. Haas, J.A. Schell and D.W. Deering. 1973. Monitoring vegetation systems in the great plains with ERTS. In *Proceeding of the ERTS-1 Symposium*, National Aeronautical and Space Administration, SP351, 309-317.

Running, S.W., C.O. Justice, V. Salomonson, D. Hall, J. Barker, Y.J. Kaufman, A.H. Strahler, A.H. Huete, J.P. Muller, V. Vanderbilt, Z.M. Wan, P. Teillet and D. Carneggie. 1994. Terrestrial remote sensing science and algorithms planned for EOS/MODIS. *International Journal of Remote Sensing*, 17: 3587-3620.

Ryeson, R.A. and P.J. Curran. 1997. Chapter 10: Agriculture (Authors/Editors). In *The Manual of Photographic Interpretation, Second Edition*, edited by W. R. Phillipson, American Society for Photogrammtery and Remote Sensing, Bethesda, Maryland.

SARA. 1986. Superfund Amendments and Reauthorization Act, Public Law 99-499. 42 U.S.C. §§ 9601 *et seq*.

SAS. 2002. SAS Users Guide. SAS Institute Inc., Cary, N.C.

Savitzky, A. and M.J.E. Golay. 1964. Smoothing and differentiation of data by simplified least squares procedures. *Analytical Chemistry*, 36: 1627-1639.

Sayn-Wittgenstein, L. 1978. Recognition of tree species on aerial photographs. Environment Canada. Canadian Forest Service Forest Management Institute Information Report, FMR-X-118, 97p.

Schilling. G.T. 2004. Spring Valley Operations Manager, U.S. Army Corps of Engineers. Personal communication.

Schmidtlein, S. 2005. Imaging spectroscopy as a tool for mapping Ellenberg indicator values. *Journal of Applied Ecology*, 42: 966–974.

Schreiber, U. 1983. Chlorophyll fluorescence as a tool in plant physiology I: The measuring system. *Photosynthesis Research*, 4: 361-373.

Schwaller M.R. and S.J. Tkach. 1985. Premature leaf senescence: remote sensing detection and utility for geobotanical prospecting. *Economic Geology,* 80: 250-255.

Schuerger, A.C., G.A. Capelle, J.A. DiBenedetto, C. Mao, C.N. Thai, M.D. Evans, J.T Richards, T.A. Blank and E.C. Stryjewski. 2003. Comparison of two hyperspectral imaging and two laser-induced fluorescence instruments for the detection of zinc stress and chlorophyll concentration in bahia grass (*Paspalum notatum Flugge*.) *Remote Sensing of Environment*, 84 (4): 572-588.

Schull, C.A. 1929. A spectrophotometric study of reflection of light from leaf surfaces. *The Botanical Gazette*, 87: 583-607.

Sigman, H. 1999. Reforming Hazardous Waste Policy. Essays in Public Policy: The Hoover Institution. http://www.hoover.org/publications/epp/93/93a.html Last accessed May 8, 2006.

Siegel, L. 1995. Land Mines - Global UXO. 1995. CPEO Military List Archive http://www.cpeo.org/lists/military/1995/msg00312.html Last Accessed January 25, 2007.

Simonett, D.S., R.G. Reeves, J.E. Estes, S.E. Bertke, and C.T. Sailer. 1983. The Development and Principals of Remote Sensing. In *The Manual of Remote Sensing, Second Edition*, edited by R.N. Colwell. Bethesda, Maryland, American Society for Photogrammetry and Remote Sensing.

Sims, D.A. and J.A. Gamon, 2002. Relationships between leaf pigment content and spectral reflectance across a wide range of species, leaf structures and developmental stages. *Remote Sensing of Environment,* 81: 337-354.

Singh, N., and L.Q. Ma. 2006. Arsenic speciation, and arsenic and phosphate distribution in arsenic hyperaccumulator *Pteris Vittata L*. and non-hyperaccumulator *Pteris Ensiformis L. Environmental Pollution,* 141: 238-246.

Slonecker, E.T., M.J. Lacerte and D. Garofalo. 2002. The value of historic imagery. *Earth Observation Magazine,* 8 (6): 39-41.

Smith, E., R. Naidu and A.M. Alston. 1998. Arsenic in the soil environment: a review. *Advanced Agronomy*, 64: 149-195.

Spurr, S.H. 1948. *Aerial Photographs in Forestry*. New York: Ronald Press Company, 340p.

Spurr, S.H. 1949. Films and filters in forest aerial photography. *Photogrammetric Engineering and Remote Sensing*, 15: 473-481.

Srivastava, M., L.Q. Ma and J.A. Gonzaga-Santos. 2006. Three new arsenic hyperaccumulating ferns. *Science of the Total Environment,* 364: 24–31.

Strachan, I.B., E. Pattey and J.B. Boisvert. 2002. Impact of nitrogen and environmental conditions on corn as detected by hyperspectral reflectance. *Remote Sensing of Environment*, 80 (20): 213-224.

Stehman, S.V. 1997. Selecting and interpreting measures of thematic classification accuracy. *Remote Sensing of Environment,* 62 (1): 77-89.

Stehman, S.V. (2000). Practical implications of design-based sampling inference for thematic map accuracy assessment. *Remote Sensing of Environment*, 72: 35-45.

Stewart, C. N., Jr. 1996. Monitoring transgenic plants using in vivo markers. *Nature Biotechnology,* 14: 682.

Stewart, C.N. Jr., R.J. Millwood, M.D. Halfhill, M. Ayalew, V.Cardoza, M. Kooshki, G.A. Capelle, K.R. Kyle, D. Piaseki, G. McCrum, and J. Di Benedetto. 2005. Laser-induced fluorescence imaging and spectroscopy of GFP transgenic plants. *Journal of Fluorescence*, 15 (5): 697-705.

Story, M., and R.G. Congalton. 1986. Accuracy assessment: a user's perspective. *Photogrammetric Engineering and Remote Sensing*, 52: 397–399.

Stout, K.K. 1986. Historical Aerial Photographic Analysis, American University, Washington, D.C. Report TS-PIC-86001M, Volumes 1 and 2. U.S. Environmental Protection Agency, Environmental Sciences Division, Las Vegas, Nevada.

Taubenhaus, J.J., W.N. Ezekiel and C.B. Neblette. 1929. Airplane photography in the study of cotton root rot. *Phytopathology,* 19: 1025-1029.

Thaman, R.R. 1974. Remote sensing of agricultural resources. In *Remote Sensing: Techniques for Environmental Analysis*, edited by J.W. Estes and L.W. Senger, Santa Barbara, California: Hamilton Publishing.

Thenkabail, P.S., R.B. Smith and E.D. Pauw. 2000. Hyperspectral vegetation indices and their relationship with agricultural crop characteristics. *Remote Sensing of Environment*, 71: 158-182.

Titus, S. 1982. Survey and analysis of present or potential environmental impact sites in Woburn, Massachusetts. In *Proceedings of the 48th Annual Meeting of the American Society for Photogrammetry, Denver, Colorado,* 538-549. American Society for Photogrammetry and Remote Sensing, Bethesda, Maryland.

Tobias, R.D. 1997. An introduction to partial least squares regression. SAS Institute, Appendices detail SAS PROC PLS Cary, N.C.: commands and parameters. http://ftp.sas.com/techsup/download/technote/ts509.pdf Last Accessed March 14, 2007.

TSCA. 1976. Toxic Substances Control Act. Public Law 94-469, 15 USC (C. 53) §§ 2601-2692.

Tu, C. and L.Q. Ma. 2002. Effects of arsenic concentrations and forms on arsenic uptake by the hyperaccumulator ladder brake. *Journal of Environmental Quality,* 31: 641-647.

Tsai F. and W. Philpot. 1998. Derivative analysis of hyperspectral data. *Remote Sensing of Environment,* 66: 41-51.

United Nations. 1969. *Chemical and Bacteriological (Biological) Weapons, and the Effect of Their Possible Use*. New York, Walden.

United Nation. 2004. Glossary of Landmine Terms. http://www.trellick.net/landmines/pages/info/glossary.html Last accessed January 25, 2007.

UNEP (United Nations Environmental Programme). 2006. Introduction to the Basel Convention. http://www.basel.int/pub/basics.html Last accessed April 22, 2006.

USA (United States Army). 1996. Handbook On The Medical Aspects Of NBC Defensive Operations Fm 8-9. HQDA (DASG-HCO, Falls Church, Virginia.

USEPA (U.S. Environmental Protection Agency). 1986a U.S. EPA Test Methods for the Evaluation of Solid Waste: Laboratory Manual Physical Chemical Methods, Method 3050: Acid Digestion of Sediment, Sludges and Soils, Volume IA, Office of Solid Waste, Washington, D.C. 20460.

USEPA (U.S. Environmental Protection Agency). 1986b U.S. EPA Test Methods for the Evaluation of Solid Waste: Laboratory Manual Physical Chemical Methods, Method 3051: Microwave Assisted Acid Digestion of Sediments, Sludges, Soil and Oils, Volume IA, Office of Solid Waste, Washington, D.C. 20460.

USEPA (U.S. Environmental Protection Agency). 2001. A Citizen's Guide to Bioremediation. EPA-F42-01-001. Office of Solid Waste and Emergency Response, Washington, D.C. http://clu-in.org/download/citizens/citphyto.pdf Last accessed January 25, 2007.

USEPA (U.S. Environmental Protection Agency). 2004. Test Methods for Evaluating Solid Waste, Physical/Chemical Methods. EPA Publication SW-846. Revision 6. U.S. Environmental Protection Agency, Washington, D.C. http://www.epa.gov/epaoswer/hazwaste/test/sw846.htm Last accessed January 25, 2007

USEPA (U.S. Environmental Protection Agency). 2005. Environmental Photographic Interpretation Center (EPIC). Photo Interpretation: Hazardous Waste Sites. Standard Operating Procedure. U.S. Environmental Protection Agency, Las Vegas, Nevada.

USEPA (U.S. Environmental Protection Agency) 2006a. What Does the Evidence Say About NPL Listing and Home Prices? http://www.epa.gov/superfund/programs/recycle/property.htm Last Accessed April 22, 2006.

USEPA (U.S. Environmental Protection Agency). 2006b. CERCLA Hazardous Substances, 40 CFR § 261. http://www.epa.gov/superfund/programs/er/hazsubs/cercsubs.htm Last accessed 22 January 2007.

Ustin, S.L., M.O. Smith and J.B. Adams. 1993. Remote sensing of ecological processes: a strategy for developing and testing ecological models using spectral mixture analysis. In *Scaling Physiological Processes: Leaf to Globe*, edited by J. R. Ehelringer and C. B. Field, 339-357. San Diego, Academic Press.

Van Atta, G.R. 1936. Filters for the separation of living and dead leaves in monochromatic photographs with a method for determination of photographic filter factors. *Journal of the Biological Photographic Association,* 4: 177-191.

Vélez-Reyes, M., S.D. Hunt, S. Morillo and H. Sierra-Gil. 2004. Effects of resolution enhancement pre-processing in atmospheric correction of hyperspectral imagery. In *Proceedings of SPIE: Algorithms and Technologies for Multispectral, Hyperspectral, and Ultraspectral Imagery X*, Vol. 5425.

Vianna N.J. and A.K. Polan. 1984. Incidence of low birth weight among Love Canal residents. *Science,* 226: 1217-1219.

Vine, M.F., L. Stein, K. Weigle, J. Schroeder, D. Degnan, C.H.J. Tse, C. Hanchette and L. Backer. 2000. Effects on the immune system associated with living near a pesticide dump site. *Environmental Health Perspectives,* 108 (12): 1113-1124.

Vrijheid, M. 2000. Health effects of residence near hazardous waste landfill sites: a review of epidemiological literature. *Environmental Health Perspectives,* Supplements 108(suppl 1): 101-112.

Vygodskaya, N.N., I.I. Gorshkova and Y.V. Fadeyeva. 1989. Theoretical estimates of sensitivity in some vegetation indices to variations in the canopy conditions. *International Journal of Remote Sensing*, 10: 1857-1872.

Wang, J,. F.J. Zhao, A.A. Meharg, A. Raab, J. Feldmann and S.P. McGrath. 2002. Mechanisms of arsenic hyperaccumulation in *Pteris vittata*; Uptake kinetics, interactions with phosphate, and arsenic speciation. *Plant Physiology*, 130: 1552-1561.

Wang, H.B., M.H. Wong, C.Y. Lan, A.J.M. Baker, Y.R. Qin, W.S. Shu, G.Z. Chen and Z.H. Ye. 2006. Uptake and accumulation of arsenic by 11 Pteris Taxa from Southern China. *Environmental Pollution*, 20: 1-9.

Wei, C.Y. and T.B. Chen. 2006. Arsenic accumulation by two brake ferns growing on an arsenic mine and their potential in phytoremediation. *Chemosphere*, 63: 1048–1053.

Wessman, C.A., J.D. Aber, D.L. Peterson and J.M. Melillo. 1988. Foliar analysis using near infrared spectroscopy. *Canadian Journal of Forest Research*, 18: 6-11.

Wessman, C.A. 1994. Remote Sensing and the Estimation of Ecosystem Parameters and Functions. In *Imaging Spectrometry - A Tool for Environmental Observations*, edited by J. Hill and J. Megier, 39-56. Dordrecht, Kluwer.

Williams, D.R. 2002. Site Discovery Inventory, Conduit Road Field Test Site Study Area. TS-PIC-20203491S, U.S. Environmental Protection Agency, Environmental Sciences Division, Las Vegas, Nevada.

Willstatter, R. and A. Stoll. 1913. Untersuchungen Uber Chlorophyll: Method Und Ergbnisse. Berlin: Springer, 435p.

Willstatter, R. and A. Stoll. 1918. Untersuchungen Uber Die Assimilation Der Kohlensaure. Berlin: J. Springer, 448p.

Wold, H. 1966. Estimation of principal components and related models by iterative Least squares, In *Multivariate Analysis*, edited by P.R. Krishnaiah, 391-420. New York, Academic Press.

Wold. H. 1975. Path with Latent Variables: The NIPALS Approach. In *Quantitative Sociology: International Perspectives on Mathematical and Statistical Model Building,* edited by H.M. Balock, 307-357. New York, Academic Press.

Wold, H. 1985. Partial Least Squares. In *Encyclopedia of statistical sciences, Volume 6*, edited by S. Kotz and N.L. Johnson, 581-591. New York, Wiley.

Wold, S. 1995. PLS for multivariate linear modeling. In *QSAR: Chemometric methods in molecular design, methods and principles in medicinal chemistry*, *Volume 2*, edited by H. van de Waterbeemd. 195-218. Weinheim, German, Verlag Chemie.

Wold, S., M. Sjolstrom and L. Erikson. 2001. PLS-regression: A Basic Tool of Chemometrics. *Chemometrics and Intelligent Laboratory Systems*, 58: 109-130.

Wood, R.W. 1910. Photography by invisible rays. *Photographic Journal*, 50: 329-338.

Wood, H.A. 1968. Accumulated data used in the air photo interpretation of agricultural land use. In *Proceedings, Second Seminar of Air Photo Interpretation in the Development of Canada*, (Ottawa), 100-114.

Xu, L., J.H. Jiang, H.L. Wu, G.L. Shen and R.Q. Yu. 2007. Variable-weighted PLS. *Chemometrics and Intelligent Laboratory Systems*, 85: 140–143.

Yoder B.J., and R.E. Pettigrew-Crosby. 1995. Predicting nitrogen and chlorophyll Content and concentrations from reflectance spectra (400 - 2500 nm) at leaf and canopy scales. *Remote Sensing of Environment*, 53: 199-211.

Zhang, W., C. Yong, C. Tu and L.Q. Ma. 2002. Arsenic speciation and distribution in an arsenic hyperaccumulating plant. *The Science of the Total Environment*, 300: 167–177.

Zhang, M., Z. Qin, X. Liu and S.L. Ustin. 2003. Detection of stress in tomatoes induced by late blight disease in California, USA using hyperspectral remote sensing. *International Journal of Applied Earth Observation and Geoinformation* 4 (4): 295-310.

Zsilinsky, V.G. 1963. Photographic interpretation of tree species in Ontario, Toronto: Ontario Department of Lands and Forests, Timber Branch.

APPENDIX A

Example of SAS commands for processing Fern Spectral Data with Partial Least Squares and Stepwise Linear Regression. Explanatory notes and comments in blue.

```
Libname ter "c:\0pcm1d";                                  * Establish Operational SAS Data Directory

Proc transpose data=ter.band out=tt;ID band;run;          * Enter Excel data in SAS
data ttt; set tt; i+1; run;                               * format and transpose.
data f; set ter.frond; i+1; run;

data ter.all;                                             * Create master SAS data set
   merge f ttt;                                           * of spectral values and frond
         by i;                                            * arsenic concentration for the first
         frond = frond+0;                                 * derivative of reflectance for the
         Lfrond = Log(frond);                             * Pteris cretica mayii data set.
         drop var0 _NAME_ _LABEL_ i;
         run;

*******************************************************************************;

symbol1 v=dot c=blue I=none;                              * Plot the input data
Proc gplot data=ter.all;                                  * for visual inspection
   plot frond *(_400--_2399);
          run;

*******************************************************************************;


Proc PLS data=ter.all cv=one cvtest(seed=12345 pval=0.10 ); * first PLS run, set cross-validation
   model frond =_400--_2399;                              * parameters and significance level
   output out=outWLT  predicted = yhat1
                yresidual = yres1
                xresidual = xres1-xres2000
                xscore    = xscr
                yscore    = yscr;
         run;

         Output out=outWLT  predicted = yhat1
                yresidual = yres1
                xresidual = xres1-xres2000
                xscore    = xscr
                yscore    = yscr;
         run;


*******************************************************************************;
```

```
axis1 label=(angle=270 rotate=90 "x score 2")                    * Plot the PLS data
     major=(number=5) minor=none;                                 * for visual inspection
axis2 label=("X-score 1") minor=none;
Title " ";
symbol1 v=dot c=blue i=none;
proc gplot data=outWLT;
     plot xscr2*xscr1=1
       / vaxis=axis1 haxis=axis2 frame cframe=white href=0 vref=0;
            run;
%let ifac = 1;
data pltanno; set outWLT;
     length text $ 25;
     retain function 'label' position '5' hsys '3' xsys '2' ysys '2'
          color 'blue' style 'swissb';
      text=%str(i); x=xscr&ifac; y=yscr&ifac;
     axis1 label=(angle=270 rotate=90 "Y score &ifac")
       major=(number=5) minor=none;
     axis2 label=("X-score &ifac") minor=none;
     symbol1 v=dot c=blue i=none;
proc gplot data=outWLT;
     plot yscr&ifac*xscr&ifac=1
       / anno=pltanno vaxis=axis1 haxis=axis2 frame cframe=white href=0 vref=0;
            run;

*******************************************************************************************;
ods output XWeights=xweights;                                    * plot the Y and X variable weights
Proc PLS data=ter.all nfac=3 details;                            * with the number of factors (nfac) from the
model frond =_400--_2399;                                        * PLS run
run;

proc transpose data=xweights(drop=NumberOfFactors InnerRegCoef)
             out =xweights;
run;
data xweights; set xweights;
     rename col1=w1 col2=w2 col3=w3 col4=w4;
run;

   data wt_anno; set xweights;
     length text $ 7;
     retain function 'label'
          position '5'
          hsys     '3'
          xsys     '2'
          ysys     '2'
          color    'blue'
          style    'swissb';
     text=%str(_name_); x=w1; y=w2;
run;

   axis1 label=(angle=270 rotate=90 "X weight 2")
        major=(number=5) minor=none;
   axis2 label=("X-weight 1") minor=none;
   symbol1 v=dot c=blue i=none;
```

```
proc gplot data=xweights;
    plot w2*w1=1 / anno=wt_anno vaxis=axis1
                haxis=axis2 frame cframe=white href=0 vref=0;
run; quit;

*******************************************************************************;

/*   Weights and Percent variance for the ind vars, #wts and pctvar=# Sig. factors */
/* The following statements produce coefficients and the VIP */
/*  Put coefficients, weights, and R**2's into data sets     */


  ods listing close;
  ods output PercentVariation  = pctvar
             XWeights          = xweights
             censcaleParms     = solution;
proc pls data=ter.all nfac=3 details;
    model frond =_400--_2399/solution;
run;
  ods listing;

*******************************************************************************;
/ * Reformat the coefficients/
  data solution; set solution;
     format frond 7.2;
     if (RowName = 'Intercept') then delete;
     rename RowName = Predictor frond   = frond;
  run;
/*

*******************************************************************************;

/  Transpose weights and R**2's.
  data xweights; set xweights; _name_='W'||trim(left(_n_));
  data pctvar  ; set pctvar  ; _name_='R'||trim(left(_n_));
  proc transpose data=xweights(drop=NumberOfFactors InnerRegCoef)
               out =xweights;
  proc transpose data=pctvar(keep=_name_ CurrentYVariation)
               out =pctvar;
  run;
  Proc Print data=pctvar;run;

*******************************************************************************;
/  Sum the squared weights times the normalized R**2's.
/  The VIP is defined as the square root of this
/  weighted average times the number of predictors.


proc sql;
     create table vip as
       select *
         from xweights left join pctvar(drop=_name_) on 1;
data vip; set vip; keep _name_ vip;
```

```
    array w{3};
    array r{3};
    VIP = 0;
    do i = 1 to 2; /* to 6, i is the number of significant factors */
      VIP = VIP + r{i}*(w{i}**2)/sum(of r1-r3);/* r3 is the number of sig factors */
      end;
    VIP = sqrt(VIP * 2000);/* 2169 is the number of x vars */
data vipbpls; merge solution vip(drop=_name_);
options ps=255 ls=80;
Proc sort data=vipbpls; by vip predictor; run;
proc print data=vipbpls;run;quit;



*******************************************************************************;

data grp;                                                   * group factors by VIP table results
   set vipbpls;                                             * drop all factors where VIP < 1
   if vip >= 2.7 then group=1;
   if 2.7 > vip >= 2 then group=2;
   if 2 > vip >= 1.5 then group=3;
   if 1.5 > vip >= 1 then group=4;
          run;
Proc sort data=grp; by group predictor ;  run;
data grp1;          set grp; where group=1;  vip1 = predictor; run;
data grp2;          set grp; where group=2;  vip1 = predictor; run;
data grp3;          set grp; where group=3;  vip1 = predictor; run;
data grp4;          set grp; where group=4;  vip1 = predictor; run;

Proc Transpose data=grp1 out=grpt1;  id predictor;  var vip1; run;        * VIP group1
modify grpt1 (label='');
 proc modify data=grpt1(label=''); out=grpt1m; run;
proc print data=grpt1 n label=''; run;

Proc Transpose data=grp2 out=grpt2;  id predictor;  var vip1; run;        * VIP group2
modify grpt1 (label='');
 proc modify data=grpt1(label=''); out=grpt1m; run;
proc print data=grpt1 n label=''; run;

Proc Transpose data=grp3 out=grpt3;  id predictor;  var vip1; run;        * VIP group3
modify grpt1 (label='');
 proc modify data=grpt1(label=''); out=grpt1m; run;
proc print data=grpt1 n label=''; run;

Proc Transpose data=grp4 out=grpt4;  id predictor;  var vip1; run;        * VIP group4
modify grpt1 (label='');
 proc modify data=grpt1(label=''); out=grpt1m; run;
proc print data=grpt1 n label=''; run;


Options ps=255 ls=100 nolabel nodate;
proc print data=grpt1; run;
```

```
proc print data=grpt2 noobs;  run;
proc print data=grpt3 noobs;  run;
proc print data=grpt4 noobs;  run;

/*
/*   END of VIP */


** group1 - vip >= 2.7 ***
        _663    _385    _379    _688    _384    _357    _368    _664    _665    _358    _383
        _666    _687    _2497   _350    _667    _686    _2518   _668    _669    _685    _670
        _671    _672    _673    _674    _684    _675    _683    _676    _682    _677    _681
        _678    _679    _680    _381    _382


** group2 - 2 7 > vip >= 2.0***
_2316  _2317  _2327  _2328  _2339  _2342  _2343  _2344  _2345  _2346  _2347  _2348  _2349
_2350  _2351  _2352  _2363  _2366  _2367  _2368  _2369  _2389  _2395  _2396  _2405  _2406
_2417  _2418  _2419  _2422  _2431  _2434  _2437  _2438  _2446   _422   _426   _438   _439
_454   _489


** group3 - 2.0 > vip >= 1.5***
_2144  _2166  _2167  _2168  _2190  _2283  _2297  _2298  _2315  _2319  _2325  _2326  _2331
_2332  _2337  _2338  _2353  _2362  _2364  _2365  _2370  _2371  _2372  _2373  _2388  _2390
_2394  _2407  _2408  _2409  _2410  _2411  _2414  _2415  _2416  _2420  _2421  _2435  _2443
_2444  _2445  _423   _427   _428   _429   _430   _432   _435   _436   _437   _440   _441
_443   _445   _446   _447   _449   _450   _451   _452   _456   _459   _466   _467   _468
_473   _474   _476   _478   _484   _485   _487   _488   _490   _491   _515   _516   _517
_518   _521   _522   _528   _529   _534   _664   _665   _666   _667   _668   _669   _670
_671   _672   _673   _674   _675   _676   _677   _678   _679   _680   _681   _682   _683

** group4 - 1.5 > vip >= 1 ***
_1000  _1001  _1002  _1003  _1004  _1005  _1006  _1007  _1008  _1009  _1010  _1011  _1012
_1013  _1014  _1015  _1016  _1017  _1018  _1019  _1020  _1021  _1022  _1023  _1024  _1025
_1026  _1027  _1028  _1029  _1030  _1031  _1032  _1033  _1034  _1035  _1036  _1037  _1038
_1039  _1040  _1041  _1042  _1043  _1044  _1045  _1046  _1047  _1048  _1049  _1050  _1051
_1052  _1053  _1054  _1055  _1056  _1057  _1058  _1059  _1060  _1061  _1062  _1063  _1064
_1065  _1066  _1067  _1068  _1069  _1070  _1071  _1072  _1073  _1074  _1075  _1076  _1077
_1078  _1079  _1080  _1081  _1082  _1083  _1084  _1085  _1086  _1087  _1088  _1089  _1090
_1091  _1092  _1093  _1094  _1095  _1096  _1097  _1098  _1099  _1100  _1101  _1102  _1103
_1104  _1105  _1106  _1107  _1108  _1109  _1110  _1111  _1112  _1113  _1114  _1115  _1116
_1117  _1118  _1119  _1120  _1121  _1122  _1123  _1124  _1125  _1126  _1127  _1128  _1129
_1130  _1131  _1132  _1133  _1134  _1135  _1136  _1137  _1138  _1139  _1140  _1141  _1142
_1143  _1144  _1145  _1146  _1147  _1148  _1149  _1150  _1151  _1152  _1153  _1154  _1155
_1156  _1157  _1158  _1159  _1160  _1161  _1162  _1163  _1164  _1165  _1166  _1172  _1404
_1405  _1406  _1407  _1408  _1409  _1410  _1411  _1412  _1413  _1414  _1415  _1416  _1417
_1418  _1419  _1420  _1811  _1884  _1885  _1886  _1887  _1888  _1889  _1890  _1891  _1892
_1893  _1894  _1895  _1896  _1897  _1898  _1899  _1900  _1901  _1902  _1903  _1904  _1905
_1906  _1907  _1908  _1909  _1910  _1911  _1912  _1913  _1914  _1915  _1916  _1917  _1918
_1919  _1920  _1921  _1922  _1923  _1924  _1925  _1926  _1927  _1928  _1929  _1930  _1931
_1932  _1933  _1934  _1935  _1936  _1937  _1938  _1939  _1940  _1941  _1942  _1943  _1944
```

_1945	_1946	_1947	_1948	_1949	_1952	_1953	_1954	_1955	_1956	_1957	_1958	_1959
_1960	_1961	_1962	_1963	_1964	_1965	_1966	_1967	_1968	_1969	_1970	_1971	_1972
_1973	_1974	_1975	_1976	_1977	_1983	_1984	_1985	_1986	_1987	_1988	_1989	_1996
_1997	_1998	_1999	_2000	_2001	_2003	_2004	_2005	_2006	_2007	_2008	_2009	_2010
_2025	_2026	_2031	_2032	_2033	_2034	_2035	_2039	_2040	_2041	_2042	_2090	_2091
_2092	_2103	_2104	_2105	_2106	_2107	_2108	_2109	_2118	_2119	_2120	_2121	_2133
_2140	_2141	_2142	_2143	_2145	_2146	_2147	_2148	_2149	_2150	_2169	_2152	_2153
_2154	_2158	_2159	_2164	_2165	_2169	_2170	_2174	_2175	_2176	_2177	_2178	_2179
_2180	_2181	_2182	_2185	_2186	_2187	_2188	_2189	_2191	_2192	_2193	_2203	_2204
_2205	_2208	_2209	_2210	_2217	_2218	_2219	_2220	_2227	_2228	_2235	_2236	_2237
_2238	_2239	_2244	_2248	_2249	_2250	_2251	_2252	_2253	_2254	_2255	_2256	_2257
_2258	_2259	_2260	_2261	_2262	_2263	_2264	_2265	_2266	_2267	_2268	_2269	_2270
_2271	_2272	_2273	_2274	_2275	_2276	_2277	_2278	_2279	_2280	_2281	_2282	_2284
_2285	_2286	_2287	_2288	_2289	_2290	_2291	_2292	_2293	_2294	_2295	_2296	_2299
_2300	_2301	_2302	_2303	_2304	_2305	_2306	_2307	_2308	_2309	_2310	_2311	_2312
_2314	_2320	_2321	_2322	_2323	_2324	_2329	_2330	_2333	_2334	_2335	_2336	_2354
_2355	_2356	_2357	_2358	_2359	_2360	_2361	_2374	_2375	_2376	_2377	_2378	_2379
_2380	_2381	_2382	_2383	_2384	_2385	_2386	_2387	_2391	_2392	_2393	_2412	_2413
_2430	_2436	_431	_434	_442	_444	_448	_453	_457	_458	_460	_461	_462	_463
_464	_465	_469	_470	_471	_472	_475	_477	_479	_480	_481	_482	_483	_486
_492	_493	_494	_495	_496	_497	_498	_499	_500	_501	_502	_503	_504	_505
_506	_507	_508	_509	_510	_511	_512	_513	_514	_519	_520	_523	_524	_525
_526	_527	_530	_531	_532	_533	_535	_536	_537	_538	_539	_540	_541	_542
_543	_544	_545	_546	_547	_548	_549	_550	_551	_552	_553	_554	_555	_556
_557	_558	_559	_560	_561	_562	_563	_564	_565	_566	_567	_568	_569	_570
_571	_572	_573	_574	_575	_576	_577	_578	_579	_580	_581	_582	_583	_584
_585	_586	_587	_588	_589	_590	_591	_592	_593	_594	_595	_596	_597	_598
_600	_601	_602	_603	_604	_605	_606	_608	_609	_610	_611	_612	_613	_614
_615	_616	_617	_618	_619	_620	_621	_622	_623	_624	_625	_626	_627	_628
_629	_630	_631	_632	_633	_634	_635	_636	_637	_638	_639	_640	_641	_642
_643	_644	_645	_646	_647	_648	_649	_650	_651	_652	_653	_654	_655	_656
_657	_658	_659	_660	_661	_662	_663	_684	_685	_686	_687	_688	_689	_690
_691	_692	_693	_694	_695	_696	_697	_698	_699	_700	_701	_702	_703	_704
_705	_706	_707	_708	_709	_710	_711	_712	_713	_714	_715	_716	_717	_718
_719	_720	_721	_722	_723	_724	_725	_726	_727	_728	_729	_730	_731	_732
_733	_734	_735	_736	_737	_738	_739	_740	_741	_742	_743	_744	_745	_746
_747	_748	_749	_750	_751	_752	_753	_754	_755	_756	_757	_758	_759	_760
_761	_762	_763	_764	_765	_766	_767	_768	_769	_770	_771	_772	_773	_774
_775	_776	_777	_778	_779	_780	_781	_782	_783	_784	_785	_786	_787	_788
_789	_790	_791	_792	_793	_794	_795	_796	_797	_798	_799	_800	_801	_802
_803	_804	_805	_806	_807	_808	_809	_810	_811	_812	_813	_814	_815	_816
_817	_818	_819	_820	_821	_822	_823	_824	_825	_826	_827	_828	_829	_830
_831	_832	_833	_834	_835	_836	_837	_838	_839	_840	_841	_842	_843	_844
_845	_846	_847	_848	_849	_852	_853	_854	_855	_856	_857	_858	_859	_861
_862	_864	_865	_866	_867	_868	_869	_870	_871	_872	_873	_880	_881	_882
_891	_892	_895	_896	_903	_904	_906	_907	_914	_915	_918	_922	_965	_976
_977	_978	_979	_980	_981	_982	_983	_984	_985	_986	_987	_988	_989	_990
_991	_992	_993	_994	_995	_996	_997	_998	_999					

```
*****   Group 1 PLS  ************************************;
Proc PLS data=ter.all cv=one cvtest(seed=12345 pval=0.10 );
   model frond =  _663     _385     _379     _688     _384     _357     _368     _664     _665     _358
           _383     _666     _687     _2497    _350     _667     _686     _2518    _668     _669     _685
           _670     _671     _672     _673     _674     _684     _675     _683     _676     _682     _677
           _681     _678     _679     _680     _381     _382;

                   Output out=outWLT  predicted = yhat1
                   yresidual = yres1
                   xresidual = xres1-xres38
                   xscore    = xscr
                   yscore    = yscr;
run;


***********    Diagnostic Check Figures and VIP table ******************************;;
axis1 label=(angle=270 rotate=90 "x score 2")
     major=(number=5) minor=none;
axis2 label=("X-score 1") minor=none;
Title " ";
symbol1 v=dot c=blue i=none;
proc gplot data=outWLT;
     plot xscr2*xscr1=1
       / vaxis=axis1 haxis=axis2 frame cframe=white href=0 vref=0;
run;
%let ifac = 1;
data pltanno; set outWLT;
     length text $ 25;
     retain function 'label' position '5' hsys '3' xsys '2' ysys '2'
          color 'blue' style 'swissb';
      text=%str(i); x=xscr&ifac; y=yscr&ifac;
     axis1 label=(angle=270 rotate=90 "Y score &ifac")
       major=(number=5) minor=none;
     axis2 label=("X-score &ifac") minor=none;
     symbol1 v=none i=none;
proc gplot data=outWLT;
     plot yscr&ifac*xscr&ifac=1
       / anno=pltanno vaxis=axis1 haxis=axis2 frame cframe=white href=0 vref=0;
run;


/* for plotting the y variables and x valiables weights*/
ods output XWeights=xweights;
Proc PLS data=ter.all nfac=4 details;
   model frond =_663       _385     _379     _688     _384     _357     _368     _664     _665     _358
           _383     _666     _687     _2497    _350     _667     _686     _2518    _668     _669     _685
           _670     _671     _672     _673     _674     _684     _675     _683     _676     _682     _677
           _681     _678     _679     _680     _381     _382;
 run;

/* ------------------------------------------------------------   */

   ods listing close;
```

```
  ods output PercentVariation  = pctvar
            XWeights          = xweights
            censcaleParms     = solution;
proc pls data=ter.all nfac=1 details;
    model frond =_663      _385      _379      _688      _384      _357      _368      _664      _665      _358
            _383      _666      _687      _2497     _350      _667      _686      _2518     _668      _669      _685
            _670      _671      _672      _673      _674      _684      _675      _683      _676      _682      _677
            _681      _678      _679      _680      _381      _382/solution;
run;
  ods listing;

proc transpose data=xweights(drop=NumberOfFactors InnerRegCoef)
             out =xweights;
run;
  data xweights; set xweights;
    rename col1=w1 col2=w2 col3=w3 col4=w4 col5=w5 col6=w6;
  run;
  data wt_anno; set xweights;
    length text $ 7;
    retain function 'label'
          position '5'
          hsys     '3'
          xsys     '2'
          ysys     '2'
          color    'blue'
          style    'swissb';
    text=%str(_name_); x=w1; y=w2;
run;

  axis1 label=(angle=270 rotate=90 "X weight 2")
       major=(number=5) minor=none;
  axis2 label=("X-weight 1") minor=none;
  symbol1 v=none i=none;
proc gplot data=xweights;
    plot w2*w1=1 / anno=wt_anno vaxis=axis1
                haxis=axis2 frame cframe=white href=0 vref=0;
run; quit;

/*   Weights and Percent variance for the ind vars, #wts and pctvar=# Sig. facotrs */
/* The following statements produce coefficients and the VIP */
/*  Put coefficients, weights, and R**2's into data sets     */
/* -------------------------------------------------------   */

  ods listing close;
  ods output PercentVariation  = pctvar
            XWeights          = xweights
            censcaleParms     = solution;
proc pls data=ter.all nfac=1 details;
    model frond =_663      _385      _379      _688      _384      _357      _368      _664      _665      _358
            _383      _666      _687      _2497     _350      _667      _686      _2518     _668      _669      _685
            _670      _671      _672      _673      _674      _684      _675      _683      _676      _682      _677
            _681      _678      _679      _680      _381      _382/solution;
run;
```

```
  ods listing;

/*
/  Just reformat the coefficients.
/-------------------------------------------------------*/
  data solution; set solution;
    format frond 7.2;
    if (RowName = 'Intercept') then delete;
    rename RowName = Predictor frond   = frond;
  run;

/*
/  Transpose weights and R**2's.
/-------------------------------------------------------*/
  data xweights; set xweights; _name_='W'||trim(left(_n_));
  data pctvar  ; set pctvar  ; _name_='R'||trim(left(_n_));
  proc transpose data=xweights(drop=NumberOfFactors InnerRegCoef)
              out =xweights;
  proc transpose data=pctvar(keep=_name_ CurrentYVariation)
              out =pctvar;
  run;
  Proc Print data=pctvar;run;

/*
/  Sum the squared weights times the normalized R**2's.
/  The VIP is defined as the square root of this
/  weighted average times the number of predictors.
/-------------------------------------------------------*/

proc sql;
    create table vip as
      select *
        from xweights left join pctvar(drop=_name_) on 1;
data vip; set vip; keep _name_ vip;
    array w{1};
    array r{1};
    VIP = 0;
    do i = 1 to 1; /* to 6, i is the number of significant factors */
      VIP = VIP + r{i}*(w{i}**2)/sum(of r1-r1);/* r3 is the number of sig factors */
      end;
    VIP = sqrt(VIP * 745);/* 33 is the number of x vars */
data vipbpls; merge solution vip(drop=_name_);
options ps=255 ls=80;
Proc sort data=vipbpls; by vip predictor; run;
proc print data=vipbpls;run;quit;

*****   outliers   ******************************;                    Check for Outliers
proc pls data=grp1 nfac=4 ;
   model frond =_663     _385     _379     _688     _384     _357     _368     _664     _665     _358
          _383     _666     _687     _2497    _350     _667     _686     _2518    _668     _669     _685
          _670     _671     _672     _673     _674     _684     _675     _683     _676     _682     _677
          _681     _678     _679     _680     _381     _382;
```

```
    output out=stdres stdxsse=stdxsse stdysse=stdysse;
    data stdres; set stdres;i+1;



        xdist = sqrt(stdxsse);
        ydist = sqrt(stdysse);
  run;
Proc Print data=stdres; run;
Symbol1 i=needles v=dot c=blue;
Symbol2 i=needles v=dot c=red;
Symbol3 i=needles v=dot c=green;
Proc gplot data=stdres;
      plot xdist*i / cframe = white ;
Proc gplot data=stdres;
      plot ydist*i / cframe=white;
run;
```

***** Group 2 PLS **; Repeat for groups 2, 3 and 4

Take top factors from each data group run and place in stepwise regression model;

```
proc reg data=ter.all;
        model frond=    _498    _499    _500    _565    _566    _567    _568    _588    _596
        _597    _603    _604    _605    _606    _607    _608    _609    _610    _611    _612
        _621    _622    _625    _626    _627    _628    _631    _632    _633    _634    _635
        _636    _639    _640    _641    _642    _643    _650    _651    _652    _654    _655
        _977    _992    _994    _995    _1114   _1115   _1472   _1663   _1664   _1683   _1777
        _1818   _1819   _2050   _2053   _2058   _2059   _2079   _2092   _2093   _2094
        _2118   _2119   _2150   _2159   _2177   _2276   _2277   _2289   _2293   _2294
        _2295   2296    _2303   _2335   _2338   _2339/selection=stepwise sle=0.25 sls=0.05;

run;
```

Test final model for collinearity;

```
proc corr data=ter.all;
        var _499 _626 _655 _977 _992 _1114 _1683 _2058;
        run;
```

APPENDIX B

Summary statistics for the three fren species grown in arsenic-amended soils as shown in Tables 6, 7 and 8 on pages 121, 122 and 123.

SUMMARY STATISTICS ***Nephrolepis exaltata***

	FROND_AS	BIOMASS	BIOCONC
N of cases	25	25	25
Minimum	0.0	0.360	0.0
Maximum	5695.0	.220	31.120
Range	5695.0	8.860	31.120
Sum	24520.0	82.120	196.060
Median	143.0	2.590	3.720
Mean	980.800	3.285	7.842
95% CI Upper	1730.040	4.271	11.925
95% CI Lower	231.560	2.298	3.759
Std. Error	363.022	0.478	1.978
Standard Dev	1815.108	2.390	9.891
Variance	3294618.833	5.711	97.839
C.V.	1.851	0.728	1.261
Skewness(G1)	1.937	1.249	1.392
SE Skewness	0.464	0.464	0.464
Kurtosis(G2)	2.227	1.242	0.575
SE Kurtosis	0.902	0.902	0.902

PEARSON CORRELATION MATRIX

	SOIL_AS	HWEEK	FROND_AS	BIOMASS	BIOCONC
SOIL_AS	1.000				
HWEEK	0.000	1.000			
FROND_AS	0.817	0.145	1.000		
BIOMASS	-0.670	0.403	-0.498	1.000	
BIOCONC	0.822	0.222	0.944	-0.596	1.000

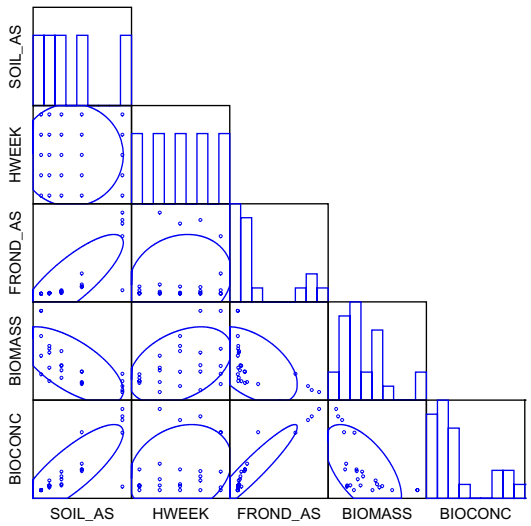

GENERAL LINEAR MODEL

Dep Var: FROND_AS N: 25 Multiple R: 0.967 Squared multiple R: 0.935

Adjusted squared multiple R: 0.922 Standard error of estimate: 506.287

Effect	Coefficient	Std Error	Std Coef	Tolerance	t	P(2 Tail)
CONSTANT	-866.125	329.40	0.000	.	-2.629	0.016
SOIL_AS	4.706	2.720	0.189	0.272	1.730	0.099
HWEEK	-69.680	25.249	-0.222	0.503	-2.760	0.012
BIOMASS	255.764	76.120	0.337	0.323	3.360	0.003
BIOCONC	190.589	21.866	1.039	0.228	8.716	0.000

ANALYSIS OF VARIANCE

Source	Sum-of-Squares	df	Mean-Square	F-ratio	P
Regression	7.39443E+07	4	1.84861E+07	72.119	0.000
Residual	5126523.302	20	256326.165		

*** WARNING ***

Case 20 is an outlier (Studentized Residual = -4.406)
Case 21 has large leverage (Leverage = 0.720)

Durbin-Watson D Statistic 1.069
First Order Autocorrelation 0.405

Plot of Residuals against Predicted Values

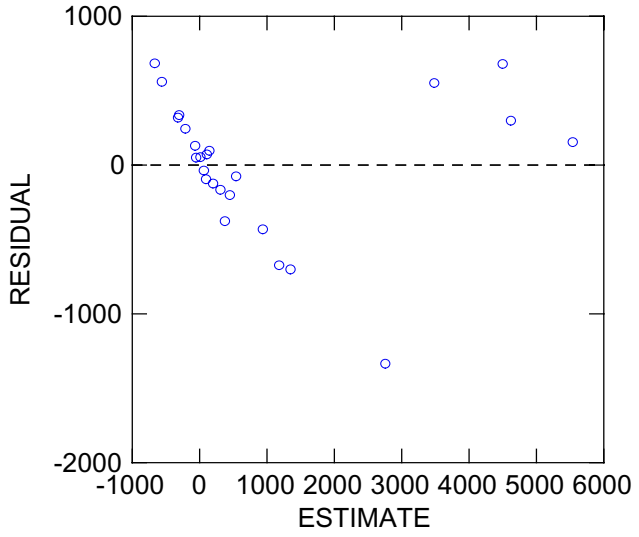

SUMMARY STATISTICS ***Pteris cretica mayii***

	FROND_AS	BIOM	BIOC
N of cases	25	25	25
Minimum	0.0	3.5	0.0
Maximum	5584.0	7.4	87.3
Range	5584.0	3.8	87.3
Sum	54662.0	129.7	966.9
Median	1868.0	5.1	41.3
Mean	2186.5	5.2	38.7
95% CI Upper	2908.5	5.6	49.8
95% CI Lower	1464.5	4.8	27.5
Std. Error	349.8	0.2	5.4
Standard Dev	1749.2	1.0	27.0
Variance	3059622.8	1.0	727.9
C.V.	0.8	0.2	0.7
Skewness(G1)	0.3	0.1	0.0
SE Skewness	0.5	0.5	0.5
Kurtosis(G2)	-1.2	-0.4	-1.0
SE Kurtosis	0.9	0.9	0.9

PEARSON CORRELATION MATRIX

	SOIL_AS	HWEEK	FROND_AS	BIOM	BIOC
SOIL_AS	1.000				
HWEEK	0.000	1.000			
FROND_AS	0.852	0.132	1.000		
BIOM	-0.592	0.383	-0.499	1.000	
BIOC	0.026	0.120	0.446	-0.175	1.000

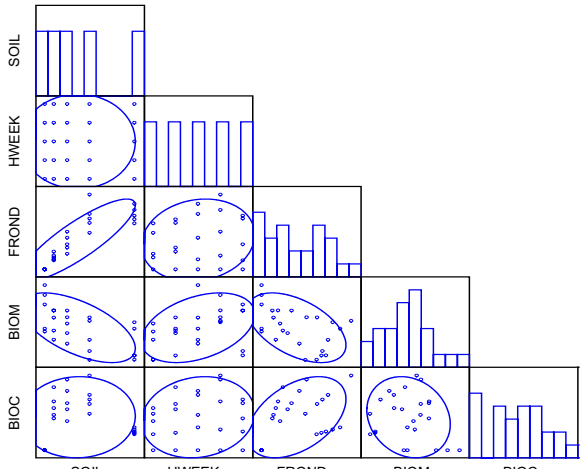

GENERAL LINEAR MOEL

Dep Var: FROND_AS N: 25 Multiple R: 0.970 Squared multiple R: 0.941

Adjusted squared multiple R: 0.929 Standard error of estimate: 462.066

Effect	Coefficient	Std Error	Std Coef	Tolerance	t	P(2 Tail)
CONSTANT	313.788	404.017	0.0	.	0.777	0.446
SOIL_AS	20.993	1.318	0.880	0.964	15.932	0.0
HWEEK	14.378	19.633	0.048	0.692	0.732	0.472
BIOMASS	-108.112	65.168	-0.110	0.674	-1.659	0.113
BIOCONC	23.800	3.247	0.406	0.960	7.329	0.0

ANALYSIS OF VARIANCE

Source	Sum-of-Squares	df	Mean-Square	F-ratio	P
Regression	6.83432E+07	4	1.70858E+07	80.025	0.0
Residual	4270104.582	20	213505.229		

*** WARNING ***
Case 10 has large leverage (Leverage = 0.576)

Plot of Residuals against Predicted Values

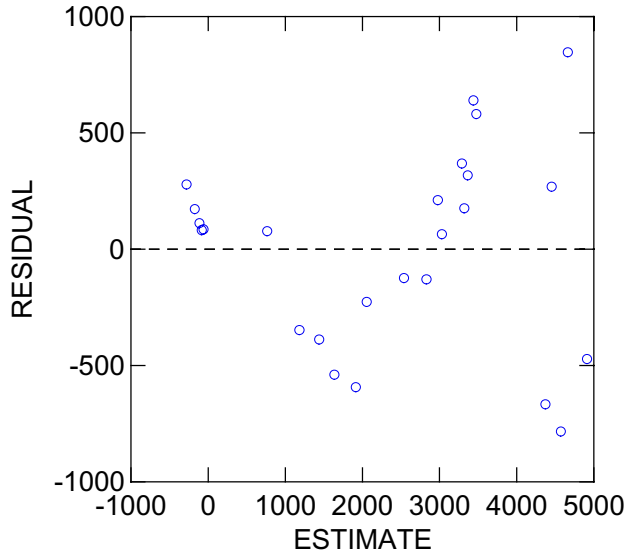

SUMMARY STATISTICS ***Pteris multifida***

	FROND_AS	BIOMASS	BIOCONC
N of cases	25	25	25
Minimum	0.0	4.190	0.0
Maximum	5510.0	12.670	93.790
Range	5510.0	8.480	93.790
Sum	59558.0	161.410	1093.040
Median	2702.0	6.240	53.820
Mean	2382.3	6.456	43.722
95% CI Upper	3100.314	7.184	55.957
95% CI Lower	1664.326	5.728	31.486
Std. Error	347.882	0.353	5.929
Standard Dev	1739.412	1.764	29.643
Variance	3025552.560	3.110	878.682
C.V.	0.730	0.273	0.678
Skewness(G1)	-0.059	1.778	-0.180
SE Skewness	0.464	0.464	0.464
Kurtosis(G2)	-1.352	5.506	-1.062
SE Kurtosis	0.902	0.902	0.902

PEARSON CORRELATION MATRIX

	SOIL_AS	HWEEK	FROND_AS	BIOMASS	BIOCONC
SOIL_AS	1.0				
HWEEK	0.0	1.0			
FROND_AS	0.883	-0.047	1.0		
BIOMASS	0.162	0.528	-0.185	1.0	
BIOCONC	-0.035	-0.092	0.359	0.102	1.0

GENERAL LINEAR MOEL

Dep Var: FROND_AS N: 25 Multiple R: 0.970 Squared multiple R: 0.941

Adjusted squared multiple R: 0.929 Standard error of estimate: 462.066

Effect	Coefficient	Std Error	Std Coef	Tolerance	t	P(2 Tail)
CONSTANT	313.788	404.017	0.0	.	0.777	0.446
SOIL_AS	20.993	1.318	0.880	0.964	15.932	0.0
HWEEK	14.378	19.633	0.048	0.692	0.732	0.472
BIOMASS	-108.112	65.168	-0.110	0.674	-1.659	0.113
BIOCONC	23.800	3.247	0.406	0.960	7.329	0.0

ANALYSIS OF VARIANCE

Source	Sum-of-Squares	df	Mean-Square	F-ratio	P
Regression	6.83432E+07	4	1.70858E+07	80.025	0.0
Residual	4270104.582	20	213505.229		

*** WARNING ***
Case 10 has large leverage (Leverage = 0.576)

Durbin-Watson D Statistic 1.476
First Order Autocorrelation 0.235

Plot of Residuals against Predicted Values

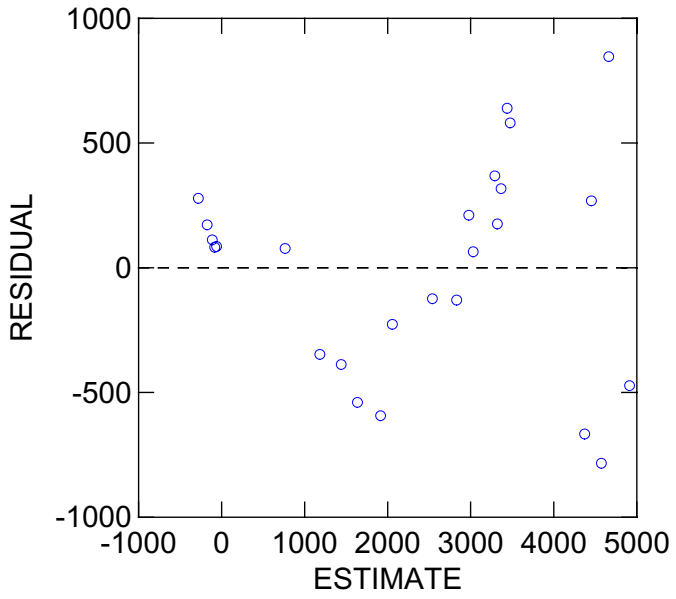

APPENDIX C

Vegetation Indices used in this study

Anthocyanin Reflectance Index 1	ARI1	(1/R550) – (1/ R700)	Gitelson et al. 2001
Anthocyanin Reflectance Index 2	ARI2	R800 (1/R550) – (1/ R700)	Gitelson et al. 2001
Atmospherically Resistant Vegetation Index	ARVI	VNIR - (2*(RED - BLUE) / vnir - (2*(RED + BLUE	Kaufman and Tanre, 1996
Blue Index	BI	BLUE/(BLUE+GREEN+RED)	Kleman & Fagerlund 1981
Cellulose Absorption Index	CAI	0.5 * (R2000 - R2200 / R2100)	Daughtry et al. 2004
Carotenoid Reflectance Index 1	CRI1	(1 / R510) – (1 / R550)	Gitelson et al. 2002.
Carotenoid Reflectance Index 2	CRI2	(1 / R510) – (1 / R700)	Gitelson et al. 2002
Enhanced Vegetation Index	EVI	2.5*((VNIR-RED)/ (VNIR+(6*RED) -(7.5*(BLUE+1)))	Running et al, 1994
GreenGNR	GGRN	GREEN/(GREEN+RED+NIR)	Bracher 1991
Green Index	GI	GREEN/(BLUE+GREEN+RED)	Kleman & Fagerlund 1981
GreenNR	GNR	GREEN(NIR/RED)	Vygodskaya et al. 1989
Green-Red	GR	GREEN/RED	Demetrides-Shah and Court 1987
Infrared Percentage Vegetation Index	IPVI	0.5 * (NDVI + 1)	Crippen 1990
Modified Chlorophyll Absorption Index	MCARI	[(R700 - R670) – 0.2 * (R700 - R550)] * (R700 / R670)	Daughtry et al., 2000
Modified Chlorophyll Absorption Index 1	MCARI1	1.2[2.5(R800-R670)-1.3 (R800-R550)]	Haboudane et al., 2004
Modified Chlorophyll Absorption Index 2	MCARI2	1.5[2.5(R800-R670)-1.3 (R800-R550)] / SQRT[(2*(R800+1)2) – (6*R800 – 5* SQRT(R670)) – 0.5]	Haboudane et al., 2004
modified Normalized Difference680	mND680	(R800-R680)/(R800 + R680+2*R445)	Sims and Gamon 2002
modified Normalized Difference705	mND705	(R750-R705)/ (R750 + R705+2*R445)	Sims and Gamon 2002
modified Red Edge Normalized Difference VI	mNDVI705	(R750-R445)/(R750 + R445)	Datt 1999; Sims and Gamon 2002
Modified Soil Adjusted Vegetation Index	MSAVI	(R800-R670)/(R800+R670+L) * (1+L)	Qi et al. (1994)
Modified Soil Adjusted Vegetation Index 2	MSAVI2	0.5 * ((2*(R800+1) - (SQRT ((2* R800	

Modified Soil Adjusted Vegetation Index 2	MSAVI2	0.5 * ((2*(R800+1) - (SQRT ((2* R800 + 1)^2 - (8 * (R800- R670)))	Haboudane et al., 2004
Moisture Stress Index	MSI	(R1599 - R819)	Hunt & Rock 1989;
modified Simple Ratio	mSR	(R800 / R670– 1) / (R800 / R670+ 1) 1/2	Chen 1996
Modified Red Edge SimpleRatio Index	mSR705	(R750 - R705) / (R750 + R705)	Datt 1999; Sims and Gamon 2002
Modified Triangular Vegetation Index 1	MTVI1	1.2 * (1.2(R800-R550)) – (1.3 * (R670- R550))	Haboudane et al., 2004
Modified Triangular Vegetation Index 2	MTVI2	1.5[1.2(R800 - R550) - 1.3 (R670 – R550)] / SQRT[(2*(R800+1)2) – (6*R800 – 5*SQRT(R670)) – 0.5]	Haboudane et al., 2004
Normalized Difference680	ND680	(R800 - R680) / (R800 + R680)	Sims and Gamon 2002
Normalized Difference705	ND705	R750 - R705) / (R750 + R705)	Sims and Gamon 2002
Normalized Difference Infrared Index	NDII	(R819 - R1649) / (R819 + R1649)	Jackson et al.,2004
Normalized Difference Lignin Index	NDLI	(LOG(1/R1754)-LOG(1/R1680))/ (LOG(1/R1754)+LOG(R1680)	Serrano et al., 2002
Normalized Difference Nitrogen Index	NDNI	(LOG(1/R1510)-LOG(1/R1680))/ (LOG(1/R1510)+LOG(R1680)	Serrano et al., 2002
Normalized Difference VI (Broadband)	$NDVI_B$	(NIR - RED)/ (NIR + RED)	Rouse et al., 1973
Normalized Difference Water Index	NDWI	(R857 - R1241) / (R857 + R1241)	Gao 1995
Near Infrared Green	NIR-G	NIR / GREEN	Demetrides-Shah and Court 1987
Normalized NIR-GREEN Index	NNGI	NIR - GREEN / NIR + GREEN	Vygodskaya et al. 1989
Normalized Difference Vegetation $Index_N$	$NVDI_N$	(R800 - R670) / (R800 + R670)	Sims and Gamon 2002
Photochemical Reflectance Index 1	PRI1	(R528 - R567) / (R528 + R567)	Gamon et al., 1992
Photochemical Reflectance Index 2	PRI2	(R531 - R570) / (R531 + R570)	Gamon et al., 1992
Photochemical Reflectance Index 3	PRI3	(R570 - R539) / (R570 + R539)	Gamon et al., 1992
Plant Senescence Reflectance Index	PSRI	(R680 - R500) / R750	Merzlyak et al., 1999
Perpendicular Vegetation Index	PVI	-.8736(RED) + .4866(NIR)	Richardson et al., 1983
Renormalized Difference Vegetation Index	RDVI	R800 - R670 / (R800 + R670)1/2	Rougean and Breon (1995)
Red Edge Value 1st derivative	REV1d	R1DREP	Curran et al., 1995
Red Edge Position	REP	R1Dmax : (R1D690 - R1D740)	Curran et al., 1995
Red Edge Reflectance	RER	RREP	Curran et al., 1995
Red Green Ratio	RGR	SUM (R600:R699) / SUM (R500 - R599)	Gamon and Surfus 1999
RedGRN	RGRN	RED/(GREEN+RED+NIR)	Bracher 1991
Red Green Index	RGI	R690 / R550	Zarco-Tejada et al., 2005
Red Index	RI	RED/(BLUE+GREEN+RED)	Kleman & Fagerlund 1981

Red Near Infrared Green	RNG	RED(NIR/GREEN)	Vygodskaya et al. 1989
Ratio Vegetation Index	RVI	NIR / RED	Jordon 1969
Red Edge Vegetation Index	RVSI	((R714 + R752) / 2) - R 733	Merton 1998
Simple Ratio Pigment Index	SRPI	R430/R680	Peñuelas et al. 1995
Soil and Atmospherically Resistant VI	SARVI	(1+L)(R800 - Rrb) / (R800 + Rrb + L)	Kaufman & Tanre 1992
Soil Adjusted Vegetation Index	SAVI	(1+ 0.5) (R800-R670)/ (R800+R670+0.5)	Huete 1988
Sum Green Index	SGI	SUM (R500: R600) / 101	Gamon and Surfus 1999
Structure Insensitive Pigment Index	SIPI	(R800 - R445) / (R800 - R680)	Penuelas et al., 1995
Simple Ratio Index	SRI	NIR / RED	Jordan 1969; Rouse et al., 1974
Simple Ratio680	SR680	R800 / R680	Sims and Gamon 2002
Simple Ratio705	SR705	R750 / R705	Sims and Gamon 2002
Triangular Vegetation Index	TVI	0.5 * (((120 * (R750-R550)) – (200 * (R670- R550)))	Broge and Leblanc 2000
Vogelman Red Edge Index 1	VOG1	(R740 / R720)	Vogelman et al., 1993
Vogelman Red Edge Index 2	VOG2	(R734 - R747) / (R715 + R726)	Vogelman et al., 1993
Vogelman Red Edge Index 3	VOG3	R734 - R747) / (R715 + R720)	Vogelman et al., 1993
Water Band Index	WBI	(R900 / R970)	Penuelas et al., 1995
Zarco and Miller	ZM	(R750 / R710)	Zarco-Tejada et al., 2001

CURRICULUM VITAE

E. Terrence Slonecker was born on March 19, 1952, in Connellsville, Pennsylvania, and is an American citizen and a Vietnam-Era Veteran of the United States Air Force. He graduated from Geibel High School, Connellsville, Pennsylvania, in 1969. He received his Bachelor of Science from Christopher Newport College, Newport News, Virginia in 1979 and a Masters of Science from George Mason University in 1991. He has been employed as an environmental scientist by the United States Environmental Protection Agency since 1989.